Dune foot behaviour and erosion of sandy coastal defences in annual storm conditions

R. R. van der Ven

TU Delft

Boskalis

Dune foot behaviour and erosion of sandy coastal defences in annual storm conditions

by

R. R. van der Ven

to obtain the degree of Master of Science

at the Delft University of Technology,

to be defended publicly on Tuesday, May 30, 2023, at 15:00.

Student number: 4472918

Project duration: September 5, 2022 – May 30, 2023

Thesis committee:

Prof. dr. ir. S. G. J. Aarninkhof,	TU Delft, chair
Prof. dr. ir. A. J. H. M. Reniers,	TU Delft
Ir. P. P. J. van Wiechen,	TU Delft, supervisor
Ir. H. T. Rijper,	Boskalis, daily supervisor

TU Delft Delft University of Technology

Boskalis

Abstract

Storm surges cause elevated water levels, potentially leading to dune erosion, which is crucial to understand due to the protective function of dunes and sandy coastal defences against flooding. Dunes are dynamic systems, extensively studied through flumes and field observations. Collecting hydrodynamic and morphological data from erosion-prone land reclamations can inform dune research and design optimisations. Loss of volume in land reclamation projects can result in setbacks, increased costs, and emissions. While dune erosion models estimate volume changes, they may deviate significantly under annual storm conditions due to calibration with normative storm conditions. Dune erosion typically occurs when the initial dune foot elevation is exceeded, resulting in a post-storm dune foot elevation at the maximum water level within the storm. Therefore, the (initial) dune foot might play an important role in the resulting erosion volume. The current knowledge on the dune foot behaviour of sandy coastal defences due to annual storm conditions is too limited and therefore the main research question of this thesis is:

How does the dune foot of sandy coastal defences behave due to annual storm conditions and what is the influence on dune erosion?

This thesis performs an analysis of two field sites with hydrodynamic and morphological measurements, RealDune-REFLEX on the Holland coast and Land Reclamation Philippines in Manila Bay in the Philippines. For Land Reclamation Philippines, the hydrodynamics are transformed using two hydrodynamic instruments and validated using an ERA5 wind-driven SWAN model. The definition of the dune foot position is based on the maxima of curvature of the dune profile above a certain threshold following the second derivative method. The maximum total water level elevation is approximated with the measured water level elevation and an empirical parametrisation of the wave runup based on offshore wave conditions and the foreshore slope.

For RealDune-REFLEX, negligible erosion occurred for maximum total water level elevations far below the dune foot. For elevations just below and exceeding the dune foot, it shows that the post-storm dune foot correlates with the maximum total water level elevations. The dune foot could translate upwards by dune erosion and downward by bed level lowering and occasional avalanching. At Land Reclamation Philippines, it was found that pre-storm, more alongshore variability was observed in the vertical and horizontal position of the dune foot compared to post-storm. Minor coastal features eroded and resulted in larger dune foot retreats on those transects. Major coastal features remained present and influenced the post-storm dune foot position.

Concluding, an increase in the maximum total water level elevations above the initial dune foot height led to the highest erosion quantities of the dune front. However, no significant linear relation was found between the initial dune foot position relative to the maximum water level elevation and the resulting dune erosion. The post-storm dune foot elevation was found to correlate significantly to the maximum total water level elevation, approximated with an empirical runup formula, for upward and downward dune foot translation due to an out-of-equilibrium upper foreshore slope. Change of the horizontal dune foot position was found to relate to some extent to the storm duration and intensity of the total water level elevation exceeding the dune foot. Dune foot retreat magnitudes can be of the same order for small and large values of this quantification method and therefore exceedance of the dune foot does not provide a proper estimation of the dune erosion volume. It is found that the mismatched volume of the initial profile with the equilibrium condition, defined as an equilibrium slope reaching from the intersection of the initial profile with the maximum total water level elevation, is a more accurate estimation of the dune erosion volume. This methodology provides a practical way of predicting erosion volumes in sandy coastal defences using simple initial conditions, making it applicable to engineering practice.

For further research, it is recommended to improve the mismatch method based on the shape and size of the equilibrium profile. Second, study the dune foot dynamics within a storm using continuous LiDAR laser measurement and therewith validate dune erosion models. Third, civil contractors should enhance the quality of surveys in periods where dune erosion is expected to establish valuable datasets. Lastly, numerical modelling of complex typhoon-induced nearshore hydrodynamics could lead to more accurate insights into the alongshore behaviour of typhoon-induced dune erosion and the validity of the methods used.

Keywords: *dune foot behaviour; dune erosion; sandy coastal defence; land reclamation; annual storm conditions; alongshore variability; erosive swash regime*

Preface

In front of you lies my master's thesis 'Dune foot behaviour and erosion of sandy coastal defences in annual storm conditions'. This will conclude my Master of Science in Hydraulic Engineering at the TU Delft. Besides, this also marks the end of my pleasant student time in Delft. Thanks to all my friends who have made this time unforgettable.

First of all, I would like to express my gratitude towards my thesis committee. As my daily supervisor at Boskalis, Huub Rijper really went to the next level with his support allowing me to be the best version of myself. My week could not start without our meetings where I could figure out my thoughts and often made me realise where the research was headed. Many thanks to Paul van Wiechen as my main contact and supervisor at the Delft University of Technology. Every meeting we had was fruitful and you provided me with in-depth knowledge about the RealDune-REFLEX project and dune erosion in general. You were always having time for a chat, even before the thesis project was up and running.

Thanks to Stefan Aarninkhof as my chair. His positive attitude towards me and the project helped me to enjoy the thesis period and made the progress meetings something to look forward to. Thanks to Ad Reniers for being part of my committee and providing valuable expertise on the analysis of hydrodynamic measurements.

I am very grateful to be given the opportunity to do this research at Boskalis. The colleagues at Hydronamic made me have a really good time. I have received great help in acquiring the data and processing it. Thanks to Johan Henrotte for providing the Land Reclamation Philippines dataset. Without his insights into potential erosion at a bund due to a typhoon, this valuable dataset would not have been acquired. Thanks to Casper Mudde for helping me set up the typhoon model and being enthusiastic about exploring this field together.

Last but certainly not least, thanks to my family. My mother, father and mormor. I can imagine that something such as the 'dune foot' is something you would only hear when conversating with me. I am very pleased to still have you with me and have supported me through my studies. Renske, doing our thesis in the same period has given us opportunities to make the best out of it. Our trip to France was a game-changer for me. Finding the last pieces of the puzzle has been key.

R. R. van der Ven
Delft, May 2023

Contents

List of Tables

List of Figures

Nomenclature

Acronyms

AWAC	Acoustic Wave and Current Profiler (ADCP)	
DC	Dune Crest	
DF	Dune Foot	
LAT	Lowest Astronomical Tide	m
LRP	Land Reclamation Philippines	
MHW	Mean High Water	m
MIA	Manila International Airport	
MSL	Mean Sea Level	m
NAP	Normaal Amsterdams Peil; Dutch national datum (~MSL)	m
RD	RealDune-REFLEX	
RMSE	Root Mean Square Error	m
SLR	Sea Level Rise	m
SSL	Storm Surge Level	m
UTC	Universal Time Coordinated	
WVR	Waverider; type of directional wave measurement buoy	

Symbols

β	Slope	
β_f	Foreshore slope	
ΔV	Volume change	$\mathrm{m^3\,m^{-1}}$
η_{act}	Measured water level elevation ($\approx \eta_{ast} + \eta_{win}$)	m
η_{ast}	Tidal component of the water level elevation	m
η_{swa}	Swash component of the water level elevation	m
$\eta_{TWL,max}$	Maximum total water level elevation in storm period	m
η_{TWL}	Total water level elevation	m
η_{wav}	Wave component of the water level elevation	m
η_{win}	Wind set-up/set-down component of the water level elevation	m

μ	Dynamic viscosity	$\mathrm{Pa\,s}$
ν	Kinematic viscosity	$\mathrm{m^2\,s^{-1}}$
ρ_s	Sediment density	$\mathrm{kg\,m^{-3}}$
ρ_w	Water density	$\mathrm{kg\,m^{-3}}$
σ	Mismatch with equilibrium conditions	$\mathrm{m^3\,m^{-1}}$
θ	Wave angle	$\mathrm{^\circ}$
c	Wave celerity	$\mathrm{m\,s^{-1}}$
d_{50}	Median grain size	$\mu\mathrm{m}$
h	Water depth	m
h	Wave length	m
H_0	Deep water wave height	m
H_{m_0}	Spectral estimate of significant wave height	m
H_s	Significant wave height	m
k	Wave number	
L_0	Deep water wave length	m
n	Wave index	
R_2	Runup elevation exceeded by 2% of the waves	m
T	Wave period	s
$T_{m_{-1,0}}$	Spectral mean wave energy period	s
$T_{m_{02}}$	Spectral mean wave period	s
w_s	Fall velocity of sediment	$\mathrm{m\,s^{-1}}$

I

Hypothesis

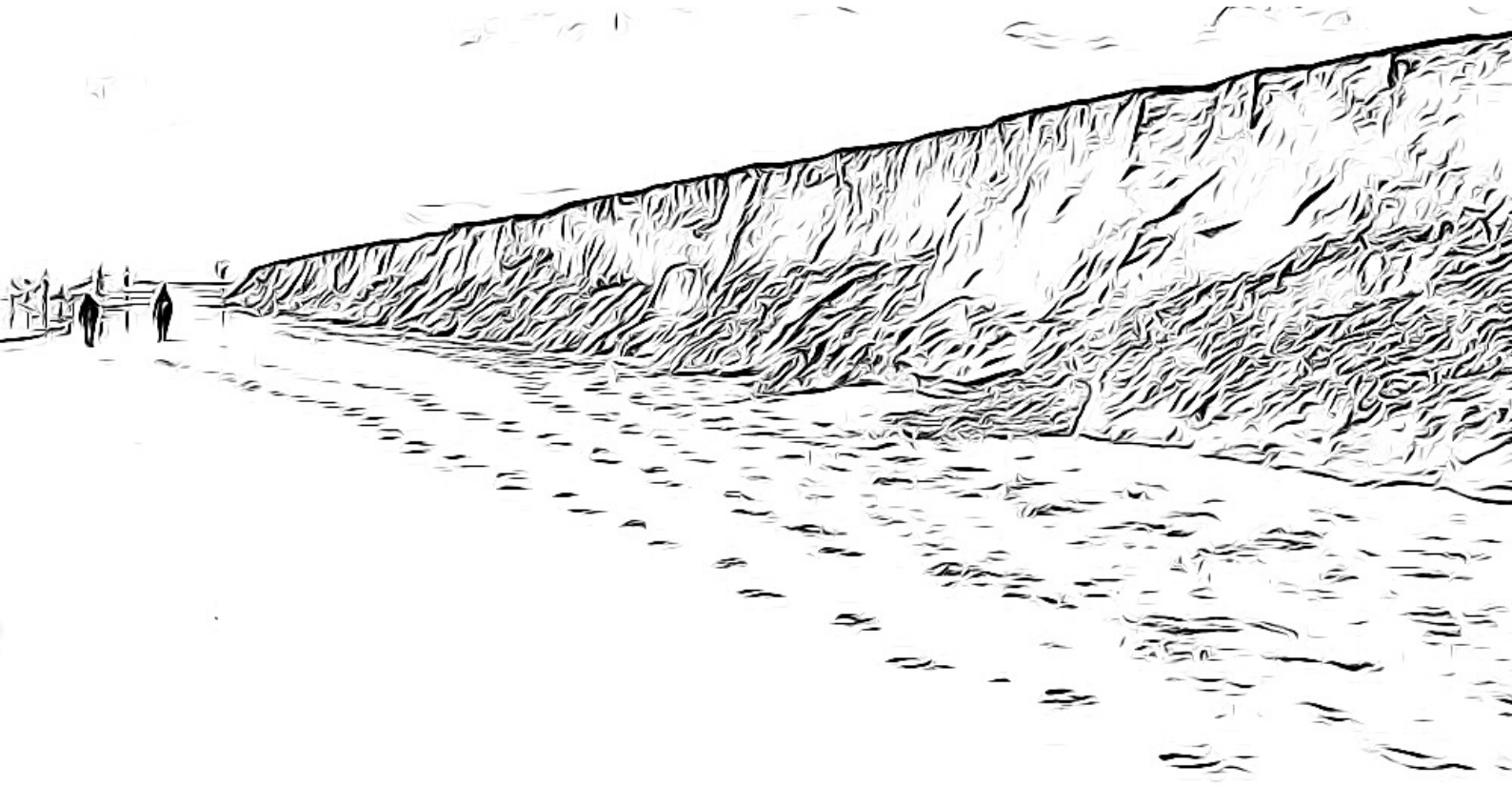

1

Introduction

1.1. Background and relevance

Storm surges leading to disastrous floods are deeply embedded in the history of the Netherlands. During storm surges, a strong wind pushes the seawater towards the coastline, leading to an increased water level with regard to the mean sea level (Dean & Galvin, 1976; Hughes & Chiu, 1981; Vellinga, 1983; Vellinga, 1986). This water level plus additional wave runup can potentially reach critical levels above the safety threshold of the coastline defences and could lead to dune erosion, inundation of land and breaches in dikes which could ultimately lead to failure and flooding of the hinterland. Presently, 26% of the Dutch land area is below NAP and is therewith directly susceptible to floods by the North Sea if there were no coastal defences such as dunes, dikes, dams and structures (Planbureau voor de Leefomgeving, 2007). In the Netherlands, approximately 70% of the 350 km coastline consists of dunes (Ruessink et al., 2012). Globally, almost 11% of the world's population lives in low-elevation coastal zones which are directly reliant on coastal protection (IPCC, 2022). With the expected rise of the mean sea level due to global warming (IPCC, 2021) and the expected intensifying extreme weather conditions such as (tropical) storm surges (IPCC, 2022), coastal resilience of our dune system is more important than ever.

Figure 1.1: Severe dune erosion and subsequent dune foot repositioning. (left) Banjaardstrand, NLD. Photo from Adriaansens (2022) (right) Elouera Beach, AUS. Photo from Trembath (2020).

Hard measures such as revetments or sea walls or sea dikes can be constructed on critical spots to prevent coastal erosion and a potential breach. However, these measures could provide certain downsides in the system. For example, groins trap sand while the potential sand demand at the adjacent coast remains and could lead to intensified coastline erosion (Basco & Pope, 2004). Soft measures against floods such as dunes and beaches are preferred above solid structures such as dams and

dikes as explained by Waterman (2010) in his work which describes an integrated coastal policy via Building with Nature. Similarly to the Netherlands, amongst other countries, the UK, Australia and the USA have sandy dune coasts which occasionally are affected by dune erosion (Figure 1.1) and make an understanding of the dunes' dynamic nature and the dune erosion processes of importance.

During storm-induced dune erosion, sand is redistributed from the dune face towards the beach and transported offshore to the outer surf zone due to the elevated water level and the wave impacts (van Thiel de Vries, 2009). Dune erosion during storm surge has been subject to multiple studies (Bruun, 1954; Delft Hydraulics Laboratory, 1978, 1984; van Thiel de Vries, 2009). Sallenger (2000) defines four storm regimes: swash, collision, overwash and inundation regime. The research in this thesis is focused on dune erosion in the collision regime, where the water attacks the dune front and does not exceed the dune crest level. The dune and beach system move around an equilibrium profile and slope under hydrodynamic and morphological processes. Generally, in winter, the beach could erode under heavy conditions and in summer sediment is deposited on the beach under moderate conditions (Wright & Short, 1984). Dunes behave somewhat differently compared to beaches. In the storm season (generally in autumn and winter), the dune could erode under heavy conditions when the sea level exceeds the dune foot level and the dune (re)grows under moderate conditions due to aeolian transport of the sand moving from the beach to the foredune (Arens, 1996; de Vries et al., 2012; de Vries et al., 2015). When storm conditions and corresponding elevated water levels are present, significant dune erosion can be observed which leads to the repositioning of the dune foot (Figure 1.2). An extensive theoretical background is provided in Chapter 2.

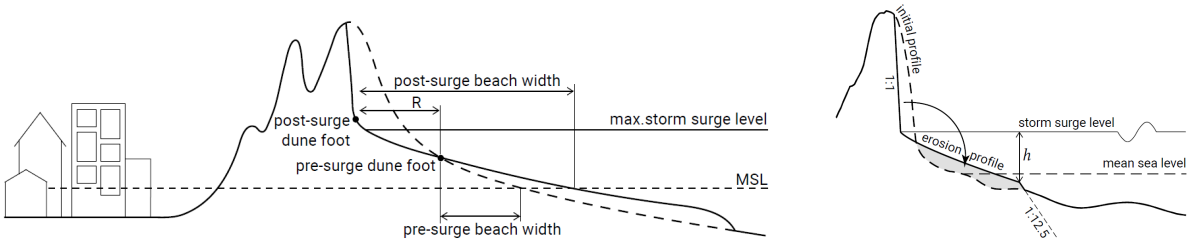

(a) Storm surge dune erosion

(b) Post-storm dune profile

Figure 1.2: Effects of storm surge on dune erosion and the change of the dune foot location (figures from Bosboom and Stive (2022)).

1.2. Problem definition and knowledge gap

Sandy coastal defences can be related to dunes, as both protect coastal areas and approximately the same conditions are governing. Such as the ability of sand to absorb wave energy, and the importance of maintaining the balance of sediment within the dune system. A sandy coastal defence could be constructed as an artificial dune to protect the hinterland from flooding or be constructed as a side slope of a land reclamation project. The dune foot is an important parameter to quantify the performance of a dune system and is often defined as the position of maximum curvature of the cross-shore profile (Smith et al., 2020). The initial slope and initial dune foot location could potentially have an impact on the performance of the sandy coastal defence, in terms of the deformation and eroded volume. In coastal engineering practices and land reclamations, loss of volume can lead to an increased risk of flooding or a setback in the project (as the project could require a certain contractually agreed slope or volume). Thus, there is a desire to minimise the loss of sand volume as it may lead to probable setbacks, elevated expenditures, and increased emissions. Combined morphological and hydrodynamic datasets gathered by (civil) contractors are used scarcely in research to verify dune theory or validate dune erosion models and could provide valuable insights.

Dune erosion models are developed to quantify the erosion volume and assess the dunes' safety. Generally, two types of models can be distinguished, (empirical) equilibrium models (e.g. DUROS+) and process-based models (e.g. XBeach). DUROS+ (van Gent et al., 2008) is a 1D equilibrium model based on the theory of Vellinga (1986) and calibrated with flume experiments based on the Dutch normative storm conditions. The use of these calibration values may reduce the reliability of dune erosion predictions for annual storm conditions that substantially diverge from normative conditions.

Annual storm conditions are defined as water levels and wave conditions which have a return period of approximately a year and are less energetic compared to extreme storm surges. XBeach (Roelvink et al., 2009) can estimate dune erosion in 1D and 2DH based on coupled hydrodynamic and morphological processes. This is a promising model for alongshore non-uniform coastal stretches and sandy coastal defences, however, the modelled erosion quantities could also deviate from reality for annual storm conditions as the challenge remains to validate the model for a wide variety of situations (van Santen et al., 2022).

The dune foot position can be a measure to assess dune erosion and dune growth. Storm conditions could influence the location of the dune foot by erosion of the dune front. However, the initial dune foot height could potentially have an influence on the degree of erosion caused by the storm. Logically, the dune foot does not affect the storm. However, the foreshore and beach in front of the dune define the wave energy that reaches the dune front. Vellinga (1986) states that the dune foot is the transition point from the 1:1 towards the parabolic shape and is, within a storm, vertically fixed at the maximal storm surge level (SSL). These findings come from small and large-scale model tests which were converted to storm surge conditions using the scale relations (Vellinga, 1986) and assume equilibrium conditions. Hence, the influence and position of the dune foot could differ in the field for the (shorter) duration of annual storm conditions.

While the dune foot has received relatively little research attention on its own, it is often mentioned in studies related to dune erosion. Such studies have observed that storm surges and the resulting elevated water levels above the dune foot can contribute to dune erosion (Sallenger, 2000) and cause the dune foot to relocate to a level close to the maximum water level elevation (Bonte & Levoy, 2015; de Winter et al., 2015; van Bemmelen et al., 2020). Alongshore pre-storm dune foot positions which were relatively lower, resulted in greater erosion quantities (Splinter et al., 2018). Horizontal dune foot retreat was found to be related to the frequency and intensity of the runup above the dune foot (Overton et al., 1988) and the amount of wave energy reaching the dune face (van Thiel de Vries, 2009).

To summarise, the current knowledge on the dune foot of sandy coastal defences is limited and could result in an over- or under-estimation of the erosion volume due to annual storm conditions. In the described former research, there is a knowledge gap in terms of the influence of the behaviour of the dune foot on dune erosion in sandy coastal defences. The initial dune foot height could potentially be an important parameter in describing the effect of individual storms on the dune. This has not come to a closing conclusion yet.

1.3. Research questions and objectives

In this thesis, the dune foot behaviour of sandy coastal defences due to annual storm conditions will be studied. The main research question of this thesis is defined as:

> How does the dune foot of sandy coastal defences behave due to annual storm conditions and what is the influence on dune erosion?

To be able to answer the main research question, three additional sub-questions are defined to split the study into comprehensible parts:

- What is the influence of the initial dune foot height on dune erosion?
- What is the influence of storm-specific hydrodynamics on the change in vertical dune foot position?
- What is the influence of the duration and intensity of the storm on the change in horizontal dune foot position?

Research on the influence of dune foot behaviour on dune erosion can lead to new insights into the behaviour of the dune during storm-induced dune erosion. If this relationship can be described, theories and models can be adjusted to properly incorporate the effect of the initial dune foot height during annual storm conditions. Models can forecast the amount of eroded volume per storm period. The main objective of this thesis research is to assess the influence and behaviour of the dune foot on dune erosion and sandy coastal defences during annual storm conditions.

1.4. Approach

Quantitative research will be conducted on two obtained large morphologic and hydrodynamic datasets: RealDune-REFLEX executed by researchers of the Delft University of Technology and Land Reclamation Philippines executed by Boskalis. These two datasets are on different field sites and differ in profile shape, sediment characteristics and hydrodynamic forcings but are both characterised by a severe out-of-equilibrium profile to the storm conditions. Both dunes are man-made and very close to the waterline. Data analysis on the morphological dataset is performed and cross-shore profiles are obtained. The study will be based on the pre- and post-storm dune profiles such that the influences of other factors than hydrodynamics are negligible on a short timescale. These cross-shore profiles are analysed based on certain parameters which are linked to the hydrodynamic forcings occurring. The methods used for data processing and analysis are stated in Chapter 4. The datasets are obtained and analysed by the author with the full consent of the owners of the datasets.

The study is limited to two datasets with a temporal variation of approximately 1 day and a varying spatial resolution. For the morphology, sampling points based on x- and y-coordinates with corresponding z-values are processed using linear interpolation to cross-shore profiles. In these interpolations, certain (alongshore) coastal features could potentially be filtered out. The hydrodynamics are sampled at a certain frequency and resampled linearly to the 30- or 10-minute interval.

1.5. Thesis outline

To be able to answer the stated research questions of this study and reach the objective, this thesis is subdivided into three main parts with nine underlying chapters.

Part 1 Hypothesis
Chapter 1: Introduction
Chapter 2: Theoretical Framework

Part 2 Analysis
Chapter 3: Situation Analysis
Chapter 4: Methodology & Data processing
Chapter 5: Case study RealDune-REFLEX
Chapter 6: Case study Land Reclamation Philippines

Part 3 Synthesis
Chapter 7: Characterisation of dune foot behaviour
Chapter 8: Discussion
Chapter 9: Conclusions & Recommendations

Chapter 1 introduces the dune foot and highlights the importance of this research. In Chapter 2, the theoretical framework provides background knowledge on dunes, dune erosion, and hydrodynamic and morphological processes. The second part focuses on the analysis. Chapter 3 introduces the field sites of RealDune-REFLEX and Land Reclamation Philippines where the two different hydrodynamic and morphological datasets are obtained. Chapter 4 states the methods used and the manner the data is processed. Chapters 5 and 6 provide the results of the case studies. Part three provides the synthesis of this study. In Chapter 7, the dune foot behaviour is characterised based on the findings of the case studies. A discussion on the outcome and methods used is provided in Chapter 8. In Chapter 9 the conclusion and recommendations provide insights resulting from this thesis and describe further research possibilities.

2

Theoretical Framework

This chapter provides a theoretical framework and serves as support for this study on the dune foot behaviour and erosion of sandy coastal defences in annual storm conditions. To gather insight into the important processes affecting dune foot behaviour, first, dunes in the coastal region are explained. Second, dune erosion processes and estimation methods are introduced. Third, the dune foot is defined and linked to dune erosion. Fourth, the hydrodynamic processes affecting dune erosion and subsequent dune foot change are described. The fifth aspect describes interventions within the cross-shore sediment balance. Concluding the literature study with the overall findings.

2.1. Dunes in the coastal region

2.1.1. Introduction

Coastal regions around the world have different characteristics and are constantly subject to changes due to natural forces. Natural dune systems or sandy protections of land reclamations are remodelled in time around an equilibrium. A dune is a terrestrial landform characterised by a mound or ridge composed of sand that is shaped by the interacting forces of wind, water, and gravity. Dunes, which may also be referred to as coastal dunes or sand dunes, form in locations where an adequate supply of sand material is available. Dunes are generally situated adjacent to active beach zones, within the supratidal region extending landward. The size and shape of dunes are determined by the different hydrodynamic and aeolian forces and site-specific characteristics. Dune systems exhibit variations in cross-shore characteristics such as grain size, vegetation, beach width, slope, slope shape, crest height, dune foot location, and dune width. Aside from coastal protection, dunes have multifarious uses ranging from recreation and biodiversity to supplying drinking water through filtration.

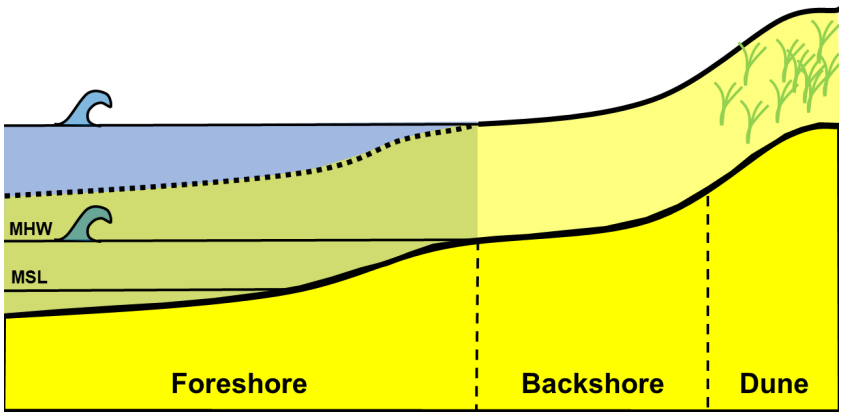

Figure 2.1: Overview of a sandy coastal dune region. MHW and MSL depict the respective water level elevation lines.

2.1.2. Sandy coastal defences

Dunes have a history of protecting low-lying countries from flooding. Within the context of land reclamation projects, the construction of sandy bunds serves the purpose of regulating the flow of fill material and managing the discharge of water from the reclamation area. Additionally, these bunds play a crucial role in ensuring safety by providing a protective barrier for individuals and machinery operating both within and on the confines of the sandy embankment. The same goes for the construction of large-scale projects such as the Hondsbossche Dunes (former Hondsbossche and Pettemer sea defence) and Maasvlakte 2, where large-scale sandy (dune) systems are constructed to protect the hinterland. Therefore dunes can be explained as sandy coastal defences. A sandy coastal defence is defined as a big heap of sand with the sea on one side and the (elevated) dry land on the other side.

Dunes and sandy coastal defences can have different characteristics in terms of vegetation, compaction, grain size and foreshore. Sandy coastal defences differ from dunes as they are relatively newly constructed and are close to the waterline making them more exposed to wave conditions. Often no beach is developed on the foreshore, therefore waves are less prone to depth-induced transformations before they reach the dune face. However, down to the grain and shape of the profile, they do show many resemblances. Therefore, the erosion processes of the sand are expected to be similar.

2.1.3. Profile characteristics

A cross-shore profile is a cross-section (or transect) of the dune, beach, and foreshore and could be extended towards a certain depth in the offshore direction depending on the interest of the research or the availability of measurements. The cross-shore profile can be taken on a location of interest and is perpendicular to the beach contour. For multiple moments in time, the development in the dune and beach profile can be observed based on these cross-shore profiles.

Over time and space, the morphology of the dune profile undergoes changes. The foreshore slope changes in shape and angle, and can be described by the beach state ranging from dissipative to reflective beaches (Short & Hesp, 1982; Wright & Short, 1984). Under storm conditions, morphological profile features are wiped and this phenomenon is called a morphological (beach) reset. Pruszak et al. (2011) states that the beach width is dependent on the dune foot and shoreline position. For narrow beaches, the dune foot location and shoreline position are interdependent. However, for wide beaches, these parameters are independent. Herein, the timescale is crucial to assess the change in dune foot and shoreline position. On short timescales, intensive storms could lead to dune foot retreat and subsequent shoreline advance due to the settlement of the dune sediment. Longer intensified storm conditions could lead to both dune foot and shoreline retreat.

2.2. Dune erosion

2.2.1. Introduction

Generally, the main constituent of dune growth is aeolian transport and the main constituent of dune erosion is erosion induced by hydrodynamics. Dune erosion is defined here as the erosion of the dune and in particular the dune face, under storm conditions due to the combined impact of water level and waves. In the collision regime (Section 2.2.2), the sand gets redistributed to the foreshore as the sand eroded from the dune face by hydrodynamic forcings deposits on the beach between the dune foot and the low-water waterline (Edelman, 1972; Vellinga, 1986). Dune erosion models are developed to calculate the dune volume change and profile development (Section 2.2.6).

2.2.2. Storm regimes

The combination of storm surge and wave runup in different magnitudes can give rise to a regime where the dune is attacked by the sea. Four storm regimes are defined by Sallenger (2000) which are separated by a threshold in terms of the dune parameters D_{HIGH} the vertical height of the dune crest, and D_{LOW} the vertical height of the dune base or dune foot. Relative to R_{HIGH} the highest vertical elevation of the water due to astronomical tide, storm surge and wave runup, and R_{LOW} the vertical height of the lowest vertical water elevation where the lower profile remains submerged. Each regime has its own specific dominant processes and net sand-transport direction (Sallenger, 2000). This study is limited to the swash and collision regime (Figure 2.2). The four storm regimes, their thresholds and the result of the regime on the dune are defined as in Table 2.1. Often, dune erosion research is focused

on the collision regime, where the dune front is attacked and the sediment balance is conserved. This regime is critical and long-term exposure can lead to overwash and eventually to inundation. However, during moderate conditions in the swash regime, the sand can move back onshore under the influence of wave forcing. When the sand is deposited on the beach, wind-induced aeolian transport is able to move the sand to the dune and (re)grow the dune (de Vries et al., 2012).

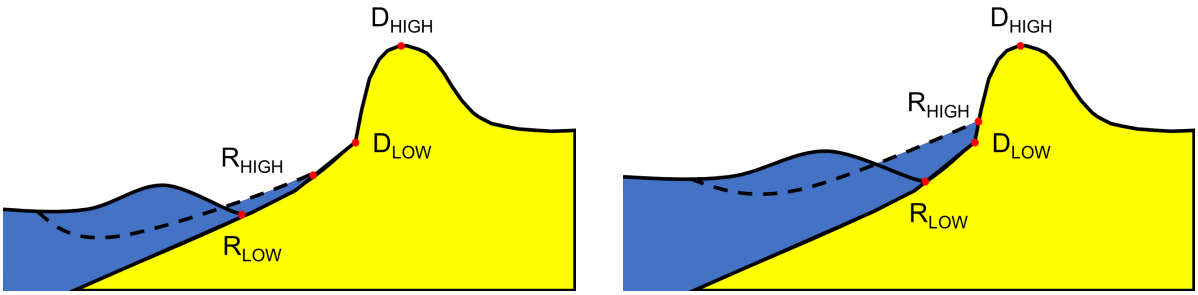

Figure 2.2: Two examples of the storm regimes and terminology defined by Sallenger (2000). (left) Swash regime. (right) Collision regime.

Table 2.1: The storm regimes described by Sallenger (2000) with their domain and description based on the range of the runup relative to the dune crest and dune foot

Regime	Domain	Description
Swash	$R_{HIGH} < D_{LOW}$ $R_{LOW} > D_{LOW}$	Runup only on the foreshore, foreshore erodes and sand transported offshore, after storm transported onshore so small net change
Collision	$D_{LOW} < R_{HIGH} < D_{HIGH}$ $R_{LOW} < D_{LOW}$	Runup on the base of the dune, dune erodes and sand transported offshore, more net erosion relative to swash
Overwash	$R_{HIGH} > D_{HIGH}$ $R_{LOW} < D_{HIGH}$	Runup exceeds dune crest, sand eroded and transported landward
Inundation	$R_{HIGH} > D_{HIGH}$ $R_{LOW} > D_{HIGH}$	Fully submerged dune in swash motion, limited evidence for massive net onshore transport

2.2.3. Sediment transport

Two stages can be distinguished in dune erosion as found by van Gent et al. (2008). The circle of uprush and backwash over the beach and dune face (drag-induced erosion) and subsequent sediment slides (avalanching) is a continuous process during the peak of the storm. Increased turbulence stirs up a larger amount of sediment and brings the sediment into suspension (Reniers, 2004; Vellinga, 1986). The sediment in suspension is transported offshore by undertow towards the lower profile (Stive, 1986). In storm-induced dune erosion, the suspended load is dominant (Ruessink et al., 1998; Vellinga, 1986). Hence, bed load is expected to be a small contributor (van Thiel de Vries, 2009). The position of the maximum sediment transport is located at the pivot point of erosion and sedimentation (zero-crossing of the volume change). This point moves in a landward direction with the retreat of the dune face (van Thiel de Vries et al., 2008).

Drag-induced erosion

The process of uprush and backwash over the dune face is called drag-induced erosion. This process picks up sediment higher up in the profile, brings most sediment in suspension and transports it to the lower profile. This is the initial stage of dune erosion which continues until the dune face is vertical or even overhanging. At this stage avalanching becomes governing, as slumps of sediment slide down the dune face with a certain frequency.

Avalanching
Avalanching is a type of failure of the dune soil where a slump slides the dune and was subject to a large extent of studies (e.g. Erikson et al. (2007), Overton et al. (1994), Palmsten and Holman (2012), and van Thiel De Vries et al. (2007)). This slump slide can occur due to two types of failure as observed in the experiments of Erikson et al. (2007): shear-type and beam-type. Shear-type is referring to failure due to the shear strength of the sediment being unable to carry the weight of the overhanging sediment. Beam type refers to failure induced by a tensile crack in the landward part of the dune face, resulting in a slump sliding down the dune face. The beam-type failure occurred in the majority of the experiments.

2.2.4. Sediment grain size and dune density
The sediment grain size and density have been found to have an impact on dune erosion. Overton et al. (1994) observed that for a decrease in sand grain size, the dune strength increased and therefore the dune erosion volume decreased. For an increased dune density the dune strength increased and the dune erosion also decreased. However, the impact of dune density showed less significance in dune erosion compared to the sediment grain size (Overton et al., 1994). The influence of sediment grain size on dune erosion remains hard to capture due to the combination of dynamic processes (transport, sorting), variable sediment properties (size, shape, distribution and composition), and challenging monitoring conditions.

2.2.5. Equilibrium theory
During storm conditions, the cross-shore profile is susceptible to a transformation over time and therewith a reset of specific morphological features. This process can be observed also in the alongshore direction. The pre-storm profile moves towards an (equilibrium) post-storm profile and can be described by equilibrium (dune erosion) theory. Edelman (1972) built upon the findings of the long-term equilibrium profiles by Bruun (1954) and found that in many cases after the storm, the upper profile was approximately identical. van de Graaff (1977) stated that the cross-shore extend of the profile transformation was far less than the reach of the long-term equilibrium profile found by Bruun (1954). Vellinga (1986) built upon the findings of van de Graaff (1977) and Vellinga (1978). He observed certain similarities in his experiments and defined an equilibrium post-storm cross-shore dune profile as a function of total water level (storm surge level), wave conditions and grain size characteristics. The profile is hypothesised to be in short-term equilibrium to the storm conditions, meaning that after the storm the profile will tend towards another equilibrium.

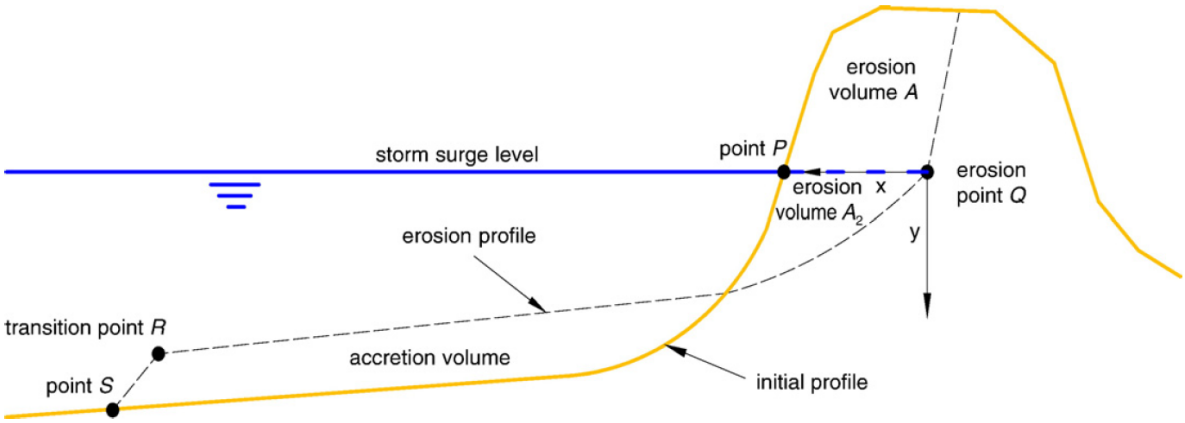

Figure 2.3: Equilbrium profile as defined by van Gent et al. (2008) (figure from van Gent et al. (2008))

The dune erosion prediction model uses an equilibrium profile sub-divided into three main sections. The first section reaches from the upper dune face with a 1:1 slope towards the post-storm dune foot position (transition point S), which is vertically fixed at the maximum storm surge level (SSL). The profile is derived for the normative conditions of $H_0 = 7.6\ m$, $T_p = 12\ s$ and $D_{50} = 225\ \mu m$. From the dune foot towards the transition point R, the dune profile follows a parabolic shape. After transition point R,

the slope of the bed is 1:12.5 until the point where sediment is conserved in the system and eroded volume equals settled volume for a fully cross-shore sediment distribution (Figure 2.3). van Gent et al. (2008) improved the method of Vellinga (1986) by including the influence of the wave period in a similar way as the wave height and sediment fall velocity have been incorporated. They found, especially in double-peaked wave spectra, that the wave period $T_{m-1.0}$ gave a better representation than the wave peak period T_p for dune erosion.

However, these erosion profiles are derived by scale relations of the prototype conditions. Bruun (1954), Dean (1977), and Hughes and Chiu (1978) had already found that the equilibrium profile can be described by the single power curve $y = p * x^{2/3}$. Vellinga (1986) states that for a complete wave climate and a wide range of wave spectra, this 2/3 power will not be valid in all cases. Therefore, also a more generalistic empirical power curve can be found as defined in Equation (2.1), where p and γ are empirically found parameters varying per site and per present conditions.

$$y = p * x^{\gamma} \tag{2.1}$$

The dune erosion prediction model, however, does come with some pitfalls which need to be accounted for in a proper calculation. Firstly, Vellinga (1986) states that the formula to predict the post-storm dune profile is based solely on the cross-shore profile. For situations with alongshore non-uniform characteristics, the effect of alongshore transport gradients needs to be investigated as this is not incorporated.

Secondly, in the dune erosion prediction model, the dune foot was fixed at the peak water level during the storm surge. In flume and field experiments, it was observed by researchers (e.g. van Thiel de Vries (2009) and van Wiechen, Rutten, et al. (2022)) that the dune foot moves in time during the storm-surge. The influence of the dune foot position, i.e. the abrupt change in slope, could potentially have an effect on the hydrodynamic conditions affecting dune erosion.

Finally, the parabolic shape of the erosion profile is described by a function of the significant offshore wave height and the settling velocity and Vellinga (1986) states that this shape of the post-storm dune profile is independent of the initial profile, however, is highly dependent on the grain size. However, in the short-term, the duration of the storm could potentially be of huge influence as it could be hypothesised that equilibrium conditions were not reached during a short-lasting storm and therefore initial conditions do have an impact on the post-storm profile. van Gent et al. (2008) and van Thiel de Vries (2009) showed that if the dune erosion process continues for a sufficiently long duration, the post-storm profile is to some extent independent of the initial profile which was stated in the theory of Vellinga (1986). van Thiel de Vries (2009) describes that varying hydrodynamic conditions showed a substantially larger erosion rate at the beginning of the tests compared to the end. This is due to the fact that a higher water depth leads to the ability of higher waves to attack the dune face. Wave impacts are reduced through a morphodynamic negative feedback mechanism. Therefore one could conclude that for certain timescales the initial profile has an influence on the eroded volume.

2.2.6. Numerical dune erosion models

In the past, due to a lack of measurements and field data, predictive methods for dune erosion were called speculative (Vellinga, 1986). Vellinga (1986) recommended developing a coastal morphology model that is capable of calculating the, among others, short-term dune profile changes for storm surge. This potential (numerical) model should be based on experiments and on made assumptions on the (morphological) processes. In this way, the relative magnitude of importance between the different parameters in the processes can be determined. Hence, to assess the safety of the hinterland from flooding, dune erosion models are created to predict the volume of dune erosion under certain hydrodynamic and morphodynamic conditions. These models could also be used for the transformation of sandy coastal defences. Two types of dune erosion models can be distinguished: (empirical) equilibrium models and process-based models.

Equilibrium models (e.g. DUROS+) make an estimation of the cross-shore dune profile development after a storm based on the conditions for a certain duration. The profile is assumed to reach a short-term equilibrium to the storm conditions when modelled and exposed for a long enough duration to these conditions. Hereafter, when normal conditions prevail, the profile returns to the long-term equilibrium.

The approach of an equilibrium model is based on a morphodynamic negative feedback mechanism between hydrodynamics and morphology. Due to elevated water levels and wave impact (hydrodynamics), the dune erodes and the sediment is transported to the foreshore (morphology). The increased bed level and reduced slope lead to the reduction of wave impacts on the dune (morphodynamics), hence the decrease in erosion. This proceeds until a steady state is reached where the dune and foreshore do not change significantly. Equilibrium models are calibrated with data gathered from flume and field experiments based on dune erosion due to storm impact.

Process-based models (e.g. XBeach) calculate the hydrodynamic and morphodynamic processes in space and time to compute the changes in the bed profile in time. The physical processes are solved numerically in the model where a grid with separate cells allows for specific characteristics per cell. This increases the complexity and required input of the model, but gives rise to the opportunity to more properly include coastal complexities compared to equilibrium models.

2.3. Dune foot

2.3.1. Introduction

An indicator to define a certain characteristic of a coastal dune system is the position of the dune foot (or dune toe). Roughly, the dune foot can be observed to be the transitional point from the beach to the dune where often vegetation begins to grow (Figure 2.1). With the definition of the dune foot, a certain baseline can be set to relate to coastline changes and dune transformations and therewith changes in dune volume. At initial construction, land reclamations can have uncurved slopes where the dune foot is rather indistinguishable. A dune foot starts to form due to the reshaping of the dune profile induced by the water level variations. These particular dune transects might be unsuitable for pre-storm dune foot analysis, however, are suitable for post-storm dune foot analysis.

2.3.2. Definition

Various dune foot definitions are present in literature. Guillén et al. (1999) stated that for the Holland coast, the dune foot was defined to be the intersection of the maximum slope of the profile between NAP +1m and NAP +5m with the NAP +1m line. In the Netherlands, the most frequently used definition of the position of the dune foot was assumed at the vertical height of NAP +3m (de Jong et al., 2014). This assumption is debated to be appropriate for a wide variety of sites as it is mostly empirical (Diamantidou et al., 2020). For the Sand Engine, the dune foot was defined at NAP +5m by Hoonhout and de Vries (2017). It is stated by Masselink et al. (2022) that the identification of the dune foot is far from trivial, therefore assumes the dune foot location for the north coast of southwest England to be the intersect of the profile with the 5-meter elevation line.

In the survey conducted by Smith et al. (2020), a group of geomorphology experts were consulted on the location of the boundary between the beach and the dune, which was defined as the dune foot. The results of the survey demonstrated that six primary classes could be established based on the determination of the dune foot location. These categories were classified according to the following characteristics: delimiter, process, surface elements, sedimentological factors, landform, and morphometric features. The majority of the experts pointed to the dune foot as a divergence in processes and/or a change in morphometry. For example, the point of maximum curvature between the coastline and dune crest when looking at the cross-shore profile or a significant or clear break in slope (Smith et al., 2020). However, the definition of the dune foot is not consistent among experts and one can still disagree about the exact dune foot location.

Diamantidou et al. (2020) proposed a general definition to define the dune foot position based on the beach and dune profile geometry and the mean high-water level and is called the second derivative method (Figure 2.4). This method has been compared to the 'NAP +3m'-method by calculating the root mean square errors (RMSE) with respect to a visual observation (complemented with satellite imagery) to define the dune foot. The second derivative method performs overall better based on a lower RMSE. A seaward and a landward boundary are set on the cross-shore profile and within this domain, dune foot detection is performed. The seaward boundary is the intersection with the mean high water level and the profile. The landward boundary is the position of the most seaward dune crest higher than 2.4 m (threshold set at NAP +6m). Within this domain, the first and second derivative of the

cross-shore profile is calculated. The cross-shore positions with first derivatives lower than 0.001 are dropped. The dune foot position is considered to be the most seaward position of the position where the second derivative is larger than the predefined threshold. Visually, this corresponds to a transition from one slope to another. In the method of Diamantidou et al. (2020), this threshold is found at 0.01. In literature, threshold values of the same magnitude are found (e.g. 0.025 (Splinter et al., 2018)). Hence, this threshold can be varies based on the dataset.

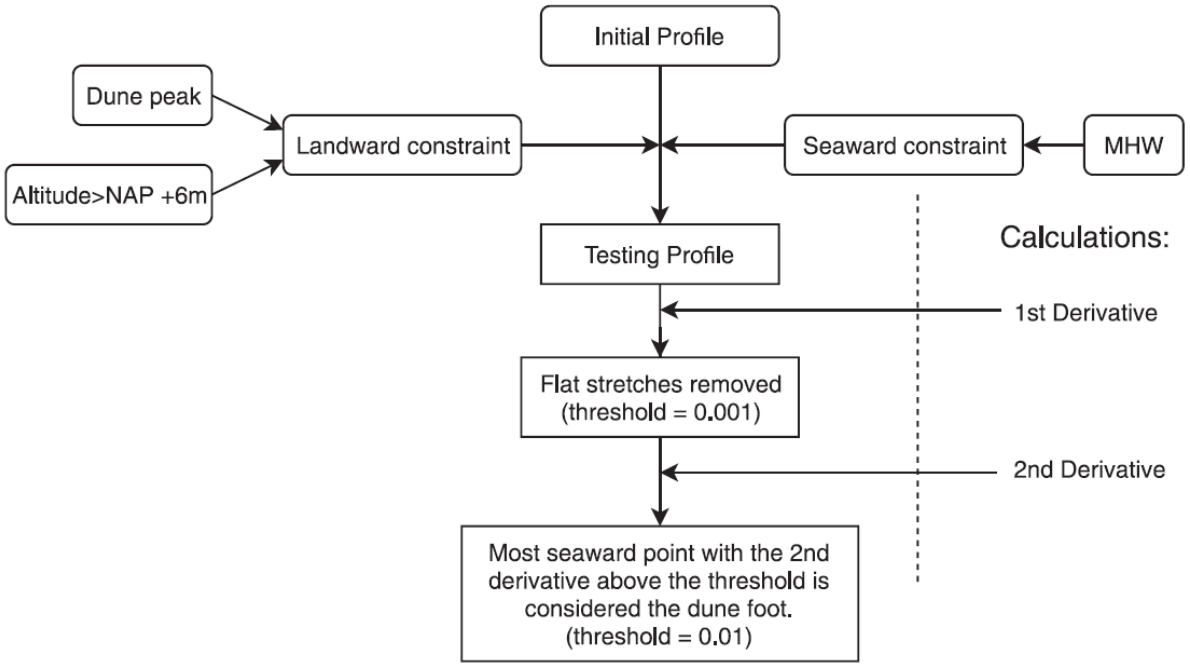

Figure 2.4: The second derivative method as proposed by Diamantidou et al. (2020) to approximate the dune foot location, schematised (figure from Diamantidou et al. (2020)).

2.3.3. Dune foot dynamics

The dune foot is not fixed to a certain cross-shore position but has a temporal variation in the vertical and horizontal direction. From field observations and experiments comes forward that mainly water levels above the dune foot are linked to dune erosion (Sallenger, 2000). Dune scarps can be formed when heavy storm conditions are present and the dune foot is at the bottom of the scarp. Below the dune foot, a smooth beach profile is observed and above the dune foot, a steep dune slope of approximately 45 degrees is found (de Winter et al., 2015; Möller & Swart, 1988; Nishi et al., 1994; Splinter & Palmsten, 2012; Vellinga, 1978). The slope is even steeper directly after erosion with approximately 61 degrees (van Wiechen, de Vries, et al., 2022). The dune foot repositions by the interaction of hydrodynamics and the morphology of the surroundings and therefore is a temporal dynamic parameter (Figure 2.5).

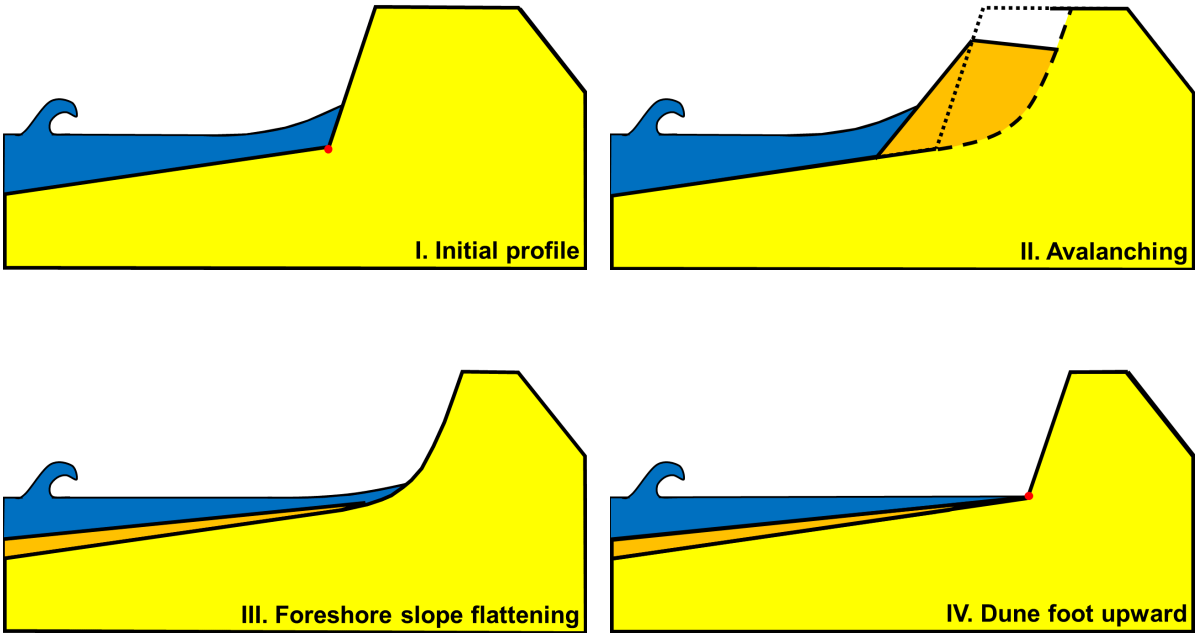

Figure 2.5: Life cycle of dune scarp evolution and subsequent dune foot repositioning.

Vertical change of dune foot position

Various flume experiments (e.g. van Thiel de Vries (2009) and Vellinga (1986)) showed that the vertical dune foot position moves throughout the storm to approximately the maximal water level elevation in the forced storm period. Giardino et al. (2012) found that a shift in dune foot position is correlated to the yearly maximal storm surge levels for the northern Holland coast. de Vries et al. (2012) presents the annual maximum water levels as one of the main drivers of dune erosion due to hydrodynamics. They found, based on the 1980 - 2000 JARKUS data, that there is a significant negative correlation between the annual maxima of the water level elevation and dune volume changes. van IJzendoorn et al. (2021) looks to SLR compared to the change in vertical dune foot position and has found that the vertical dune foot change outpaces SLR for the Holland coast.

Following, that the post-storm dune foot is found at the maximum water level and the wave runup level of a naturally occurring storm (Bonte & Levoy, 2015; de Winter et al., 2015; van Bemmelen et al., 2020). Splinter et al. (2018) takes the dune foot position as the most seaward local maxima of curvature above the threshold of 0.025 and compares total water levels with evolving dune foot elevations. She concluded that alongshore varying transects with a lower pre-storm dune foot position and total water levels exceeding this elevation resulted in greater dune erosion. While total water levels below the dune foot (swash regime) resulted in very little to no erosion. Splinter et al. (2018) states that the pre-storm elevation of the dune foot is a key driver in the alongshore variability in dune erosion and higher dune foot elevations result in lower erosion amounts. However, contradictory to these findings, Suanez et al. (2012) observed periods of water level exceeding the dune foot elevation while no erosion was present. These high water levels were stated to be not sufficiently energetic for dune erosion and repositioning of the dune foot.

Horizontal change of dune foot position

Overton et al. (1988) states that the total dune retreat, or the erosion volume, is dependent on the frequency and intensity of the runup above the dune foot. Giardino et al. (2012) found that migration of the dune foot is often related to changes in beach width and storminess. van Thiel de Vries (2009) studied the influence of the wave period on dune erosion. He has found that a larger wave period results in an increased dune face retreat and consequently an increased dune erosion volume. With an increase of 50% of the wave period, the dune erosion volume has increased by 25% after 1 hour,

24% after 2 hours and 15% after 6 hours. The slope around the still water level becomes more gentle. Approximately 10 to 15% more wave energy reaches the dune face. The time and depth-averaged flow velocity remains of the same magnitude while the dune orbital flow velocity shows an increase of around 15%. Also the sediment concentration near the bed and the time and depth-averaged concentration increase with respectively O(100%) and O(60%). The increase in dune erosion could be explained by the higher offshore directed mean sediment transport. van Gent et al. (2008) and van Thiel de Vries (2009) showed that an increased wave period led to increased dune face retreat and therewith a landward move of the horizontal dune foot position. However, the wave period showed no significant influence on the vertical dune foot location.

Alongshore variability
Ruessink and Jeuken (2002) has found for the Holland coast for 160 km coastline and 100 to 150 years of measurements that the dune foot behaviour is largely dominated (80%) by alongshore non-uniform character, which is linked to sand wave patterns. The remainder of variability is alongshore uniform and is linked to yearly fluctuations and the alongshore uniform residual dune foot vertical position can be related to the occurred maximal water level between two measurements.

Stockdon et al. (2007) derived a simple storm-impact scaling model based on the maximal water level and the dune foot elevation. She shows that the storm regime formulation of Sallenger (2000) is a reasonable estimate for hurricane-induced dune erosion. Observed in the research was that in the collision regime (and overwash regime), slopes flatten and in the swash regime slopes steepen. Also, in areas where the slope was steeper, higher runup elevations and more shoreline change were observed. Bonte and Levoy (2015) takes the foreshore beach slope as the slope between the mean water level and the initial foot position as introduced by Stockdon et al. (2007). Bonte and Levoy (2015) observe that the dune foot retreats along a certain slope with a difference in slope between the east and west sides of the profile measurements. The runup was affected when there was a huge alongshore variation. The difference in foreshore slope affects the swash direction and speed and therefore the impact on the dune.

2.3.4. Dune foot in dune erosion models

In certain dune erosion models, the dune foot is parameterised and serves as an initial value, a continuously updated parameter, or an end state. Here, the focus is on the models DUROS+ ((van Gent et al., 2008)), LEH04 (Larson et al., 2004), PH12 (Palmsten & Holman, 2012), and XBeach (Roelvink et al., 2009).

DUROS+ is based on the equilibrium dune theory and assumes that the post-storm dune foot is located at the storm surge level which is approximately the spatial mean of the water level elevation plus additional runup (van Gent et al., 2008). The model of Larson et al. (2004) uses the dune foot height z_b in his analytical wave-impact model and relates it with the runup R height to the eroded volume ΔV and with the number of waves colliding with the dune face t/T. In simplified form:

$$\Delta V = 4C_s \left(R - z_b\right)^2 \frac{t}{T} \tag{2.2}$$

The model of Palmsten and Holman (2012) uses the wave impact model of Larson et al. (2004) and improves this model with a Gaussian distribution for the runup and elevation of the dune foot based on the number of waves N_c. XBeach (Roelvink et al., 2009) uses a definition for a maximum dry slope and wet slope to incorporate the process of avalanching. The dune foot position is influenced herein as avalanching occurs due to the maximum wet slope being exceeded above this point and that will slightly change the position of the dune foot.

Splinter and Palmsten (2012) stated in parameters that a dune is in collision regime if the following equation holds for the total water level elevation $R_2 + \bar{\eta} + tide > z_b(0)$ with $z_b(0)$ as the initial dune foot elevation. She found that the initial dune foot position, defined as the position with the maximum slope change, has an influence on the effectiveness of the models of Larson et al. (2004) and Palmsten and Holman (2012) in the estimation of the erosion and dune foot retreat calculation. She states that especially in field data, the dune foot is hard to distinguish due to no obvious change in slope. XBeach was found to be more sensitive to site-specific calibration. The formulation of Palmsten and Holman

(2012) was found to perform reasonably with the default values and the use of the 2% exceedance value of the runup R_2 and a probability distribution for the predicted collisions.

These models use the position of the dune foot as an important parameter in the calculation of the dune volume change. Consequently, it appears that the precise positioning of the dune foot before the storm, after the storm, and during the storm plays a crucial role in ensuring adequate model performance.

2.4. Hydrodynamic processes

2.4.1. Introduction

The coastal region is the boundary of land where it meets the sea and its hydrodynamics. These hydrodynamics can be described using linear wave theory and are elaborated on nearshore wave transformation. Nearshore, incoming waves shoal and refract as depth decreases. The wave spectrum (energy/variance density spectrum) moves from short to long waves. The short waves break close to the shore, while the long waves do not break and increase in amplitude, therewith becoming relatively more important for dune erosion with a developing foreshore (van Thiel de Vries et al., 2008).

2.4.2. Linear wave theory

Linear wave theory describes how gravity waves propagate through oceanic and coastal waters based on their harmonics. The theory assumes that water is inviscid, incompressible and irrotational. The linear wave theory approximation is only valid for waves where the amplitude is small compared to wavelength $a \ll L$ and depth $a \ll d$ (small-amplitude approximation). The theory is based on the mass and momentum balance equations and solved with boundary conditions at the bottom and the surface of the fluid. The free surface elevation η of the harmonic wave can be derived.

$$\eta(x,t) = a \sin(\omega t - kx) \tag{2.3}$$

The kinematics can be applied to the propagation of a harmonic wave and expressed with the dispersion relationship (Equation (2.4)). This relates the radian frequency ω to the wave number k. Waves of different wavelengths travel at different phase speeds and therefore waves disperse.

$$\omega^2 = \left(\frac{2\pi}{T}\right)^2 = gk \tanh kh \tag{2.4}$$

Or rewritten for the wavelength, with the formulation for the wave number $k = 2\pi/L$:

$$L = \frac{gT^2}{2\pi} \tanh\left(\frac{2\pi h}{L}\right) \tag{2.5}$$

The dispersion relationship is implicit and can be solved iteratively. From this relation, the wave propagation speed c and index n can be derived.

$$c = \sqrt{\left(\frac{g}{k} * \tanh kd\right)} \tag{2.6}$$

$$n = \frac{1}{2}\left(1 + \frac{2kd}{\sinh 2kd}\right) \tag{2.7}$$

For deep water wave characteristics (depicted with subscript 0), it results in $\tanh kh \to 1$ and $kh \to \infty$. When waves move towards the nearshore, waves transform and can be described with linear wave theory up until wave breaking. Here, non-linearities take over. For very shallow water $\tanh kh \to kh$ and $kh \to 0$. The three main processes affecting nearshore waves are shoaling, refraction and diffraction. The influence on the wave height of shoaling can be estimated through Equation (2.8) and refraction can be estimated through Snell's Law in Equation (2.9). Diffraction is not part of the scope of this thesis.

$$K_{sh} = \sqrt{\frac{c_1}{c_2}\frac{n_1}{n_2}} \tag{2.8}$$

$$K_{ref} = \sqrt{\frac{\cos\theta_1}{\cos\theta_2}} \tag{2.9}$$

2.4.3. Water level

The water level η, or the still water level, is the average over a short time interval of the continuous water level elevation signal. The water level is the elevation for which hydrostatic pressure can be assumed. Around this signal, an elevation arises which can be linked to waves. The water level η is not a force on itself, but a result of different hydrodynamic processes acting. The total water level on the beach or against the dune can be decomposed in astronomical, wind, wave setup and swash-related components (van Wiechen, Rutten, et al., 2022), as described by Equation (2.10).

$$\eta_{TWL} = \eta_{ast} + \eta_{win} + \eta_{wav} + \eta_{swa} \tag{2.10}$$

The astronomical component is based on the tide and has a diurnal or semi-diurnal character based on the location. The wind component is dependent on the fetch length and wind speed and direction. The wave component is related to wave setup, which is the superelevation of the mean water level. This is a result of wave breaking and subsequent cross-shore gradient in radiation stresses (Longuet-Higgins & Stewart, 1964). The swash component is related to the upward and downward motion of the wave around this mean water level.

2.4.4. Setup, swash and runup

The wave setup and individual wave swash motion components can be approximated by the formulation of Stockdon et al. (2006) for the maximum runup elevation of the wave on the foreshore slope. Splinter et al. (2012) have found that runup parameters R_2 and R_{16} can be used to quantify dune volume change and dune foot retreat. Splinter and Palmsten (2012) found that R_2 gave a lower average error in dune foot retreat and is a better predictor in the collision regime in the field. The use of R_2 is often used in dune erosion and scarp-related research (e.g. Bonte and Levoy (2015), Splinter et al. (2018), Stockdon et al. (2007), and van Bemmelen et al. (2020)). The empirical parametrisation of Stockdon et al. (2006) for the extreme runup is defined based on the 2% exceedance of the runup peaks R_2 for all beaches except extremely dissipative beaches.

$$R_2 = 1.1\left(0.35\beta_f \left(H_0 L_0\right)^{1/2} + \frac{\left[H_0 L_0 \left(0.563\beta_f^2 + 0.004\right)\right]^{1/2}}{2}\right) \tag{2.11}$$

Where β_f is the foreshore slope. Stockdon et al. (2007) uses the foreshore beach slope β_f as the area over which significant swash activity is present for hurricane-induced conditions. This area was defined as the mean beach slope between the dune (dune foot) and the MHW shoreline. The R_2 formulation uses the deep-water equivalents of the wave height and wavelength.

2.5. Cross-shore sediment balance

In the context of coastal dune systems, the collision regime is characterised by a state in which the volume of sediment eroded from the dune face is deposited at the foreshore, resulting in an equilibrium between erosion and deposition volumes. However, there are certain scenarios in which the redistribution of sediment within the dune system cannot be fully attributed to cross-shore hydrodynamic processes. This is because other factors, such as alongshore transport, aeolian transport and human interventions, may also play a significant role.

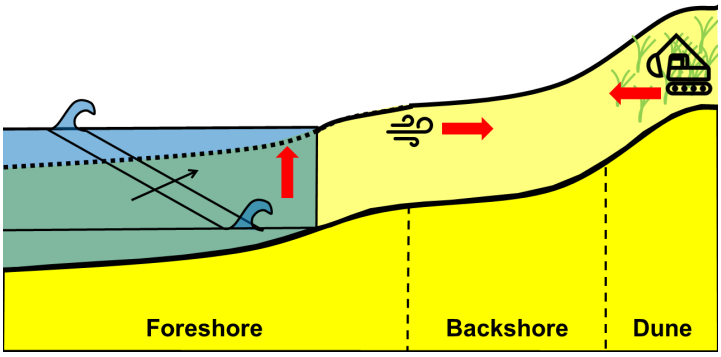

Figure 2.6: Overview of the significant factors influencing the sediment balance: alongshore transport, aeolian transport and human intervention.

2.5.1. Alongshore transport

Alongshore transport, also known as littoral drift, is a coastal process responsible for the transport of sediment parallel to the coastline. Alongshore transport plays a major role in shaping and maintaining the dynamic features of coastal regions, such as beaches and dunes. The main driver of alongshore transport is the effect of alongshore currents which are induced by oblique incident waves. Alongshore non-uniform features of the foreshore, beach, and dune could induce alongshore transport and therewith a change in the cross-shore sediment balance (Bonte & Levoy, 2015).

2.5.2. Aeolian transport

Aeolian (wind-induced) transport refers to the wind-driven transport of particles and implies that the dunes do not only transform due to impact by sea, instead, dunes can also erode and grow due to aeolian processes. The capacity to dune erosion of hydrodynamic forcing is of the same order as the capacity of aeolian processes to dune growth (de Vries et al., 2012). Important is, to know whether you can assume that the dune foot position does not change significantly in time due to aeolian processes and only due to hydrodynamic processes. Generally, aeolian transport of sand occurs for wind velocities higher than 5 to 10 m/s. Precipitation limits aeolian transports as the sand becomes wet which makes it non-erodible by the wind. Large wind velocities often go hand-in-hand with precipitation, hence aeolian transport occurs only for relatively mild conditions (Arens, 1996). The sediment supply for dune growth due to aeolian transport was found to not originate from the upper beach and therefore may originate from the lower beach or the intertidal zone (de Vries et al., 2015). Dune accretion after a storm event was found to occur principally at the dune foot (Suanez et al., 2012). For single storm events with pre- and post-storm profiles in the order of days, there can be assumed that the influence of aeolian transport on the dune volume change is negligible.

2.5.3. Human intervention

The net sediment volume in a certain confined cell can be influenced by human interventions. Roughly, a distinction can be made between direct and indirect interventions. Nourishments, dry land displacement and construction of hard structures are examples of direct intervention. Nourishments are depositions of sand to reinforce the dune and beach system. There is a positive net sand volume change within the system. This might explain an extreme increase in volume in a certain range of cross-shore profiles. Indirect interventions are harder to distinguish. Alongshore or offshore interventions can lead to a change in the equilibrium conditions, which could result in intensified erosion or sedimentation.

2.6. General conclusions

The dune foot position is defined by taking the most seaward peak of the second derivative of the elevation profile above a certain threshold (Diamantidou et al., 2020). Dune erosion and subsequent dune foot repositioning within a storm are attributed to hydrodynamic and morphological processes and relate with the duration and intensity of the storm. However, cross-shore sediment balance can be disrupted by factors such as alongshore transport, aeolian transport, and human intervention.

The post-storm dune foot elevation is often related to the maximum total water level elevation within a storm period in the collision regime. The total water level elevation can be calculated by adding the tide, wind setup, and wave and swash components ($\eta_{TWL} = \eta_{ast} + \eta_{win} + \eta_{wav} + \eta_{swa}$). An approximation of the wave and swash component can be made by the empirical parametrisation of the runup as defined by Stockdon et al. (2006).

Foreshore slope, a significant parameter of the dune profile, influences the runup elevation and is defined as the region of significant swash action. For events with high runup elevations reaching the dune front, the foreshore slope is approximated by the slope between mean high water (MHW) and the dune foot (Stockdon et al., 2007).

II

Analysis

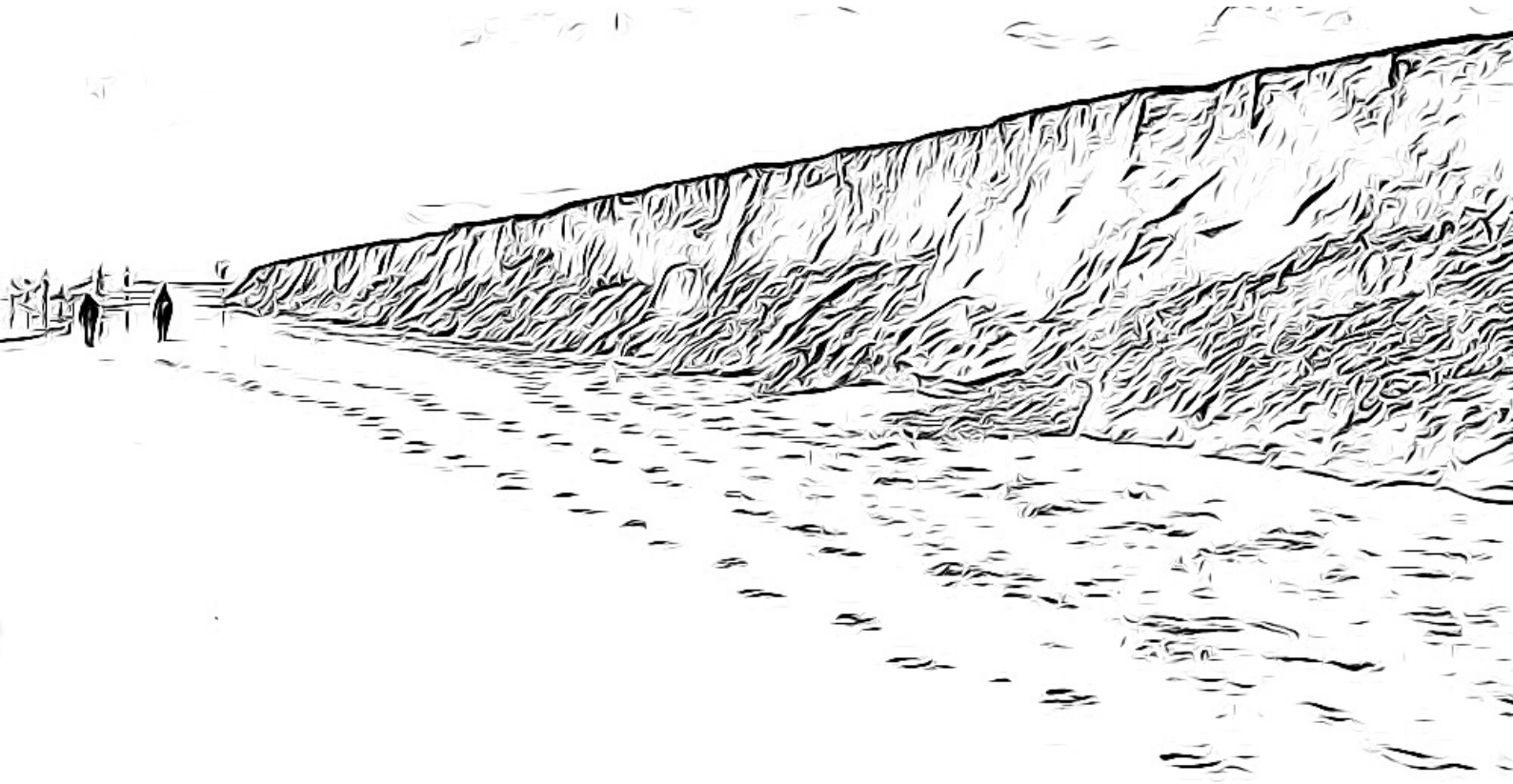

3

Situation Analysis

For the purpose of this study on the dune foot behaviour of sandy coastal defences during annual storm conditions, two sites are investigated: RealDune-REFLEX and Land Reclamation Philippines. In this chapter, the main site characteristics, metocean conditions and instrumentation of these two sites are introduced.

3.1. RealDune-REFLEX

3.1.1. Introduction

The RealDune-REFLEX project (RD), is a large-scale manipulative field experiment conducted and supervised by researchers from TU Delft with support from different partners in the field of hydraulic engineering. For this field experiment, two real-life scale dunes are constructed close to the waterline on the Sand Engine located near Kijkduin (Figure 3.2). The Sand Engine is a large, man-made peninsula consisting of over 20 million cubic meters of sand that were deposited here in a pre-defined shape using a ”Building with Nature” approach. The dunes of RealDune-REFLEX were built at the end of October 2021 and were measured from November 2021 until January 2022 (TU Delft, 2022). This experiment was performed to gain more knowledge on the driving processes of dune erosion. During this period of three months, three significant storms passed by which led to the most significant storm-induced erosion of the dunes. In this three-month period, the northern dune (Dune 2) eroded entirely.

(a) Before experiment; aerial

(b) During experiment; close-up

Figure 3.1: An impression of the RealDune-REFLEX field measuring site. (Left photograph from TU Delft (2022) and right photograph from Mischa Keijser).

3.1.2. Site characteristics

The site of the field experiment is located in the Netherlands along the Holland coast on the Sand Engine surrounded by the North Sea (Figure 3.2). The Sand Engine is an innovative coastal engineering project and was initiated in response to the increasing threat of coastal erosion and sea level rise, which is a significant concern for low-lying areas like the Netherlands.

Figure 3.2: Map of the RealDune-REFLEX site location at the Sand Engine (edited imagery from Google (2023))

The location and orientation of the dunes at the RealDune-REFLEX were defined for the RealDune-REFLEX experiment to ensure capturing oblique incident waves. The site consisted of two large-scale dunes with measurements of 150 m length, 20 meters wide and 5.5 meters high. The two dunes are defined based on an origin and an orientation. The origin corresponds to the mid-point of the dune. The orientation corresponds to the transect which is perpendicular to the dune. The origin of Dune 1 has UTM coordinates for zone 31U (581040, 5767173) and orientation of the transect of 296 degrees with respect to the north. The origin of Dune 2 has UTM coordinates for zone 31U (581297, 5767631) and the orientation of the transect of 310 degrees with respect to the north. At the field site, Dune 1 is the southern dune and Dune 2 is the northern dune (Figure 3.1a). The instrumentation of the measuring site will be further discussed in Section 3.1.4

The sediment of both Dune 1 and Dune 2 of RealDune-REFLEX consisted of the same characteristics. The sediment is slightly fine gravelly medium sand, unimodal and well-sorted. The sediment size d_{50} is 362.3 μm. The sample statistics and grain size distribution is provided in Appendix C

3.1.3. Metocean conditions

The metocean conditions for RealDune-REFLEX are subdivided into water levels and tide (Figure 3.3), wave height and direction (Figure 3.4b), and wind speed and direction (Figure 3.4a). MHW is found at 1.13 +m NAP and LAT at -0.94 +m NAP. The main waves are coming from the North and the south-west.

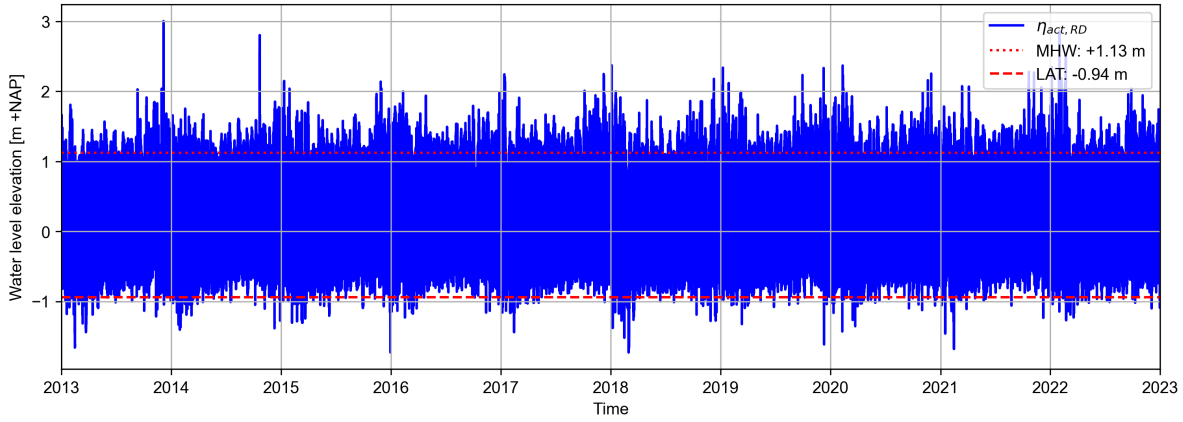

Figure 3.3: Water level elevation estimations in NAP for the RealDune-REFLEX field site over the period 2013 to 2022 based on the average of Hoek van Holland harbour and Scheveningen harbour.

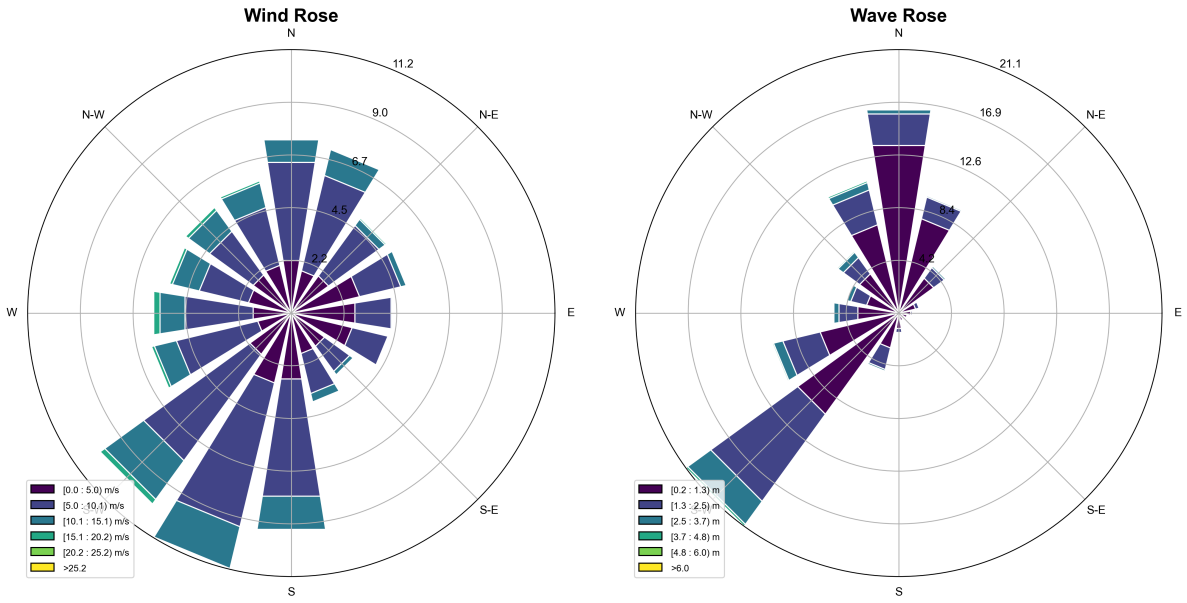

(a) Hoek van Holland wind rose

(b) Europlatform wave rose

Figure 3.4: RealDune-REFLEX wind and wave roses for the direction coming from. (left) Wind data was measured at the RWS Hoek van Holland 10-meter elevation measurement station from 2021-02-01 to 2022-12-31. (right) Wave data was measured at the RWS Europlatform in the North Sea at approximately 32 meters of water depth from 2013-01-01 to 2022-12-31.

3.1.4. Instrumentation

Dune 1 and Dune 2 are measured with an RTK along a pre-defined transect located in the middle of the dune with an almost daily frequency. In between, measurements with an RTK mounted on a wheelbarrow or an RTK on a quad were performed to measure the area around the dunes. The three storms which were identified to result in significant erosion were recorded from 6 to 8 November, 30 November to 2 December and 5 to 6 January. These elevation measurements are extracted from the dataset. The overview of the instrumentation and the pre-defined transects at the field experiment site are depicted in Figure 3.5.

Figure 3.5: The layout of the RealDune-REFLEX field measuring site. The measurement devices are shown with their respective location and orientation to Dune 1 and Dune 2. The RBR sensors are located on the mid-transect for Dune 1 and Dune 2. The Signature ADCP (depth $d \approx 14\ m$) and the Europlatform (depth $d \approx 32\ m$) are located offshore. The Europlatform. tidal gauge of Hoek van Holland and the tidal gauge of Scheveningen are not depicted in this figure.

The tidal water level elevation is measured at the harbour of Scheveningen and the harbour of Hoek van Holland. The average between these two tidal stations is used for the RealDune-REFLEX site as the RealDune-REFLEX site is approximately in the middle of these two measurements. This comes down to a shift of the peak of approximately 15 minutes which is verified against local pressure sensor measurements.

The wave conditions are captured by the measurements at the Europlatform (Storm 1, 2 and 3), two RBR pressure sensors (Storm 2 and 3) each in line with the transect of Dune 1 and Dune 2 and an offshore Signature AWAC at approximately 14 meters of water depth (Storm 2 and 3).

3.2. Land Reclamation Philippines

3.2.1. Introduction

Land Reclamation Philippines (LRP) is a land reclamation project designed and executed by Boskalis in Manila Bay in the Philippines (Figure 3.7). The land reclamation is constructed by the dredging and disposal of sand and has unprotected sandy slopes around the reclamation during the construction phase. After the dredging is completed, these sandy slopes will be constructed with slope protection to withstand future typhoons. During the construction phase, a typhoon passed right over the bay resulting in severe erosion of the unprotected sandy slopes. The tropical storm exhibited its maximum intensity over LRP between the 29th and 31st of October 2022. The Philippine area is known to have more tropical cyclones than anywhere else in the world. Each year, on average 20 typhoons pass this region. With 70% of typhoons passing, the peak of the typhoon season is from July to October (PAGASA, 2022).

(a) Before typhoon (2022-10-29)

(b) After typhoon (2022-11-03)

Figure 3.6: The slope of Land Reclamation Philippines. Significant erosion due to typhoon-induced hydrodynamics. Note that the water level elevations of the two photos do not coincide.

An impression is given of the severity of the erosion on the slope (Figure 3.6). In contrast, other slopes were less prone to erosion, while being at least equally or more exposed. Notably, these slopes are approximately 1:12 in contrast to the eroded slope, which is roughly 1:4. These findings suggest that slope may play a crucial role in the erosion process. For this study, the slopes of 1:4 were chosen as the main region of interest due to the observed severe erosion and the superior accuracy of the available morphological dataset in this location.

3.2.2. Site characteristics

The site is located in Manila Bay. The bay is located in the Philippines in the northern hemisphere and is connected to the South China Sea and spans approximately 1,994 square kilometres (Figure 3.7).

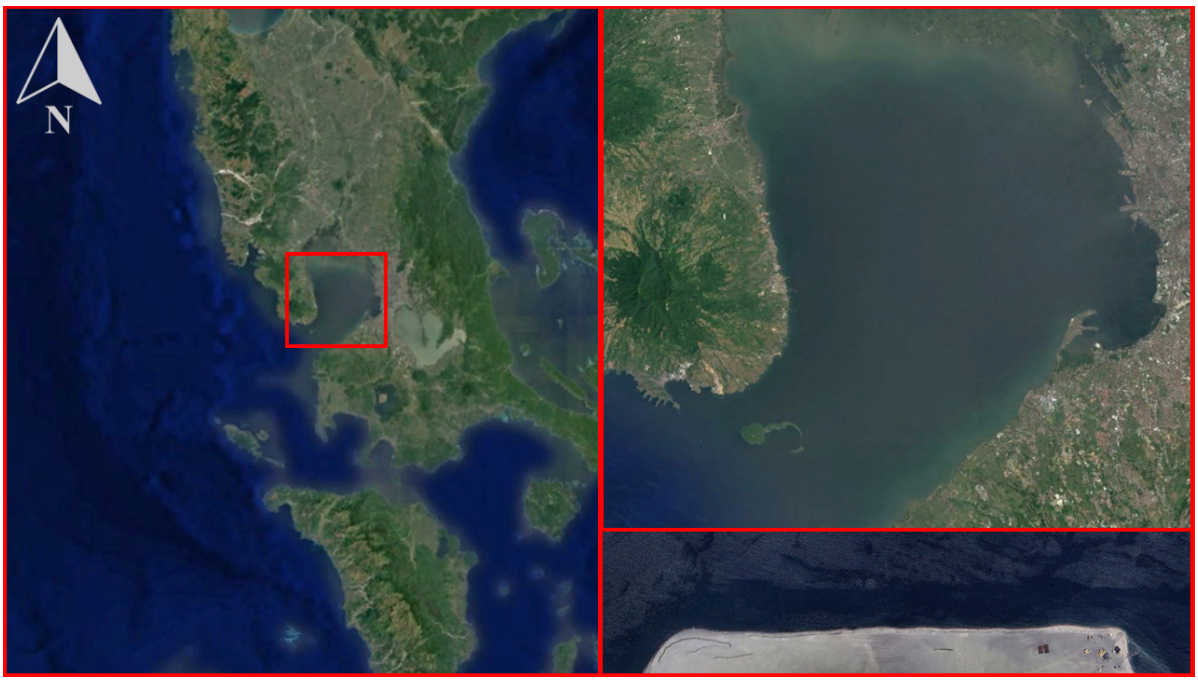

Figure 3.7: Field site location of Land Reclamation Philippines (edited imagery from Google (2023)) (left) South China Sea and the Philippines. (right upper) Manila Bay. (right lower) Field site Land Reclamation Philippines.

The sediment of the slope of interest is sampled onboard the hopper dredger at three moments (begin, mid, end) of the hopper cycle for eleven cycles from 2022-06-19 to 2022-07-17. The sediment is discharged using a spreader pontoon and the slopes above water are created using a dozer. Therefore it is assumed that the sediment samples at the hopper are representative of the sediment type of these slopes. During the land reclamation, samples are taken at eleven different cycles with three samples per cycle, as described. The mean of all these samples is taken and assumed representative. The sediment normative characteristics are $d_{50} = 778\ \mu m$ and $d_{60}/d_{10} = 5.071$.

3.2.3. Metocean conditions

The water level elevation measured at UHSLC is corrected for the MSL over the period 1985 to 2016. This period is chosen as a reference datum as the elevation measurements are project specific to this datum. An offset of -0.7 m due to instrument relocation is corrected. Outliers are removed. The water level elevation shows a linear upward trend due to SLR and land subsidence (Figure 3.8) and is not corrected as the reference datum remains MSL over the period 1985 to 2016. The main wind direction is from the southwest and the main wave direction is from the west and northwest (Figure 3.9).

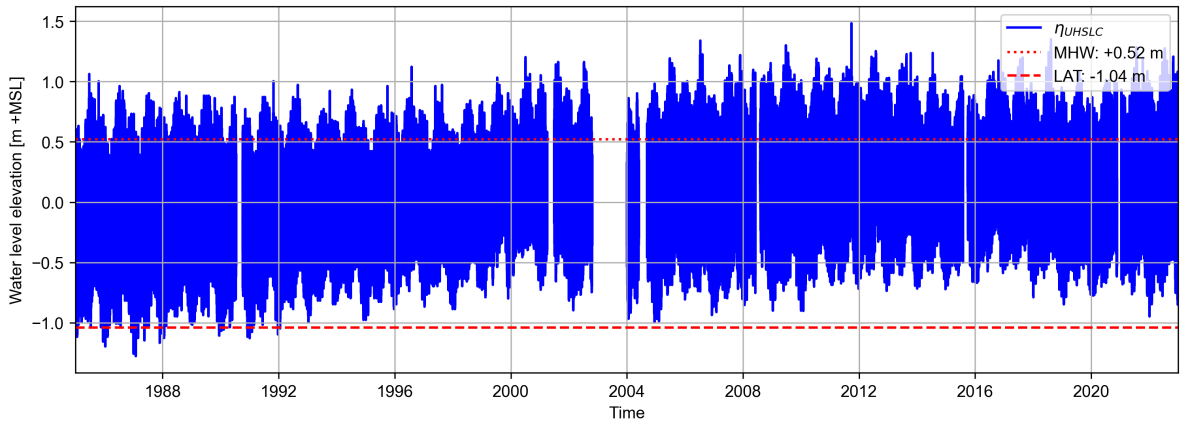

Figure 3.8: Tidal water level elevation record for Land Reclamation Philippines based on the UHSLC measurements from 1985-01-01 to 2022-12-31 (Caldwell et al., 2015). The time series is corrected for MSL calculated over the period 1985 to 2016.

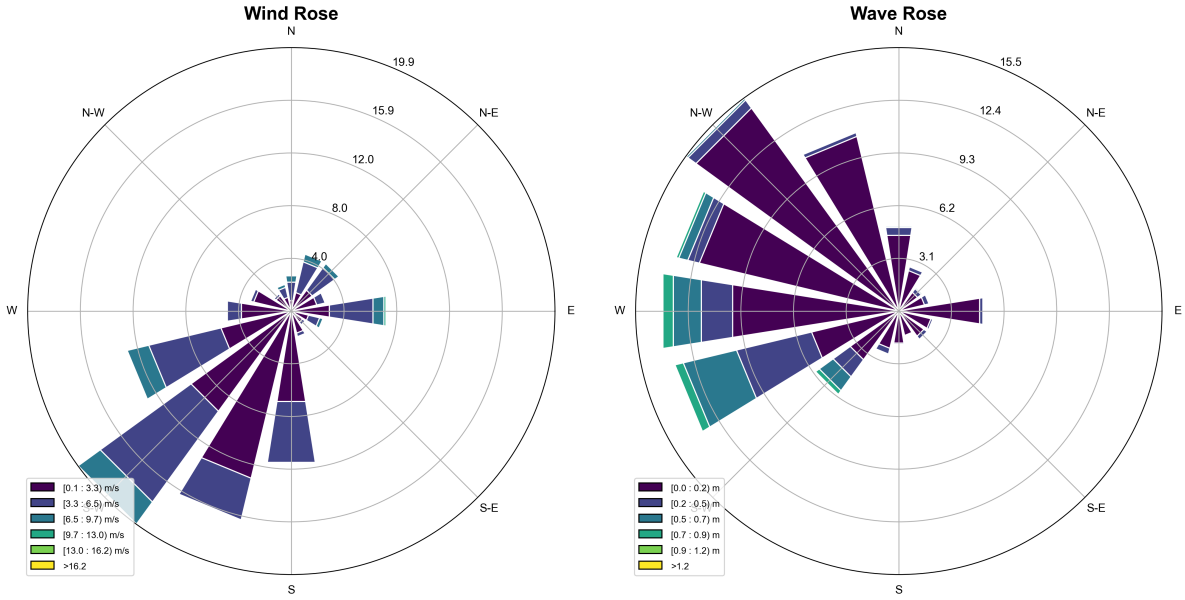

(a) MIA wind rose

(b) LRP wave rose

Figure 3.9: The wind and wave roses which are governing for Land Reclamation Philippines. The wind rose is constructed from the available data at the wind measuring station at the land platform of Manila International Airport. This period is from 2021-11-05 to 2023-02-26. The wave rose is constructed from the Waverider data (depth $d \approx 9\ m$) near the project LRP. The period of measurement here is from 2022-09-06 to 2022-12-08 with a gap in the data during the typhoon of interest around 2022-10-30 and between 2022-09-20 and 2022-10-13.

3.2.4. Instrumentation

Land Reclamation Philippines is located in a bay (Figure 3.7) with elevation measurements of the land reclamation (Figure 3.10). The slope and bathymetry are measured pre-storm on 2022-10-27 at 09:00 and post-storm on 2022-10-31 at 16:00 on the slopes of interest. To be able to quantify certain transects, the slope is subdivided into 26 transects each spaced 50 meters with names Kp150 to Kp1400 (Figure 3.10). Between these Kp-lines, additional transects are defined which are each spaced 10 meters coming to a total of 126 transects. These measurements were pre-processed to a grid with 1x1 meter spatial resolution. The survey data for LRP is provided in LAT and the project-specific conversion of LAT to MSL is -1.04 (Figure 3.8). The Waverider and AWAC are located in the bay, additional settings and resolution of the instruments are provided in Appendix F.

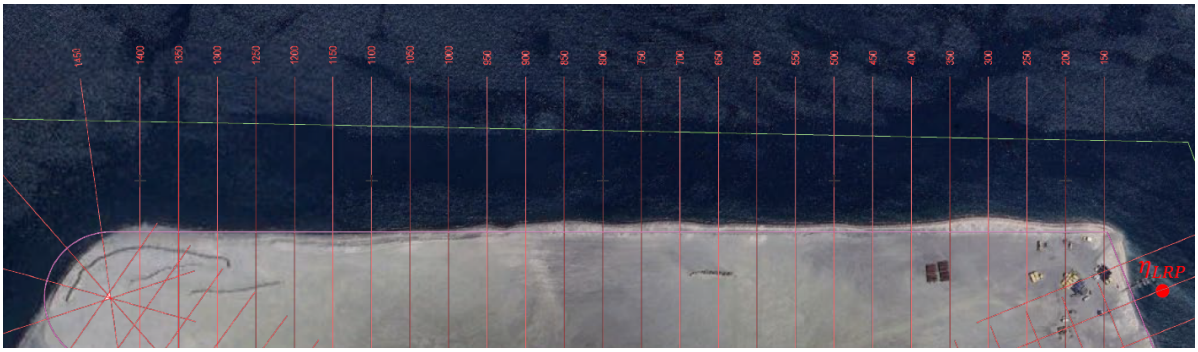

Figure 3.10: LRP site layout with Kp-lines 1400 to 150 overlay. The LRP tidal gauge is located on the side of the land reclamation.

3.3. Overview and differences of field sites

To provide insights into the similarities and differences between the two sites and the different measurements, an overview of the storm periods are provided in Table 3.1. Both field sites contain out-of-equilibrium dune profiles which are affected by storm-induced dune erosion.

Table 3.1: Situation analysis overview of the field sites and respective measurements during storm periods.

Site	Storm	Date	# transects	d_{50} [μm]
RD	1	2021-11-06 10:00 to 2021-11-08 13:00	2	362.3
	2.1	2021-11-30 18:00 to 2021-12-01 09:00	2	362.3
	2.2	2021-12-01 07:00 to 2021-12-01 21:00	2	362.3
	2.3	2021-12-01-19:00 to 2021-12-02 10:00	2	362.3
	2.4	2021-12-02 08:00 to 2021-12-02 19:00	2	362.3
	3	2022-01-05 09:00 to 2022-01-06 12:00	2	362.3
LRP	Nalgae	2022-10-29 to 2022-10-31	126	777.6

Differences between the RealDune-REFLEX and Land Reclamation Philippines measurements arise in terms of spatial and temporal resolution. These differences originate from the fact that RealDune-REFLEX is a project especially set up for research purposes, while LRP is measured to ensure the design and progress of the land reclamation. RealDune-REFLEX is measured approximately every day during the entire measurement campaign of three months. The same mid-dune transects are measured at these times. Therefore the temporal evolution of RealDune-REFLEX over the same transect could be a very interesting aspect to look at. For Land Reclamation Philippines, the spatial evolution and alongshore variability of the dune foot and foreshore slope could be of interest as the entire alongshore slope of the land reclamation is measured.

4

Methodology & Data processing

4.1. Introduction

This thesis focuses on field measurements of dune erosion (sandy coastal defences) during annual storm conditions on a daily timescale. The measurements described in Chapter 3 are performed in advance of this research and performing the measurements is not part of the scope of this thesis. The origin of the data gathering for the two field sites is different. The RealDune-REFLEX experiment was purely conducted for research purposes and the measurements for Land Reclamation Philippines were part of a large-scale land reclamation project. The data processing in this chapter is split up into hydrodynamics, typhoon-induced wave conditions, morphology and parametrisation. The introduced parameters will be used for the analysis of this study. All time series in this thesis are converted to UTC.

4.2. Hydrodynamics

Hydrodynamic measurements are obtained for both case studies. The water level elevation and wave conditions are extracted from the data following the described procedure.

4.2.1. Data overview

RealDune-REFLEX

For RealDune-REFLEX, the overview of the hydrodynamic data is described in Table 4.1.

Table 4.1: Instrument overview of the RealDune-REFLEX site. Location, owner, raw data and processed parameter of interest are provided.

Instrument	Location	Owner	Raw	Parameter
Tidal gauge	Hoek van Holland	RWS	η_{HvH}	$\eta_{act,SE}$, $\eta_{ast,SE}$
Tidal gauge	Scheveningen	RWS	η_{Sche}	$\eta_{act,SE}$, $\eta_{ast,SE}$
Europlatform	North Sea	RWS	-	$H_{1/3,0}$, $T_{1/3,0}$, θ_0
RBR	Dune 1	TU Delft	pressure, $F_s = 8\ Hz$	η, H_{m0}, $T_{m-1.0}$
RBR	Dune 2	TU Delft	pressure, $F_s = 8\ Hz$	η, H_{m0}, $T_{m-1.0}$
Signature	Offshore, $d \approx 14\ m$	TU Delft	pressure, elevation, $F_s = 4\ Hz$	η, H_{m0}, $T_{m-1.0}$

Land Reclamation Philippines
For Land Reclamation Philippines, the overview of the hydrodynamic data is described in Table 4.2.

Table 4.2: Instrument overview of the Land Reclamation Philippines site. Location, owner, raw data and processed parameter of interest.

Instrument	Location	Owner	Raw	Parameter
Tidal gauge	Right side LRP	Boskalis	-	η_{act}
Tidal gauge	Manila	UHSLC	-	η_{act}
Waverider	Bay, $d \approx 9\ m$	Boskalis	-	H_{m0}, T_{m02}, θ
AWAC	Bay, $d \approx 14\ m$	Boskalis	-	H_{m0}, T_{m02}, θ

4.2.2. Data transformation

The available hydrodynamic datasets vary significantly between RealDUne-REFLEX and Land Reclamation Philippines. The hydrodynamic methodology is described schematically in Figure 4.1.

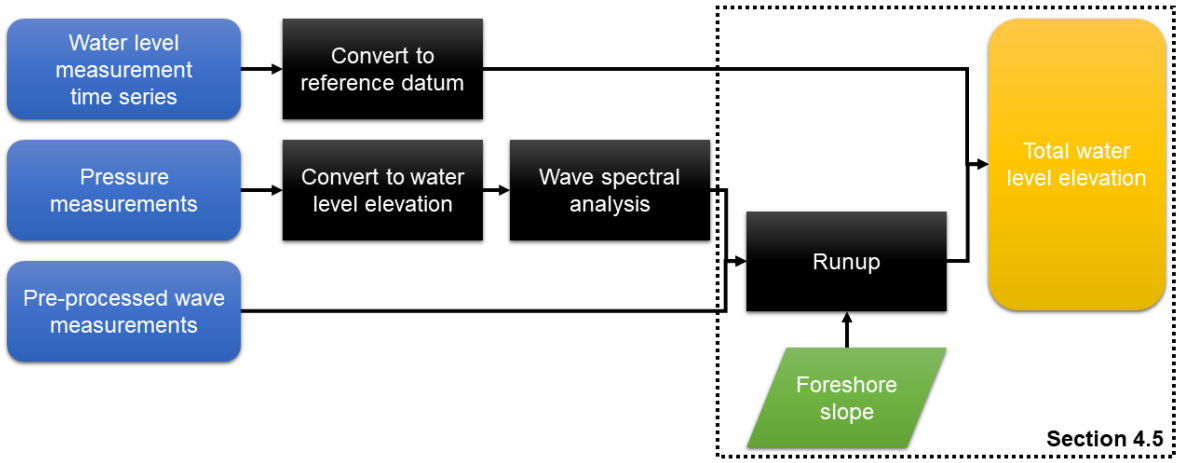

Figure 4.1: Flowchart for the methodology regarding the hydrodynamics. Hydrodynamic input: blue. Morphological input: green. Process: black. Output: yellow.

RealDune-REFLEX
Water level time series of the tidal gauge of Hoek van Holland and the tidal gauge of Scheveningen are averaged for all timesteps and the best estimate time series for the water level elevation at the RealDune-REFLEX site is obtained. The site is approximately in the middle of the two tidal stations along the Holland coast. The signature elevation is corrected for a bed level offset of 63 cm and the RBR is measured with respect to NAP and corrected for a varying bed level offset. The water level elevation of the signature is corrected to NAP using an RMSE approach to subtracting an offset with steps of 0.001 over a reference period with mild wave conditions. Offset with the lowest RMSE resulted in the best estimate for the NAP reference datum. For the Europlatform, the water depth is approximately 32 meters, for the offshore Signature ADCP the average depth was 14 meters. For the RBRs, the depth was varying significantly and the RBRs have become dry at times.

Pressure time series obtained by the RBR sensors were converted to surface elevation time series based on linear wave theory (Appendix B.1). The variance density spectrum of the water surface elevation for the Signature and the RBR is calculated using wave spectral estimates and the spectral estimates for the wave height and wave period are obtained (Appendix B.2). The spectral moments are calculated over the frequencies between 0.004 Hz and 1 Hz to cut-off low- and high-frequency noise. For Storm 1, the measurements of Eurolatform were used as the other instruments were not active at that time. For Storm 2 and Storm 3, the measurements of the Signature at a 14-meter depth were used for this analysis.

Land Reclamation Philippines
The water level elevation of the tidal gauge at LRP is corrected to MSL using the water level data of UHSLC (Caldwell et al., 2015). The mean of the entire time series over the period 1985-2016 is subtracted from the value per timestep and therefore assumed that MSL equals $\eta = 0$. This procedure is also performed for the AWAC with converted mean pressure above the ADCP (including the bed level offset of 70 cm). The water depth was varying around approximately 9 meters for the Waverider and 14 meters for the AWAC.

During the typhoon, the Waverider near LRP lacked measurements. In order to overcome this particular issue, measurements obtained by the AWAC located close to MIA were transformed to the location of the Waverider which was in close proximity to LRP. The procedures followed as well as the subsequent transformation process have been elaborated in detail in Section 4.3. The mean wave period T_{m02} is used as this parameter was measured by both the Waverider and the AWAC. The spectral mean energy wave period $T_{m-1.0}$ is preferred for dune erosion-related calculations, however, was not incorporated in the instrument settings and is therefore not known.

4.2.3. Data results
The resulting hydrodynamic measurements consist of a continuous signal during the period of interest, resampled to a time interval of 10 minutes for RealDune-REFLEX and resampled to 30 minutes for Land Reclamation Philippines. The parameters which will be used in the research are:

- Water level elevation to reference NAP/MSL [m]; η_{act}
- Wave height [m]; H_{m0}
- Wave period [s]; RD: $T_{m-1.0}$ and LRP: T_{m02}
- Wave direction [°]; θ

4.3. Typhoon wave conditions Land Reclamation Philippines

The missing Waverider measurements at LRP (Section 4.3.1) are estimated by means of wind-induced SWAN modelling (Section 4.3.2) to get an insight into the typhoon-induced behaviour in the bay. Thereafter, the AWAC measurements are transformed to the Land Reclamation Philippines location (Section 4.3.3) and validated according to linear wave theory (Section 4.3.4).

4.3.1. Incomplete wave measurements Waverider

The Waverider near the Land Reclamation Philippines reclamation site, unfortunately, failed to provide measurements during the onset of the typhoon. While it was able to supply output conditions before and after the typhoon, the measurements of the offshore wave conditions adjacent to the reclamation site during the most significant erosion event remain absent from the dataset. Close to another project of Boskalis 'Manila International Airport', or in short MIA, an AWAC was deployed offshore (Figure 3.7).

Measurements were taken during peak typhoon conditions but from a location on another location of the bay where different wave conditions are present (Figure 4.2). The individual measurement points are plotted and show that the measurements during the peak of the typhoon did not succeed for the Waverider at LRP. The direction of the waves during the typhoon peak is rather uniform for the two locations.

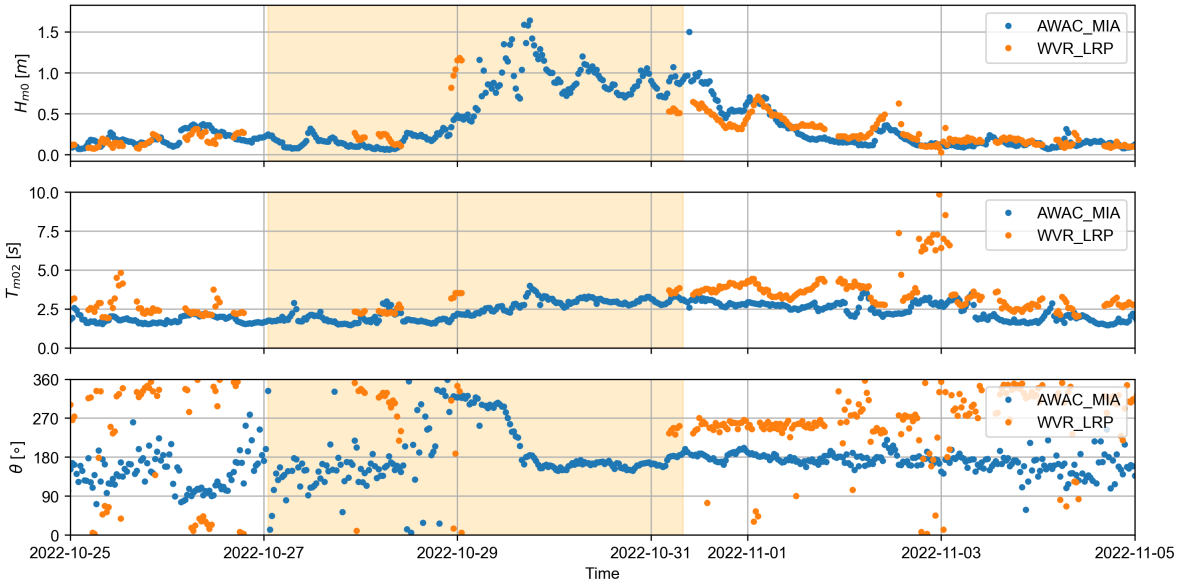

Figure 4.2: The H_{m0}, T_{m02} and θ measurements of the Waverider at LRP and the AWAC at MIA. Missing measurements for the Waverider during the typhoon peak.

4.3.2. Typhoon modelling

To gain insight into the behaviour of the wave conditions during a typhoon at the two locations, a typhoon model is set up using the software Triangle and SWAN. An unstructured triangular mesh is constructed and non-stationary simulations are performed. The model is set up using the guidelines of a Boskalis in-house typhoon model (Hoek & Klein, 2022).

The grid and grid's resolution are defined in Google Earth (Google, 2023), by defining open boundaries, closed boundaries and areas of interest with a specific resolution. These boundaries are exported and used as input to create a triangular grid in the region, where additional smoothening of the grid is applied. The raw boundaries are created in Google Earth which are applied and combined with the grid resolution to the final unstructured grid of the model. The resolution of each area is predefined. The outer sea is set at 20000x20000, closer to the bay 5000x5000 and in the bay 1000x1000. Details are applied at three locations of interest and importance. The mouth of the bay is of importance as the bathymetry is subject to a rapid incline due to the shelf sea and is detailed with 500x500. Also, some

islands in the mouth could interfere with the converging streamlines. Details of 200x200 are applied to the LRP and MIA regions as the output points will be located here. The unstructured grid has 24469 nodes and 46680 elements.

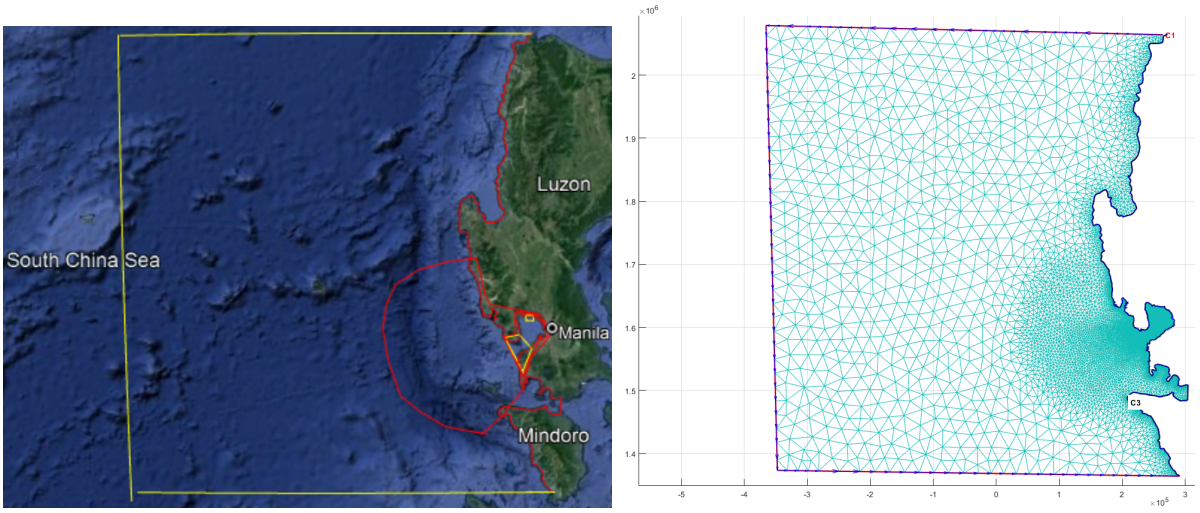

(a) Boundaries on map

(b) SWAN unstructured grid

Figure 4.3: The boundaries and grid for the unstructured SWAN typhoon model for the Land Reclamation Philippines case. Three open boundaries are defined and one closed land boundary from SW up to the NW.

On this grid, a depth file is interpolated linearly. Outside the bay, a depth file of the GEBCO database is used (GEBCO, 2022) and inside the bay, a higher resolution Boskalis depth file is used. The wind data is retrieved from the ERA5 database which has a spatial resolution of 0.25 degrees and an hourly interval in time (ECMWF, 2022). This ERA5 wind field (Figure 4.4) is also interpolated with linear interpolation to the triangular grid. In the SWAN non-stationary calculations, a timestep of 10 minutes and a maximum of 200 iterations is chosen to reach 99.5% accuracy.

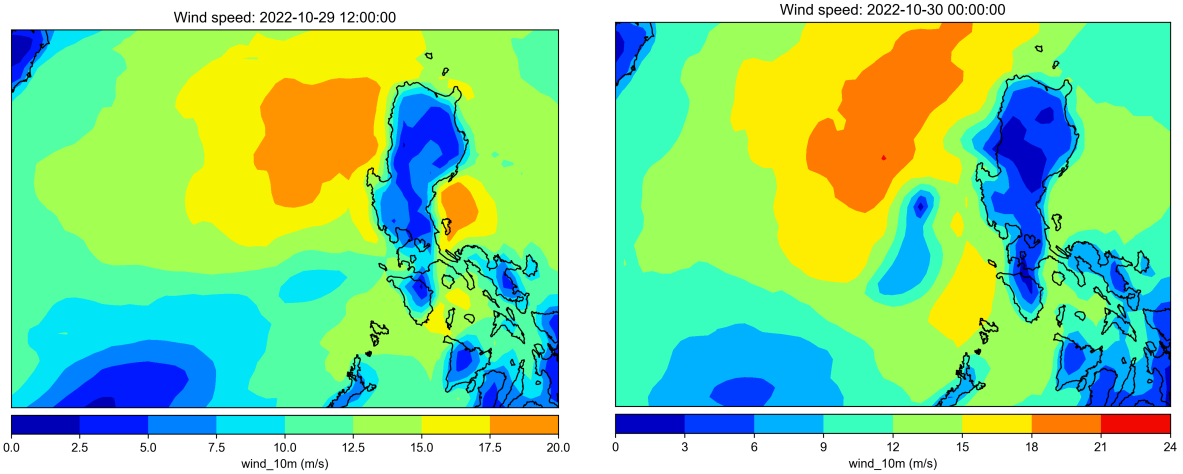

(a) 2022-10-29 12:00

(b) 2022-10-30 00:00

Figure 4.4: The ERA5 wind field for the region around the bay for two time-steps with a 12-hour difference in between. (left) The eye of the typhoon can be observed in the middle of the sea. (right) The eye is approximately above the bay.

The model is set up and runs from 25-10-2022 at 00:00 to 01-11-2022 at 23:00. Two output locations are chosen, MIA and LRP. A spatial overview of the propagation of the significant wave heights is plotted for six timesteps (Figure 4.5). During the peak of the typhoon, the model underestimates the wave heights (Figure 4.6). The wave direction has a huge spread in the period before and during the typhoon passes the bay. After the typhoon passes the temporal variation of the wave direction is very low. The sudden change of wave direction can be linked to the eye of the typhoon moving over the bay around 12:00 2022-10-29.

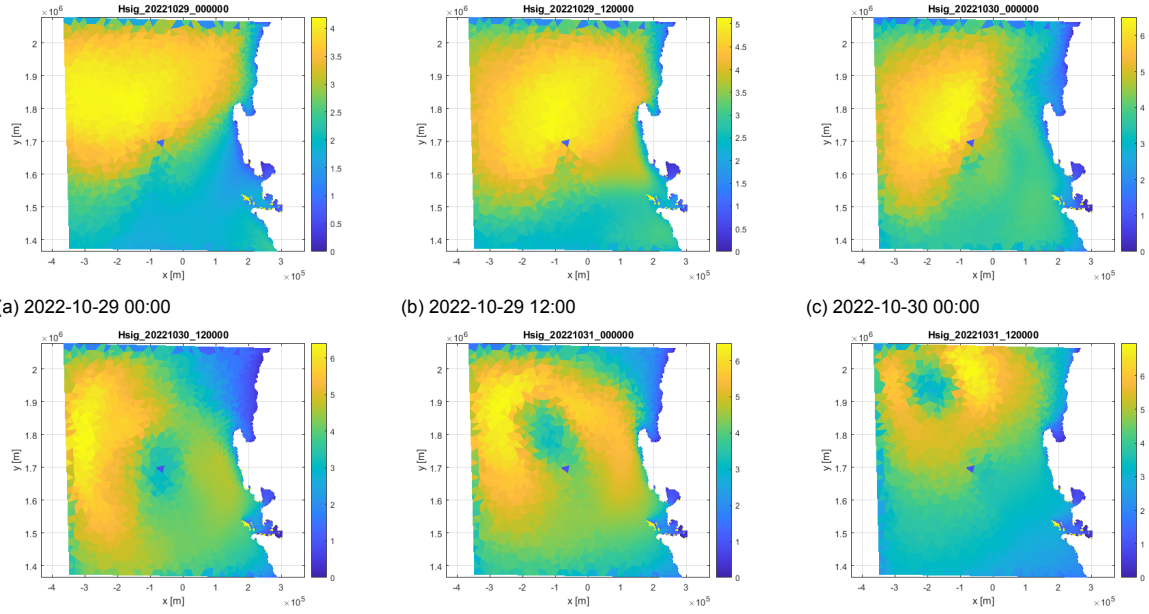

(a) 2022-10-29 00:00 (b) 2022-10-29 12:00 (c) 2022-10-30 00:00

(d) 2022-10-30 12:00 (e) 2022-10-31 00:00 (f) 2022-10-31 12:00

Figure 4.5: An overview of the spatial propagation of the significant wave height modelled by the typhoon model for the Land Reclamation Philippines case. The overview shows six timesteps from 2022-10-29 at 00:00 to 2022-10-31 at 12:00.

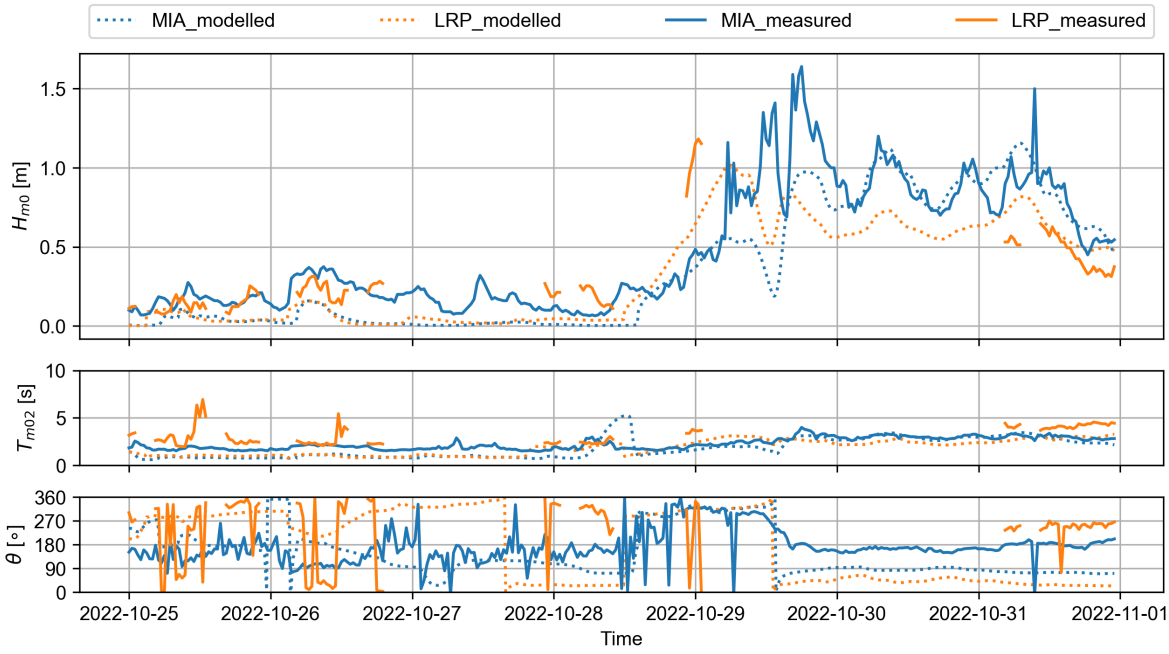

Figure 4.6: Measurements of H_{m0}, T_{m02} and θ in the bay for Land Reclamation Philippines (LRP) and Manila International Airport (MIA) compared to the results of the typhoon model.

The modelled wave heights show some resemblance to the measured data but are not very accurate. The differences between the actual measurements and the predicted values using the model are quantified with the Root Mean Square Error (RMSE) as follows:

$$RMSE = \sqrt{\sum_{i=1}^{n} \frac{\left(y_{pred,i} - y_{meas,i}\right)^2}{N}} \tag{4.1}$$

The root mean square error serves as a statistical measure for the discrepancy between the model and measured values. With regard to the analysis of the typhoon period, the RMSE was determined for MIA and LRP, with values of 0.217 m and 0.245 m, respectively. These findings reveal the average differences between the observed and modelled data for the duration of the typhoon period. Looking at the model outcome, it can be concluded that the model underestimates the wave height H_{m0} at the peak of the typhoon and therefore the model outcomes are not reliable enough to use the modelled signal of the wave height for the further calculations. However, two interesting features can be highlighted. There is a slight phase lag between the signal of LRP and MIA of the order of 2 hours and also a scale factor in the difference in wave height at the typhoon's peak.

4.3.3. MIA to LRP transformation

The AWAC located near MIA recorded wave heights throughout the duration of the typhoon. The introduction of the time and scale shift theory may provide greater accuracy in determining wave conditions. The time series of both measurements were resampled to a temporal resolution of 30 minutes. A comparable typhoon event, where measurements were taken by both the Waverider and the AWAC, was utilized to transform the MIA dataset. The selection criteria mandate heightened wave heights in comparison to average conditions, coinciding with consistency in wave direction and a limited standard deviation of the directional signal over a prescribed duration. In the entire time series, only one event did apply to these criteria. This period is from 14-10-2022 09:30 to 18-10-2022 06:00 and is called Typhoon Neneng (or Nesat). Within this reference period, the wave heights were elevated above the mean. However, the wave heights did not reach the elevated levels of Typhoon Nalgae.

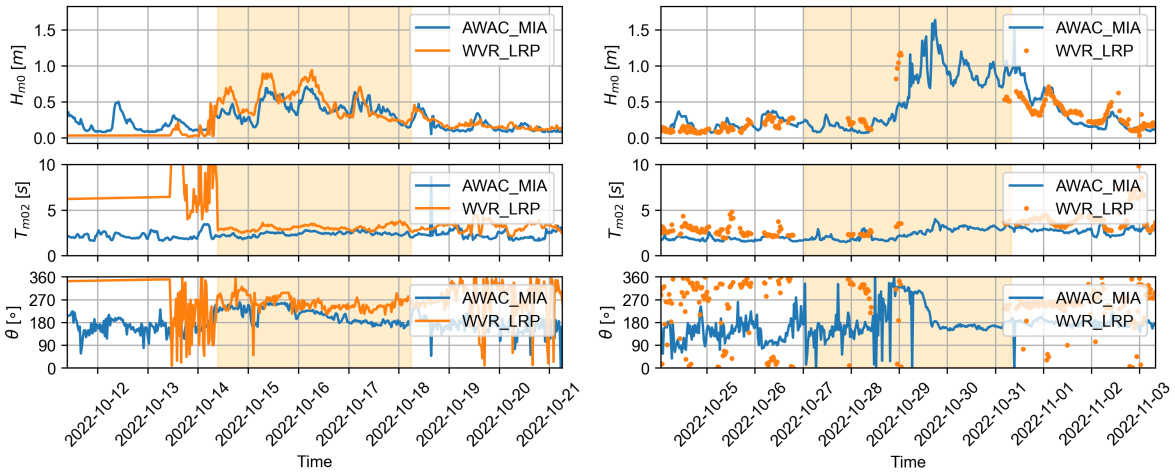

Figure 4.7: Initial wave conditions for the WVR and the AWAC before the time series of the AWAC is transformed.

To shift the time series of MIA, the interval during the chosen reference period is shifted at a timestep of 30 minutes. For each shift, including the initial condition, the RMSE is calculated over the cut-off periods between MIA and LRP. The shift for which the RMSE was the lowest, meaning the lowest difference between the two different time series, was chosen as the normative shift for the entire time series. This resulted in two timesteps backwards which correspond with a timeshift of -60 minutes for MIA, which means that the peak of the high wave heights arrived an hour earlier at LRP than at MIA.

For height scaling, the time-shifted time series for the wave height H_{m0} and wave period T_{m02} are scaled with a factor varying from 0 to 2 with steps of 0.001. The values are multiplied with the scaling factor and for every scaling, the RMSE is calculated. The scaling factor with the lowest RMSE results in the scaling factor which is applied for further calculations. For H_{m0} this factor is 1.19 and for T_{m02} this factor is 1.27. The shift and scaling results in the adjusted time series for the reference period and the storm period of interest (Figure 4.8).

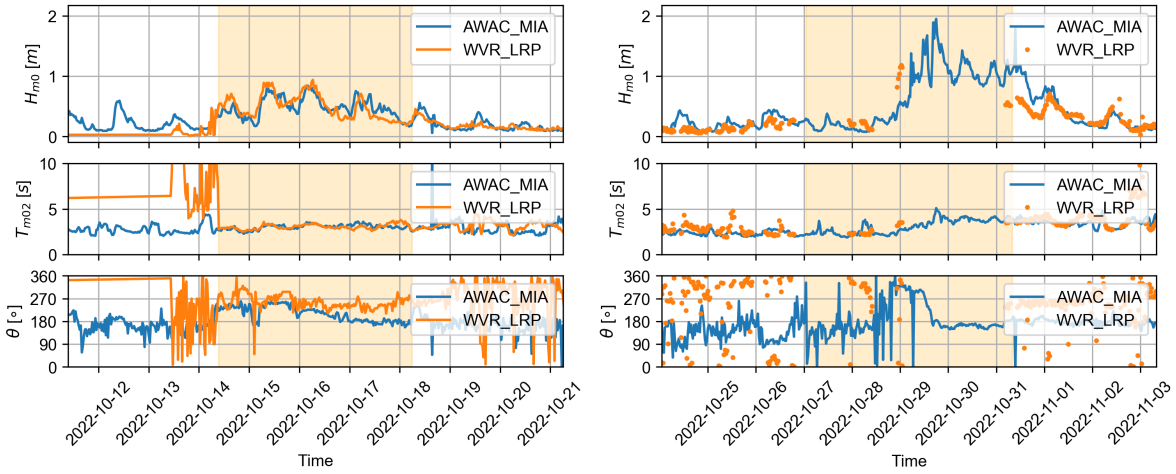

Figure 4.8: Transformed wave conditions for the WVR and the AWAC after the time series of the AWAC is shifted in time and scaled in height.

4.3.4. Validation of the transformation

The waves hypothesised to reach LRP first and MIA second, travel at a certain speed towards the shore. The wave propagation speed can be described with Equation (2.6) and the wavelength with Equation (2.5). From LRP to MIA, the wave speed is assumed to change predominantly through the influences of three processes: shoaling, refraction and diffraction. The wave propagation speed will be affected by the bottom when the water depth h decreases below $h/L < 0.5$ which is approximately the limit of deep water wave conditions. To get an order of magnitude for the wave celerity the upper and lower limits are calculated which correspond with deep water conditions and shallow or intermediate water conditions. The actual wave speed would be somewhere in between those limits as the bay has characteristics from deep water and intermediate water. The difference in the path of the waves is not known fully. Therefore the distance they have to cover to arrive at the Waverider (depth = 8 m) at LRP and the AWAC (depth = 14 m) at MIA is approximately 10 to 20 km. In the entrance and middle of the bay, deep water is assumed. The lower depth limit of 8 meters, with a mean wave period of approximately 3.03 s corresponds with intermediate water.

In deep water, the wave celerity and respectively the duration of arrival are, with the smallest distance:

$$c = c_0 = \frac{gT}{2\pi} = 4.731\ m/s \Longrightarrow \Delta t = \frac{10 * 10^3}{4.731} = 35.29\ minutes \tag{4.2}$$

In intermediate water depth, the wave celerity and respectively the duration of arrival are, with the largest distance:

$$c = \frac{gT}{2\pi} \tanh\left(\frac{Th}{2\pi}\right) = 4.727 \Longrightarrow \Delta t = \frac{20 * 10^3}{4.727} = 70.52\ minutes \tag{4.3}$$

With a Δt between 35.29 minutes and 70.52 minutes, the order of magnitude of a shift of two timesteps of 30 minutes backwards in time seems to be a reasonable estimate of the shift. Therefore, a -60 minute shift will be used for further analysis.

4.4. Morphology

Elevation measurements are obtained for both case studies. The pre- and post-storm cross-shore profiles are extracted from the data following the described procedure.

4.4.1. Data overview

RealDune-REFLEX

The RealDune-REFLEX morphology measurements are performed with an RTK mounted on a wheelbarrow or on a quad and with a stand-alone RTK. The location of RDx- and RDy-coordinates is measured along with a z-value for the elevation with NAP as the reference datum. The raw measurements contain a point cloud of XYZ values measured. The RealDune-REFLEX measurements are performed almost every day during the period of the measurement campaign. However, not every day the same region or path has been walked. For most days, at least the pre-defined transect along Dune 1 and Dune 2 was measured from the dune foot towards around -1 +m NAP. At two moments, an extensive survey was performed with a large density of points in the point cloud. These datasets were used to complete the cross-shore profile from the dune foot towards behind the dune as was assumed that the dune was almost untouched behind the dune foot.

Land Reclamation Philippines

The XYZ measurements for LRP are in UTM region 51N and are measured with SBES for the wet elevations and with a drone for the dry elevations. These measurements are pre-combined and interpolated to a 1x1 grid by the surveyors on site. The reference datum for the elevation is LAT. The elevations of LRP are transformed from LAT to MSL to compare with the water level elevations. The site-specific value for the relation of LAT to MSL is -1.04 (Figure 3.8).

4.4.2. Data transformation

The point cloud GPS data points were processed using a Python-based program (griddata) from 3D XYZ measurements to 2D cross-shore profiles by linear interpolation. The results of the interpolation process are evaluated for potential errors. Due to irregularities in measurement locations and potential deviations from an ideal 2D cross-shore profile, these data points must be transformed to align with a specified, predefined transect. The landward boundary is defined on the right and the seaward boundary on the left. Around the defined transect, a polygon of 2 meters wide (1 meter at each side of the transect) is cut off and only the points inside the polygon remain. This makes sure no far-away points are used for the interpolation. GPS coordinates were interpolated linearly to the defined transects with 10 grid points per meter ($\Delta y = 0.1\ m$). The procedure is schematised in Figure 4.9.

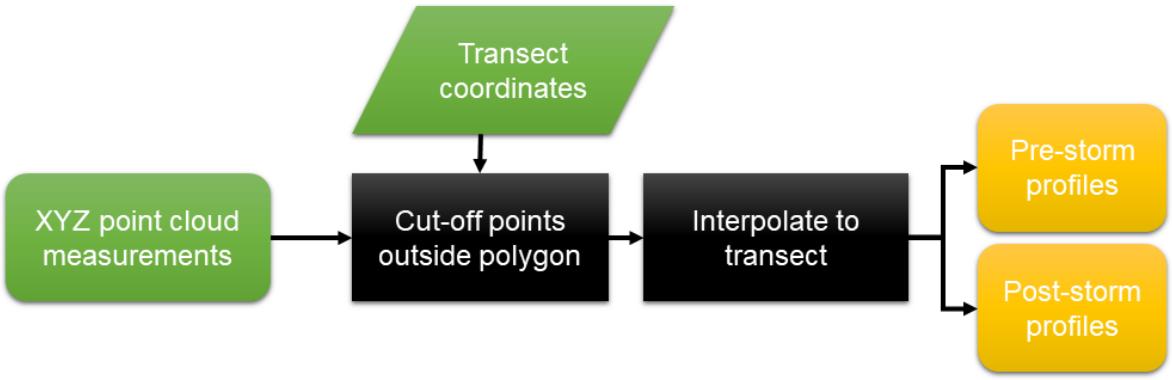

Figure 4.9: Flowchart for the methodology regarding the morphology. Morphological input: green. Process: black. Output: yellow.

4.4.3. Data results

The morphological output for the two locations is:

- Pre- and post-storm cross-shore profiles at pre-defined transects

4.5. Parametrisation

The parameters of interest are each calculated following a specific procedure. An overview of how they relate within a cross-shore profile is provided (Figure 4.10).

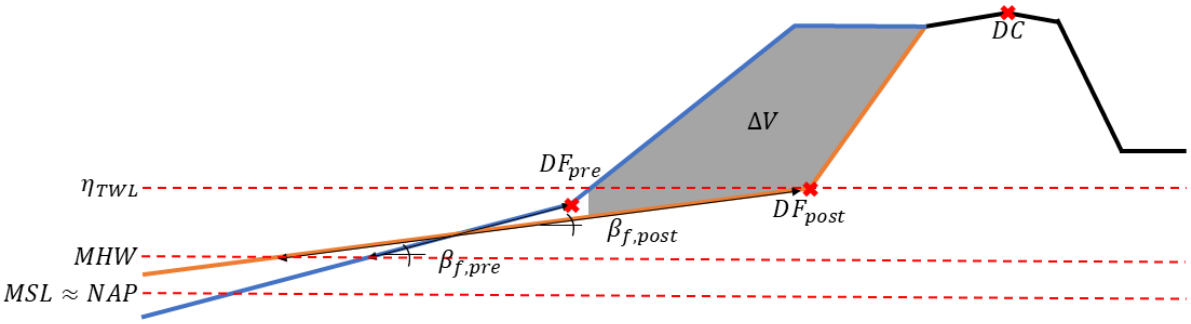

Figure 4.10: An overview of a cross-shore dune profile with the parameters of interest for this study. Subscript 'pre' corresponds to the pre-storm parameter and the subscript 'post' to the post-storm parameter.

4.5.1. Dune foot position

The definition for the dune foot in this research is based on the morphological characteristic of the position of maximum curvature of the cross-shore profile. An adjusted method of the second derivative method of Diamantidou et al. (2020) (Section 2.3.2) is used to extract the dune foot position from the cross-shore profile.

Assuming the landward boundary is on the right and the seaward boundary is on the left, all points right of the dune crest and left of the MHW crossing are dropped. Within this region of interest, the first derivative is calculated over the cross-shore profile using a gradient function which is second-order accurate central differences. All points with a first derivative (slope) lower than 0.001 are removed to drop all flat stretches. Then, the second derivative (rate of change of slope) is calculated using a gradient function over the remainder of the first derivative and all points which have a lower value for the second derivative than 0.01 are dropped as recommended by Diamantidou et al. (2020). The most seaward local maximum above a threshold height of 0.1 of the second derivative is taken as the dune foot position. This cross-shore location is interpolated to the cross-shore profile to get the elevation of the dune foot.

The dune foot position is calculated for the pre-storm profile and for the post-storm profile. With these two locations, the change in the z-direction and the x-direction can be calculated for each storm period.

4.5.2. Volume change

Dune erosion is a phenomenon that can be characterized using several metrics, including eroded volume (measured in m^3/m or m^2/m), crest retreat (measured in m/m), and foot retreat (measured in m/m). The dune volume change is taken as the difference in area between the pre- and post-storm profile between the vertical boundaries of the crossing with the maximum total water level in the storm period and the dune origin (defined at the landward boundary). This method is used as it can handle a variety of slopes and is not dependent on the dune foot position.

To calculate the volumes of erosion and deposition, we integrate the profile difference over the appropriate areas using a spacing of 0.1 meters between data points. The resulting values are expressed in units of m^3/m. This methodology allows us to accurately quantify changes in dune volume and understand the dynamics of erosion and deposition in a coastal environment.

4.5.3. Foreshore slope

The foreshore slope, denoted as β_f, is an important parameter that describes the region of significant swash activity on the beach. In the study conducted by Stockdon et al. (2006), the region of swash activity was defined as the area between $\bar{\eta} \pm 2\sigma$, where $\bar{\eta}$ is the mean water level and σ is the standard deviation of the continuous water level signal. However, this definition was insufficient for regimes of collision and overwash in hurricanes, as described by Stockdon et al. (2007). Therefore, an adjusted definition as described by Stockdon et al. (2007) is used in this study.

The upper threshold of the swash region is limited at the dune foot and the lower threshold is the crossing with the MHW line as suggested by Stockdon et al. (2007). In situations where the dune foot is not found properly. The upper threshold becomes the maximal measured water level elevation (without runup) in the storm. The lower threshold remains the MHW line. Mean High Water (MHW) is the average height of all high tides. It is calculated by taking the mean of all the peak values of the water level elevation signal with certain spacing between two peaks. This is performed to take only one high water peak per tidal cycle. The foreshore slope is the best-fit slope over this region between the dune foot and MHW. The line which results in the lowest RMSE is taken as normative.

To quantify the runup, it is assumed that the foreshore slope changes linearly in time due to the hydrodynamic conditions from the pre-storm measurement towards the post-storm measurement.

4.5.4. Wave runup

The η_{TWL} consists of four components as described by Equation (2.10). The influence of the water level setup and the wave swash and runup is parameterized to quantify the storm impact. The influence of the total water level on the dune foot position is studied by taking an approximation of the total water level. This approximation is based on the empirical parametrisation of the maximum runup elevation defined by Stockdon et al. (2006). Herewith, Equation (2.10) can be reduced with field measurements to Equation (4.4) where R_2 is the 2% exceedance value of the runup peaks on natural beaches

$$\eta_{TWL} = \underbrace{\eta_{ast} + \eta_{win}}_{\eta_{act}} + \underbrace{\eta_{wav} + \eta_{swa}}_{R_2} \tag{4.4}$$

The actual water level η_{act} is the water level elevation which can be measured outside the region where wave setup and setdown are present. The formulation for $R2\%$ is defined by Stockdon et al. (2006) as Equation (2.11). With the foreshore slope β_f, deep water wave height H_0 and deep water wave length L_0. An exception is made by Stockdon et al. (2006) only for extremely dissipative beach conditions where $\xi_0 < 0.3$. Here, the parametrization is $R_2 = 0.043(H_0 L_0)^{1/2}$. However, these dissipative conditions were not present in this research. For a better comparison, the deep water wave characteristics H_0 and L_0 are used in the formulation. Hence, the instrument measurements were reverse-shoaled to deep water equivalent conditions using linear wave theory and a shore normal approach (Section 2.4.2). This procedure, however, neglects refraction, diffraction, white-capping, friction and local generation (Stockdon et al., 2006). The procedure follows by finding a shoaling factor K_{sh} to calculate the deep water equivalent of the measured wave height. The intermediate water parameters are divided by the deep water equivalents (subscript 0).

$$H_0 = \frac{H_{m0,meas}}{K_{sh}} = H_{m0,meas} * \sqrt{\frac{c_g}{c_{g,0}}} = H_{m0,meas} * \sqrt{\frac{n * c}{\frac{1}{2} * c_0}} \tag{4.5}$$

To calculate the wave number k, the linear dispersion relation is rewritten to solve for wavelength L. The linear dispersion relation is implicit and therefore an initial value of L_0 for the wavelength was used to iterate 100 times to approximate the wavelength at intermediate depth. Herewith, the deep water wave height and deep water wavelength are found which are used in the runup formula. The water depth d was varied based on the mean water level elevation and the corrected bed level offset in the time step. To assess the normative conditions for the hydrodynamic conditions, the sum per timestep is taken of the water level and the runup resulting in the total water level η_{TWL} as described in Equation (2.10). To assess the relation of η_{TWL} to the vertical dune foot position, the maximum value $\eta_{TWL,max}$ averaged over 10 minutes (RD) or 30 minutes (LRP) of η_{TWL} is taken to be representative.

4.6. Methodological assumptions

The method used has come with some assumptions. These need to be taken into consideration when the results are analysed. Assumed regarding the hydrodynamical methodology:

- Hydrodynamic conditions are resampled and interpolated to 10 minutes and 30 minutes. Herewith, the average over this period is taken for the hydrodynamic conditions. This could lead to a slight underestimation of the maximum hydrodynamic conditions at the peak of the storm.
- The wave conditions of Land Reclamation Philippines are transformed from the opposite side of the bay to a location close to the land reclamation. This encompasses a shift in time and a scaling factor for H_{m0} and T_{m02}. This approximation is validated to be within the limits calculated with linear wave theory and assumed that linear wave theory is valid. However, the precise hydrodynamics in the bay are complex and are not measured to the full extent.
- The wave runup is approximated following the empirical parametrisation of the runup of Stockdon et al. (2006) and requires the deep water equivalent of the wave height and wavelength. The measurements are reverse-shoaled taking only a shoaling factor into account. This procedure, however, neglects refraction, diffraction, white-capping, friction and local generation. Which could be of importance in Manila Bay where Land Reclamation Philippines is located.
- Set-down due to wave breaking was assumed to be negligible as the used water level elevations were not in the breaker zone in contrast with the RBRs.

Assumed regarding the morphological methodology:

- Morphological elevation measurements are interpolated over the pre-defined transect, and therefore certain foreshore, beach or dune features can be averaged out. These are assumed to be negligible to the outcome of the study as morphological features are often averaged out quickly in the storm.
- The foreshore slope (area of significant swash action) runs from MHW and is limited at the dune foot. For periods with lower water level elevation, there could be a limited amount of swash in this area. However, this study is limited to storm conditions where water level elevations rise towards and above the dune foot.
- There is assumed that the foreshore slope changes linearly in time from the pre-storm profile to the post-storm profile. This assumption is made to be able to make a more accurate prediction of the varying runup (and therefore total water level elevation) with the storm conditions.
- No aeolian transport is taken into account in dune volume change as is assumed that this has no significant contribution on the short time scale of this study.

5

Case study RealDune-REFLEX

This chapter focuses on the analysis and results of the measurements done during the RealDune-REFLEX measuring campaign. First, the hydrodynamics during the measurement period are visualised. The hydrodynamics are split into water level elevation and wave characteristics. Then, one of the storms is highlighted and all parameters are described. In Chapter 7, the results of this case study will be highlighted and a comparison with the case study of Chapter 6 will be made.

5.1. Introduction

The RealDune-REFLEX dataset is very suitable for the analysis of the dune foot behaviour in time as the elevation measurements are performed with a daily frequency and therefore the daily timescale influence of the hydrodynamics on the dune foot can be depicted. The measurements are performed for one transect in the middle of Dune 1 and for one transect in the middle of Dune 2 and only alongshore for a few moments in time. Therefore, the alongshore variability of the dune foot behaviour along one dune can not be addressed with this dataset.

5.2. Hydrodynamics

The hydrodynamics are split per storm period and subdivided into intervals where GPS height measurements are performed. Three storms are identified with Storm 2 split up into four periods. A total of six storm periods are defined and measured at low water with a number of high waters in between.

	Begin	End	# High waters
Storm 1	2021-11-06 11:00:00	2021-11-08 13:00:00	4
Storm 2.1	2021-11-30 18:00:00	2021-12-01 07:00:00	1
Storm 2.2	2021-12-01 07:00:00	2021-12-01 19:00:00	1
Storm 2.3	2021-12-01 19:00:00	2021-12-02 08:00:00	1
Storm 2.4	2021-12-02 08:00:00	2021-12-02 17:00:00	1
Storm 3	2022-01-05 09:00:00	2022-01-06 10:00:00	2

Table 5.1: An overview of the identified storms for the RealDune-REFLEX case. Three storms are identified. In Storm 2, the dunes are measured five times resulting in four intermediate storm periods.

5.2.1. Water level elevation

The water level elevation for the entire duration of the measuring period of RealDune-REFLEX is plotted and shows a semi-diurnal tidal cycle and a neap-spring tidal cycle (Figure 5.1). Within the highlighted storm periods, the water level elevation is elevated above the MHW to heights between 2 and 2.5 meters. The tidal signal shows two high and low tides per day.

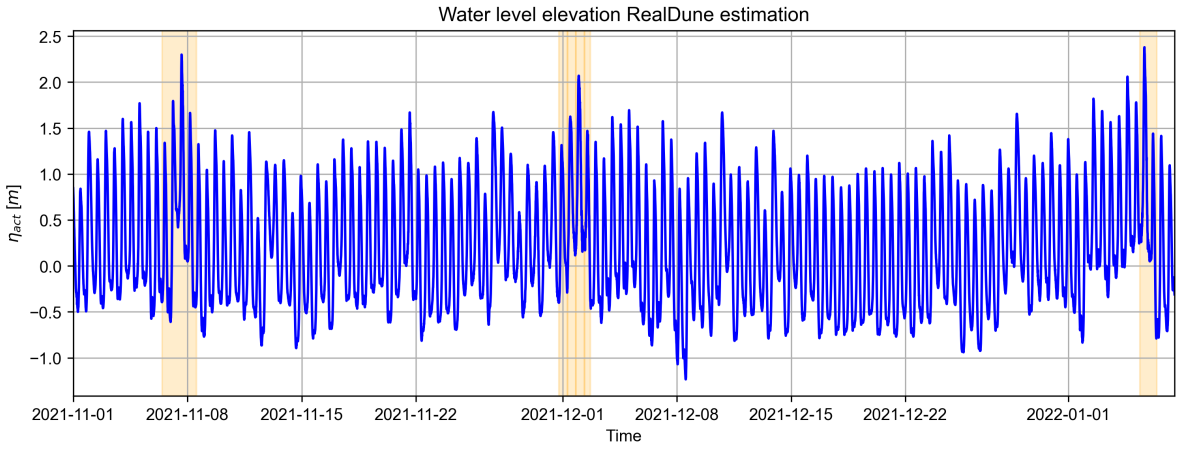

Figure 5.1: Water level elevation overview for the RealDune-REFLEX measurement campaign from 2021-11-01 to 2022-01-07. The storm periods of interest are highlighted in yellow. These periods show an elevated high water peak compared to the MHW.

5.2.2. Wave height, period and direction

The wave characteristics during the entire measurement campaign of RealDune-REFLEX are plotted (Figure 5.2). Within the highlighted storm periods, the wave heights of especially Storm 2 and Storm 3 are elevated to offshore heights of approximately 4 meters.

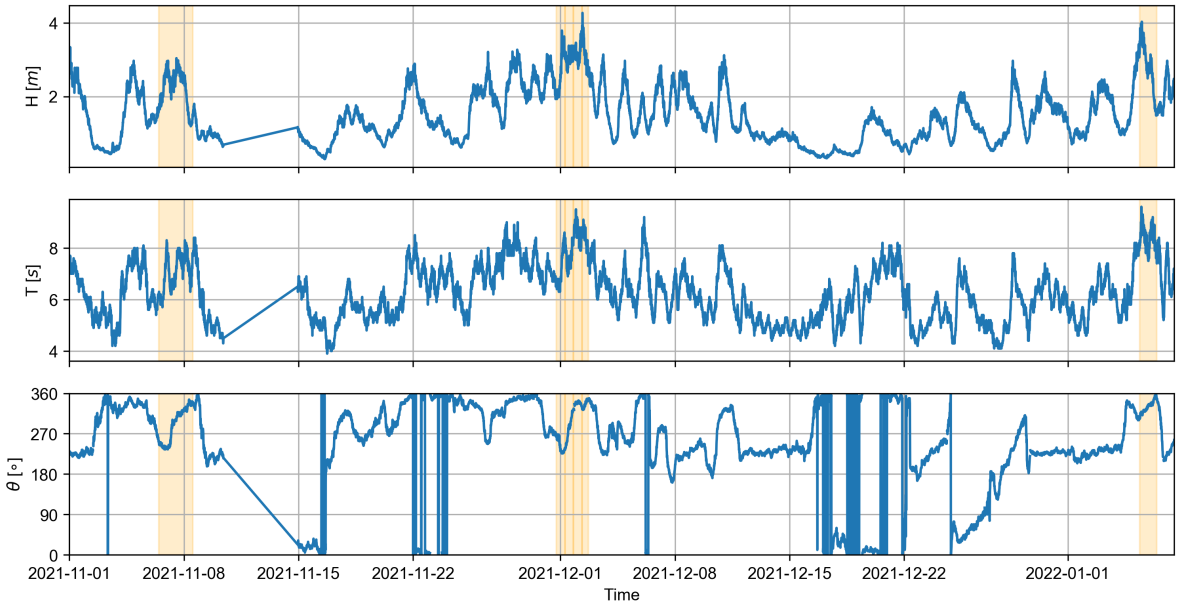

Figure 5.2: Offshore wave height, period and direction overview for the entire measurement campaign of RealDune-REFLEX. Measured at Europlatform with a local depth of approximately 32 meters. The storm periods are highlighted in yellow.

5.2.3. Storm-specific conditions

This section shows the storm-specific hydrodynamics for one high water period of Storm 2.3 in Figure 5.3. Similar plots for the other storm periods are provided and analysed in Appendix D. This overview shows how the water level η varies with one high water. The wave characteristics are shown for this specific storm. Thereafter, the foreshore slope β_f is given based on the before and after measurement of the profile and assumed that the foreshore slope transforms linearly throughout the storm. Herewith, the runup R_2 is calculated following Equation (2.11). Finally, η_{TWL} is calculated as the sum of the measured water level elevation η_{act} and the calculated runup R_2.

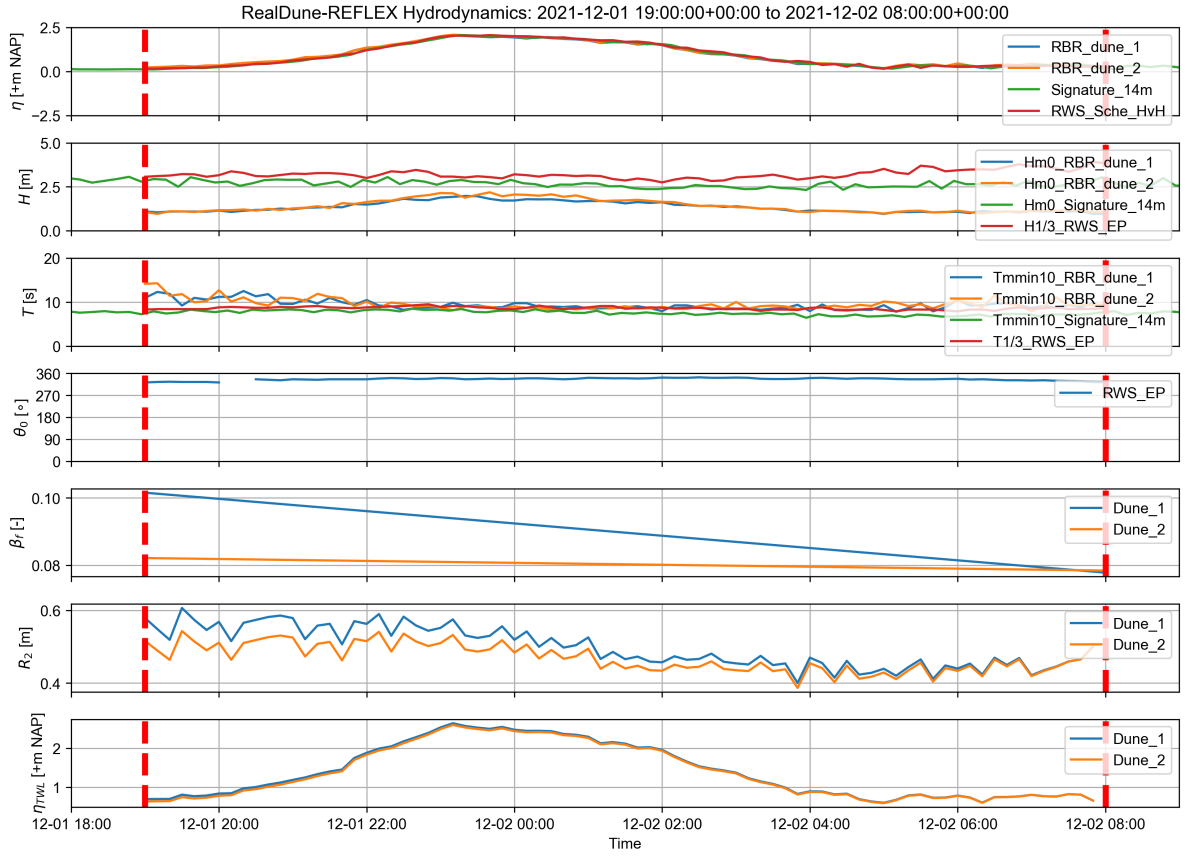

Figure 5.3: The storm-specific RealDune-REFLEX Hydrodynamics for Storm 2.3 of 1-2 December 2021 with bed level measurements on 2021-12-01 19:00 to 2021-12-02 08:00 (red dashed line) for one high water around 23:00. R_2 runup elevations are calculated per time step with H, T and β_f as input. The temporal total water level elevation η_{TWL} is the sum of η and R_2. Offshore wave angle $\theta_0 \approx 340°$.

The actual water level elevation, which is composed of a tide component and a wind setup component, is elevated to a height of approximately 2 +m NAP during the peak of high tide. The wave heights vary between offshore and nearshore. Offshore for the Europlatform and Signature, H_{m0} varies around 3 meters and nearshore for the RBR around 2 meters. For the RBR sensors during the rise of the tide, the wave heights increase and during the fall of the tide the wave heights decrease. This shows that the wave heights at the location of the RBR are already depth limited and the higher waves are already broken. When depth increases, higher waves can reach the RBR sensor. This phenomenon occurs for both Dune 1 and Dune 2. The wave period $T_{m-1.0}$ is approximately 10 seconds at high tide for all sensors. With low water, the $T_{m-1.0}$ of the RBR sensors are elevated. This could be due to the fact that with lower water depths, the shorter waves break more early and a larger fraction of the longer waves remain in the signal.

The initial foreshore slope $\beta_{f,pre}$ between Dune 1 and Dune 2 varies significantly. The post-storm foreshore slope is approximately the same. This results in the runup being slightly higher of the order of 5 cm for Dune 1 compared to Dune 2 at the beginning of the storm. For the calculation of the runup, the offshore wave height, and wave period of the Signature are used. The total water level elevation η_{TWL} follows from the sum of the time series of the water level elevation η and the approximated runup R_2. The maximum total water level elevation is the maximum value in this time domain. For Storm 2.3, $\eta_{TWL,max}$ for Dune 1 is 2.653 meters and $\eta_{TWL,max}$ for Dune 2 is 2.607 meters.

5.3. Morphology

The RealDune-REFLEX dataset is very suitable for morphological analysis over time, as the same dune transect was attacked three times during the measurement campaign. Therewith a developing profile can be observed. This transformation in time is depicted for Dune 1 and Dune 2 (Figures 5.5 and 5.6). For Dune 1 and Dune 2, one cross-shore profile is depicted (Figures 5.7 and 5.8). This pre- and post-storm profile corresponds to the storm hydrodynamics of Storm 2.3 (Figure 5.3). All cross-shore profiles on the predefined transects of RealDune-REFLEX Dune 1 and Dune 2 are provided in Appendix E.

5.3.1. Temporal evolution

In this section, the temporal evolution of RD is highlighted. The top view of the Sand Engine is plotted for two measurements (Figure 5.4). The foreshore bathymetry of RealDune-REFLEX can be observed for this longer period of approximately a month with the respective morphological difference in between. Significant foreshore erosion is found in front of both Dune 1 and Dune 2. Sand bar increase is found around 100 metres from the coast in between the two dune transects.

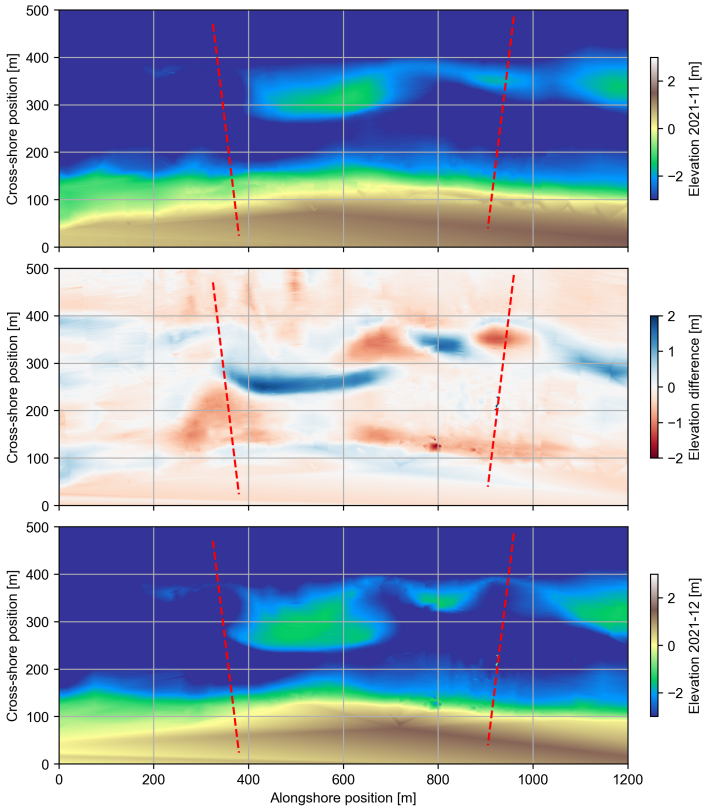

Figure 5.4: Spatial overview of the alongshore and cross-shore position and their respective elevation of RealDune-REFLEX with the shoreline rotated 57 degrees in a clockwise direction. The left dashed red line corresponds with the transect of Dune 1 and the right with Dune 2. (upper panel) SHORE measurement for November. (middle panel) The difference in elevation between these two measurements. (lower panel) SHORE measurement for December.

The dune foot was found to not retreat under a constant slope over the measuring campaign. Instead, the retreat was dependent on the water level elevation and the runup induced by the wave conditions within one storm period. The retreat within one storm period could occur under a certain slope with a threshold (e.g. van Thiel de Vries (2009)). However, the measurement frequency was too low to assess this theory for the case studies in this research. The vertical dune foot position was found to correlate to the maximum total water level elevation. Also for periods where the $\eta_{TWL,max}$ was below the dune foot, the dune foot could reposition downwards which could potentially be related to an out-of-equilibrium upper foreshore slope.

The cross-shore profile of Dune 1 for multiple periods during the measurement campaign is plotted (Figure 5.5). The dune crest was located approximately at 5.5 +m NAP and the hinterland at 4.5 +m NAP. The initial profile shows a gentle slope with no clear inflection point. In time, the dune erodes with a steep scarp and an evident dune foot between the scarp and the foreshore slope. The dune foot translates upwards but also downwards through time. This is different from what dune theory suggests that the dune foot would translate upwards approximately at the maximum water level elevation if the dune is in the collision regime. The profiles show a slightly decreasing bed level in time at the foreshore slope.

The dune foot retreats in the horizontal direction but does not do this under a certain slope as was observed by Bonte and Levoy (2015) within the storm. As these measurements are not measured through the storm but instead at multiple times within three months, it could be hypothesized that the dune foot only retreats under a certain slope for the same storm conditions. For some periods the dune foot stayed approximately at the same position, these occurred for periods where the total water level elevation was below the dune foot and the out-of-equilibrium upper foreshore slope.

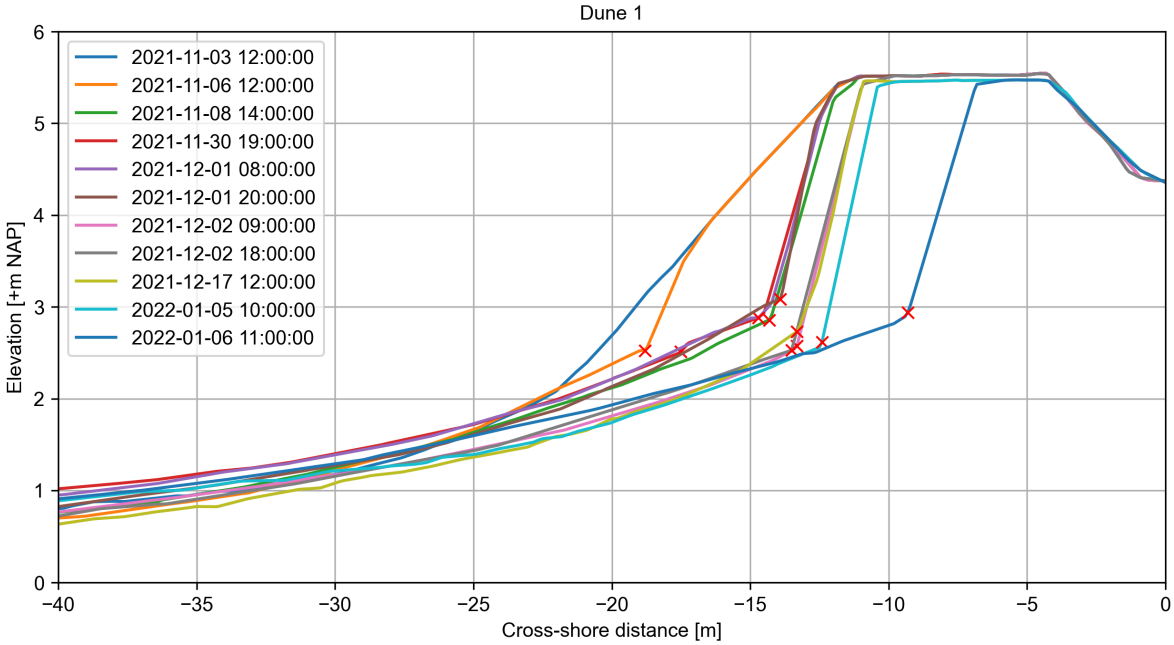

Figure 5.5: The cross-shore profiles for RealDune-REFLEX Dune 1 for all the defined storm periods within the measuring campaign. The cross-shore distance is plotted against the elevation of the profile. The lower profile reaches approximately 1 +m NAP. The dune foot position is depicted with a red cross for each dune profile. The dune foot could not be found on the profile of 2021-11-03 at 12:00.

The cross-shore profile of Dune 2 for multiple periods during the measurement campaign is plotted (Figure 5.6). The dune crest was located approximately at 5.5 +m NAP and the hinterland at 3 +m NAP. No dune foot could be found for the initial profile with a gentle slope. The dune retreats with a starting scarp and follows in time with a similar steep scarp as Dune 1.

Significantly more erosion is observed for Dune 2 compared to Dune 1 and therefore significantly more horizontal dune foot translation. For measurement at 2022-01-06 11:00 shows that the dune eroded almost entirely, giving rise to the overwash regime. Overwash was also observed for this period during the measurement campaign. The waves approach under a more developed foreshore for Dune 1 for the majority of the storms (NW/NNW) and therefore Dune 2 is more exposed than Dune 1 (Figure 5.4). Significantly more bed level lowering of the foreshore slope was observed for Dune 2 ($\Delta z \approx 0.8\ m$) compared to Dune 1 ($\Delta z \approx 0.5\ m$) at the initial base of the dune.

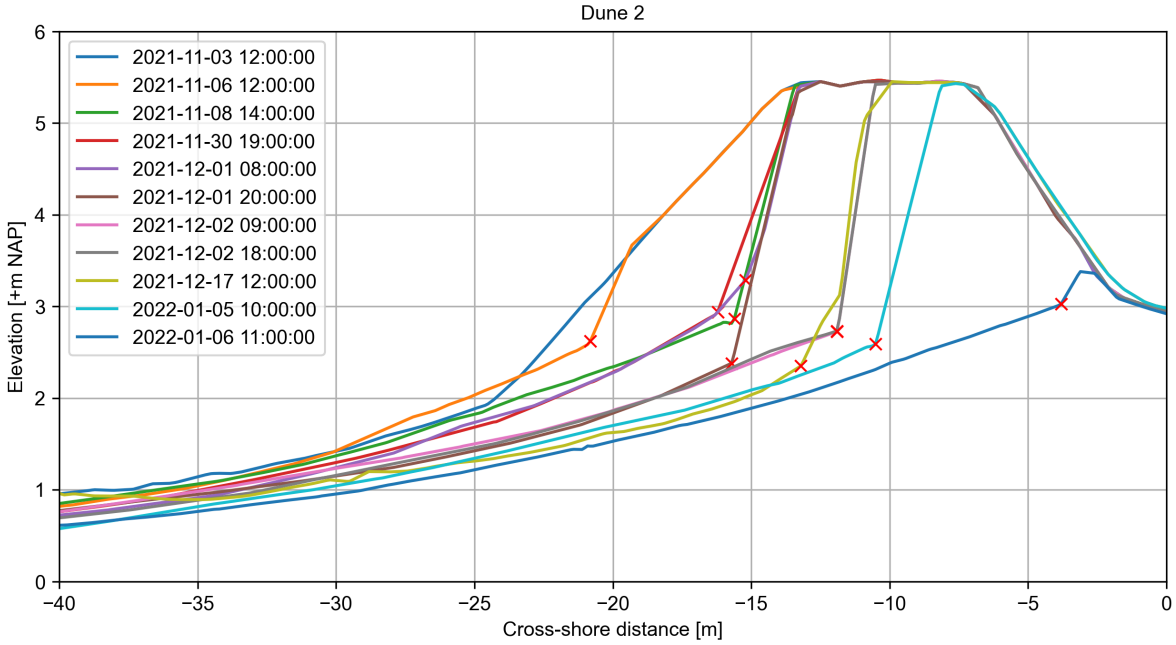

Figure 5.6: The cross-shore profiles for RealDune-REFLEX Dune 2 for all the defined storm periods within the measuring campaign. The cross-shore distance is plotted against the elevation of the profile. The lower profile reaches approximately 1 +m NAP. The dune foot position is depicted with a red cross for each dune profile. At the profile of 2021-11-03 at 12:00 the dune foot could not be found. The dune profile of 2022-01-06 11:00 is almost completely eroded and was subject to overwash.

5.3.2. Cross-shore profile Dune 1

From all cross-sections of Dune 1, Storm 2.3 is highlighted (Figure 5.7) which corresponds with the storm conditions of Figure 5.3. For this period, $\eta_{TWL,max}$ was lower than the initial dune foot elevation of Dune 1. Hence, the swash regime would be governing. However, significant erosion of the dune face through avalanching was observed by the field campaign crew.

The post-storm dune foot $DF_{z,post}$ position corresponds neatly to the $\eta_{TWL,max}$ and suggests that the dune foot can also translate downwards when the dune foot elevation is not exceeded. The pre-storm foreshore slope of Dune 1 shows an offset compared to the best-fit slope. A significant decrease through the storm in slope was observed (Figure 5.3) which corresponds with the bed lowering (Figure 5.7). The presence of a non-equilibrium upper foreshore slope during storm events may cause sediment of the foreshore to be transported offshore or alongshore via swash motion, prompting the profile to adjust toward an equilibrium slope.

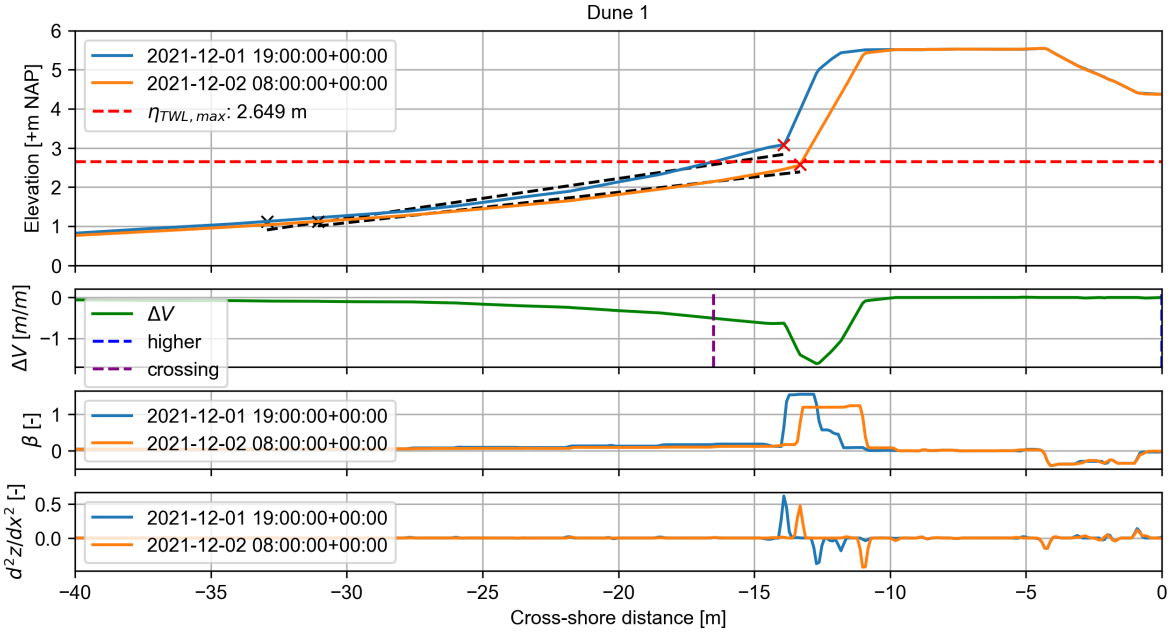

Figure 5.7: Cross-shore profile for Storm 2.3 of Dune 1 with post-storm dune foot at approximately $\eta_{TWL,max}$. The blue line corresponds to the pre-profile and the orange line to the post-profile. The post-storm dune foot DF_{post} is lowered compared to the pre-storm dune foot DF_{pre}. The black dashed lines represent the foreshore slopes β_f. (2nd panel) Volume change. (3th panel) Plot of the first derivative (slope β). (4th panel) Plot of the second derivative (rate of change of slope) with dune foot at the seaward maximum.

The $DF_{z,post}$ for all transects with significant erosion corresponds approximately to $\eta_{TWL,max}$ (Appendix E). A slight offset is found for Dune 2 over Storm 2.2. In this period, the bed lowered and the dune foot translates downward ($DF_{z,post} = 2.380\ m$) but remains 30 cm above $\eta_{TWL,max} = 2.081\ m$. This could potentially be explained by the fact that the slope did not reach equilibrium within the duration of the high water.

5.3.3. Cross-shore profile Dune 2

A cross-shore profile for the same storm conditions of Storm 2.3 as described (Figure 5.3) and previously shown for Dune 1 (Figure 5.7), is provided for Dune 2 (Figure 5.8). An exceedance of the dune foot level has led to significantly more erosion over this period than for Dune 1. The erosion led to a dune foot repositioning backwards and upwards corresponding to approximately η_{TWL}.

It is remarkable to observe that for the same storm conditions, the dune foot could lower at Dune 1 and decrease at Dune 2. This could be explained by an out-of-equilibrium upper foreshore slope as negligible lowering of the bed can be observed compared to Dune 1. The $\eta_{TWL,max}$ of Dune 1 is approximately 5 centimetres higher as the foreshore slope is steeper resulting in a higher estimated runup elevation.

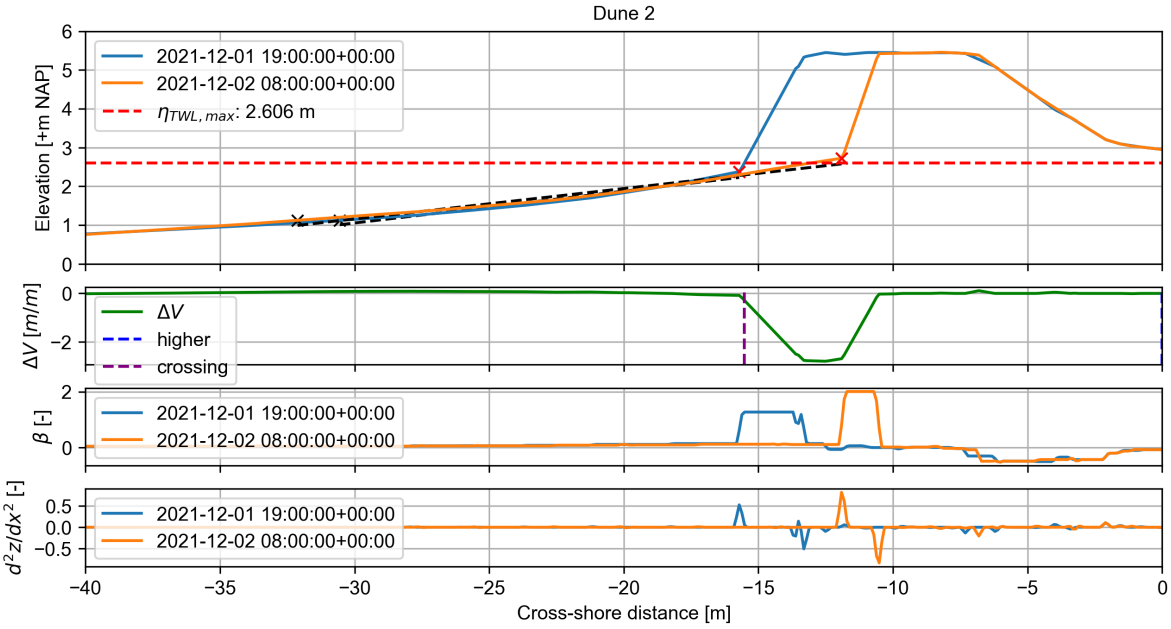

Figure 5.8: Cross-shore profile for Storm 2.3 of Dune 2 with the post-storm dune foot at approximately η_{TWL}. The blue line corresponds to the pre-profile and the orange line to the post-profile. The black dashed lines represent the foreshore slopes β_f. (2nd panel) Volume change. (3th panel) Plot of the first derivative (slope β). (4th panel) Plot of the second derivative (rate of change of slope) with dune foot at the seaward maximum.

5.4. General conclusions

Based on the results of the RealDune-REFLEX dataset analysis, can be concluded that the dune foot can translate upwards and downwards in the same storm for different dunes, reaching approximately the estimated $\eta_{TWL,max}$ in both dunes. Significant bed lowering near the dune can be observed for both dunes, giving rise to the idea of an out-of-equilibrium slope in the upper foreshore slope. This could induce dune erosion and downward dune foot translation in the swash regime. Small to negligible erosion quantities were observed for storm periods where the $\eta_{TWL,max}$ reached far below the initial dune foot position $DF_{z,pre}$ and the upper foreshore slope.

Significantly more dune erosion and subsequent horizontal dune foot change are observed for Dune 2 than for Dune 1 in the same period under approximately the same offshore and nearshore wave conditions excluding orientation and foreshore. The dune foot does not translate under a certain slope in different storms.

6

Case study Land Reclamation Philippines

6.1. Introduction

The Land Reclamation Philippines dataset is very suitable for analysis in space as the elevation measurements are performed over the entire side slope of the land reclamation, compared to RealDune-REFLEX where only one transect is measured for both dunes. This gives the opportunity to study the dune foot behaviour in the alongshore direction under the same hydrodynamic conditions, wave angle and sediment size.

6.2. Hydrodynamics

The hydrodynamic conditions for Land Reclamation Philippines are provided for a longer period for the water level elevations and wave conditions. The storm-specific parameters during Typhoon Nalgae (highlighted in yellow) are combined and provided in an overview.

6.2.1. Water level elevations

The water level elevations close to the reclamation site are measured with a tide gauge. The start date of the measurements is 2022-08-12 at 06:00:00 to 2022-11-24 at 07:36:00. The typhoon period is highlighted in yellow in Figure 6.1.

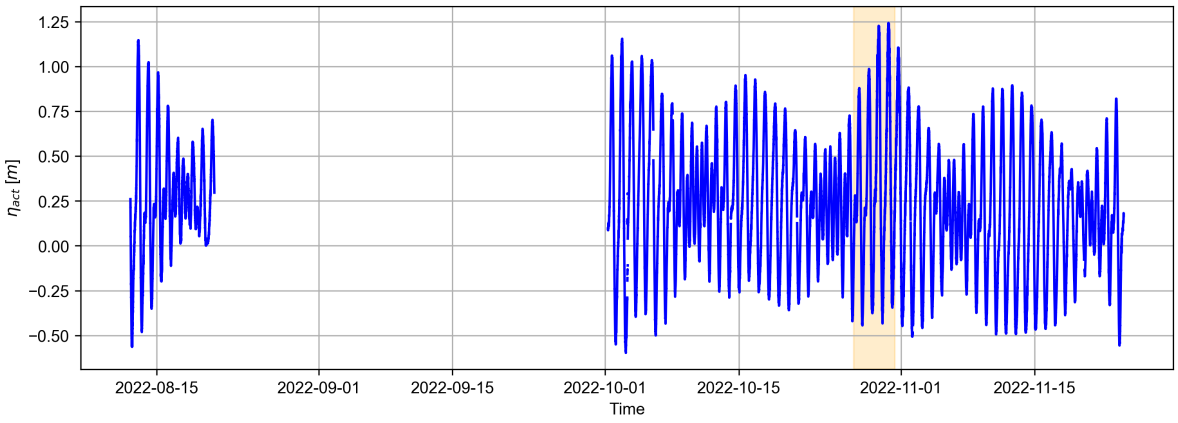

Figure 6.1: The water level elevation for Land Reclamation Philippines measured at the tide gauge at LRP. The time series reaches from 2022-08-12 06:00:00 to 2022-11-24 07:36:00. The almost horizontal line shows a lack of measurements during this period. The typhoon period of interest is highlighted in yellow.

6.2.2. Wave height, period and direction

The wave characteristics of LRP were approximated in Section 4.3 with the transformation of AWAC measurement near MIA to the location of the Waverider near LRP. These wave characteristics are measured with the AWAC from 2021-09-01 01:00:00 to 2022-12-06 23:30:00. The average significant wave heights in this period are low and most of the time do not exceed 0.5 meters (Figure 6.2). In the typhoon storm period, a huge sudden peak of wave height is observed reaching almost 2 meters. The average mean wave periods within this period are of order 4 to 5 seconds.

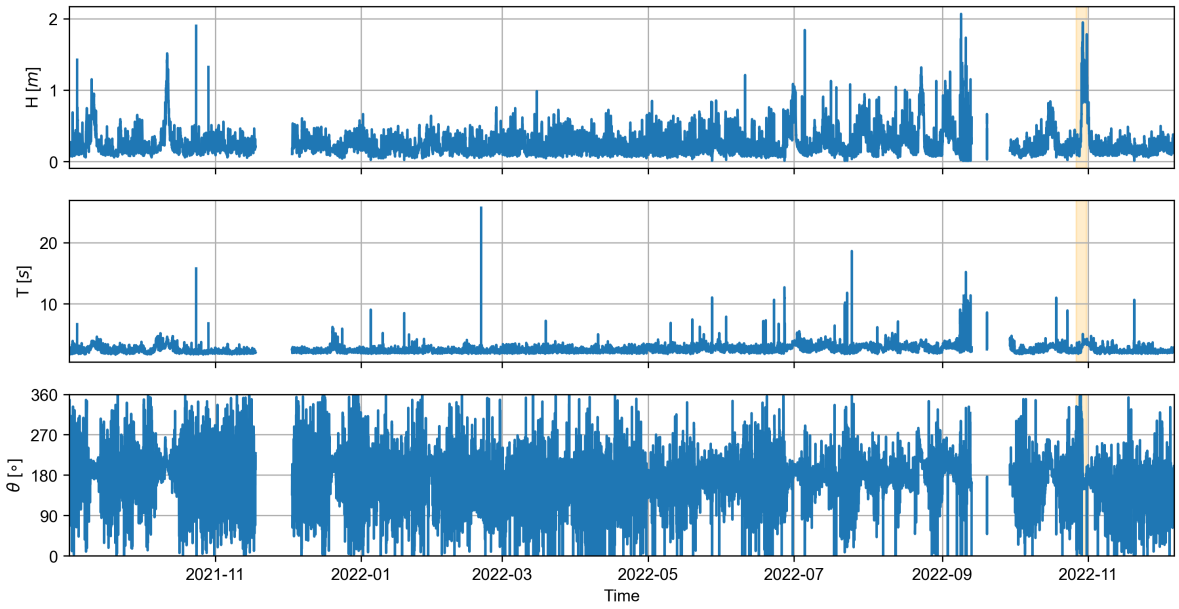

Figure 6.2: An overview of the AWAC wave characteristics H, T and θ of Land Reclamation Philippines. The measurements are shown from 2021-09-01 01:00:00 to 2022-12-06 23:30:00. The typhoon period of interest (Typhoon Nalgae) is highlighted in yellow. This period shows highly elevated wave heights and elevated wave periods.

6.2.3. Storm-specific conditions

The parameters during the typhoon, with slope elevation measurements around approximately 2022-10-27 01:00:00 and 2022-10-31 08:00:00 are processed to correspond with the variation in foreshore slope (Figure 6.3). The estimated peak period of the storm is from 2022-10-28 00:00:00 to 2022-11-01 03:00:00 with the peak of the storm on 2022-10-29 between 16:30 and 17:00. Also, the incomplete measurements of the Waverider (LRP in Figure 6.3) are shown as a reference and for an indication of more accurate wave angles with respect to the shore-normal.

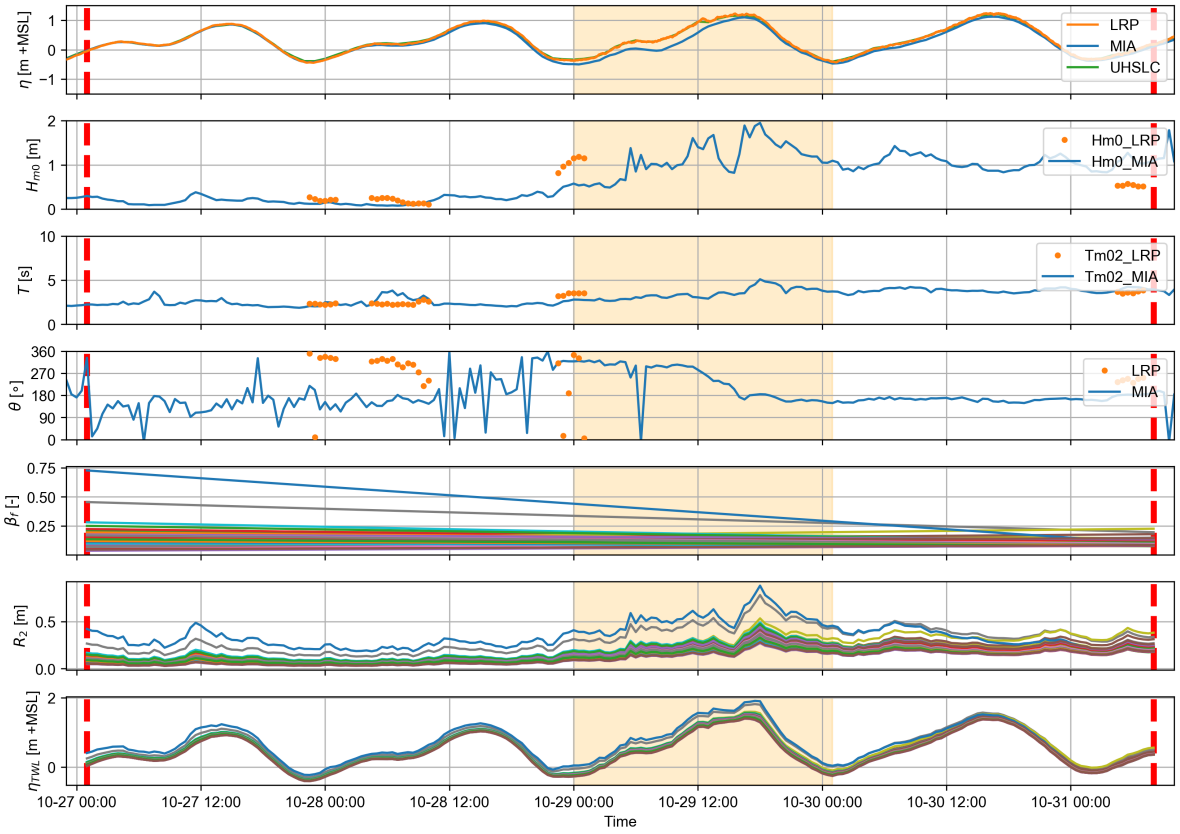

Figure 6.3: The (typhoon) storm-specific hydrodynamics for Land Reclamation Philippines for the period of 2022-10-28 00:00:00 to 2022-11-01 03:00:00. The bed level measurements are performed on 2022-10-27 00:00 to 2022-10-31 07:00 (red dashed line) The peak of the tide coincided approximately with the peak elevation of the wave heights resulting in the peak of the storm on 2022-10-29 between 16:30 and 17:00. The wave characteristics H_{m0}, T_{m02} and β_f are used to estimate the R_2 runup elevations using the formula of Stockdon et al. (2006). (lower panel) The total water level elevation η_{TWL} is found by the sum of the water level elevation and the runup.

At Land Reclamation Philippines, the wave angle is approximately 250 degrees and at MIA the wave angle is approximately 160 degrees. However, significant erosion could have occurred for the period starting around 2022-10-29 at 12:00:00. Here the wave angle commences at estimated 330 degrees turning towards 250 degrees at LRP. In other words, the waves approach more obliquely towards the slope in time. Two outliers of the foreshore slope are defined which are Kp1250 and Kp920 ($\beta_{f,pre} > 0.4$). Of these three transects, the average of the foreshore slope was taken from the two adjacent transects and therewith the maximum total water level elevation is adjusted (Figure 6.5).

6.3. Morphology

The Land Reclamation Philippines morphological measurements are especially suitable for the specific analysis of the dune foot behaviour in the alongshore direction. Along the slope, elevation differences between pre- and post-storm are compared. In this section, three regions of interest are highlighted and an example cross-shore profile is given. These regions are defined as 'severe erosion', 'dune intervention' and 'average erosion'. All the other cross-shore profiles are depicted for reference in Appendix G. The left edge (Kp1410 onwards) of the reclamation site showed significant erosion, however, is not included in this study as the orientation of the coastline with respect to the waves is different and edge effects are expected to be significant.

6.3.1. Alongshore variability

In this section, the alongshore variability of the slope is highlighted (Figure 6.4). The top view of the side slope before and after the storm and the height difference between those measurements provide insights into the morphological development induced by the storm conditions. Before the storm, the side slope shows multiple alongshore variable coastal features. After the storm, these are wiped out. The transition between the beach and the dune is less spread and the beach width is more uniform. The foreshore area shows a net decrease in sediment quantity and it is likely that alongshore transport took account for this loss. Sediment is lost in the cross-shore towards the right edge of the reclamation site (middle panel Figure 6.4). The slope close to the water line experienced severe erosion with up to a 4-meter vertical change. The transects at the left edge of the reclamation site show significantly more erosion than the other transects. This is in line with expectations as the waves were propagating from the west. The fact that this area is more exposed to these waves and the waves approach less obliquely reinforces this hypothesis. Around Kp1200, the difference plot shows a huge dune growth on the slope. It is most likely that the slope is reinforced locally to guarantee the stability of a pipe stockpile (Figure 6.8).

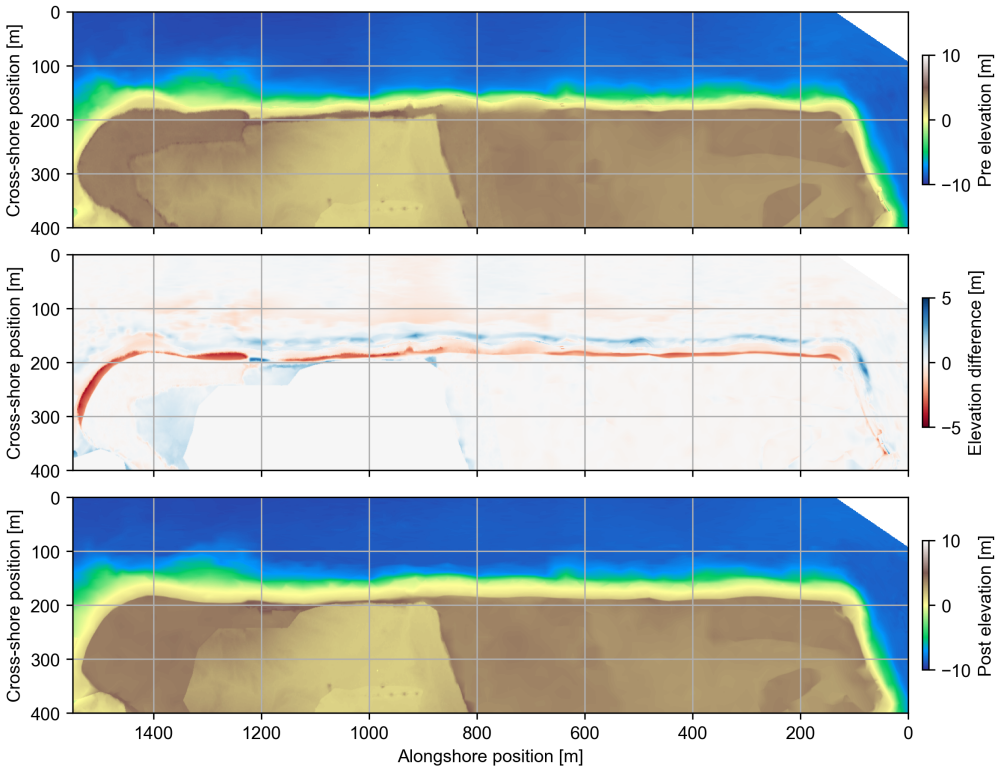

Figure 6.4: The spatial overview of the alongshore and cross-shore position and their respective elevation of Land Reclamation Philippines. (upper panel) Pre-storm elevations. (middle panel) The difference in elevation between the pre- and post-storm elevation. Negative values correspond with erosion quantities and positive values with deposition. (lower panel) Post-storm elevations.

The surface elevation plots are quantified to a certain cross-shore profile in the alongshore direction corresponding to Kp150 to Kp1400 with a spacing of 10 meters in between (Figure 6.5). In total, 126 transects are calculated for Land Reclamation Philippines. As stated before, the slopes can be subdivided into three areas based on their mean erosion quantities. The severely attacked left area exhibits erosion quantities of order two larger than the mean of the other transects. The less exposed areas show erosion quantities of the same order with an alongshore variability of the erosion quantity with interesting slight wiggling erosion quantities. These can be explained by a reset of alongshore variability in the dune and foreshore. The pre-storm elevations show a variety of features and differences in elevations. In the post-storm spatial elevation plot (lower panel Figure 6.4), these features seem to be reset.

Vertical dune foot position
The pre-storm dune foot elevation $DF_{z,pre}$ shows a huge spread in the alongshore direction (3th panel Figure 6.5). Post-storm, less spread can be observed in the dune foot elevation. The initial dune foot elevation seems to have no significant influence on the post-storm dune foot position for these storm conditions where (almost) all alongshore transects were in the collision regime and translated upwards. The approximation for the maximum water level elevation $\eta_{TWL,max}$ using the measured water level elevation with the additional runup with the formulation of Stockdon et al. (2006) corresponds very well with the post-storm dune foot elevation $DF_{z,post}$. The average offset is +8 cm, meaning the dune foot is on average positioned 8 cm higher than the approximated maximum total water level elevation. For this case study, the $\eta_{TWL,max}$ did not vary significantly alongshore. When huge differences in foreshore slope are found, greater differences in runup elevation can be found and therefore a more spread dune foot elevation.

Horizontal dune foot position
The variation of the initial horizontal dune foot position $DF_{x,pre}$ of individual transects towards adjacent transects is greater than the variation of the post-storm horizontal dune foot position $DF_{x,post}$ (2nd panel Figure 6.5). This can be explained by minor coastal features being wiped out by storm conditions. The post-storm horizontal position of the dune foot shows dependency on the initial horizontal dune foot position as major alongshore variations remained and protruding stretches of the order of approximately 100 metres and longer were not averaged out. The horizontal dune foot change could be a quantification of the degree of erosion and shows some correlation with the volume change ΔV (lower panel Figure 6.5). This can be observed at Kp410 to Kp450 compared to Kp150 to Kp410. For the transects around Kp800, the initial dune profile was less developed and no significant scarp and dune foot was found.

Foreshore slope
The variability of the initial foreshore slope $\beta_{f,pre}$ is greater compared to the post-storm foreshore slope $\beta_{f,post}$. This reinforces the finding of a morphological reset. On average $\beta_{f,post}$ is more gentle and is in line with the equilibrium dune theory of Vellinga (1986) that the initial (severe out-of-equilibrium) profile moves towards an equilibrium shape ($\beta_{f,pre} > \beta_{f,post}$). For nearly all transects this was reached by a lowering of the foreshore bed as the sediment was deposited lower in the profile or transported alongshore (Figure 6.4). The foreshore slope was found to be of influence within the runup elevations and is therefore able to induce alongshore variations in dune foot (re)positioning.

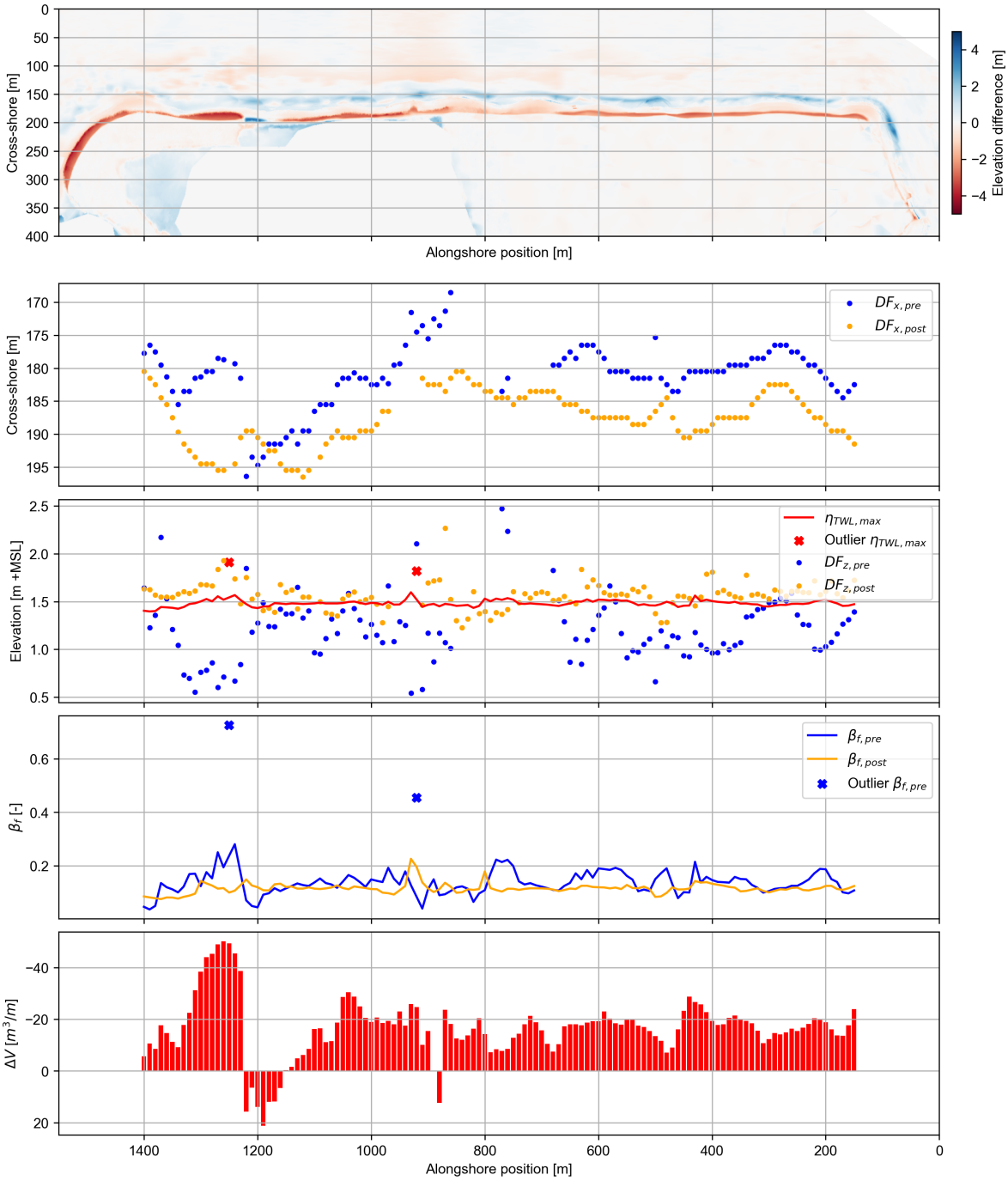

Figure 6.5: Overview of dune foot, foreshore slope and dune volume change measurements. (upper panel) Plot of the spatial differences in pre- and post-storm elevation. (middle panels) For each transect spaced 10 meters apart, the parameters of interest $DF_{x,pre}$, $DF_{x,post}$, $DF_{z,pre}$, $DF_{z,post}$, η_{TWL}, $\beta_{f,pre}$, and $\beta_{f,post}$ are calculated. (lower panel) Resulting dune volume change ΔV.

6.3.2. Cross-shore profiles

Severe erosion (Kp1400 to Kp1230)

Severe erosion is observed for the range of cross-shore profiles Kp1310 to Kp1230 (Kp1300 in Figure 6.7). Here, significantly more erosion up to an order two higher per transect is calculated. These profiles were subject to 10-15 metres of horizontal dune foot retreat and around one metre of vertical dune foot change. The initial foreshore slope was relatively steep and led to (relatively to the other transects) elevated estimated runup values. Pre-storm, this dune front protrudes relative to the adjacent transects. Therefore, this area was slightly more exposed resulting in larger erosion quantities.

(a) 2022-10-29 (b) 2022-11-03

Figure 6.6: Left edge of the reclamation site and section with severe erosion for the Land Reclamation Philippines site. Cross-shore profiles Kp1310 to Kp1230 are located on the left side around the land edge.

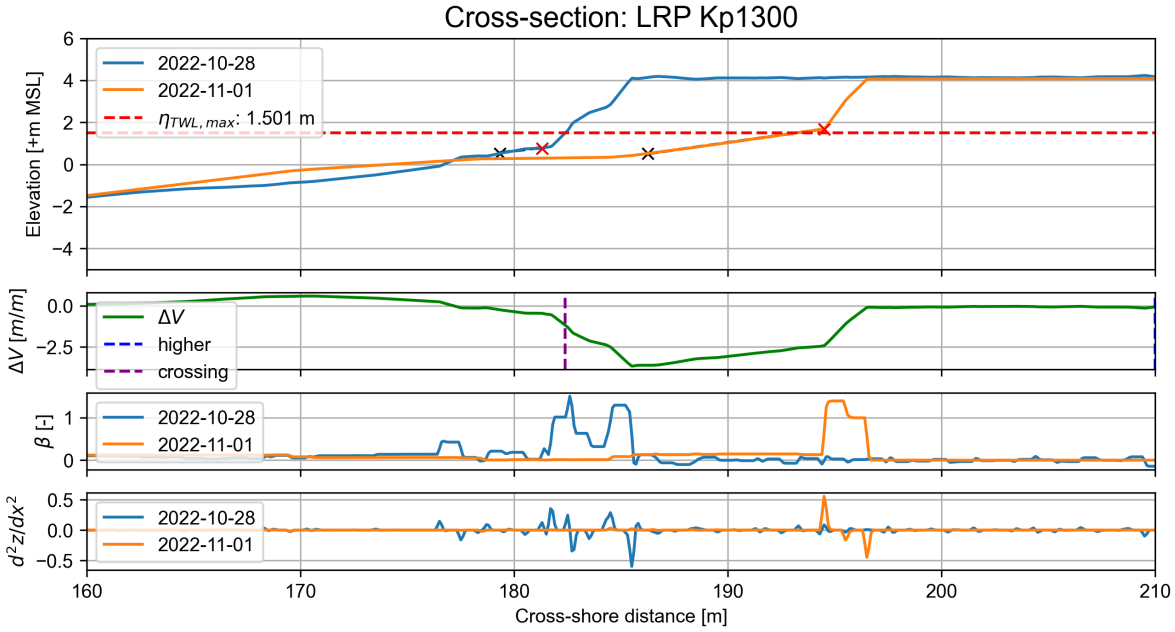

Figure 6.7: Cross-shore profile of LRP Kp1300 in the region 'severe erosion'. The dune foot retreated by 13.2 meters and translated upwards by 0.92 meters. The $\eta_{TWL,max}$ was very slightly below the post-storm dune foot elevation. The foreshore slope is narrow for the pre-storm profile and wide for the post-storm profile. (2nd panel) The plot of the volume change. The area between 'higher' and 'crossing' is defined as the dune volume change.

Dune intervention (Kp1220 to Kp1060)
Huge dune progradation is observed for Kp1220 to Kp1180 (Kp1200 in Figure 6.9). Here, the back slope and hinterland of the dune also show some growth. It is likely that sediment is added to the area Kp1220 to Kp1060 of the slope between the two elevation measurements by means of anthropogenic intervention. It is most likely that the intervention was performed just after the pre-storm measurements as the dune foot is located around $\eta_{TWL,max}$ and huge sediment increases are observed in the profile below MSL. This sand probably originates from the dune face of these transects or originates from the updrift area where severe erosion is observed. Photographs of the difference between the pre- and post-storm reinforce this theory. It could be observed that the land reclamation has a pipe stockpile with a protruding dune in front (Figure 6.8).

(a) 2022-10-29 (b) 2022-11-03

Figure 6.8: Photos providing evidence for the human intervention at a certain segment of Land Reclamation Philippines. (left) Situation before the typhoon. (right) Situation after the typhoon.

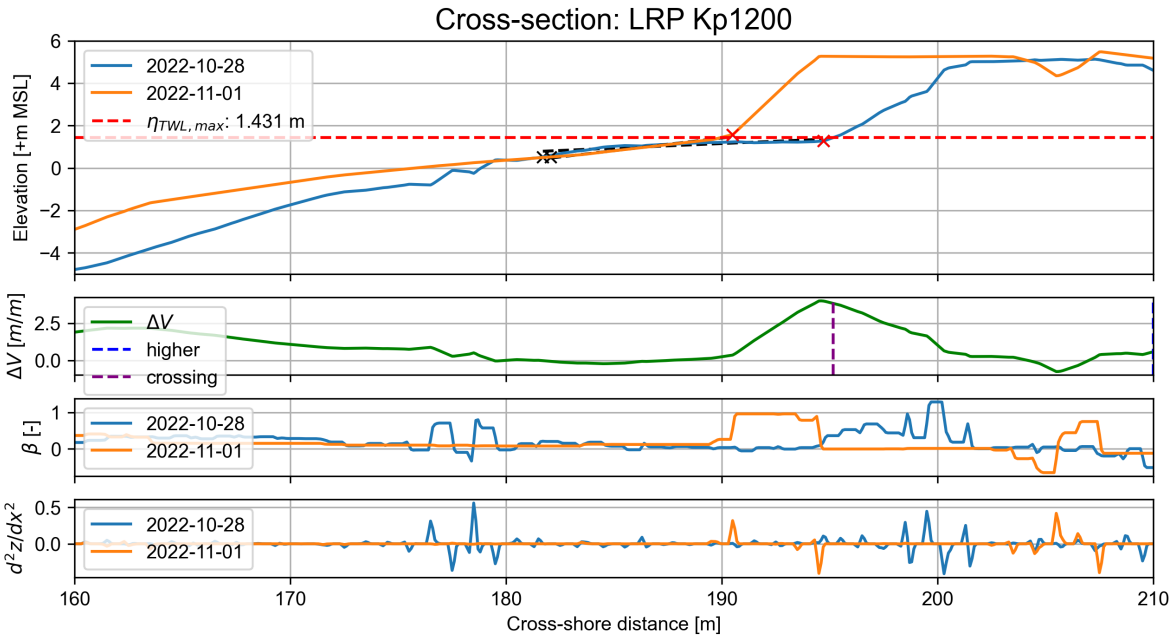

Figure 6.9: Cross-shore profile of LRP Kp1200. The transect shows huge dune progradation which cannot be related to the storm hydrodynamics.

Average erosion (Kp1050 to Kp150)
For the remainder of the transects, excluding the regions mentioned above and the regions close to the edges of the reclamation site, erosion quantities close to an average were observed. The cross-shore profile Kp600 is an example of this region. In this region, the pre-storm dune foot is exceeded and the post-storm dune foot is slightly above $\eta_{TWL,max}$ for almost all of the transects. For approximated region Kp900 to Kp650, initial dune foot positions were undefined as the dune slope was gentle and no significant initial scarp was present. Therefore, it is unable to assess this area on the influence of the initial dune foot position.

(a) 2022-10-29 (east to west)

(b) 2022-11-03 (west to east)

Figure 6.10: Section with average erosion for the Land Reclamation Philippines site. This section reaches from Kp1050 to Kp150.

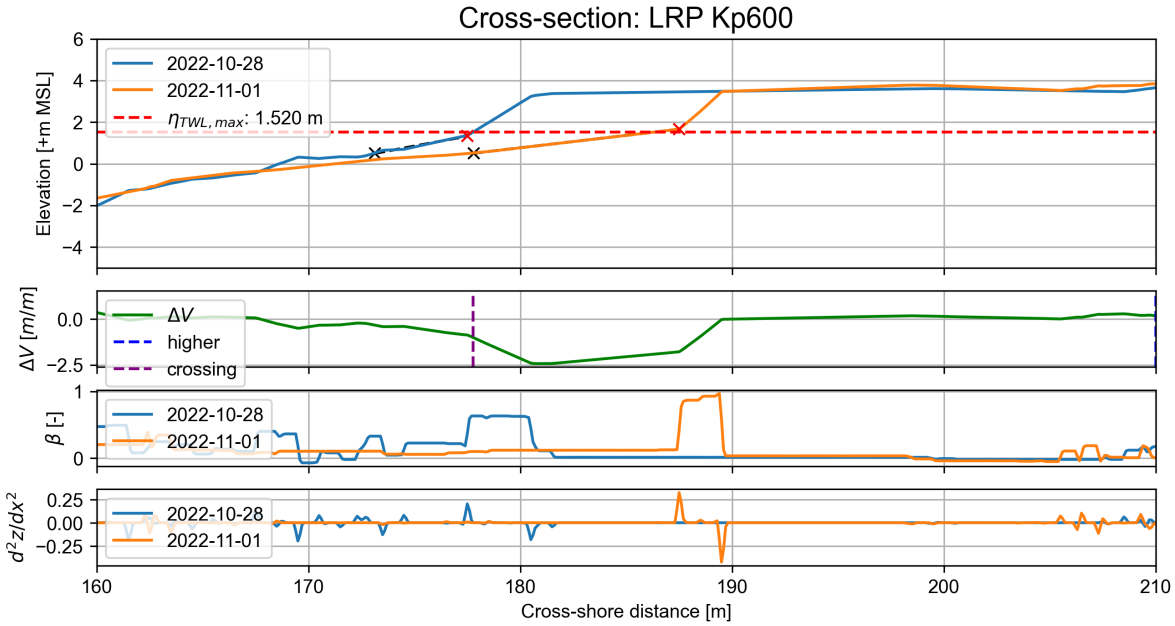

Figure 6.11: Cross-shore profile of LRP Kp600. The transect shows average dune erosion compared to the other transects of Land Reclamation Philippines.

6.4. General conclusions

Based on the results of the Land Reclamation Philippines dataset analysis, three main areas can be distinguished within this dataset: severe erosion, dune intervention and average erosion. Where the area of average erosion comprises the majority of the transects. Deviations from this mean can be related to minor coastal features. Lowering of the foreshore bed was observed for nearly all transects to move towards the erosion profile. More alongshore variability is found for the initial foreshore slope relative to the post-storm foreshore slope. For the majority of transects, the foreshore slope flattened.

Upward translation of the dune foot is found for the majority of the transects. The post-storm dune foot elevation is located at the maximum total water level elevation $\eta_{TWL,max}$ ($\eta_{act} + R_2$) with an average offset of +8 cm. More alongshore variability is found in both the pre-storm vertical and horizontal dune foot positions relative to the post-storm positions. The post-storm dune foot is rather independent of the pre-storm dune foot for these storm conditions and the initial dune profile. Moreover, the post-storm dune foot position is found to be dependent on the initial horizontal dune foot position, which can be related to the presence of major alongshore variabilities.

III

Synthesis

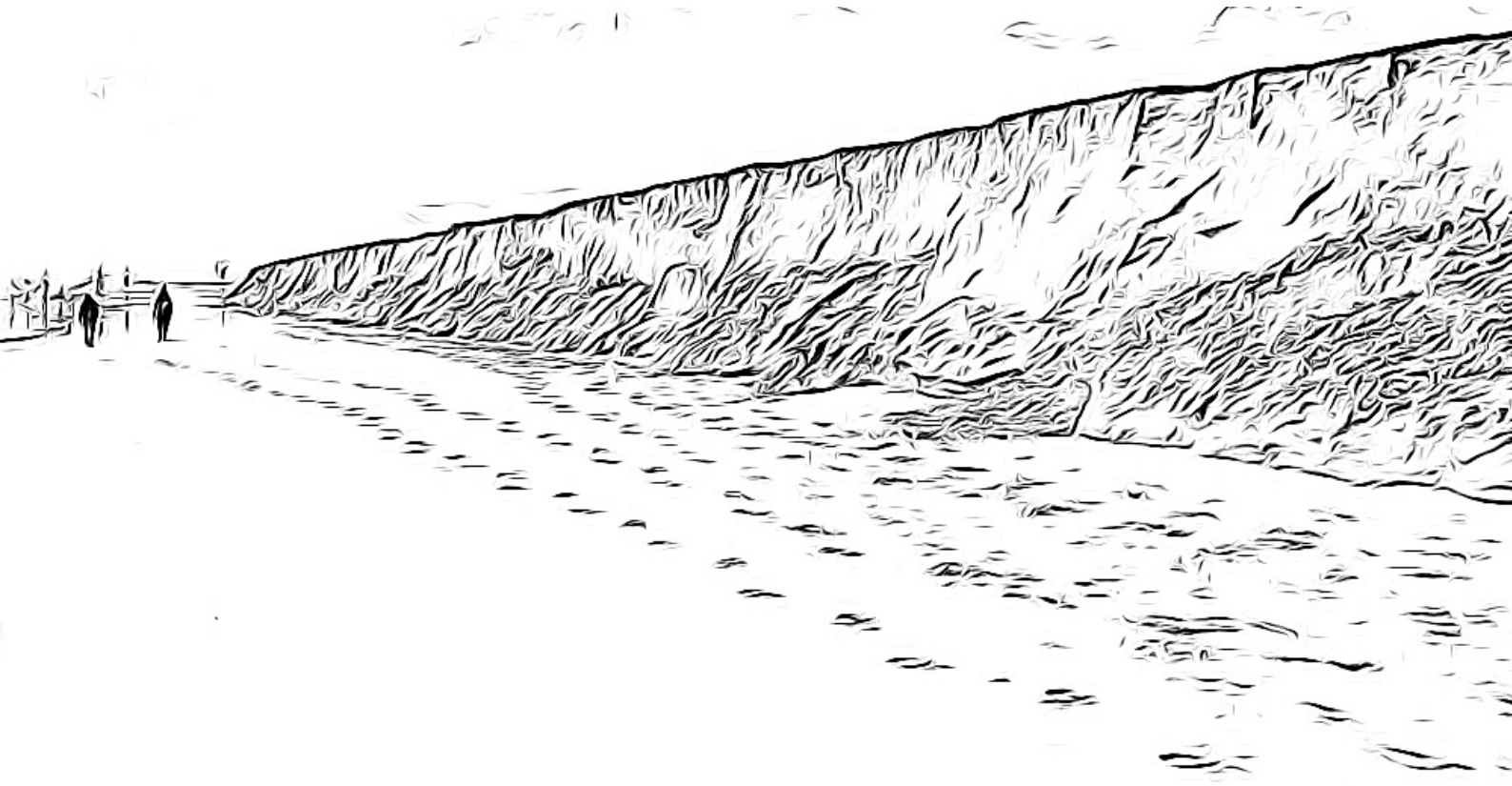

7

Characterisation of dune foot behaviour

This chapter provides a synthesis based on the findings from the case studies at RealDune-REFLEX and Land Reclamation Philippines. Herewith, the dune foot behaviour of sandy coastal defences in annual storm conditions is characterised based on the main driving factors.

7.1. Initial profile characteristics

The initial conditions of the slope of the sandy coastal defence are characterised in this study by the initial dune foot elevation and the initial foreshore slope. The exceedance of the dune foot elevation by the total water level elevation was seen as the commencement of the collision regime and therewith dune erosion (Sallenger, 2000) and subsequent horizontal dune foot retreat. The foreshore slope is an essential factor in the runup formulation, which influences the reach of the runup elevation and therewith potential erosion. The initial parameters DF_z, DF_x and β_f are quantified and assessed on their correlation with their corresponding post-storm equivalent (Figure 7.1). Looking at the correlation graphs of the dune foot position, most of the transects show upward dune foot translation and horizontal dune foot retreat. The foreshore slope is less steep post-storm for the majority of the transects at LRP. However, for RealDune-REFLEX also steepening of the foreshore slope is observed which is typical for the swash regime. Transects for both sites, where the maximum total water level elevation is below the initial dune foot position, are related to less to negligible dune foot retreat.

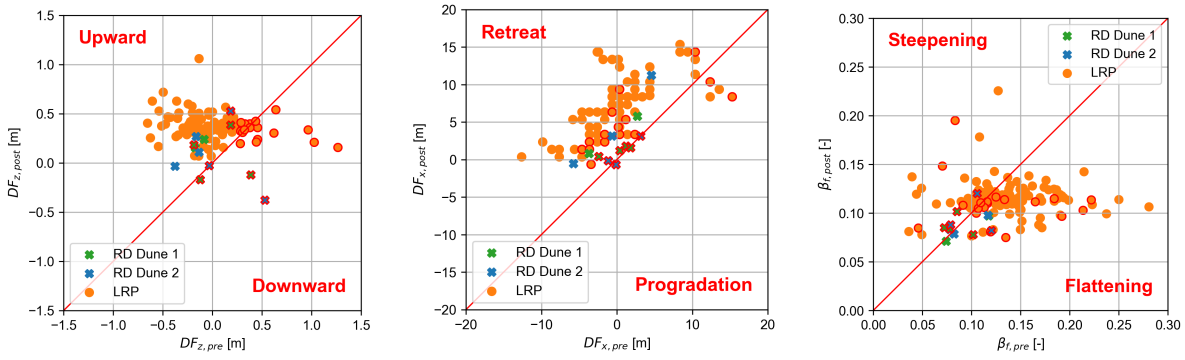

Figure 7.1: Correlation figures of the initial parameters respectively DF_z, DF_x and β_f and their corresponding post-storm equivalent subtracted with the mean of the initial values. The no-change line is indicated in red. Transect points where $\eta_{TWL,max} < DF_{z,pre}$ are outlined with red.

The calculated parameters of the cross-shore profiles of RealDune-REFLEX and Land Reclamation Philippines are combined and an overview is provided of the eroded volume, the maximum total water level $\eta_{TWL,max}$, the foreshore slope β_f and the initial dune foot elevation $DF_{z,pre}$ (Figure 7.2). Four regimes can be distinguished based on the dune volume change and the total water level relative to the dune foot height (Table 7.1 and Figures 7.2 and 7.3).

Table 7.1: Dune regimes based on the dune volume change and the total water level elevation relative to the dune foot elevation

Quadrant	Regime	ΔV	$\eta_{TWL,max} - DF_{z,pre}$
1	Collision dune growth	+	+
2	Swash dune growth	+	-
3	Erosive swash regime	-	-
4	Traditional collision regime	-	+

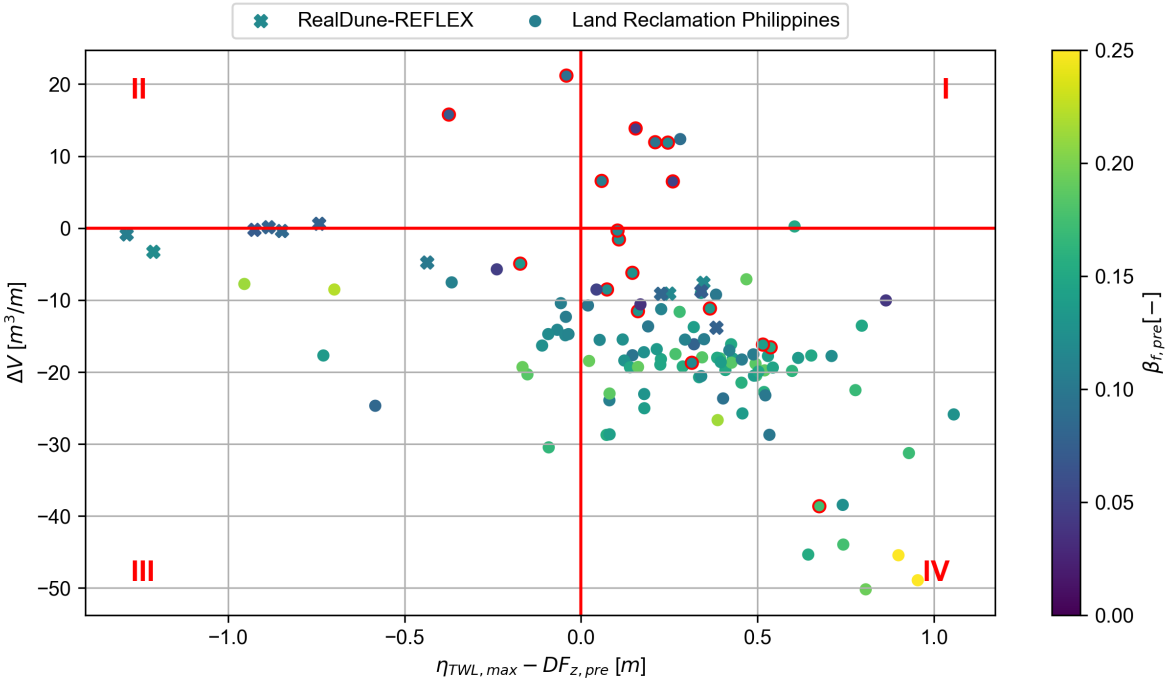

Figure 7.2: The influence of the initial dune foot height $DF_{z,pre}$ and the maximal total water level elevation $\eta_{TWL,max}$ on dune volume change. The red solid lines divide the graph into four quadrants. The colour-grading shows the pre-storm foreshore slope $B_{f,pre}$. RealDune-REFLEX is shown with crosses and Land Reclamation Philippines with circles.

It can be observed that the erosion volume tends to increase with the degree of exceedance relative to the initial dune foot position. However, no clear trend is found. For maximum total water level elevations far below the dune foot, no significant erosion was observed. For water levels just below the dune foot, erosion volumes of the same order can be found relative to large exceedances. Hence, the initial dune foot elevation might not be the governing factor regarding the magnitude of the erosion volumes. The initial foreshore slope tends to be steeper for transects which were subject to larger amounts of erosion.

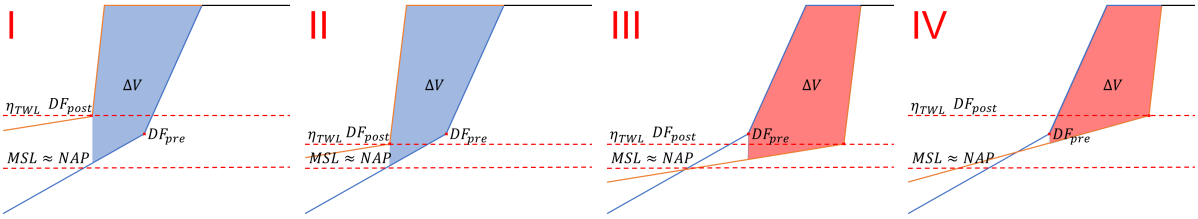

Figure 7.3: Cross-shore profiles examples of the four regimes based on the initial dune foot location and the approximated maximum total water level elevation.

Collision dune growth (I)
In the first quadrant, collision dune growth could potentially be observed on certain transects. This regime, however, is very rare as the dune foot elevation is exceeded by the water level which is often related to dune erosion. When the beach is submerged and high wind speeds are prevailing (in combination with high precipitation), the origin of the sediment increase is probably not due to wind-driven transports. In this case, human intervention is more likely. For the LRP case, it was stated that the increase in sediment was due to the reinforcement of the side slope at this stretch. However, there is an example within other research of the collision regime where dune accretion was observed (Cohn et al., 2018). Here, elevated η_{TWL} could cause dunes to accrete and therefore discusses the being of collisional waves to solely be erosional to dunes.

Swash dune growth (II)
In the swash dune growth regime, quadrant 2, positive values of dune volume change are observed with a water level elevation below the dune foot. Therefore, this regime is probably governed by either aeolian transport, human intervention or swash accretion of the foreshore. During periods between storms, the dune face is known to accrete due to aeolian transport coming from the beach. As in this study, only storm periods are examined on a short time scale of the order of 1 day, so it is not likely that aeolian transport was the main constituent. It is probable that human intervention led to these significant dune volume increases (Section 6.3).

Erosive swash regime (III)
In the traditional swash regime (quadrant 3) as described by Sallenger (2000), negligible dune erosion is expected. In this study, a phenomenon at RealDune-REFLEX was observed when two storms follow each other shortly. The maximum total water level elevation did not exceed the dune foot during the period of high water, however, still avalanching of the dune face was observed undermining the dune and leading to significant dune erosion. Therefore, an erosive swash regime was introduced for quadrant 3. A minority of cross-shore profiles of LRP are found in this regime (Figure 7.2) and were related to a lowering of the bed. No visual observations can confirm if the lowering of the bed resulted in avalanching. It seems that erosion volumes of the same order can be reached by both upward and downward dune foot translation for both sites.

Traditional collision regime (IV)
The traditional collision regime (quadrant 4) as described by Sallenger (2000) commences when the water level elevation exceeds the dune foot. The total water level exceeds the dune foot leading to erosion of the dune by avalanching of the dune face. Most of the cross-shore profiles appear to be in this regime, as was expected with the analysis of storm conditions with two severe out-of-equilibrium profiles. For higher exceedances of the dune foot, larger erosion volumes were expected. Looking to Figure 7.2, this correlation can be found however is not clear. Looking at the foreshore slope, higher erosion quantities can be found for steeper slopes. This relation is not clear for RD as the differences in the foreshore slope are smaller.

7.2. Vertical translation

Vertical repositioning was found from previous research to relate to the storm surge level (Bonte & Levoy, 2015; de Winter et al., 2015; van Bemmelen et al., 2020; Vellinga, 1986). They found that approximately a 1:1 relation was found for water level elevations above the dune foot. The total water level $\eta_{TWL,max}$ relative to the initial dune foot height $DF_{z,pre}$ is found to be an accurate measure of the vertical dune foot translation for RealDune-REFLEX and Land Reclamation Philippines (Figure 7.4).

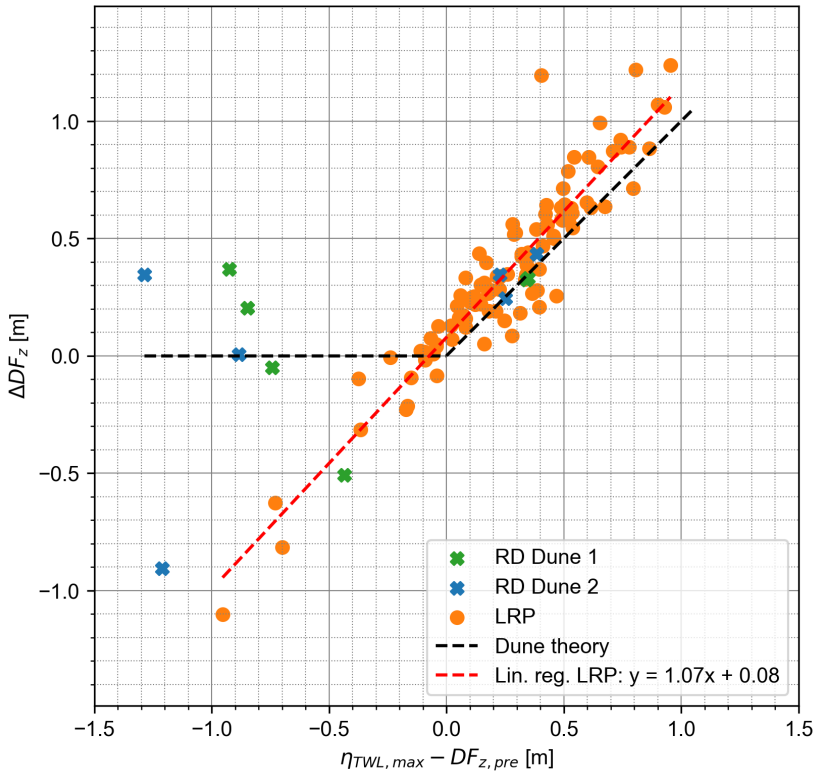

Figure 7.4: Correlation graph of the maximum total water level above the initial dune foot height and the change in dune foot height. Positive ΔDF_z values correspond to an upward translation of the dune foot. A theoretical line is shown for a 1:1 relation between dune foot height change and the overheight of the water level.

For RealDune-REFLEX, the dune foot translated upwards and downwards corresponding to the $\eta_{TWL,max}$ for six transects which are in line with theory. For water level elevations below the dune foot, the dune foot could lower to the maximal total water elevation reached in the storm period. Through erosion of the upper foreshore slope, the dune front was being undermined which led to avalanching of the dune face and resulted in significant erosion (Figure 7.5).

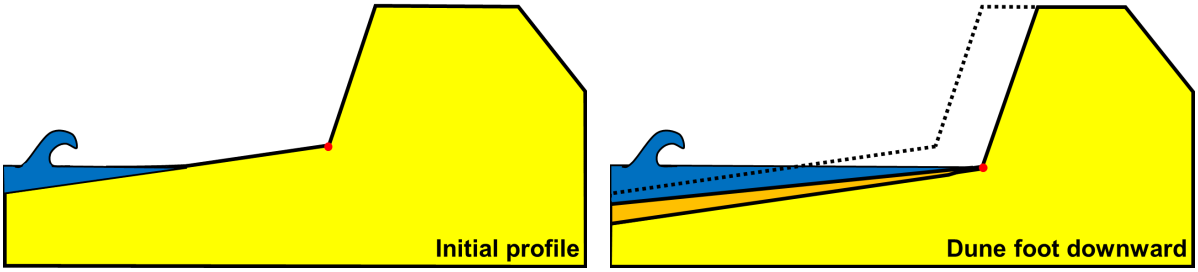

Figure 7.5: Schematisation of downward dune foot translation relative to the initial profile.

For three storm periods (three times Dune 1 and two times Dune 2), the dune foot translated significantly upwards (between 0 and 0.5 m) while respectively the water levels were below the dune foot. These can be explained by the instabilities of the dune face and the inability within this period of the swash motion to transport the slump sediment in the offshore direction. Here, the difficulties in the definition of the dune foot and the second derivative method come with their shortcomings. Two periods show minor dune foot elevation changes (in the order of the measurement error) where $\eta_{TWL,max}$ was below the dune foot which is in line with theory.

The cross-sections of Land Reclamation Philippines show an accurate linear relation ($R^2 = 0.88$) between the change in vertical dune foot position and the total water level elevation above the dune foot. The slope of the line with a value of 1.07 matches closely to the theoretical slope of 1:1. The slope coefficient of 1.07 may suggest that, as exceedances of the dune foot increase, additional dune erosion mechanisms become more significant, consequently leading to a post-storm dune foot elevation that surpasses the approximated maximal total water level elevation. Alternatively, it is plausible that the method employed generates less precise estimations for higher (and lower) determined dune foot positions. However, no clear evidence was found supporting these hypotheses. Downward translations are found for LRP at transects in the middle of the reclamation site where the slopes were gentle and no significant pre-storm scarp was present. However, dune foot positions were difficult to distinguish in this region with the used method, therefore it might be unjust to state that downward dune foot translation occurred for these transects (Figure 7.6).

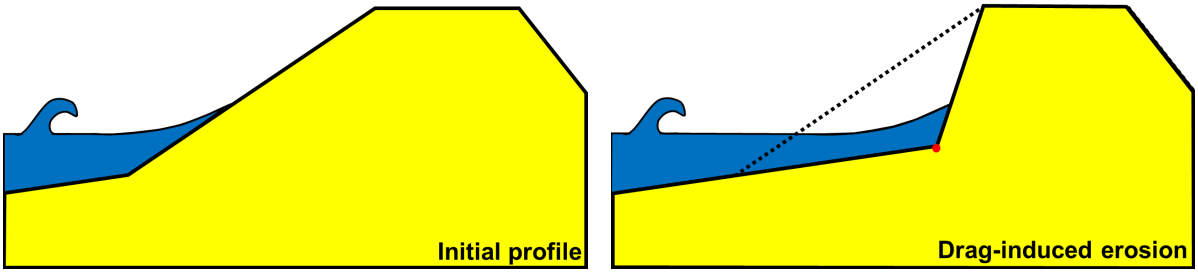

Figure 7.6: Schematisation of drag-induced erosion of a gentle initial slope.

7.3. Horizontal translation

In literature, a relation was found between horizontal changes of the dune foot and the intensity and duration of a storm (Giardino et al., 2012; Overton et al., 1988). The initial quantification of the storm-specific duration and intensity was based on the exceedance of the dune foot. The duration is defined as the time $DF_{z,pre}$ was exceeded by the total water level elevation until the total water level elevation dropped below $DF_{z,post}$. The intensity of the storm is defined as the height of η_{TWL} above the (estimated) dune foot elevation. For these approximations of the intensity and duration of the dune foot exceedance, it was assumed in this study that the dune foot would progress linearly through the storm in between pre-storm and post-storm morphological measurement (Figure 7.7). These relations were examined (Figure 7.8).

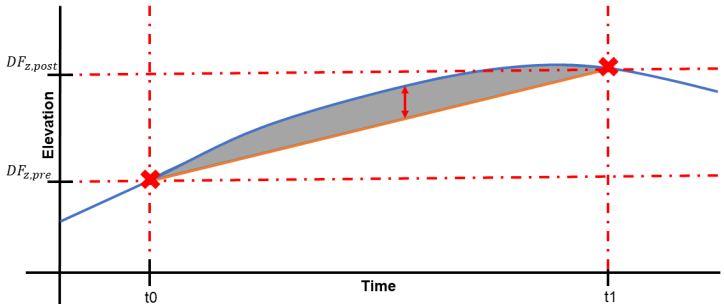

Figure 7.7: Methodology of the duration and intensity of the storm. The blue line depicts the total water level elevation. The orange line depicts the linear translation of the dune foot height. The integral of the intensity over the duration (grey area) quantifies the impact of the storm conditions.

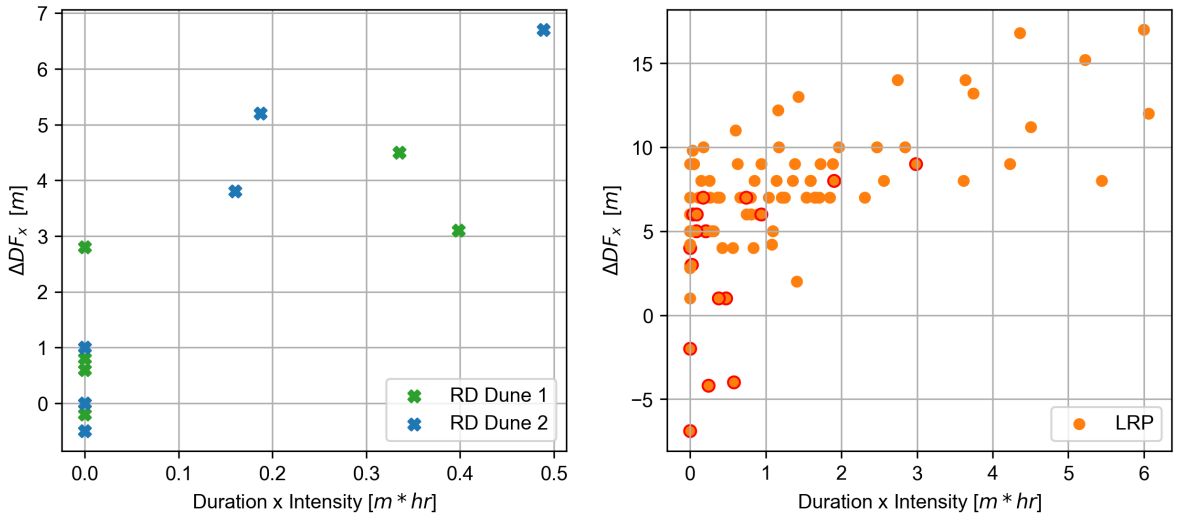

Figure 7.8: Influence of the duration and intensity of the total water level elevation on the horizontal dune foot change. Each marker corresponds to a transect within a storm period. (left panel) RealDune-REFLEX (right panel) Land Reclamation Philippines. Red encircled dots represent the intervened transects.

For an increase in the duration and intensity of the storm, a higher horizontal dune foot translation is observed. The horizontal dune foot change curve is flattening for higher values of 'Duration x Intensity' for both datasets (Figure 7.8) and is limited to profile characteristics and therefore could reach an equilibrium based on the storm conditions. This limit could be explained by an equilibrium dune profile and the associated negative feedback mechanism which reduces the wave impact reaching the dune front by a developing foreshore profile. Both for RD and LRP, this curve is observed however strongly varying in duration and intensity height.

These results show that the horizontal dune foot change is dependent on the duration and intensity of the storm. However, dune foot translations of the same order were found for transects where the dune foot was not exceeded and for transects which were subject to the hydrodynamic forcings for an intense period. Within all the storm periods, the orientation of the dunes and sediment characteristics are assumed to be constant. Differences at RealDune-REFLEX may be explained by a varying water level, wave height, wave period and wave angle. Differences at Land Reclamation Philippines are expected to be due to alongshore variabilities in the foreshore slope and protruding minor coastal features. Note that erosion can be present for situations where $\Delta DF_x = 0$, due to bed level lowering and downward dune foot translation.

7.4. Mismatch of the foreshore

In Section 7.1, it was shown that the initial dune foot position relative to the runup is not an accurate measure to quantify dune erosion volumes. Section 7.2 shows that the dune foot can also translate downwards corresponding to the maximum total water level elevation and resulting in dune erosion (Figure 5.7). The method of duration and intensity of the storm above the dune foot position is stated to be an inaccurate measure to quantify dune erosion (Section 7.3). Instead, it was hypothesised that the (upper) foreshore slope might be out-of-equilibrium with the storm conditions and which results in erosion of the dune for water levels below the dune foot.

Dune equilibrium theory states that the erosion volume equals the accretion volume (Figure 2.3). Combined with the equilibrium slope, the concept is able to quantify the erosion volume related to the mismatch in volume. This theory is based on three assumptions:

1. Post-storm dune foot is positioned at the maximum total water level elevation.
2. Post-storm foreshore slope is equal to the equilibrium slope.
3. Hypothetical equilibrium slope starts at the intersection of the maximum total water level elevation with the pre-storm profile.

The area between the line of equilibrium slope and the initial profile is defined as a mismatch σ with equilibrium conditions (Figure 7.9). This area is the sum of the resulting missing positive volumes and is calculated between 0 and 30 meters seaward. This stretch is chosen as this is the maximum that the RealDune-REFLEX dataset encompassed (Equation (7.1)).

$$\sigma = \int_{z_{dune}-30*\beta_{eq}}^{z_{dune}} \left(z_{equi} - z_{initial}\right) dx \tag{7.1}$$

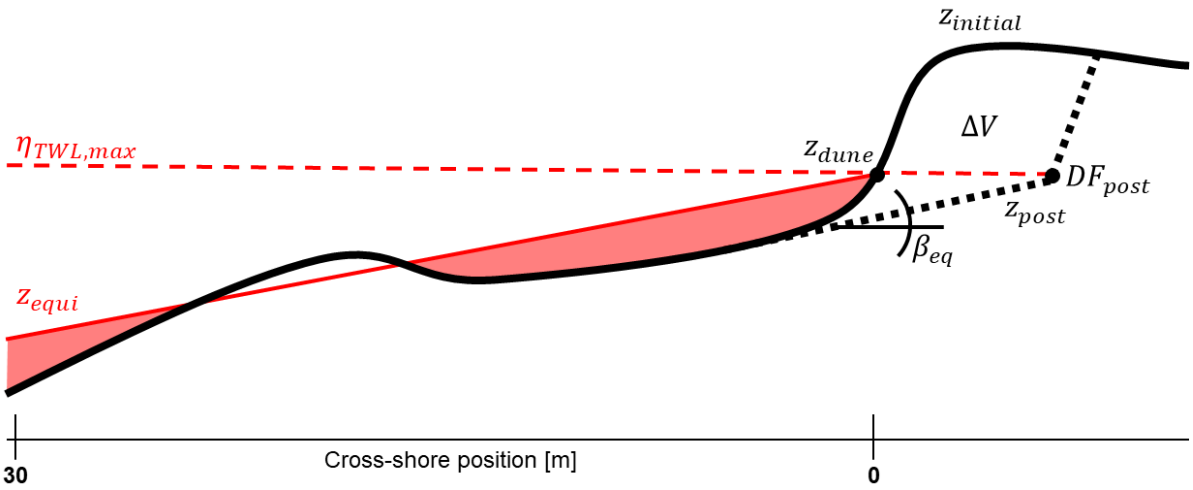

Figure 7.9: Supportive schematisation of the methodology of the mismatch between the initial profile and the equilibrium conditions

The erosion volumes of RealDune-REFLEX Dune 1 correspond significantly to the mismatch of volume under a slope coefficient of -0.66 and for Dune 2 at -1.02 (left panel Figure 7.10). For Land Reclamation Philippines, the erosion volumes and corresponding mismatch do not show a linear trend but are spread over a large range of mismatch around a mean erosion value of approximately $-17\ m^3/m$ (right panel Figure 7.10). This could indicate a strong dependency of a transect on the adjacent transects induced by the wave direction.

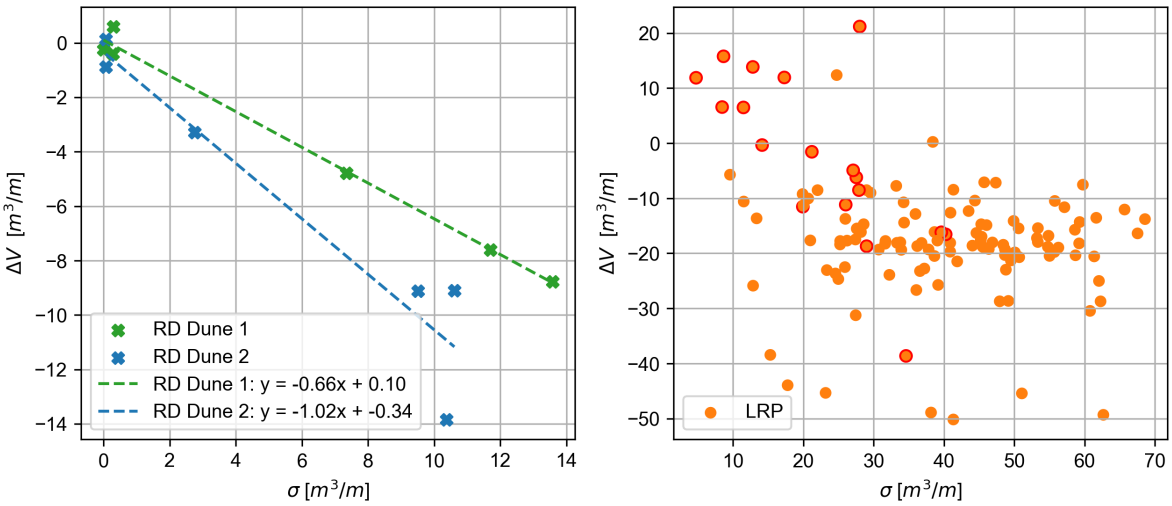

Figure 7.10: Mismatch of the foreshore with the estimated equilibrium profile. (left panel) RealDune-REFLEX Dune 1 and Dune 2. (right panel) Land Reclamation Philippines with intervened transects Kp1230 to Kp1060 encircled in red.

7.5. Application for engineering purposes

The mismatch method can be used for a quick estimation of the erosion volume of sandy coastal defences based on the initial profile, offshore wave conditions, water level variations and sediment characteristics. From the observations of this study, it became evident that the exceedance of the dune foot might not be the commencement of erosion for sandy coastal defences. However, a certain out-of-equilibrium slope was hypothesised which induces erosion. This might relate to the formation of beach scarps at steep nourished beaches as described by van Bemmelen et al. (2020).

The calculated mismatch volumes with corresponding erosion volumes are fitted using linear regression for RealDune-REFLEX Dune 1 and Dune 2 and Land Reclamation Philippines (Figure 7.11). The reliability of the fit is very high for RD Dune 1 ($R^2 = 0.99$) and for RD Dune 2 ($R^2 = 0.91$), however low for LRP ($R^2 = 0.14$). The transects which show no anthropogenic interventions (Kp1050 to Kp150) are alongshore averaged every 100 meters and fitted through zero. The slope coefficient of Dune 2 is -1.02, Dune 1 is -0.66 and LRP is -0.43. A slope coefficient of -0.66 represents that for every $3\ m^3/m$ mismatch of volume, $2\ m^3/m$ of the dune will erode. Based on Figure 7.11 a dune erosion volume of $1\ m^3/m$ is expected for varying mismatch of approximately 1 to 2.5 m^3/m. This value could vary due to the obliquity of the waves, median grain size, storm duration and alongshore non-uniformities.

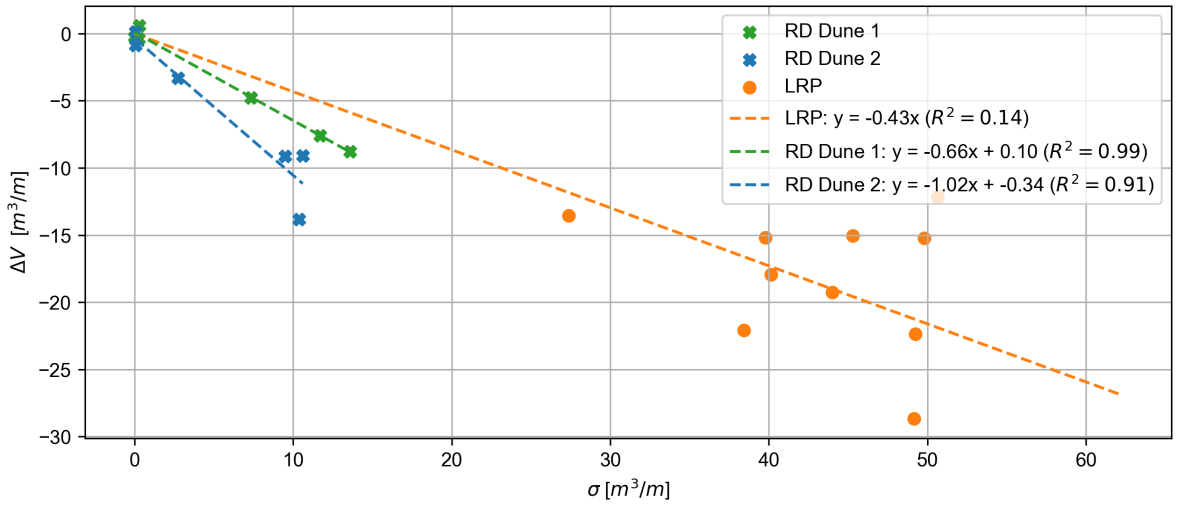

Figure 7.11: Mismatch foreshore with equilibrium profile. Transects of LRP are alongshore averaged over every 100 meters ranging

This method is based on two datasets where RealDune-REFLEX contains two dunes with different orientations and is valid for the collision regime for initial profiles with very few coastal features. Anticipating the potential limitations of the proposed methodology, it is crucial to acknowledge that its applicability may be compromised in the event of overwash occurrences, primarily due to the lack of sediment redistribution towards the foreshore. Moreover, the seaward extent of 30 meters could be considered restrictive, thereby necessitating an evaluation to ascertain whether an extension of this range would be appropriate. It is assumed that the storm duration is sufficiently long and the profile is in equilibrium with the conditions of the maximum total water level elevation. The integration of the temporal variation is not taken into account.

To be able to forecast the erosion volumes based on this method of mismatch with equilibrium conditions, the method is decomposed in the required inputs. The hydrodynamics are captured in the maximum total water level elevation which is composed of the astronomical tide, wind setup and the additional wave runup calculated with Equation (2.11). This provides the crossing with the hypothetical initial profile where the equilibrium slope begins.

The equilibrium slope according to Vellinga (1986) and further improved by van Gent et al. (2008) was found to be a function of wave height H, wave period T and median grain size d_{50}.

$$\beta_{eq} = f\,(H, T, d_{50}) \tag{7.2}$$

The foreshore slope was defined as the best-fit slope (lowest RMSE) over the region between the MHW and the dune foot. The equilibrium post-storm profile can be estimated using the erosion profile equation of van Gent et al. (2008). This profile can be constructed between the post-storm dune foot position (x_0, z_0), which will equal the maximum total water level elevation, and the crossing with MHW when solved for x using Equation (7.3).

$$\left(\frac{7.6}{H_s}\right) z = 0.4714 \left[\left(\frac{7.6}{H_s}\right)^{1.28} \left(\frac{12}{T_{m-1.0}}\right)^{0.45} \left(\frac{w_s}{0.0268}\right)^{0.56} x + 18\right]^{0.5} - 2.0 \tag{7.3}$$

Herein, the fall velocity w_s is dependent on the median grain size d_{50} and can be approximated by the Stokes formula. However, in these extreme weather conditions, it is expected that conditions are beyond the Stokes regime. Therefore van Rijn (1993) proposed an approximation which is more applicable to these conditions and grain sizes in the range $100\ \mu m < d_{50} < 1\ mm$.

$$w_s = \frac{10\nu}{d_{50}} \left[\sqrt{1 + \frac{0.01\,(\rho_s - \rho_w)\, g d_{50}^3}{\rho_w \nu^2}} - 1\right] \tag{7.4}$$

The fall velocity formula takes into account the kinematic viscosity $\nu = \mu / p_w$, the sediment density $\rho_s \approx 2650\ kg/m^3$ and the water density $\rho_w \approx 1025\ kg/m^3$.

This method provides a rapid approximation for the magnitude of erosion volume at sandy coastal defences using a linear relationship based on the mismatched volume and site-specific constant a.

$$\Delta V_{dune} = a * \sigma \tag{7.5}$$

This method assumes a duration where an equilibrium state to the storm conditions is reached. The horizontal dune foot retreat can be calculated from the erosion volume by dividing it by the sediment availability of the dune. This is defined as the height of the dune front which is the elevation difference between the dune foot and the dune front crest. The magnitude can change in time as the dune retreats and another magnitude of the doot relative to the crest arises.

$$\Delta DF_x = \frac{\Delta V_{dune}}{DC_{z,pre} - DF_{z,pre}} \tag{7.6}$$

7.6. General conclusions

Larger erosion volumes are found for transects where there was a higher maximum total water level elevation relative to the initial dune foot height. However, no clear trend was found and volumes of the same order are found for water levels below the dune foot and for water levels significantly exceeding the dune foot.

The post-storm vertical dune foot position is located at approximately the maximum total water level elevation. The dune foot can translate upwards as seen in regular dune erosion occasions but also downwards when the upper foreshore slope is out-of-equilibrium.

The horizontal dune foot change is found to be related to the duration and intensity of the total water level elevation above the dune foot. However, dune foot retreat magnitudes can be of the same order for small and large values of the 'Duration x Intensity'-parameter.

The amount of mismatch with the foreshore volume has been found to be a more reliable method to quantify the dune erosion volume and a significant linear relation has been found. The proposed methodology offers a viable approach for predicting erosion volumes in sandy coastal defences, utilising straightforward initial conditions, thereby demonstrating its applicability in the field of engineering practice.

8

Discussion

The findings within this study are critically reviewed on reliability and evaluated to place the results within the context of existing literature and the theoretical framework. The discussion will subsequently handle the separate chapters of this thesis, starting with the methodology and data processing, then the case studies of RealDune-REFLEX and Land Reclamation Philippines. Finalising the discussion with a reflection on the characterisation of the dune foot behaviour.

8.1. Methodology & Data processing

Dune foot location approximation method

The dune foot location estimation method can be discussed based on the definition of the dune foot. For some situations, a dune face could just have had a periodic slump due to the instability of the dune front and the swash motion thereafter was not able to fully transport this sediment offshore. Then the method for the dune foot estimation based on the second derivative could find the point below this slump while others could discuss that the dune foot is the point above this slump. Also, for the section of LRP transect Kp900 to Kp690 the pre-storm slope of the land reclamation was gentle and straight and no obvious change of slope was observed for these newly established dune profiles. Therefore the method could not define a dune foot position on those pre-storm profiles (Figure 8.1). This also demonstrates the insignificance of the dune foot as a quantification parameter in sandy coastal defences. These transects are disregarded in this study for analysis based on the pre-storm dune foot and therefore could introduce a certain bias in the results for the domain of those transects.

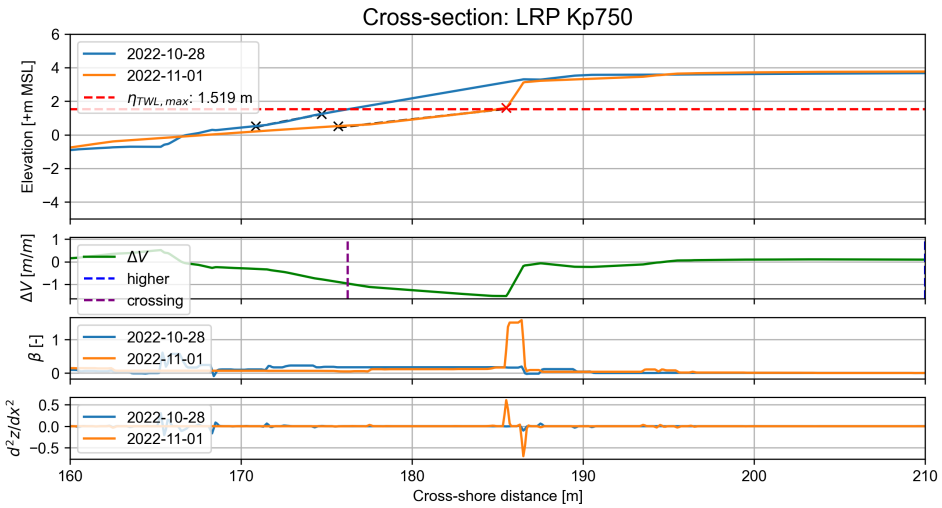

Figure 8.1: Cross-section LRP Kp750, an example of an indistinguishable initial dune foot position.

Use of offshore wave conditions
The total maximum water level elevation is approximated by combining the measured water level elevation η_{act} with the runup formula of Stockdon et al. (2006). This formula requires reverse shoaling of the measured wave conditions to corresponding offshore wave conditions. The method assumes a shore normal approach and therefore disregards, among other factors, refraction and diffraction. Sudden changes in the bathymetry (sand banks) or alongshore variabilities (coastal features) could have a huge impact on the wave characteristics nearshore and the resulting visually observed runup elevation. Wave conditions were resampled to 10 and 30 minutes which could have led to an underestimation of the maximum wave conditions. Therefore the maximum water level elevations, duration and intensity of the storm could have been slightly underestimated. However, the approximation of the total water level elevation in this study resulted in maximum total water levels around the dune foot position which was expected from previous research. In order to increase the temporal and spatial reliability of the η_{TWL}, the actual total water level elevations could be measured using video techniques (e.g. Bonte and Levoy (2015)). Therewith, the sampling rate of the runup could be increased compared to RealDune-REFLEX (10 min.) and Land Reclamation Philippines (30 min.).

8.2. Case study RealDune-REFLEX

Supplementation of elevation measurements
The XYZ elevation measurements, obtained via RTK GPS, do not constitute a continuous point cloud within a uniform grid. During specific intervals, a limited amount of points were measured at varying positions along pre-defined transects, extending from approximately NAP to the dune foot. For other periods, the entire dry area in front of both dunes and the areas on top of the dunes were measured (excluding the scarp itself). In order to assess the volume change of the dune (normative transect), some daily measurements were completed with the elevation measurements of the closest day where the area was measured under a higher spatial resolution. This went under the assumption that the resulting calculated dune volume change within this period was negligible.

The constructed cross-shore profile and subsequent calculated dune volume change could vary slightly due to settlements, compaction of the dune, aeolian growth at the dune front, aeolian transport from the dune crest (which was observed at the field site), and influences of precipitation. These deviations in the calculated volume changes tend to be small with regard to the observed erosion quantities induced by the hydrodynamic conditions at the site.

Variation in compaction
As the elevations along the transects of Dune 1 and Dune 2 are measured on a daily timescale during the three-month period, the temporal evolution of the dunes can be investigated. Therefore, the water level elevation and wave conditions (including the wave angle) varied per storm period and the resulting dune erosion can be directly linked to these governing hydrodynamics. It was assumed that the orientation of the dune, sediment size and compaction of the dune remained constant throughout the measuring campaign.

Overton et al. (1994) showed that higher compaction (or density) of the dune, resulted in a decreased amount of dune erosion. However, density showed to be of less significance than the sediment size which was approximately equal for both dunes over time. Increased compaction of the dune could have introduced a certain bias influencing the degree of erosion of the dunes during the measuring campaign. The error which might be introduced is expected to be of lower significance than the influence of the sediment size on dune erosion. Moreover, during the construction of both dunes, the compaction is performed thoroughly by a bulldozer and therefore the remainder of settlement and strength increase due to compaction might be negligible.

8.3. Case study Land Reclamation Philippines

Visual observations of erosion conditions

Although visual observations could prove beneficial for determining the conditions responsible for significant erosion at the Land Reclamation Philippines field site, they are unfortunately absent. Consequently, the directional variation in which waves approach the coastline at this location remains uncertain. The trail of the typhoon went right over the bay, probably leading to a strong varying wind field and therefore varying wave field in terms of direction and wave heights.

The empirical runup formula of Stockdon et al. (2006) did not include wave angle nor state about the validity domain, however, Stockdon et al. (2007) found that the runup parametrisation was valid for spatial variable hurricane impacts. In this study, looking at the main wave directions it was assumed that the waves leading to the most severe erosion were generated just outside the bay and propagated into the bay. Therefore the most significant erosion probably occurred at the peak of the typhoon on 2022-10-29 between 16:30 and 17:00. During the peak typhoon period, the wave direction changes from 330 degrees (NNW) to 250 degrees (WSW).

Additionally, a water level difference is present between the bay's north and south sides during this period. Erosion resulting from typhoon-induced hydrodynamics may diverge from storm surge-induced erosion, as classical storm surges typically exhibit a relatively constant wave direction throughout the high water phase. Moreover, sediment transporting processes can vary in relative magnitude and equilibrium conditions can change throughout the typhoon. This can be very interesting as the difficulties and mismatches of unrestricted field measurements with regard to restricted flume experiments reach their pinnacle.

Inaccurate reference datum

Due to the LRP project's nature, measurements of hydrodynamics and morphology are less frequent and less accurate compared with the RealDune-REFLEX research project. Water level elevations are measured at a tidal gauge every minute and were related to an instrument-specific reference datum. Those water levels are related to the UHSLC mean sea level over the period 1985 to 2016, serving as the project-specific reference datum wherein bed level elevations were measured.

However, the UHSLC tidal gauge was not used for this definition nor did the method express whether outliers were dropped or corrected. The UHSLC tidal gauge showed a strong trend over the years which indicates either sea level rise or land subsidence in which sea level rise is expected to be relatively small (Figure 3.8). Therefore, the reference datum for mean sea level for the bed level elevation and the water level elevations can vary up to a maximum of circa 5 cm.

Offset maximum total water level elevation

The linear regression line of the total water level elevation and the post-storm dune foot elevation intersects the y-axis at 0.08 where a value of 0 was expected from the theory. This could show that the maximal total water level elevation was underestimated by approximately 0.08 meters, assuming the dune foot is located exactly at the approximated maximum total water level elevation.

It could be hypothesised that (1) runup values following the Stockdon et al. (2006) formula are underestimated by the use of offshore wave conditions for typhoon-generated waves over the bay. (2) The translation of LAT to MSL for the morphological data was not in line with the reference datum MSL of the water level elevation. (3) The influence of highly oblique incident waves and varying directions led to varying refraction and therefore can be preferred to include the offshore wave angle in the runup parametrisation. In the current method, a shore normal approach was assumed.

8.4. Characterisation of dune foot behaviour

In this study, dune erosion theory is linked to the erosion of man-made sandy dikes and the erosion of unprotected land reclamation slopes. Generally, land reclamations have a less developed foreshore and might have different sediment characteristics and dune strength. Within this thesis, observations have been made based on the erosion quantities at both field sites. These show that bunds and artificially created dunes could relate well. Moreover, the erosion of sandy coastal defences compares significantly to the erosion of real coastal dunes. At both field sites, a steep erosion scarp forms and an erosion profile is formed with a flattened slope in front of the dune. Likewise was observed in various dune erosion experiments (e.g. van Thiel de Vries (2009) and Vellinga (1986)).

Bias in the temporal variation of the dune foot position

Variation of the dune foot position was limited to hydrodynamic and morphological processes in this study. There was assumed that aeolian processes did not affect the position of the dune foot on a short time scale. However, Suanez et al. (2012) found that dune accretion after a storm occurred primarily at the dune foot. With a low morphological measurement frequency, the temporal variation of the dune foot could have been influenced due to aeolian transport. Nonetheless, bed level measurement frequency was expected to be frequent enough to reduce the implications of aeolian dune foot migration. Moreover, the expected error of the bed-level measurements is in the order of these variations.

Size and shape of the equilibrium slope

In the method of mismatch with a hypothetical equilibrium slope, the slope is taken linearly from the crossing of the initial profile with the maximum total water level elevation over the pre-defined transect. Although the erosion profile is known to be concave, the linear slope provides for a simplistic method over the first 30 meters seaward. To further improve the method, a parabolic shape $y = p * x^y$ can be used over a greater distance seaward.

The transects are defined perpendicular to the coastal profile following the initial bathymetry. Alongshore variability can be induced by coastal features and oblique incident waves. The alongshore variable character of the dunes at LRP might influence the results of this method. van Thiel de Vries et al. (2011) state that higher dunes in the presence of lower dunes could lead to a larger erosion volume at the higher dunes, as a larger volume of sand will slump off the dune and be used to develop a storm profile in the foreshore of the low dune areas. However, this might lead to less horizontal dune foot change as the equilibrium is reached more rapidly and provide an improper estimation of the resulting erosion. However, in this study, the alongshore dune heights were relatively uniform and it is expected that the influence of protruding coastal features is larger than the local height of the dune. These could have significantly influenced the erosion volume of certain transects and the development of the foreshore at other transects.

Applications for engineering purposes

The described application is a quick estimation method for the dune erosion volume at sandy coastal defences based on the initial profile, offshore wave conditions, water level variations and sediment characteristics. The found linear relationship between the mismatch and the erosion volume shows variation between the three different field sites. Moreover, the method has a huge spread for LRP within one storm period. The 126 transects of LRP are transformed by means of alongshore averaging over 100 meters from the transects which are not intervened to reduce the distortion in the results.

Variations could arise based on sediment characteristics such as compaction and median grain size. Also, the influence of wave obliquity is not included in this approach and might explain the differences between the mismatch relative to the erosion volumes of RealDune compared to Land Reclamation Philippines.

9

Conclusions & Recommendations

The objective of this research was to obtain a better understanding of the dune foot behaviour of sandy coastal defences due to annual storm conditions. The focus was on the influence of the dune foot on dune erosion and the change in dune foot position due to storm-specific hydrodynamics. This was studied by doing extensive literature research, an analysis of the constructed dunes of RealDune-REFLEX with different orientations and the typhoon-induced erosion at the side slopes of the land reclamation at Land Reclamation Philippines. This chapter contains the conclusions and recommendations of this research and provides answers to the research questions.

9.1. Conclusions

To provide a conclusion on the findings of this study, the three sub-research questions are answered first and thereafter the main research question is answered.

> What is the influence of the initial dune foot height on dune erosion?

The initial dune foot height and the relative maximum total water level elevation were used to explain occurrences of positive and negative dune volume change. The division is an extension of the regime theory of Sallenger (2000) and explains 'collision dune growth', 'swash dune growth', 'erosive swash regime', and 'traditional collision regime'. Dune growths of sandy coastal defences under storm conditions were related to human interventions.

For the majority of the transects of both case studies, a maximum total water level elevation above the initial dune foot height (traditional collision regime) led to the highest erosion quantities of the dune front. However, no significant linear relation was found between the initial dune foot position relative to the maximum water level elevation and the resulting dune erosion. For water levels lower than the initial dune foot height (erosive swash regime), lowering of the foreshore was observed. For some periods this led to minor erosion of the dune front, however, some periods resulted in significant dune erosion and subsequent downward repositioning of the dune foot. Bed lowering could lead to instability of the dune face while it is not attacked with wave impacts and eventually led to avalanching of the dune face at the RealDune-REFLEX site.

> What is the influence of storm-specific hydrodynamics on the change in vertical dune foot position?

The measured water level elevations and storm-specific hydrodynamic conditions used in combination with the approximation of the wave runup as defined by Stockdon et al. (2006), were found to correlate significantly with the post-storm dune foot elevations. This occurred for the majority of the transects where the maximum total water level elevation exceeded the initial dune foot elevation.

For periods where the maximum total water level elevations did not exceed the dune foot elevation but were high up on the foreshore, occurrences have been found where the dune foot translated downwards due to bed lowering and avalanching of the dune face. This is different from standard dune erosion theory and regime theory. These findings led to the hypothesis of an out-of-equilibrium upper foreshore slope. Periods in which approximated maximum total water level elevations were significantly lower than this upper foreshore slope showed no significant change in dune foot elevation.

What is the influence of the duration and intensity of the storm on the change in horizontal dune foot position?

Change of the horizontal dune foot position was found to relate to some extent to the duration and intensity of the storm defined as the time and height of the total water level elevation above the continuous dune foot position. Higher duration and intensity of the storm generally led to greater horizontal dune foot changes. Alongshore differences in the horizontal dune foot change can be explained by pre-storm minor alongshore variabilities while major alongshore variable features remained present. Observed is that the horizontal dune foot changes potentially approach a limit based on the storm hydrodynamics and the foreshore profile. This could be explained by a negative feedback mechanism from a developing foreshore.

This parameterisation method shows that dune foot retreat magnitudes can be of the same order for small and large values of the quantification method for the duration and intensity. Furthermore, it is notable that zero values within the parameterisation can result in average dune foot retreat distances. Consequently, it can be deduced that the exceedance of the dune foot does not provide a proper estimation of the erosion of out-of-equilibrium sandy coastal defences.

With the conclusion of the three sub-questions, the main research question could be answered. The main research question states:

How does the dune foot of sandy coastal defences behave due to annual storm conditions and what is the influence on dune erosion?

Cross-shore dune foot repositioning has been found to relate to storm-specific hydrodynamics. The dune foot can move upwards and downwards corresponding to the maximal total water level elevation. The upward movement was related to dune erosion in the collision regime. Downward movement was found to relate to an erosive swash regime where an out-of-equilibrium upper foreshore slope led to the scarp-like lowering of the foreshore slope. This bed lowering led to instabilities of the dune face and avalanching was observed resulting in significant dune erosion. The post-storm dune foot elevation of these out-of-equilibrium sandy coastal defences is independent of the pre-storm dune foot elevation for storms with sufficient duration and intensity to reach the dune foot equilibrium elevation at approximately the maximum total water level elevation.

The exceedance of the maximum water level elevation relative to the initial dune foot position is found to not properly represent the erosion volume. Also, the horizontal dune foot change related to the duration and intensity of the total water level elevation exceeding the dune foot is found to not be an accurate measure to estimate dune erosion and subsequent dune foot retreat. It is found that the mismatched volume of the initial profile with the equilibrium condition, defined as an equilibrium slope reaching from the intersection of the initial profile with the maximum total water level elevation, is a more reliable estimation of the dune erosion volume and a significant linear relation has been found. This methodology provides a practical way of predicting erosion volumes in sandy coastal defences using simple initial conditions, making it applicable to engineering practice.

9.2. Research recommendations

Based on the findings in this report, further research on several topics is recommended. Investigating these topics may yield a better understanding of dune foot behaviour in dune erosion models and lead to enhanced erosion volume estimations of sandy coastal defences due to annual storm conditions.

9.2.1. Improvement of the mismatch method

The dune erosion volume estimation via the mismatch method relied on the assumption of a linear equilibrium slope. Commencing at the intersection of the initial profile with the maximum total water level elevation, the slope was computed, extending 30 meters seaward from the origin. This range was restricted by the RealDune-REFLEX dataset measurement depth availability. Enhancements to this approach could include modifying the equilibrium profile and incorporating the temporal variation of both total water level elevation and the dune profile.

The cross-shore erosion profile of a dune is a concave profile, as was observed in dune erosion experiments (e.g. van Gent et al. (2008) and Vellinga (1986)). This parabolic shape profile starts at the post-storm dune foot until a certain far seaward position depending on the wave conditions. To improve the mismatch method, the linear slope could be replaced by a fit with a parabolic equilibrium slope of the form $y = p * x^y$ (as described in Section 2.2.5) and reach further seaward. The current method assumes that the post-storm foreshore slope coincides with the equilibrium slope, which may not necessarily hold for brief storm events. Moreover, the foreshore slope was assumed to be purely cross-shore derived from restrictive flume experiments. Further research is suggested to investigate curve alterations in relation to the wave angle of incidence and pronounced alongshore features, as observed at Land Reclamation Philippines with significant alongshore transport volumes.

Currently, only the mismatch below the equilibrium conditions is calculated. Nonetheless, incorporating erosion volume mismatch values above the equilibrium slope (i.e., available sediment) from the lower profile could accommodate sandy coastal features in the model, thereby partially compensating for potential dune erosion volume.

To include the temporal variation of the volume mismatch magnitude, the total water level elevation varied over time could be included in the calculation and therewith the starting point of the equilibrium slope. This variation in time is described by Equation (9.1).

$$\sigma_{storm} = \int_{t_{pre-storm}}^{t_{post-storm}} \sigma_t \, dt \tag{9.1}$$

Also the updated profile and therefore start point of the equilibrium slope changes through time. This could be included in the timestep of the model. However, this might introduce extra complexity for quick estimation and therefore be out of the scope of the uses of this method.

The foreshore was found to be of more significance to the erosion volume than the dune foot as an initial profile parameter and therefore recommended to perform further research on the shape and size of the equilibrium slope in alongshore variable areas under oblique incident waves.

9.2.2. Dune foot dynamics during the storm for dune erosion models

Dune foot dynamics following the dune foot migration during the storm can be of interest to investigate with LiDAR laser measurements. With these measurements, an accurate view of the dune foot translation through the storm can be determined and the dune foot behaviour could be captured to a greater extent. In this thesis, it was assumed that the dune foot moves linearly in time between the pre-storm dune foot DF_{pre} and the post-storm dune foot DF_{post}. This assumption can either be validated or adjusted based on these LiDAR measurements. Also, the scarp-like erosion of the foreshore could be investigated as a significant contributor to dune erosion. The translation of the dune foot within the storm or between subsequent waves can be used to validate and improve dune erosion models (e.g. Larson et al. (2004)).

In Section 2.3.4 the presence of the dune foot in (several) both equilibrium and numerical dune erosion models was introduced. Splinter and Palmsten (2012) found that some dune erosion models were dependent on the initial dune foot position. This study found that for land reclamations, the dune

foot can be rather indistinguishable for some side slopes. Especially in annual storm conditions, this phenomenon might be more pronounced. Therefore, it is recommended to perform further research on the effect of the dune foot position on the erosion volume in dune erosion models relative to these LiDAR measurements.

9.2.3. Enhance measurement quality of exposed land reclamations

In this thesis, it was shown that the influence of annual storm conditions could lead to significant amounts of erosion in sandy coastal defences. Therefore, similar studies can be executed to better comprehend the influence of annual storm conditions and to estimate the resulting erosion. Varying hydrodynamic conditions, wave obliquity, profile geometries, and sediment characteristics could give inclusion and applicability to a wider range of sites. Usable and complete field measurement datasets, especially pre- and post-storm dune profiles, are scarce. Other, similar, sites with comparable forcings such as manipulative field campaigns, bunds or low-energy environments are shown to be of interest. It is advised that Boskalis, as a contractor, persist in surveying and enhancing measurement quality in order to perform dune erosion analysis on more datasets of land reclamations made by Boskalis.

Important for the gathering of a valuable dataset, is to anticipate potential bund erosion and perform proper measurements of the required wet and dry pre-storm slopes. Post-storm, the wet and dry eroded slopes need to be measured again. When side slopes are measured for an extended alongshore reach, the influence of alongshore variability can be assessed. Optimal conditions could be realised when bed-level measurements are performed with only one high water event in between. Although, safety is priority number one when performing the measurements. In between the bed level measurements, it is important to capture the hydrodynamics with a pressure or elevation sensor under a high sampling frequency (4 to 8 Hz) and export the raw time series from the instrument. Herewith, wave spectral analysis can be performed and the spectral shape could be investigated. The height elevations of both water levels and bed level elevations need to be set to the same reference datum. Additional photographs are helpful to conclude on certain outliers.

With high-quality datasets on the erosional behaviour of sandy coastal defences due to (annual) storm conditions, Boskalis can set up a research program and therewith significantly collaborate in research projects and profit from their outcomes. With these insights, the design and work method could be optimised to reduce sediment losses, setbacks in the project, additional CO2 emissions and reduce safety hazards. To achieve this, it is recommended that someone within the engineering department is responsible for the dataset acquiring incentive and overview of quality assurance.

9.2.4. Numerical modelling of typhoon-induced nearshore hydrodynamics

The typhoon occurrence at Land Reclamation Philippines is typical, with nearly 20 annual events in this region (PAGASA, 2022). Anticipated increasing frequency and severity of such storms are linked to climate change (IPCC, 2022). In order to be able to provide a more accurate estimation of the typhoon-induced erosion of sandy coastal defence slopes, it is recommended to further study the influence of nearshore hydrodynamics on dune erosion using a coupled wind-driven (SWAN and ERA5 as in Section 4.3.2) and dune erosion numerical model (e.g. XBeach). Herewith, an alongshore differentiating spatial overview of wave characteristics could be modelled and exported at every transect of 10 meters. These could provide (when reverse-shoaled to offshore conditions) a better prediction for the runup for this case study of LRP as was shown for hurricanes along the US east coast by Stockdon et al. (2007). These improved nearshore wave conditions could potentially provide a better correlation with the maximum total water level elevation (based on R_2 or potentially R_{max}) and the post-storm dune foot elevation. Therewith, the validity of the methodology of this study under typhoon-induced storm conditions can be reinforced.

References

Adriaansens, W. (2022). Corrie verandert het Banjaardstrand in een soort krijtrotsen van Dover; 'Zo erg heb ik het nog nooit gezien'. https://www.pzc.nl/bevelanden/corrie-verandert-het-banjaardstrand-in-een-soort-krijtrotsen-van-dover-zo-erg-heb-ik-het-nog-nooit-gezien~a739efb6/

Arens, S. M. (1996). Rates of aeolian transport on a beach in a temperate humid climate. *Geomorphology*, *17*(1-3 SPEC. ISS.). https://doi.org/10.1016/0169-555x(95)00089-n

Bagnold, R. A. (1941). The Physics of Blown Sand and Desert Dunes. *The Geographical Journal*, *98*(2). https://doi.org/10.2307/1787211

Basco, D. R., & Pope, J. (2004). Groin Functional Design Guidance from the Coastal Engineering Manual. *Journal of Coastal Research*, 121–130. http://www.jstor.org/stable/25736249

Bertin, X., de Bakker, A., van Dongeren, A., Coco, G., André, G., Ardhuin, F., Bonneton, P., Bouchette, F., Castelle, B., Crawford, W. C., Davidson, M., Deen, M., Dodet, G., Guérin, T., Inch, K., Leckler, F., McCall, R., Muller, H., Olabarrieta, M., … Tissier, M. (2018). Infragravity waves: From driving mechanisms to impacts. *Earth-Science Reviews*, *177*, 774–799. https://doi.org/10.1016/J.EARSCIREV.2018.01.002

Bishop, C. T., & Donelan, M. A. (1987). Measuring waves with pressure transducers. *Coastal Engineering*, *11*(4), 309–328. https://doi.org/10.1016/0378-3839(87)90031-7

Bonte, Y., & Levoy, F. (2015). Field experiments of beach scarp erosion during oblique wave, stormy conditions (Normandy, France). *Geomorphology*, *236*, 132–147. https://doi.org/10.1016/J.GEOMORPH.2015.02.014

Bosboom, J., & Stive, M. J. F. (2022). *Coastal Dynamics* (1.1). TU Delft Open. https://doi.org/10.5074/T.2021.001

Bruun, P. (1988). The Bruun Rule of Erosion by sea-level rise: a discussion on large- scale two- and three-dimensional usages. *Journal of Coastal Research*, *4*(4).

Bruun, P. (1954). Coast Erosion and the Development of Beach Profiles. *US Army Corps of Engineers*, (44).

Bruun, P. (1962). Sea-Level Rise as a Cause of Shore Erosion. *Journal of the Waterways and Harbors Division*, *88*(1). https://doi.org/10.1061/jwheau.0000252

Caldwell, P. C., Merrifield, M. A., & Thompson, P. R. (2015). Sea level measured by tide gauges from global oceans.

Cohn, N., Ruggiero, P., de Vries, S., & Kaminsky, G. M. (2018). New Insights on Coastal Foredune Growth: The Relative Contributions of Marine and Aeolian Processes. *Geophysical Research Letters*. https://doi.org/10.1029/2018GL077836

Datawell. (2023). Directional Waverider DWR-G. https://datawell.nl/products/directional-waverider-dwr-g/

Dean, R. G., & Galvin, C. J. (1976). Beach erosion: Causes, processes, and remedial measures. *C R C Critical Reviews in Environmental Control*, *6*(3). https://doi.org/10.1080/10643387609381643

Dean, R. G. (1977). Equilibrium Beach Profiles: U.S. Atlantic and Gulf Coasts. *Ocean Engineering Report*, *12*.

de Jong, B., Keijsers, J. G., Riksen, M. J., Krol, J., & Slim, P. A. (2014). Soft engineering vs. a dynamic approach in coastal dune management: A case study on the North Sea barrier Island of Ameland, the Netherlands. *Journal of Coastal Research*, *30*(4). https://doi.org/10.2112/JCOASTRES-D-13-00125.1

Delft Hydraulics Laboratory. (1978). *Duinafslag ten gevolge van de stormvloed op 3 januari: toetsing van de voorlopige richtlijn* (tech. rep.). Delft Hydraulic Laboratory. Delft.

Delft Hydraulics Laboratory. (1984). *Duinafslag ten gevolge van de stormvloed op 1 en 2 februari 1983* (tech. rep.). Delft Hydraulics Laboratory. Delft.

de Vries, S., Southgate, H. N., Kanning, W., & Ranasinghe, R. (2012). Dune behavior and aeolian transport on decadal timescales. *Coastal Engineering*, *67*. https://doi.org/10.1016/j.coastaleng.2012.04.002

de Vries, S., Harley, M. D., De Schipper, M. A., & Ruessink, G. (2015). Dune growth due to aeolian sediment transport and the role of the beach and intertidal zone. https://doi.org/10.1142/9789814689977{_}0043

de Winter, R. C., Gongriep, F., & Ruessink, B. G. (2015). Observations and modeling of alongshore variability in dune erosion at Egmond aan Zee, the Netherlands. *Coastal Engineering*, *99*, 167–175. https://doi.org/10.1016/J.COASTALENG.2015.02.005

de Winter, R. C., & Ruessink, B. G. (2017). Sensitivity analysis of climate change impacts on dune erosion: case study for the Dutch Holland coast. *Climatic Change*, *141*(4). https://doi.org/10.1007/s10584-017-1922-3

Diamantidou, E., Santinelli, G., Giardino, A., Stronkhorst, J., & de Vries, S. (2020). An Automatic Procedure for Dune Foot Position Detection: Application to the Dutch Coast. *Journal of Coastal Research*, *36*(3). https://doi.org/10.2112/JCOASTRES-D-19-00056.1

Eckhart, C. (1952). Propagation of gravity waves from deep to shallow water. *Gravity waves*. U.S. Govt. Print. Off.

ECMWF. (2022). ERA5 hourly data on single levels from 1979 to present. https://www.ecmwf.int/en/forecasts/datasets/reanalysis-datasets/era5

Edelman, T. (1972). Dune erosion during storm conditions. *Coastal Engineering Proceedings*, *1*(13). https://doi.org/10.9753/icce.v13.66

Erikson, L. H., Larson, M., & Hanson, H. (2007). Laboratory investigation of beach scarp and dune recession due to notching and subsequent failure. *Marine Geology*, *245*(1-4), 1–19. https://doi.org/10.1016/J.MARGEO.2007.04.006

GEBCO. (2022). GEBCO 2022 Grid (sub-ice topo/bathy). https://www.gebco.net/data_and_products/gridded_bathymetry_data/

Giardino, A., Santinelli, G., & Bruens, A. (2012). *The state of the coast (Toestand van de kust). Case study: North Holland* (tech. rep.). Deltares. Delft.

Google. (2023). Google Earth Pro.

Guillén, J., Stive, M. J., & Capobianco, M. (1999). Shoreline evolution of the Holland coast on a decadal scale. *Earth Surface Processes and Landforms*, *24*(6). https://doi.org/10.1002/(SICI)1096-9837(199906)24:6<517::AID-ESP974>3.0.CO;2-A

Harley, M. D., Turner, I. L., Splinter, K. D., Phillips, M. S., & Simmons, J. A. (2016). Beach response to Australian east coast lows: A comparison between the 2007 and 2015 events, Narrabeen-Collaroy Beach. *Journal of Coastal Research*, *1*(75). https://doi.org/10.2112/SI75-078.1

Hoek, J., & Klein, M. (2022). Guideline for Cyclone Modelling with software Triangle and SWAN.

Holthuijsen, L. H. (2007). *Waves in Oceanic and Coastal Waters*. Cambridge University Press.

Hoonhout, B., & de Vries, S. (2017). Aeolian sediment supply at a mega nourishment. *Coastal Engineering*, *123*. https://doi.org/10.1016/j.coastaleng.2017.03.001

Hughes, S. A., & Chiu, T. Y. (1981). Beach and dune erosion during severe storms. *University of Florida, Coastal and Oceanographic Engineering Department, (Technical Report) UFL/COEL-TR*.

Hughes, S. A., & Chiu, T. Y. (1978). Variations in beach profiles when approximated by a theoretical curve. *Univ Fla Coastal Oceanogr Eng Lab Rep UFL COEL TR*, (39).

IPCC. (2021). *Climate Change 2021: The Physical Science Basis. Contribution of Working Group I to the Sixth Assessment Report of the Intergovernmental Panel on Climate Change* (tech. rep.). Cambridge. https://doi.org/10.1017/9781009157896

IPCC. (2022). *Climate Change 2022: Impacts, Adaptation and Vulnerability. Contribution of Working Group II to the Sixth Assessment Report of the Intergovernmental Panel on Climate Change* (tech. rep.). Intergovernmental Panel on Climate Change. https://doi.org/10.1017/9781009325844

Kawamura, R. (1951). *Study of sand movement by wind* (tech. rep. No. 3-4).

Larson, M., Erikson, L., & Hanson, H. (2004). An analytical model to predict dune erosion due to wave impact. *Coastal Engineering*, *51*(8-9), 675–696. https://doi.org/10.1016/J.COASTALENG.2004.07.003

Lippmann, T. C., & Holman, R. A. (1990). The spatial and temporal variability of sand bar morphology. *Journal of Geophysical Research: Oceans*, *95*(C7), 11575–11590. https://doi.org/https://doi.org/10.1029/JC095iC07p11575

Longuet-Higgins, M. S., & Stewart, R. w. (1964). Radiation stresses in water waves; a physical discussion, with applications. *Deep-Sea Research and Oceanographic Abstracts*, *11*(4). https://doi.org/10.1016/0011-7471(64)90001-4

Masselink, G., Brooks, S., Poate, T., Stokes, C., & Scott, T. (2022). Coastal dune dynamics in embayed settings with sea-level rise – Examples from the exposed and macrotidal north coast of SW England. *Marine Geology*, *450*, 106853. https://doi.org/10.1016/J.MARGEO.2022.106853

Masselink, G., Castelle, B., Scott, T., Dodet, G., Suanez, S., Jackson, D., & Floc'h, F. (2016). Extreme wave activity during 2013/2014 winter and morphological impacts along the Atlantic coast of Europe. *Geophysical Research Letters*, *43*(5), 2135–2143. https://doi.org/https://doi.org/10.1002/2015GL067492

Möller, J. P., & Swart, D. H. (1988). Extreme Erosion Event on an Artificial Beach. *Coastal Engineering 1988*, 1882–1896. https://doi.org/10.1061/9780872626874.140

National Research Council. (1995). *Beach Nourishment and Protection*. The National Academies Press. https://doi.org/10.17226/4984

Nickling, W., & Davidson-Arnott, R. (1990). Aeolian sediment transport on beaches and coastal sand dunes. *Proceedings of Symposium on Coastal Sand Dunes*, (June).

Nishi, R., Sato, M., & Wang, H. (1994). Field Observation and Numerical Simulation of Beach and Dune Scarps. *Coastal Engineering 1994*, 2434–2448. https://doi.org/10.1061/9780784400890.177

Nortek. (2023). AWAC - 600 kHz. https://www.nortekgroup.com/products/awac-600-khz

Overbeck, J. R., Long, J. W., & Stockdon, H. F. (2017). Testing model parameters for wave-induced dune erosion using observations from Hurricane Sandy. *Geophysical Research Letters*, *44*(2), 937–945. https://doi.org/https://doi.org/10.1002/2016GL071991

Overton, M. F., Fisher, J. S., & Young, M. A. (1988). Laboratory Investigation of Dune Erosion. *Journal of Waterway, Port, Coastal, and Ocean Engineering*, *114*(3), 367–373. https://doi.org/10.1061/(ASCE)0733-950X(1988)114:3(367)

Overton, M. F., Pratikto, W. A., Lu, J. C., & Fisher, J. S. (1994). Laboratory investigation of dune erosion as a function of sand grain size and dune density. *Coastal Engineering*, *23*(1-2), 151–165. https://doi.org/10.1016/0378-3839(94)90020-5

PAGASA. (2022). Tropical Cyclone Information.

Palmsten, M. L., & Holman, R. A. (2012). Laboratory investigation of dune erosion using stereo video. *Coastal Engineering*, *60*(1), 123–135. https://doi.org/10.1016/J.COASTALENG.2011.09.003

Planbureau voor de Leefomgeving. (2007). *Correctie formulering over overstromingsrisico Nederland in IPCC-rapport* (tech. rep.). Planbureau voor de Leefomgeving. Den Haag. https://www.pbl.nl/correctie-formulering-over-overstromingsrisico#:~:text=Op%20basis%20van%20de%20actuele,gevoelig%2Fkwetsbaar%20is%20voor%20overstromingen.

Pruszak, Z., Ostrowski, R., & Schönhofer, J. (2011). Variability and correlations of shoreline and dunes on the southern Baltic coast (CRS Lubiatowo, Poland). *Oceanologia*, *53*(1), 97–120. https://doi.org/10.5697/oc.53-1.097

Psuty, N. P. (1990). Foredune mobility and stability. In K. Nordstrom, N. Psuty, & B. Carter (Eds.), *Coastal dunes, form and process* (pp. 159–176). Wiley.

Reniers, A. J. H. M. (2004). Morphodynamic modeling of an embayed beach under wave group forcing. *Journal of Geophysical Research*, *109*(C1), C01030. https://doi.org/10.1029/2002JC001586

Reniers, A. J., MacMahan, J. H., Thornton, E. B., & Stanton, T. P. (2007). Modeling of very low frequency motions during RIPEX. *Journal of Geophysical Research: Oceans*, *112*(7). https://doi.org/10.1029/2005JC003122

Reniers, A. J., Thornton, E. B., Stanton, T. P., & Roelvink, J. A. (2004). Vertical flow structure during Sandy Duck: observations and modeling. *Coastal Engineering*, *51*(3), 237–260. https://doi.org/10.1016/J.COASTALENG.2004.02.001

Roelvink, D., Reniers, A., van Dongeren, A., van Thiel de Vries, J., McCall, R., & Lescinski, J. (2009). Modelling storm impacts on beaches, dunes and barrier islands. *Coastal Engineering*, *56*(11-12). https://doi.org/10.1016/j.coastaleng.2009.08.006

Ruessink, B. G., Boers, M., van Geer, P. F., de Bakker, A. T., Pieterse, A., Grasso, F., & de Winter, R. C. (2012). Towards a process-based model to predict dune erosion along the Dutch Wadden coast. *Geologie en Mijnbouw/Netherlands Journal of Geosciences*, *91*(3). https://doi.org/10.1017/S0016774600000494

Ruessink, B. G., & Jeuken, M. C. (2002). Dunefoot dynamics along the Dutch coast. *Earth Surface Processes and Landforms*, *27*(10). https://doi.org/10.1002/esp.391

Ruessink, B. G., Kleinhans, M. G., & van den Beukel, P. G. L. (1998). Observations of swash under highly dissipative conditions. *Journal of Geophysical Research: Oceans*, *103*(C2), 3111–3118. https://doi.org/https://doi.org/10.1029/97JC02791

Sallenger, J. (2000). Storm impact scale for barrier islands. *Journal of Coastal Research*, *16*(3).

Senechal, N., Abadie, S., Gallagher, E., MacMahan, J., Masselink, G., Michallet, H., Reniers, A., Ruessink, G., Russell, P., Sous, D., Turner, I., Ardhuin, F., Bonneton, P., Bujan, S., Capo, S., Certain, R., Pedreros, R., & Garlan, T. (2011). The ECORS-Truc Vert'08 nearshore field experiment: presentation of a three-dimensional morphologic system in a macro-tidal environment during consecutive extreme storm conditions. *Ocean Dynamics*, *61*(12), 2073–2098. https://doi.org/10.1007/s10236-011-0472-x

Seymour, R., Guza, R. T., O'Reilly, W., & Elgar, S. (2005). Rapid erosion of a small southern California beach fill. *Coastal Engineering*, *52*(2), 151–158. https://doi.org/10.1016/J.COASTALENG.2004.10.003

Sherman, D., & Hotta, S. (1990). Aeolian sediment transport: theory and measurement. In K. F. Nordstrom, N. P. Psuty, & B. B. Carter (Eds.), *Coastal dunes, form and process*. Wiley.

Short, A. D., & Hesp, P. A. (1982). Wave, beach and dune interactions in southeastern Australia. *Marine Geology*, *48*(3-4), 259–284. https://doi.org/10.1016/0025-3227(82)90100-1

Smith, A., Houser, C., Lehner, J., George, E., & Lunardi, B. (2020). Crowd-sourced identification of the beach-dune interface. *Geomorphology*, *367*. https://doi.org/10.1016/j.geomorph.2020.107321

Splinter, K. D., Kearney, E. T., & Turner, I. L. (2018). Drivers of alongshore variable dune erosion during a storm event: Observations and modelling. *Coastal Engineering*, *131*, 31–41. https://doi.org/10.1016/j.coastaleng.2017.10.011

Splinter, K. D., & Palmsten, M. L. (2012). Modeling dune response to an East Coast Low. *Marine Geology*, *329-331*, 46–57. https://doi.org/10.1016/J.MARGEO.2012.09.005

Splinter, K. D., Palmsten, M. L., Holman, R. A., & Tomlinson, R. B. (2012). Comparison of measured and modeled run-up and resulting dune erosion during a lab experiment. https://doi.org/10.1142/9789814355537{_}0059

Stive, M. (1986). A model for cross-shore sediment transport. *Coastal Engineering*.

Stockdon, H. F., Holman, R. A., Howd, P. A., & Sallenger, A. H. (2006). Empirical parameterization of setup, swash, and runup. *Coastal Engineering*, *53*(7), 573–588. https://doi.org/10.1016/J.COASTALENG.2005.12.005

Stockdon, H. F., Sallenger, A. H., Holman, R. A., & Howd, P. A. (2007). A simple model for the spatially-variable coastal response to hurricanes. *Marine Geology*, *238*(1-4). https://doi.org/10.1016/j.margeo.2006.11.004

Suanez, S., Cariolet, J. M., Cancouët, R., Ardhuin, F., & Delacourt, C. (2012). Dune recovery after storm erosion on a high-energy beach: Vougot Beach, Brittany (France). https://doi.org/10.1016/j.geomorph.2011.10.014

Trembath, M. (2020). Sand dunes collapse into sea at Elouera beach with erosion expected to spread. https://www.theleader.com.au/story/6852395/cronulla-beaches-battered/

TU Delft. (2022). RealDune – Dune erosion during storm surges. https://www.tudelft.nl/citg/over-faculteit/afdelingen/hydraulic-engineering/sections/coastal-engineering/research/realdune

van de Graaff, J. (1977). Dune erosion during a storm surge. *Coastal Engineering*, *1*(100), 99–134. https://doi.org/10.1016/0378-3839(77)90010-2

van Bemmelen, C. W., de Schipper, M. A., Darnall, J., & Aarninkhof, S. G. (2020). Beach scarp dynamics at nourished beaches. *Coastal Engineering*, *160*. https://doi.org/10.1016/j.coastaleng.2020.103725

van Gent, M. R., van Thiel de Vries, J., Coeveld, E. M., de Vroeg, J. H., & van de Graaff, J. (2008). Large-scale dune erosion tests to study the influence of wave periods. *Coastal Engineering*, *55*(12). https://doi.org/10.1016/j.coastaleng.2008.04.003

van IJzendoorn, C. O., de Vries, S., Hallin, C., & Hesp, P. A. (2021). Sea level rise outpaced by vertical dune toe translation on prograding coasts. *Scientific Reports*, *11*(1). https://doi.org/10.1038/s41598-021-92150-x

van Rijn, L. (1993). Principles of Sediment Transport in Rivers, Estuaries and Coastal Seas. *Principles of Sediment Transport in Rivers , Estuaries and Coastal Seas*.

van Santen, R., McCall, R., Wilmink, R., Coumou, L., Quataert, E., Pluis, S., Steetzel, H., de Goede, R., & van Kuik, N. (2022). Improvements and validation of XBeach for the safety assessment of

the Dutch coast. *NCK*. https://www.nck-web.org/boa-2022/505-improvements-and-validation-of-xbeach-for-the-safety-assessment-of-the-dutch-coast-part-2-morphodynamics

van Thiel de Vries, J. (2009). *Dune erosion during storm surges* (Doctoral dissertation).

van Thiel De Vries, J., Clarke, L. B., Aarninkhof, S. G., Coeveld, E. M., Holman, R. A., Palmsten, M. L., Reniers, A. J., Stive, M. J., & Uijttewaal, W. S. (2007). Interaction of dune face and swash zone. *Coastal Sediments '07 - Proceedings of 6th International Symposium on Coastal Engineering and Science of Coastal Sediment Processes*. https://doi.org/10.1061/40926(239)155

van Thiel de Vries, J., Dongeren, A. V., McCall, R., & Reniers, A. (2011). The effect of the longshore dimension on dune erosion. *Coastal Engineering Proceedings*, *1*(32). https://doi.org/10.9753/icce.v32.sediment.49

van Thiel de Vries, J., Gent, M. R. v., Walstra, D. J., & Reniers, A. J. (2008). Analysis of dune erosion processes in large-scale flume experiments. *Coastal Engineering*, *55*(12). https://doi.org/10.1016/j.coastaleng.2008.04.004

van Wiechen, P., de Vries, S., Reniers, A. J. H. M., & Aarninkhof, S. G. J. (2022). Dune erosion during storm surges: A review of the observations, physics and modelling of the collision regime. *Journal of Coastal Engineering*.

van Wiechen, P., Rutten, J., Mieras, R., Anarde, K., Tissier, M., & de Vries, S. (2022). Avalanching of the dune face: field observations and equilibrium theory.

Vellinga, P. (1978). Movable bed model tests on dune erosion. *Coastal Engineering Proceedings*, *1*(16). https://doi.org/10.9753/icce.v16.122

Vellinga, P. (1983). Predictive computational model for beach and dune erosion during storm surges. *DELFT, THE NETHERLANDS, DELFT HYDRAUL. LAB., FEB. 1983*, (294)).

Vellinga, P. (1986). *Beach and Dune Erosion during Storm Surges* (Doctoral dissertation). Delft Hydraulics Laboratory. Delft.

Waterman, R. E. (2010). *Integrated Coastal Policy via Building with Nature* (Doctoral dissertation). Technische Universiteit Delft. Delft. http://resolver.tudelft.nl/uuid:fa9a36f9-7cf8-4893-b0fd-5e5f15492640

Weggel, J. R. (1995). A primer on monitoring beach nourishment projects. *Shore & Beach*, *63*(3).

Wright, L. D., & Short, A. D. (1984). Morphodynamic variability of surf zones and beaches: A synthesis. *Marine Geology*, *56*(1-4), 93–118. https://doi.org/10.1016/0025-3227(84)90008-2

Appendices

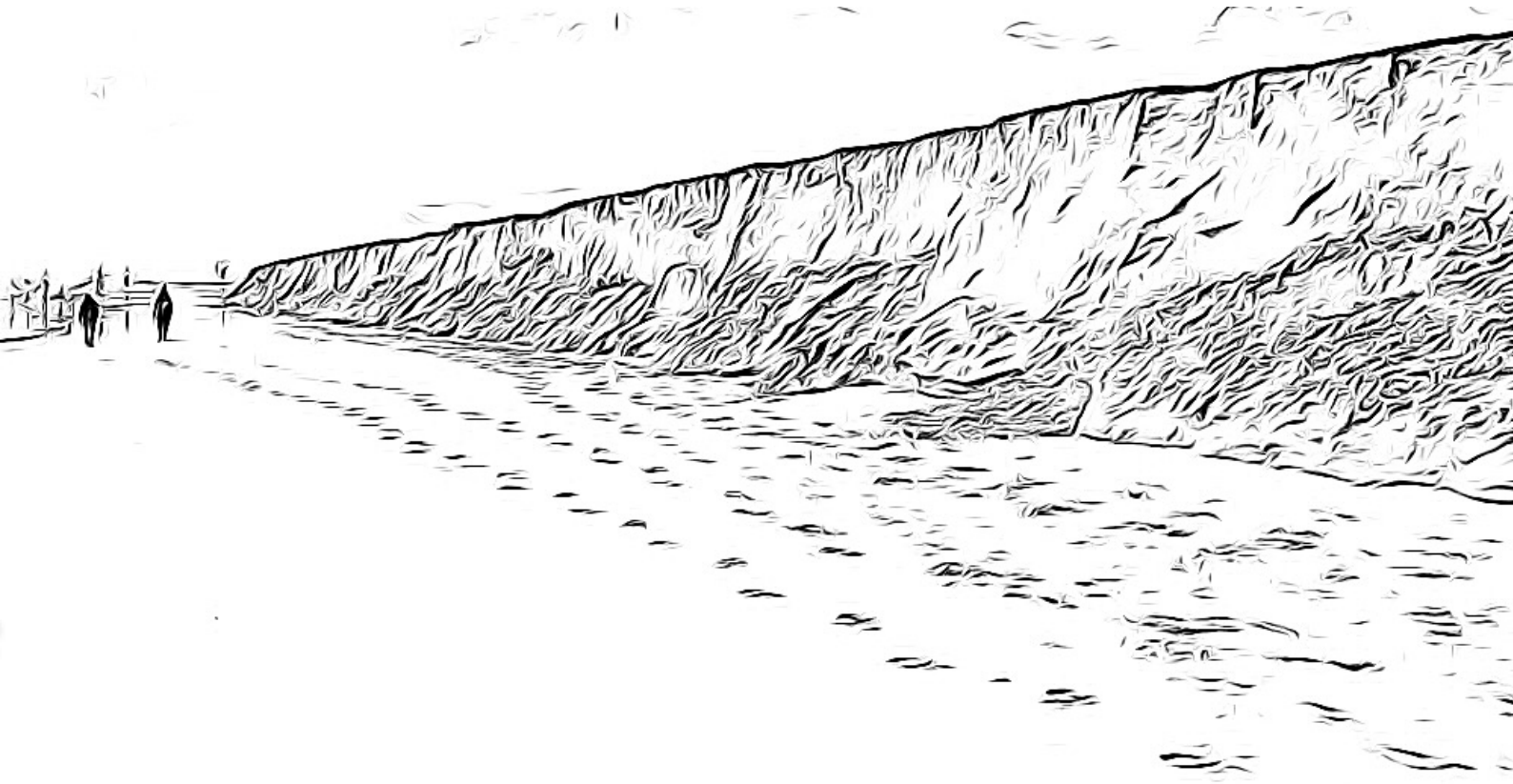

A

Supportive literature study

The theoretical framework presented in Chapter 2 encompassed a brief description of dune equilibrium theory, dune erosion experiments, aeolian transport and sea level rise. This appendix provides a more thorough background on these dune erosion-related subjects.

A.1. Equilibrium theory

A cross-shore profile is a cross-section of the dune, beach, and foreshore and could be extended towards a certain depth offshore depending on the interest of the research or the availability of measurements. The cross-shore profile can be taken on a location of interest and is perpendicular to the beach contour. Which such a figure for multiple moments in time, the development in the dune and beach profile can be observed.

During storm conditions, the cross-shore profile is susceptible to a transformation over time and therewith a reset of specific morphological features. This process can be observed also in the alongshore direction. The pre-storm profile moves towards an (equilibrium) post-storm profile and can be described by equilibrium (dune erosion) theory. Edelman (1972) built upon the findings of the long-term equilibrium profiles by Bruun (1954) and found that in many cases after the storm, the upper profile was approximately identical. van de Graaff (1977) stated that the cross-shore extend of the profile transformation was far less than the reach of the long-term equilibrium profile found by Bruun (1954). Vellinga (1986) built upon the findings of van de Graaff (1977) and Vellinga (1978). He observed certain similarities in his experiments and defined an equilibrium post-storm cross-shore dune profile as a function of total water level (storm surge level), wave conditions and grain size characteristics. The profile is hypothesised to be in short-term equilibrium to the storm conditions, meaning that after the storm the profile will tend towards another equilibrium. The dune erosion prediction model uses an equilibrium profile sub-divided into three main sections. The first section reaches from the upper dune face with a 1:1 slope towards the post-storm dune foot position (transition point S), which is vertically fixed at the maximum storm surge level (SSL). The profile is derived for the normative conditions of $H_0 = 7.6\ m$, $T_p = 12\ s$ and $D_{50} = 225\ \mu m$. From the dune foot towards the transition point R, the dune profile follows a parabolic shape described by:

$$\frac{7.6}{H_{0s}} * y = 0.4714 \left[\left(\frac{7.6}{H_{0s}} \right)^{1.28} * \left(\frac{w_s}{0.0268} \right)^{0.56} * x + 18 \right]^{0.5} - 2.00 \tag{A.1}$$

This, offshore located, transition point R is located at the cross-shore x- and y- coordinates:

$$\begin{aligned} x_R &= 250 * \left(\frac{H_{0s}}{7.6} \right)^{1.28} * \left(\frac{0.0268}{w_s} \right)^{0.56} \\ y_R &= 5.717 * \left(\frac{H_{0s}}{7.6} \right) \end{aligned} \tag{A.2}$$

After transition point R, the slope of the bed is 1:12.5 until the point where sediment is conserved in the system and eroded volume equals settled volume for a fully cross-shore sediment distribution as shown in Figure A.1.

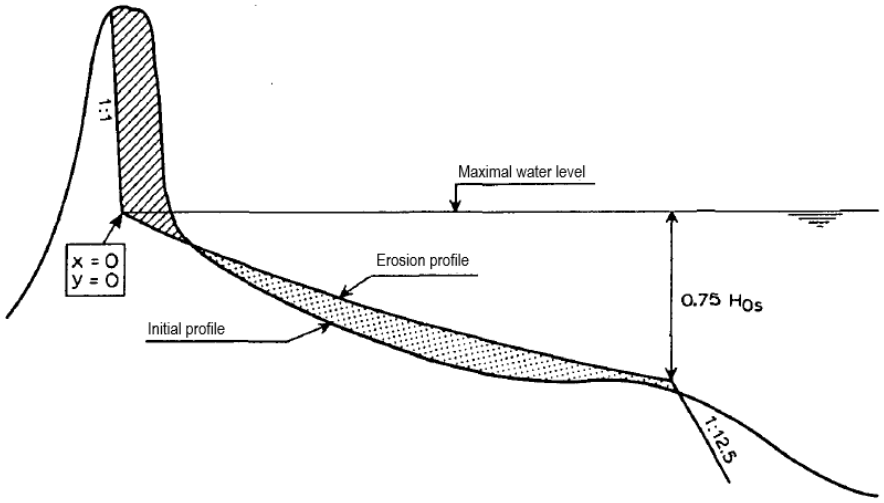

Figure A.1: Equilbrium profile as defined by Vellinga (1986) (figure edited from Vellinga (1986))

van Gent et al. (2008) improved the method of Vellinga (1986) by including the influence of the wave period in a similar way as the wave height and sediment fall velocity are incorporated. They found, especially in double-peaked wave spectra, that the wave period $T_{m-1.0}$ gave a better representation than the wave peak period T_p for dune erosion. Therewith the expression for the post-storm dune erosion profile reads:

$$\frac{7.6}{H_{0s}} * y = 0.4714 \left[\left(\frac{7.6}{H_{0s}} \right)^{1.28} * \left(\frac{10.9}{T_{m-1.0}} \right)^{0.45} \left(\frac{w_s}{0.0268} \right)^{0.56} * x + 18 \right]^{0.5} - 2.0 \tag{A.3}$$

and

$$\begin{aligned} x_R &= 250 * \left(\frac{H_{0s}}{7.6} \right)^{1.28} * \left(\frac{0.0268}{w_s} \right)^{0.56} \\ y_R &= \left(\frac{H_{0s}}{7.6} \right) * \left[0.4714 * \left(250 * \left(\frac{10.9}{T_{m-1.0}} \right)^{0.45} + 18 \right)^{0.5} - 2 \right] \end{aligned} \tag{A.4}$$

However, these erosion profiles are derived by scale relations of the prototype conditions. Bruun (1954), Dean (1977), and Hughes and Chiu (1978) had already found that the equilibrium profile can be described by the single power curve $y = p * x^{2/3}$. Vellinga (1986) states that for a complete wave climate and wide range of wave spectra, this 2/3 power will not be valid in all cases. Therefore, also a more generalistic empirical power curve can be found as defined in Equation (2.1), where p and γ are empirically found parameters varying per site and per present conditions.

$$y = p * x^{\gamma} \tag{A.5}$$

The dune erosion prediction model, however, does come with some pitfalls which need to be accounted for in a proper calculation. Firstly, Vellinga (1986) states that the formula to predict the post-storm dune profile is based solely on the cross-shore profile. For situations with alongshore non-uniform characteristics, the effect of alongshore transport gradients needs to be investigated as this is not incorporated.

Secondly, in the dune erosion prediction model, the dune foot was fixed at the peak water level during the storm surge. In flume and field experiments, it was observed by researchers (e.g. van Thiel de Vries

(2009) and van Wiechen, Rutten, et al. (2022)) that the dune foot moves in time during the storm-surge. The influence of the dune foot position, i.e. the abrupt change in slope, in the effect of the hydrodynamic conditions on dune erosion is not yet understood to the full extent.

Finally, the parabolic shape of the erosion profile is described by a function of the significant offshore wave height and the settling velocity and Vellinga (1986) states that this shape of the post-storm dune profile is independent of the initial profile, however, is highly dependent on the grain size. However, in the short-term, the duration of the storm could potentially be of huge influence as it could be hypothesised that equilibrium conditions were not reached during a short-lasting storm and therefore initial conditions do have an impact on the post-storm profile.

A.2. Dune erosion experiments and measurements

To be able to properly implement a dune erosion model, a better understanding of the site-specific processes could be needed. This can be achieved by studies on monitoring or experimental field data regarding certain unknown aspects. Monitoring data is often not complete and does not have clear statements of site-specific parameters according to Weggel (1995) and data which is collected in a monitoring program is often not usable for a specific research goal and the crucial questions remain unanswered (National Research Council, 1995). Nowadays, more datasets monitored by governments are available which could provide for the research goals (de Vries et al., 2012; van IJzendoorn et al., 2021). However, combined morphological and hydrodynamic datasets gathered by (civil) contractors are used scarcely in research to verify dune theory or validate dune erosion models.

In order to gain insight into dune erosion processes in the collision regime, measurements were performed which proved to be valuable. The timescale of those measurements is important as the impact assessment of one storm requires the pre- and post-storm dune profile. Generally, three types of measurements can be distinguished: Field observations, laboratory experiments and manipulative field campaigns (van Wiechen, de Vries, et al., 2022). Field observations are performed at dunes which are subject to real-life conditions and forcings which makes sure every aspect is included. Laboratory experiments are performed in a confined environment where the hydrodynamic forcings (e.g. wave height, wave period, water level) can be imposed as desired. Manipulative field campaigns are somewhere in between, a field setup is configured in a way that the processes occur for more frequent events and imply (near) real-life conditions.

This research aims to examine the impact of annual storm conditions on the dune foot behaviour of sandy coastal defences, using a combination of real-scale field measurements and relevant insights gathered from laboratory experiments and manipulative field campaigns. To effectively assess the influence of annual storm conditions on the morphodynamics of sandy coastal defences, it is essential to record and analyse both the morphological characteristics of the dune and beach, as well as the hydrodynamic forces acting on the coastal system. To record the morphological characteristics of the dune and beach in the field, a range of advanced technological tools and techniques can be used, including Real-Time Kinematic Global Positioning Systems (RTK GPS) (Harley et al., 2016; Masselink et al., 2016; Seymour et al., 2005), Light Detection and Ranging (LiDAR) systems (Bonte & Levoy, 2015; de Winter et al., 2015; Overbeck et al., 2017), and image analysis (Lippmann & Holman, 1990). Additionally, the bathymetry of the coastal area can be surveyed using a single-beam (SBES) or multi-beam echo sounder (MBES) attached to a small boat, surveying vessel or jetski. Meanwhile, the hydrodynamic forces acting on the coastal system can be observed and recorded using various instruments such as wave buoys, pressure sensors, and acoustic (ADCP) and electromagnetic velocimeters (ESV) (de Winter et al., 2015; Reniers et al., 2004; Senechal et al., 2011; Seymour et al., 2005).

A.3. Aeolian transport

To enhance the prediction for aeolian transport volumes, the first equations were developed based on aeolian processes for desert dunes and in wind tunnels (Bagnold, 1941; Kawamura, 1951). These are relatively simple conditions compared to the more complex situation of aeolian transport in coastal dunes (Psuty, 1990). Here, other factors influencing aeolian transport are amongst others: beach width, rainfall, surface moisture, sediment characteristics, crust formation and vegetation (Arens, 1996; Nickling & Davidson-Arnott, 1990; Sherman & Hotta, 1990). For instance, has been found that milder beach slopes accommodate for more aeolian transport, resulting in more dune growth (de Vries et al., 2012).

Generally, aeolian transport of sand occurs for wind velocities of >5-10 m/s. Precipitation limits aeolian transports as the sand becomes wet which makes it non-erodible by the wind. Large wind velocities often go hand-in-hand with precipitation, hence aeolian transport occurs only for relatively mild conditions (Arens, 1996). However, quantitative knowledge on the processes of coastal dune building is still limited (de Vries et al., 2012). Aeolian transport includes three main aeolian processes:

- Suspension: fine sand particles that are moved by wind and remain in suspension in the air.
- Saltation: wind induces turbulence close to the ground which disturbs the sand particles and set them in motion. Gravity attracts them back to the bed which they impact and set other particles in motion before they bounce off again. This is the most common form of aeolian transport.
- Surface creep: coarse sand particles moved by the wind along the ground.

Dune volume changes are found to be linear in time for the Holland coast based on the JARKUS dataset and are in the order of $0 - 40\ m^3/m/yr$ and occur especially during calm periods (de Vries et al., 2012). This is important to take into account when looking at dune erosion events on larger timescales. Dune erosion events occur for high wind velocities where precipitation is likely. Precipitation limits the availability of the sand for aeolian transport (Arens, 1996). The sediment supply for dune growth due to aeolian transport was found to not originate from the upper beach and therefore may originate from the lower beach or the intertidal zone (de Vries et al., 2015).

When looking at a monthly, quarterly or yearly timescale the effect of dune volume change due to aeolian transport cannot be disregarded without notice, as it has been shown that it is significant on yearly basis (de Vries et al., 2012). For these timescales, it is important to properly include a reliability interval to not underestimate the erosion volumes due to storm surges. Additionally, it has been found by de Vries et al. (2012) that it cannot be concluded that there is faster dune recovery in the year after an erosion event and therefore assumed, that aeolian-induced dune growth is approximately linear in time for a longer period.

A.4. Sea Level Rise

Dune erosion is often linked to Sea Level Rise (e.g. Bruun (1962)). Sea Level Rise (SLR) refers to the mean global sea level change compared to a certain reference point in time, for instance, the year 1900. Sea level rise can be linked as a consequence of global warming. Over the last 100 years, the sea has already risen to a higher level. Unfortunately, this rise is expected to be reinforced over the coming 100 years (IPCC, 2021). The rise will not be equally distributed over all water bodies, therewith some regions will face more rise in the water level elevation than the mean.

The Intergovernmental Panel on Climate Change introduces five scenarios, each having its own characteristics and resulting SLR confidence interval. These scenarios are called Shared Socioeconomic Pathways (SSP) and consist of a first number based on a strategy and a second number based on the expected level of radiative forcing (W/m^2) in 2100. The scenarios vary from SSP1 (Sustainability – Taking the Green Road) to SSP5 (Fossil-fueled Development – Taking the Highway) (IPCC, 2021).

Based on these scenarios, a confidence interval of the projected Global Mean Sea Level (GMSL) change is provided. By 2150 an SLR of around 1 meter will be likely (Figure A.2).

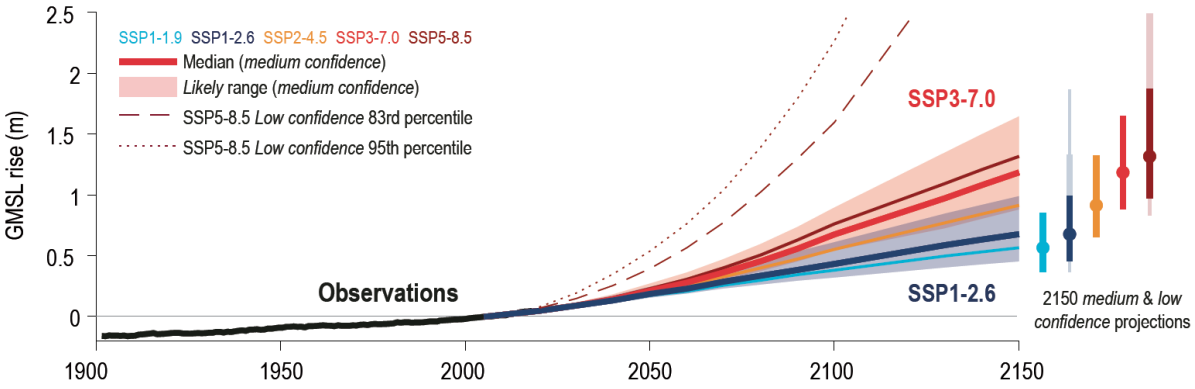

Figure A.2: Global mean sea level (GMSL) change on different time scales and under different SSP scenarios (figure from IPCC (2021))

The general effect of SLR on dunes can be described by a simple formula from the theory of Bruun (1962) which relates SLR to the dune volume change:

$$(y + a)^{3/2} = p\,(x + 100a) \tag{A.6}$$

With p an empirical parameter is found using field data in line with the equilibrium profile $y^{3/2} = px$ and a the amount of SLR. According to Bruun (1988) it is important to note that the Bruun rule (Bruun, 1962) is designed for a two-dimensional use and not for three-dimensional use (with alongshore variations). Numerical modelling with XBeach performed by de Winter and Ruessink (2017) reinforces the relation of SLR being the driving processes of intensified dune erosion.

B

Supplementary data processing for RealDune-REFLEX hydrodynamics

The raw hydrodynamic measurements of the continuous water level elevation of the RealDune-REFLEX dataset require thorough pre-processing before the wave characteristics can be attributed to certain storm periods. This appendix first provides a description of how the pressure measurements are converted to water level elevations and second how wave characteristics are extracted from water level time series.

B.1. Pressure to water level elevation

The RBR pressure sensors of Dune 1 and Dune 2 measure at a sampling frequency of $F = 8\ Hz$. The instruments measure time t in Unix seconds and pressure p in Pascal. The gravity acceleration $g = 9.81\ m/s^2$ and the density of the seawater $\rho_w = 1025\ kg/m^3$.

The RBR measured pressure at the site consists of three components. The atmospheric pressure p_{atm}, the hydrostatic pressure $p_{hydrostatic}$ and the wave-induced pressure p_{wave} (Equation (B.1). Hydrostatic pressure assumes stationary and incompressible fluid which is not valid in this situation as the wave-induced pressure influences the pressure in the moving water. The water particles in a wave move in ellipses which are caused by wave-induced pressure gradients. Continuous pressure measurements in the water, lead to the measurement of the total pressure which includes the wave-induced pressure.

$$p = p_{atm} + p_{hydrostatic} + p_{wave} = p_{atm} + \rho g h + \rho g a \frac{\cosh\left[k\left(d+h\right)\right]}{\cosh\left(kd\right)} \sin\left(\omega t - kx\right) \tag{B.1}$$

First, the pressure time series are corrected for the atmospheric pressure $p_{atm} = p_0$ which is measured at Hoek van Holland.

$$p - p_0 = \rho g h \tag{B.2}$$

The pressure time series is then converted from pressure Pascal to the pressure height in meters.

$$h = \frac{p}{g * \rho} \tag{B.3}$$

The mean water depth over the interval is computed using the mean of the pressure height and the mean height above the bed which was measured every day by the RealDune-REFLEX team and assumed to increase or decrease linearly through time in between measurements.

$$h = \overline{p} + h_{bed} \tag{B.4}$$

The pressure is detrended with a double smoothing function with a window of 10 minutes. The mean is calculated over this period and subtracted from the pressure signal, so the pressure height signal varies around zero. A Fast Fourier Transformation (FTT) is applied on the detrended pressure signal. The block length is the entire length of the 10-minute interval. The smallest frequency which is solved for is $f_1 = 0.001667\ Hz$ with steps of $\Delta f = 0.001667\ Hz$ until the cut-off frequency $f_{cut-off} = 1\ Hz$.

A factor is calculated to account for the wave-induced pressure and to obtain an estimation of the actual water surface elevation η. For this estimation, the wave number k is required. The initial estimate of k is estimated following the Eckhart (1952) formulation.

$$k = \frac{\alpha}{h}\sqrt{\frac{\cosh\alpha}{\sinh\alpha}} \tag{B.5}$$

with α defined as:

$$\alpha = \frac{(2\pi)^2 h}{g(1/f_1)^2} \tag{B.6}$$

With this initial value for the wave number k, the dispersion relation is solved for k for all frequencies.

$$\omega^2 = gk\tanh kh \tag{B.7}$$

A factor K_p (pressure response factor) is calculated following the method of Bishop and Donelan (1987).

$$K_p = \frac{\cosh(k*h)}{\cosh(k*h_{bed})} \tag{B.8}$$

The minimum factor is 0.2 chosen in this study following Bishop and Donelan (1987) range of 0.2 to 0.4. If $(h-h_{bed})/(2\pi/k) > 0.2$ then the maximum factor of the range where $(h-h_{bed})/(2\pi/k) \leq 0.2$ is substituted for this value. These factors per step are multiplied with the Fourier series. The water level elevation η is obtained by taking the real part of the inverse Fourier transformation over this factorised time series.

B.2. Wave spectral analysis

The elevation time series of the RBR at Dune 1 ($F_s = 8\ Hz$), RBR at Dune 2 ($F_s = 8\ Hz$) and the offshore Signature at 14-meter water depth ($F_s = 4\ Hz$) can be transformed to a mean water level elevation and to wave characteristics per time interval. The time interval of the wave record should be long enough to obtain reliable statistics and short enough to be stationary usually a duration in the order of 15 to 30 minutes). In this study, 10 minutes is chosen as an estimate for the wave characteristics over a shorter time interval was preferred. The period of interest is defined as the storm period related to the elevation measurements. This period is subdivided into time intervals of 10 minutes.

The measured RBR elevations are converted to NAP with measurements of the bed and elevation of the instruments to the bed. The signature instrument setup is set at a height of 0.63 cm above the bed. Thus, the signature altimeter measurements are all increased by 0.63 cm. The mean of the water level elevations over the 10-minute time interval is considered as the water level elevation over this entire period. The water level elevation time series are detrended before the wave analysis is performed.

A zero-crossing analysis is performed on the elevation time series using a zero-down-crossing method. This procedure conducts an analysis of all the waves in the time series and calculates the raw wave height and wave period of all the successive waves. This method uses the measured time series and is used as a reference to the wave spectral analysis in this study. The wave characteristics based on the time series can be described using the equations stated. The mean wave height H_{mean} is the mean of the entire time series and the significant wave height (H_s or $H_{1/3}$) is the mean of the highest one-third

of the waves.

$$H_{mean} = \overline{H} = \frac{1}{N}\sum_{i=1}^{N} H_i \tag{B.9}$$

$$H_s = H_{1/3} = \frac{1}{N/3}\sum_{j=1}^{N/3} H_j \tag{B.10}$$

The wave period per wave within this zero-down-crossing method (T_0) is the time difference between the first and the second crossing with the zero-line. The mean zero-crossing period (T_{mean} or T_z) is defined as the mean period of all the waves in the record. The significant wave period (T_s or $T_{1/3}$) is defined as the mean wave period over the one-third largest waves.

$$T_{mean} = \overline{T}_0 = T_z = \frac{1}{N}\sum_{i=1}^{N} T_{0,i} \tag{B.11}$$

$$T_s = T_{1/3} = \frac{1}{N/3}\sum_{j=1}^{N/3} T_{0,j} \tag{B.12}$$

Another method to extract the wave characteristics from the elevation signal is wave spectral analysis where the variance density spectrum is obtained. The wave spectral analysis is performed on the detrended water level elevation signal. The continuous (or raw) variance density spectrum can be described with Equation (B.13).

$$E(f) = \lim_{\Delta f \to 0} \frac{1}{\Delta f} E\left\{\frac{1}{2}\underline{a}^2\right\} \tag{B.13}$$

In this research, the variance density spectrum will be solved by dividing the time series into blocks and performing a one-dimensional discrete Fourier Transform or Fast Fourier Transform (FFT) on the blocks following the method provided in Holthuijsen (2007). In this study, the block length is chosen as the entire length of the time interval ($D = F_s * 60 * 10$). This corresponds to solving with a $\Delta f = 0.00167$ for waves with a maximum of 10 minutes ($f_1 = 0.00167\ Hz$), 5 minutes ($f_2 = 0.00333\ Hz$), 2.5 minutes ($f_3 = 0.00500\ Hz$), up to the Nyquist frequency ($F_N = F_s\ 2$). The Fast Fourier Transformation is performed on the block.

The sea surface elevation is written as a Fourier series using trigonometry in Equation (B.14). The amplitudes A_i and B_i (or Fourier coefficients) of the sea surface elevation are described by Equations (B.15) and (B.16)

$$\eta(t) = \sum_{i=1}^{N} [A_i \cos(2\pi f_i t) + B_i \sin(2\pi f_i t)] \tag{B.14}$$

$$A_i = \frac{2}{D}\int_D \eta(t)\cos(2\pi f_i t)dt \tag{B.15}$$

$$B_i = \frac{2}{D}\int_D \eta(t)\sin(2\pi f_i t)dt \tag{B.16}$$

The variance at each frequency is calculated with:

$$E_i = \frac{1}{2}a_i^2 = \frac{1}{2}\left(A_i^2 + B_i^2\right) \tag{B.17}$$

The variance density spectrum of the wave record is obtained by averaging over the blocks (in this study one block is used) and dividing by Δf.

Then, the spectral moments are calculated based on the variance density spectrum. These frequencies can be discriminated into short and infragravity waves and low- and high-frequency noise. Short waves

are related to wave frequencies of 0.04 Hz to 1 Hz. Below 0.04 Hz to 0.004 Hz, waves are defined as infragravity waves (Bertin et al., 2018). Especially infragravity waves are found to be important contributors in dune erosion and barrier breaching (Roelvink et al., 2009). Frequencies below 0.004 Hz are related to very low-frequency motions (VLFs) and could be related to rip-current vortices (Reniers et al., 2007). High frequencies above 1 Hz are disregarded as the noise is related to non-physical variations (e.g. instrument noise) (Holthuijsen, 2007). For this analysis, the cut-off frequencies are defined as the lower boundary of 0.004 Hz and the upper boundary at 1 Hz to include both infragravity waves and short waves while the low- and high-frequency noise is disregarded. The nth-order moments of the variance density spectrum (with $n = [..., -1, 0, 1, ...]$) are calculated using

$$m_n = \int_{0.004}^{1} f^n E(f) df \tag{B.18}$$

The wave characteristic height and periods are calculated using their spectral estimates and f_{peak} is defined as the frequency at the peak of the energy density spectrum. The spectral estimate of the significant wave height is defined with Equation (B.19)

$$H_{m_0} = 4 * \sqrt{m_0} \tag{B.19}$$

The peak period T_p, the spectral mean wave energy period $T_{m_{-1.0}}$, the mean period at the mean frequency of the spectrum $T_{m_{01}}$, and the mean zero-crossing period $T_{m_{02}}$ can be defined using the variance density spectrum. By the use of a lower-order spectral wave period, more weight is given to the lower frequencies.

$$T_p = \frac{1}{f_{peak}} \tag{B.20}$$

$$T_{m_{-1.0}} = \frac{m_{-1}}{m_0} \tag{B.21}$$

$$T_{m_{01}} = \frac{1}{f_{mean}} = \frac{m_0}{m_1} \tag{B.22}$$

$$T_{m_{02}} = \overline{T}_0 = \sqrt{\frac{m_0}{m_2}} \tag{B.23}$$

Concluded, these spectral wave heights and periods are calculated per 10-minute time interval over the entire storm period of variable length. They are taken into account for the hydrodynamic analysis in this study and will be related to the morphological developments.

C

Sediment statistics for RealDune-REFLEX

This appendix provides the sample statistics (Figure C.1) and the grain size distribution (Figure C.2) for the sediment of RealDune-REFLEX Dune 1 and Dune 2. The two dunes are constructed from approximately the same sediment.

SIEVING ERROR: 0.3%

SAMPLE STATISTICS

SAMPLE IDENTITY: **TU Delft sed. calibration 220202** ANALYST & DATE: BvD, 25-05-2022

SAMPLE TYPE: Unimodal, Well Sorted TEXTURAL GROUP: Slightly Gravelly Sand

SEDIMENT NAME: Slightly Fine Gravelly Medium Sand

	µm	ϕ
MODE 1:	390.0	1.364
MODE 2:		
MODE 3:		
D_{10}:	236.0	0.843
MEDIAN or D_{50}:	362.3	1.465
D_{90}:	557.6	2.083
(D_{90} / D_{10}):	2.362	2.471
(D_{90} - D_{10}):	321.5	1.240
(D_{75} / D_{25}):	1.542	1.532
(D_{75} - D_{25}):	155.7	0.625

GRAIN SIZE DISTRIBUTION

GRAVEL:	0.2%	COARSE SAND:	13.7%
SAND:	99.8%	MEDIUM SAND:	74.4%
MUD:	0.0%	FINE SAND:	11.5%
		V FINE SAND:	0.1%
V COARSE GRAVEL:	0.0%	V COARSE SILT:	0.0%
COARSE GRAVEL:	0.0%	COARSE SILT:	0.0%
MEDIUM GRAVEL:	0.0%	MEDIUM SILT:	0.0%
FINE GRAVEL:	0.1%	FINE SILT:	0.0%
V FINE GRAVEL:	0.1%	V FINE SILT:	0.0%
V COARSE SAND:	0.1%	CLAY:	0.0%

	METHOD OF MOMENTS			FOLK & WARD METHOD		
	Arithmetic	Geometric	Logarithmic	Geometric	Logarithmic	Description
	µm	µm	ϕ	µm	ϕ	
MEAN ($\bar{x}$):	388.1	358.6	1.479	359.1	1.477	Medium Sand
SORTING (σ):	243.3	1.426	0.512	1.396	0.482	Well Sorted
SKEWNESS (Sk):	19.02	0.100	-0.100	-0.035	0.035	Symmetrical
KURTOSIS (K):	591.1	11.52	11.52	1.109	1.109	Mesokurtic

Figure C.1: RealDune-REFLEX sample statistics

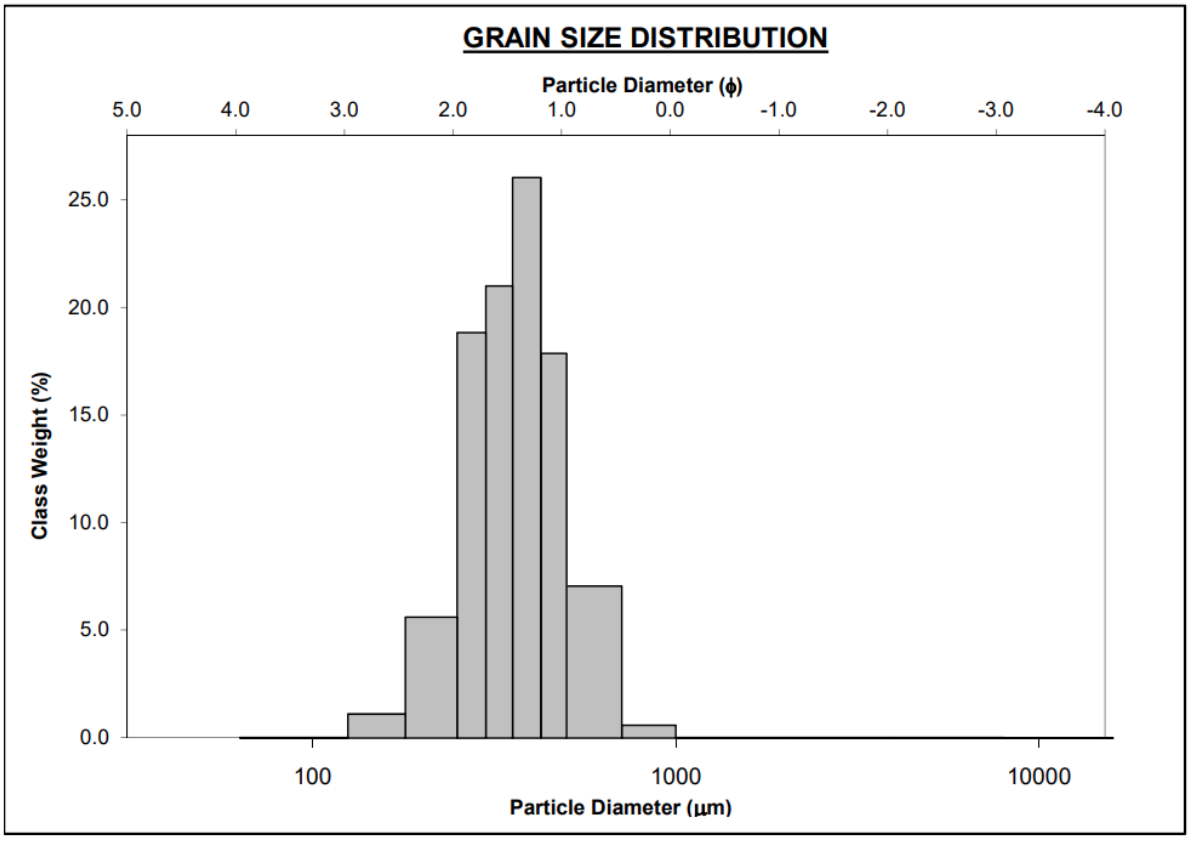

Figure C.2: RealDune-REFLEX grain size distribution

D

Storm-specific hydrodynamics for RealDune-REFLEX

This appendix provides an extensive hydrodynamic overview of the different storm periods of RealDune-REFLEX. Each storm period is depicted and briefly described. The date and time of the morphological measurements are illustrated with a red dashed line. The gradual increase in wave height towards the peak of the high water measured by the RBR can be explained by the fact that waves are depth-limited at the shallow area where the RBR is positioned.

The storm of 1 to 2 December 2021 is measured on 5 moments in time, hence giving four intervals of potential erosion. These measurements hold significant value, as the presence of a singular high water event between them allows for the conclusion that erosion during this interval resulted from that specific high water occurrence and runup.

D.1. Storm 1 (7-8 November 2021)

The storm with morphological measurements on 2021-11-06 at 11:00 and 2021-11-08 at 13:00 had no RBR and Signature measurement data available, hence the results are based on the Rijkswaterstaat measurements at the Europlatform. The third high water was the highest and is expected to have caused the majority of the erosion.

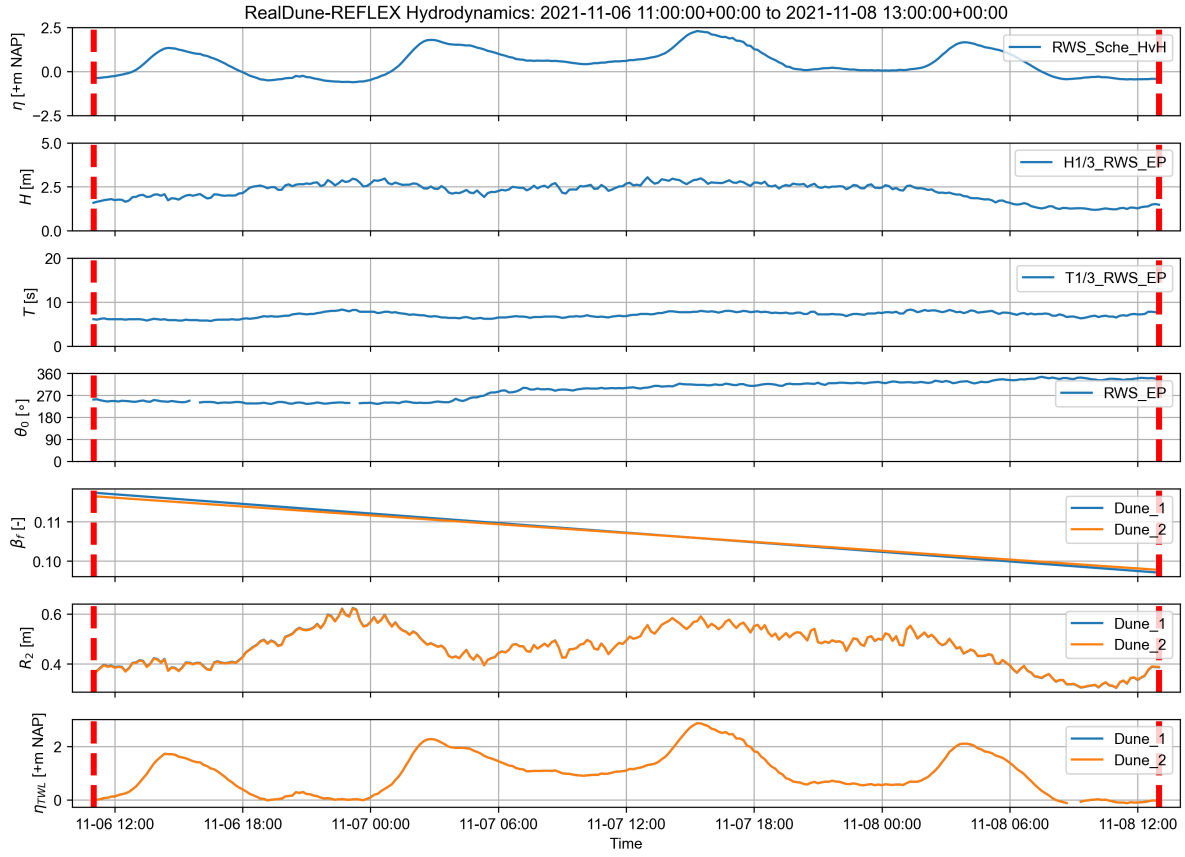

Figure D.1: RealDune-REFLEX Hydrodynamics Storm 1 with measurements on 2021-11-06 11:00 to 2021-11-08 13:00

D.2. Storm 2 (1-2 December 2021)

Storm 2.1 has measurements from 2021-11-30 at 18:00 to 2021-12-01 at 07:00. Runup is based on the Signature measurements. Runup values are approximately 5-10 cm larger for Dune 2 relative to Dune 1.

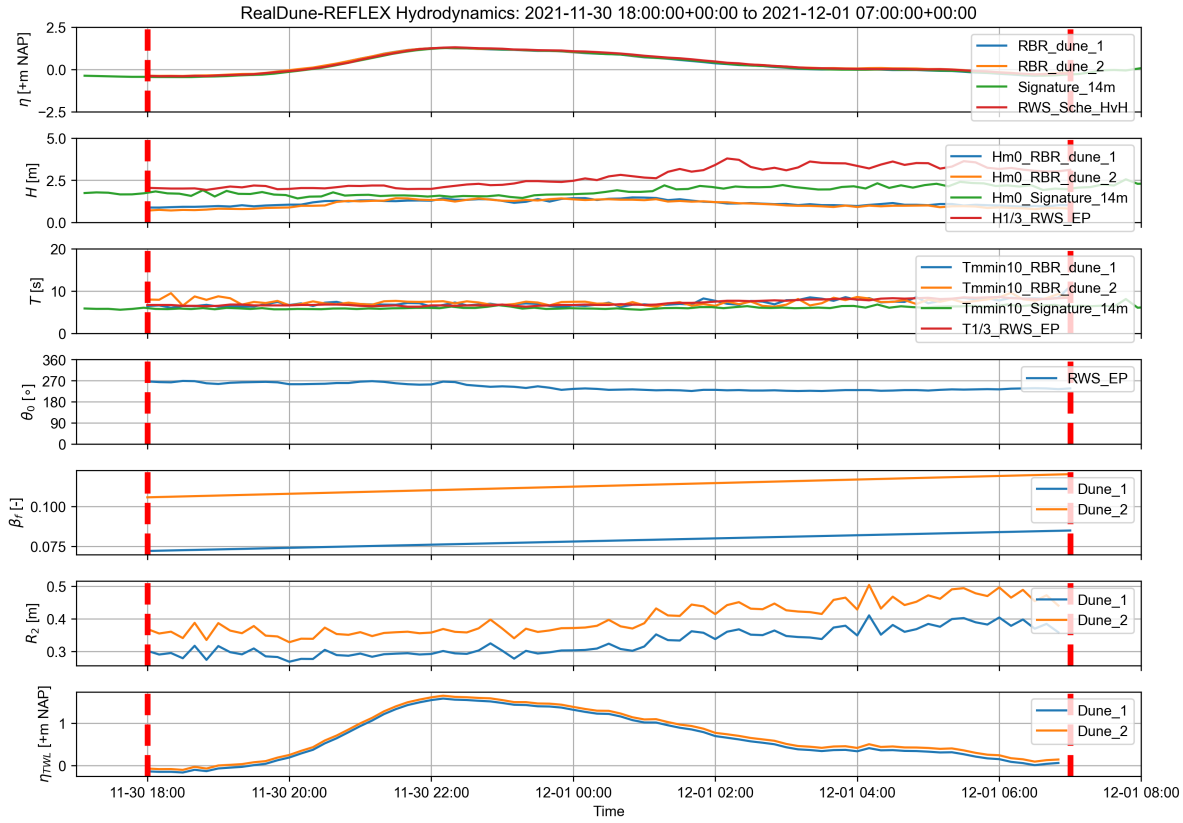

Figure D.2: RealDune-REFLEX Hydrodynamics Storm 2.1 with measurements on 2021-11-30 18:00 to 2021-12-01 07:00

Storm 2.2 has measurements from 2021-12-01 at 07:00 to 2021-12-01 at 19:00. Runup is based on the Signature measurements. The magnitude of estimated runup values fluctuates during the storm; initially, Dune 2 exhibits a roughly 10 cm higher runup, while 12 hours later a 10 cm higher runup for Dune 1 was observed. This can be attributed to a strong foreshore slope change, with Dune 1 becoming steeper and Dune 2 flattening.

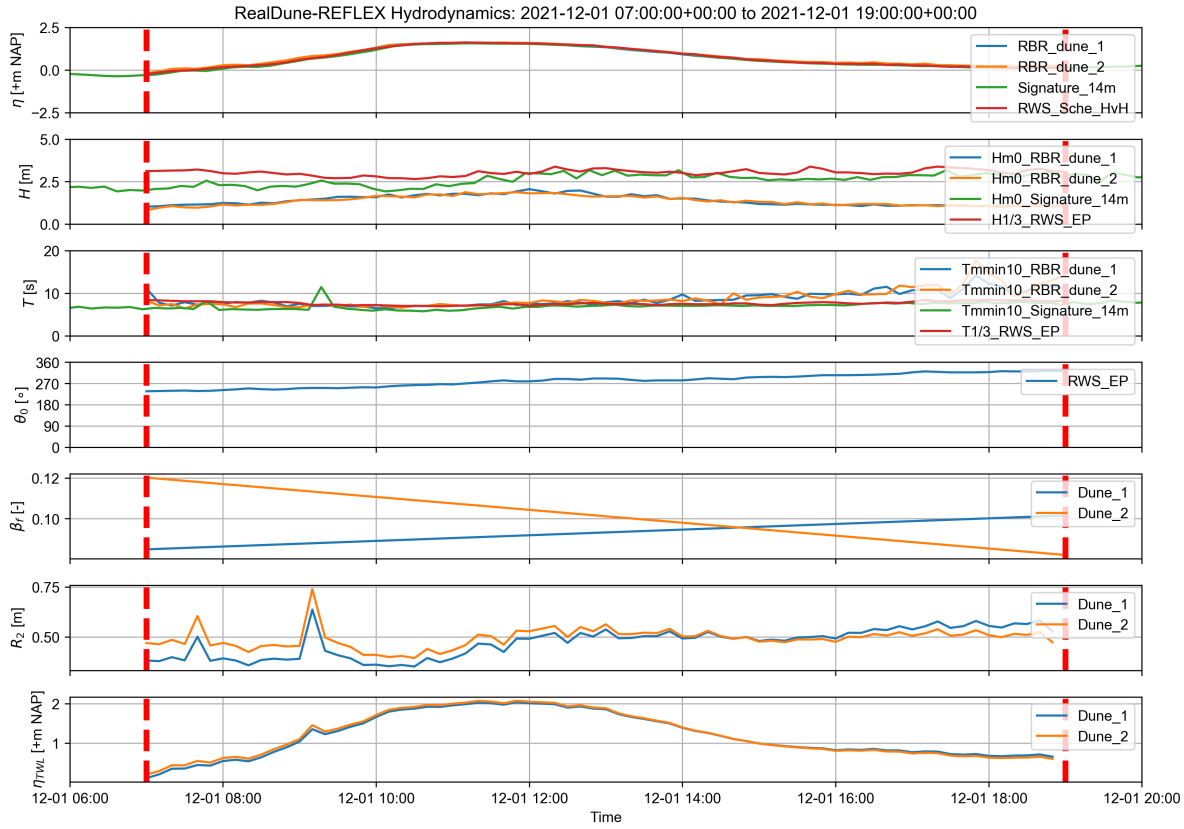

Figure D.3: RealDune-REFLEX Hydrodynamics Storm 2.2 with measurements on 2021-12-01 07:00 to 2021-12-01 19:00

Storm 2.3 has measurements from 2021-12-01 at 19:00 to 2021-12-02 at 08:00. Runup is based on the Signature measurements. The foreshore slope of Dune 2 remains rather constant while the foreshore slope of Dune 1 flattens.

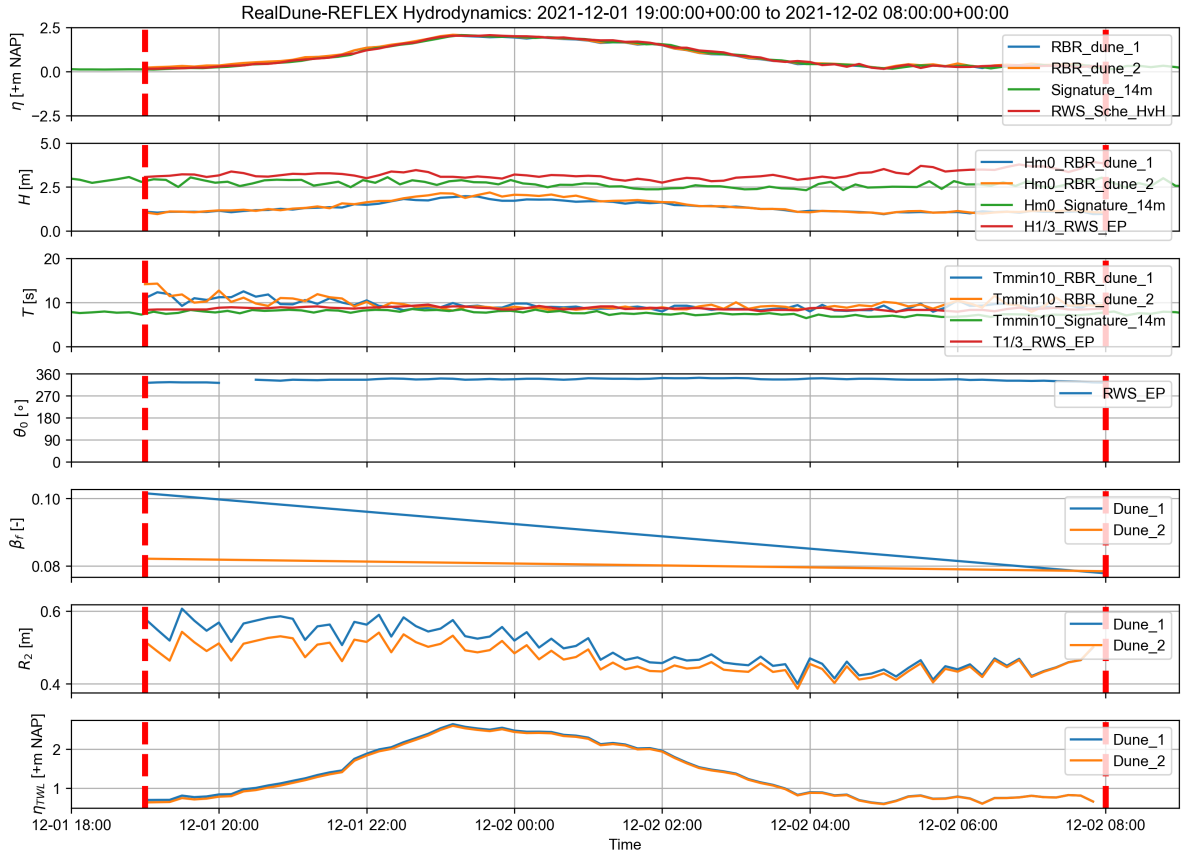

Figure D.4: RealDune-REFLEX Hydrodynamics Storm 2.3 with measurements on 2021-12-01 19:00 to 2021-12-02 08:00

Storm 2.4 has measurements from 2021-12-02 at 08:00 to 2021-12-02 at 17:00. Runup is based on the Signature measurements. The foreshore slope of Dune 1 and Dune 2 both steepen which is typical for the swash regime. Runup values are of the same order for Dune 1 and Dune 2.

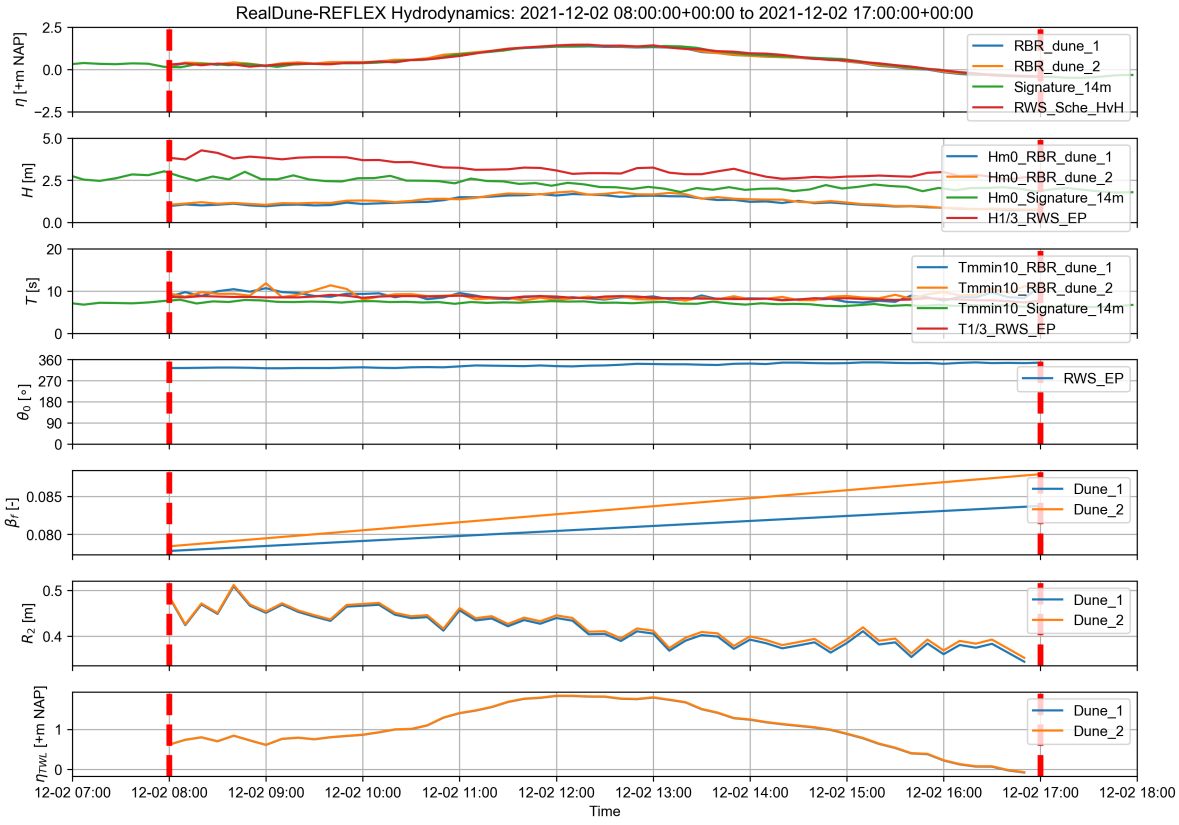

Figure D.5: RealDune-REFLEX Hydrodynamics Storm 2.4 with measurements on 2021-12-02 08:00 to 2021-12-02 17:00

D.3. Storm 3 (5-6 January 2022)

Storm 3 has measurements from 2022-01-05 at 09:00 to 2022-01-06 at 10:00. Runup is based on the Signature measurements. The RBR was repositioned between Storm 2 and Storm 3 and moved higher up the profile. Therefore, the RBR has become dry at low water. Due to the fact that the RBR is in or beyond the breaker zone, these wave heights are depth limited and only the longest waves arrive near the dune as they remain unbroken.

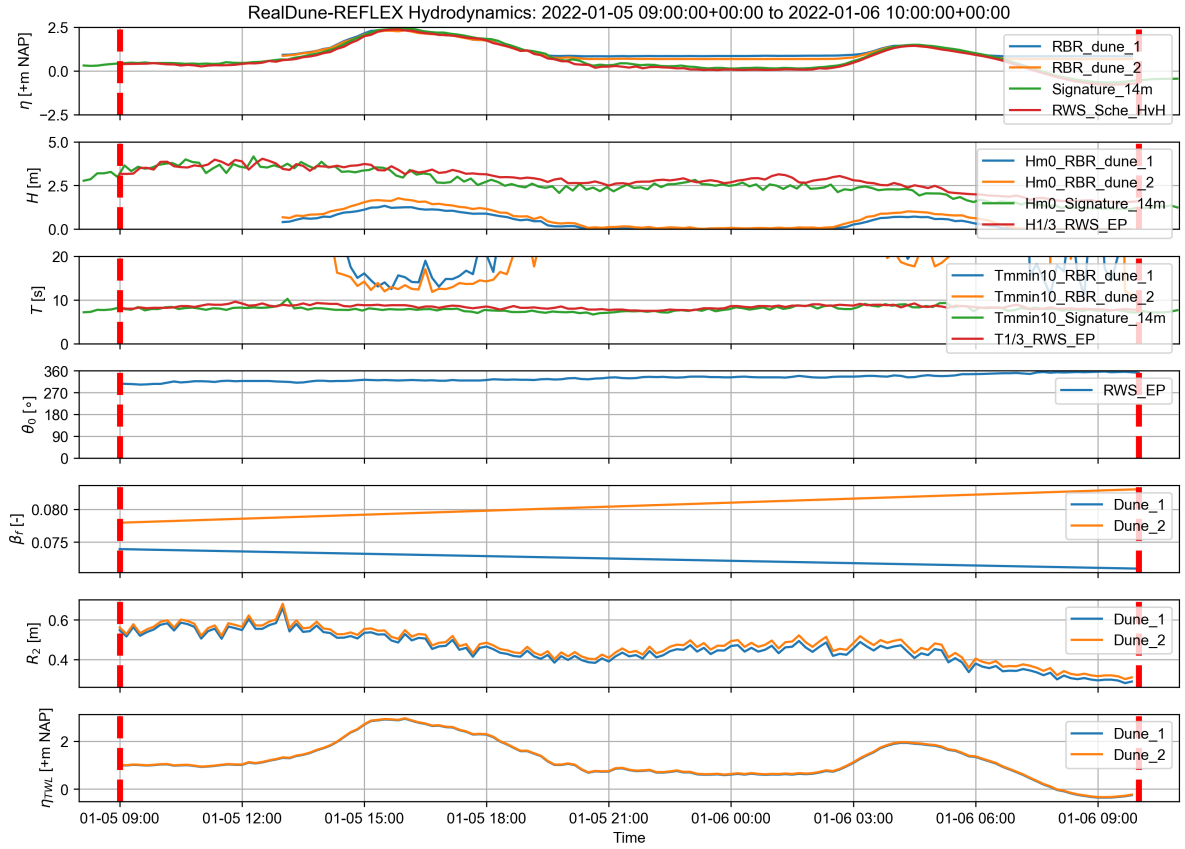

Figure D.6: RealDune-REFLEX Hydrodynamics Storm 3 with measurements on 2022-01-05 09:00 to 2022-01-06 10:00

E

Cross-shore profiles for RealDune-REFLEX

This Appendix provides all the cross-shore profiles for the RealDune-REFLEX case study over the pre-defined transects of Dune 1 and Dune 2. Each figure contains the pre- and post-storm profile of a Dune 1 or Dune 2 over one storm period. In Sections 5.3.2 and 5.3.3 the cross-sections and their results are explained.

E.1. Storm 1 (7-8 November 2021)

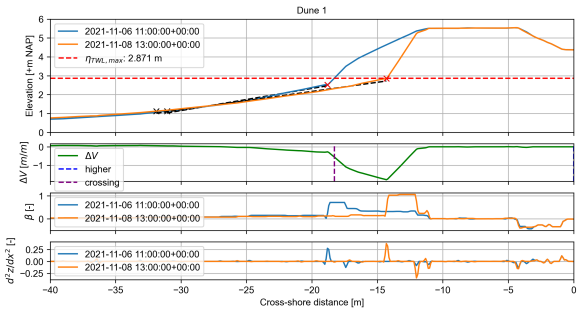

(a) Dune 1 2021-11-06 12:00 to 2021-11-08 14:00

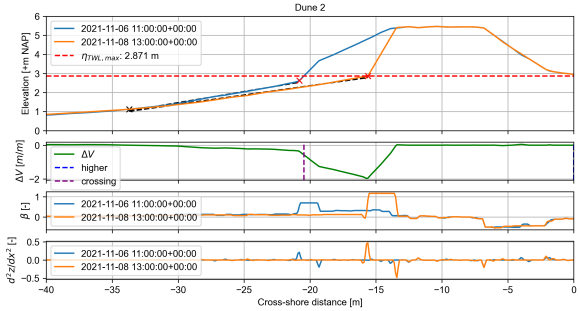

(b) Dune 2 2021-11-06 12:00 to 2021-11-08 14:00

E.2. Storm 2 (1-2 December 2021)

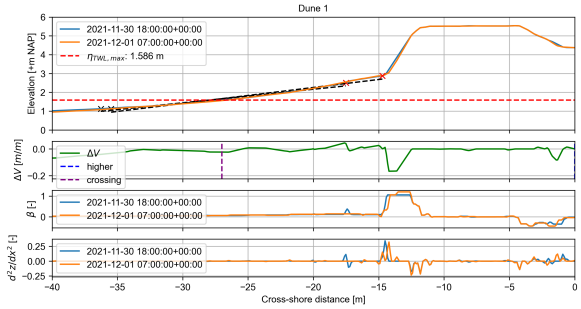

(a) Dune 1 2021-11-30 19:00 to 2021-12-01 08:00

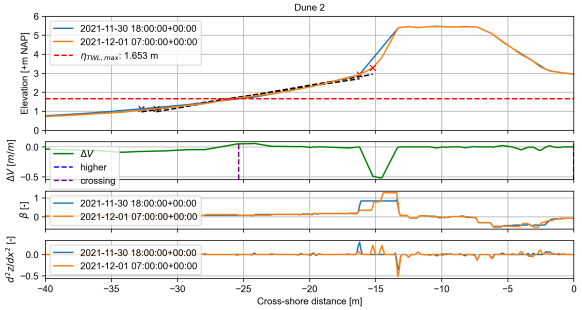

(b) Dune 2 2021-11-30 19:00 to 2021-12-01 08:00

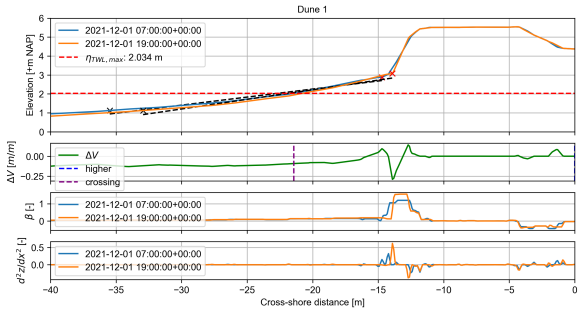

(c) Dune 1 2021-12-01 08:00 to 2021-12-01 20:00

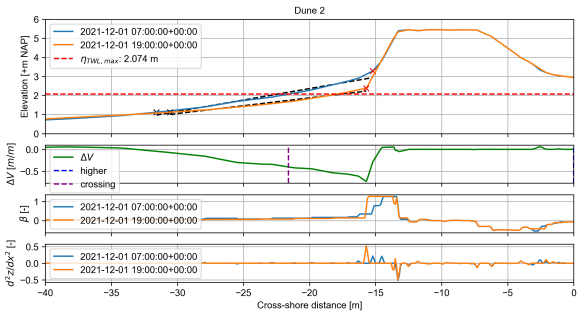

(d) Dune 2 2021-12-01 08:00 to 2021-12-01 20:00

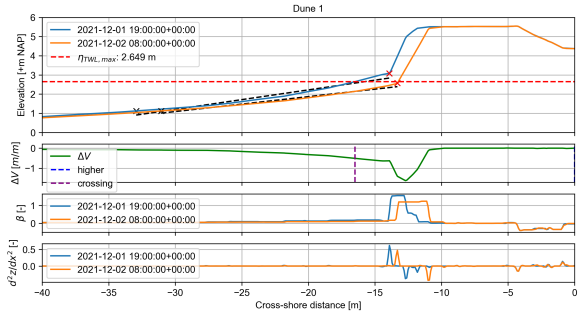

(e) Dune 1 2021-12-01 20:00 to 2021-12-02 09:00

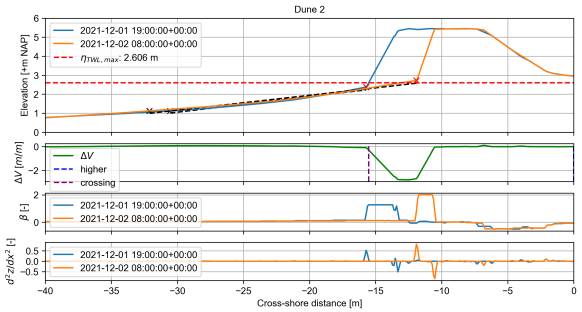

(f) Dune 2 2021-12-01 20:00 to 2021-12-02 09:00

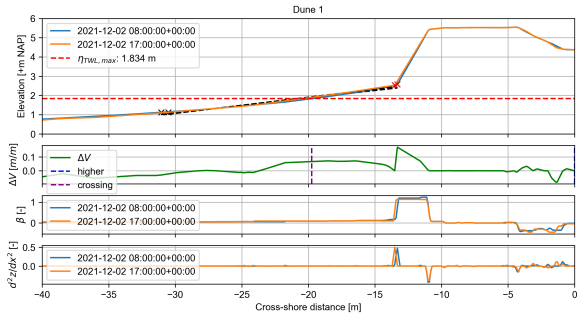

(g) Dune 1 2021-12-02 09:00 to 2021-12-02 18:00

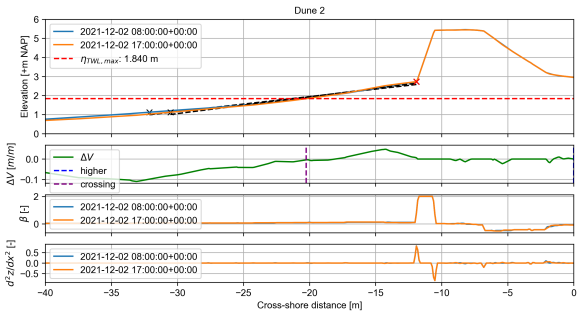

(h) Dune 2 2021-12-02 09:00 to 2021-12-02 18:00

E.3. Storm 3 (5-6 January 2022)

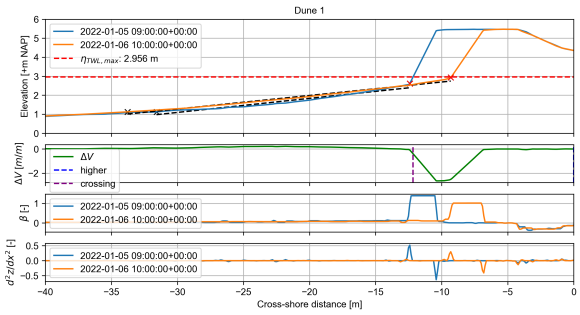

(a) Dune 1 2022-01-05 10:00 to 2022-01-06 11:00

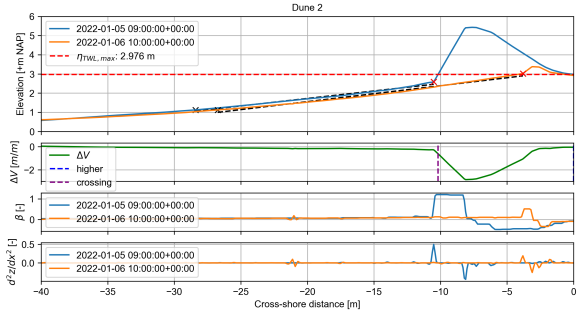

(b) Dune 2 2022-01-05 10:00 to 2022-01-06 11:00

F

Wave instruments for Land Reclamation Philippines

This appendix provides information on the settings, spectral resolution and validity domain of the wave measurement instruments at Land Reclamation Philippines. This is a description based on the manuals of both the Waverider and the AWAC.

F.1. Waverider

The Datawell 'Directional Waverider GPS' (Waverider or DWR-G) is a wave-measuring instrument with GPS. The wave buoy can measure directional waves and does not need calibration. The specifications are provided in Table F.1. The Waverider is located at an average water depth of approximately 14 meters.

Module	Subject	Description
Wave motion sensor	Sensor	Single GPS (not differential)
	Precision	1-2 cm + 0.5% moored, vertical (1σ)
	Periods	1.6 s - 100 s
	Calibration	Not required ever
	Exclusion	GPS signals do not penetrate through water, occasional data gaps may occur
	Exclusion	Measurements fail at position changes > 100 m in < 100 s, e.g. when used free floating or towed at constant velocities > 1 m/s
Wave data	Data	North, west, vertical
	Resolution	1 cm (north 2 cm, LSB "north" is GPS data gap indicator)
	Range	–20 m - +20 m
	Rate	1.28 Hz
	Reference	WGS84
	Measurements	θ, θ_{peak}, H_{m_0}, $T_{m_{01}}$, $T_{m_{02}}$, T_p, $T_{m_{24}}$, $T_{m_{-2.0}}$
Spectral data	Frequency resolution	0.005 Hz below 0.10 Hz and 0.010 Hz above
	Frequency range	0.025 Hz - 0.60 Hz
	Direction resolution	1.5°
	Direction range	0° - 360°
Standard features	GPS position	Every 30 min, precision 5 m

Table F.1: Specifications Waverider DWR-G at Land Reclamation Philippines (Datawell, 2023)

F.2. AWAC

The Nortek 'Acoustic Wave And Current profiler' (AWAC) is a type of acoustic doppler current profiler (ADCP). The type which is used, is the 600 kHz variant. The AWAC is positioned in a metal frame at 70 cm above the bed (Figure F.1). The specifications are provided in Table F.2. The AWAC is located at an average water depth of approximately 9 meters.

Figure F.1: LRP AWAC 600 kHz MIA frame

Module	Subject	Description
Wave measurement	Maximum depth	60 m
	Data types	Pressure, one velocity along each beam, AST
	Sampling rate velocity (output)	1 Hz
	Sampling rate AST (output)	2 Hz
	Measurements	η, θ, θ_{peak}, H_{m_0}, H_{max}, $H_{1/3}$, T_z, $T_{m_{02}}$, T_p
Wave estimates	Range	-15 to 15 m
	Accuracy/resolution (H_s)	< 1% of measured value / 1 cm
	Accuracy/resolution (Dir)	2° / 0.1°
	Period range	1-50 s
	Cut-off period (Hs)	5 m depth: 0.5 sec, 20 m depth: 0.9 sec, 60 m depth: 1.5 sec
	Cut-off period (dir)	5 m depth: 1.5 sec, 20 m depth: 3.1 sec, 60 m depth: 5.5 sec
Real-time clock	Accuracy	±1 min/year

Table F.2: Specifications AWAC 600 kHz at Manila Internation Airport (Nortek, 2023)

G

Cross-shore profiles for Land Reclamation Philippines

This Appendix provides all the transects for LRP. As described in Section 6.3, the transects along the land reclamation can be divided into three regions:

- **Kp1400 - Kp1230**: Severe erosion
- **Kp1220 - Kp1060**: Dune intervention
- **Kp1050 - Kp150**: Average erosion

Each of these transects from Kp150 towards Kp1400 with a spacing of 10 meters is depicted in this appendix. The transects are analysed based on the cross-shore profile, volume change, slope and second derivative of the cross-shore profile.

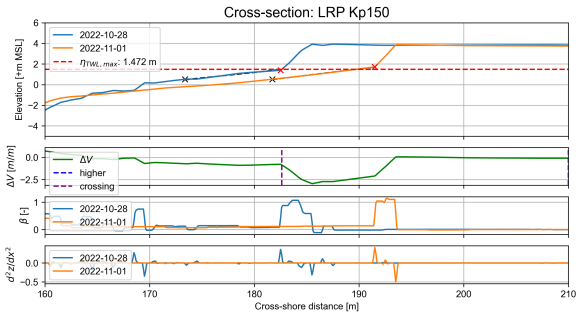

LRP transect Kp150

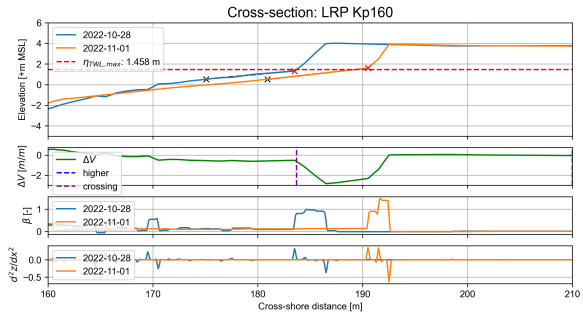

LRP transect Kp160

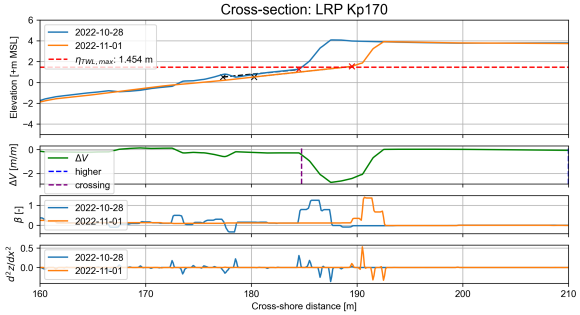

LRP transect Kp170

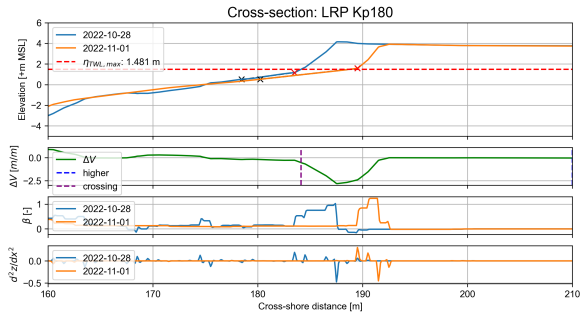

LRP transect Kp180

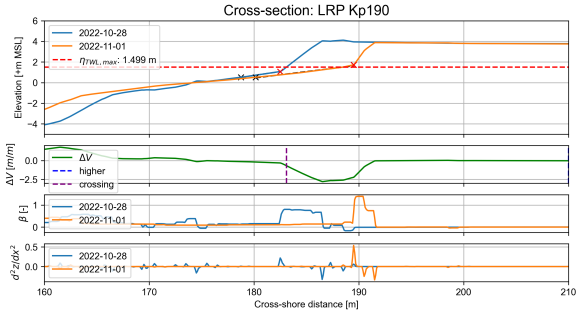

LRP transect Kp190

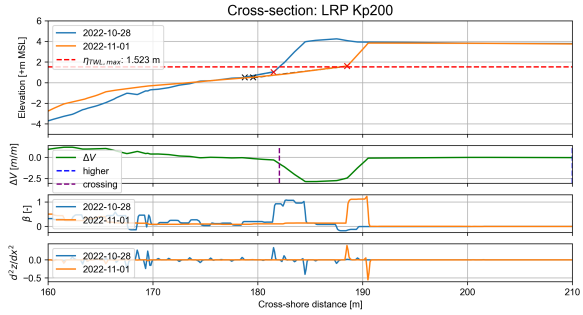

LRP transect Kp200

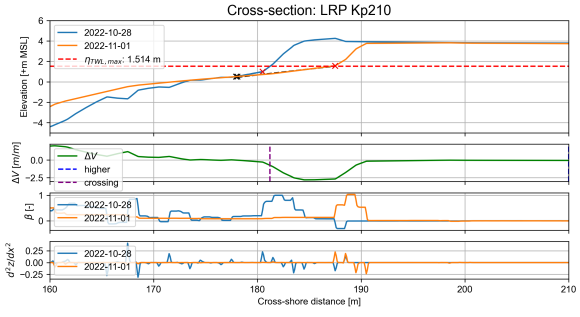

LRP transect Kp210

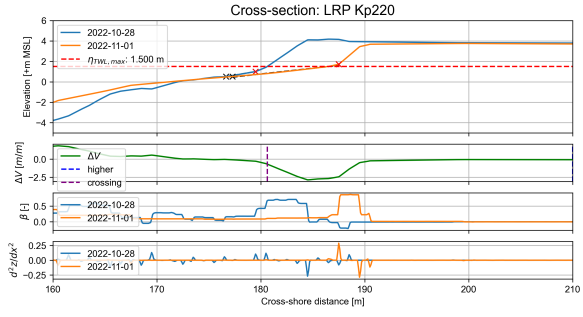

LRP transect Kp220

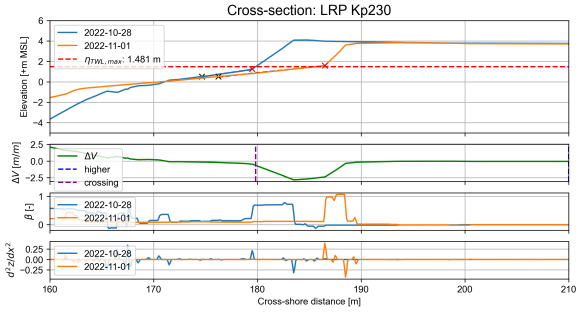

LRP transect Kp230

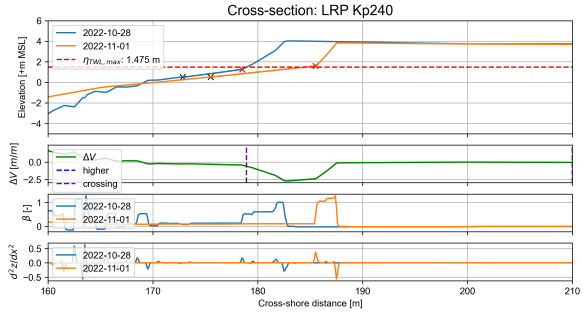

LRP transect Kp240

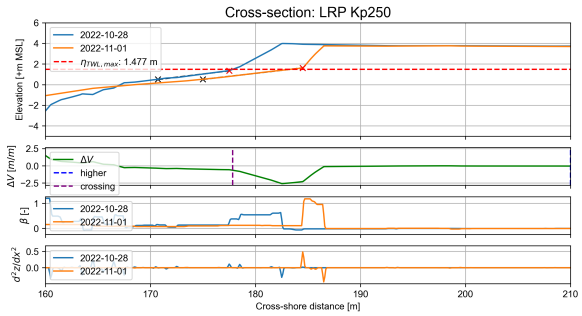

LRP transect Kp250

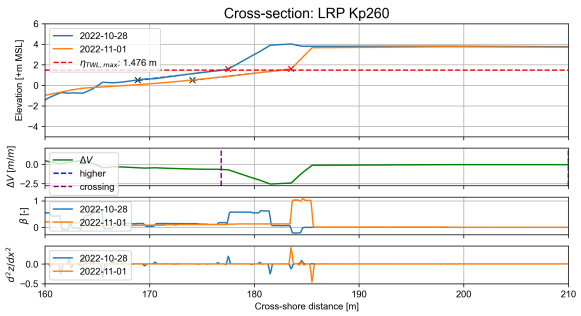

LRP transect Kp260

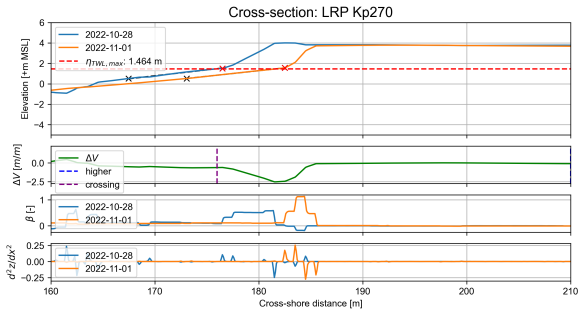

LRP transect Kp270

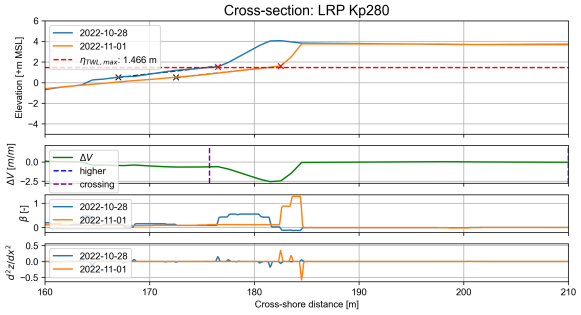

LRP transect Kp280

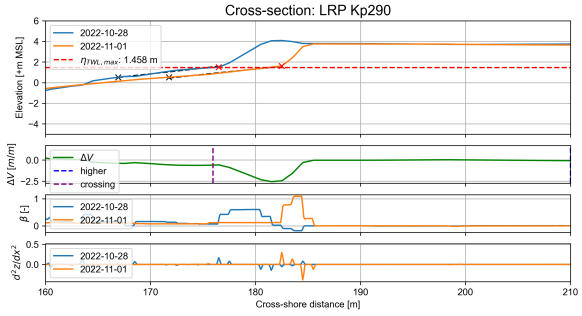

LRP transect Kp290

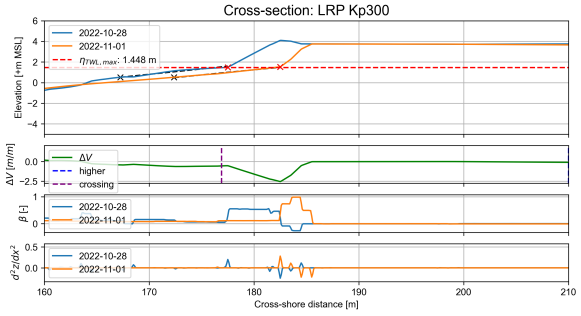

LRP transect Kp300

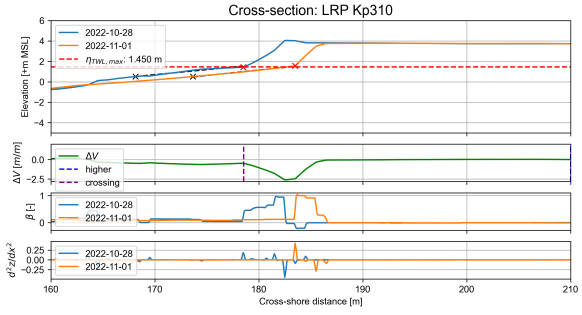

LRP transect Kp310

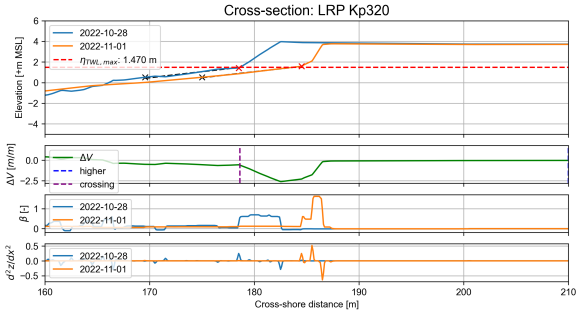

LRP transect Kp320

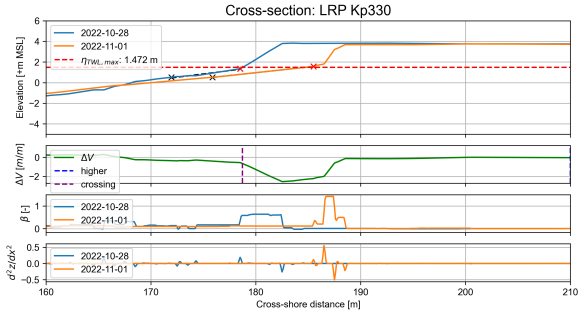

LRP transect Kp330

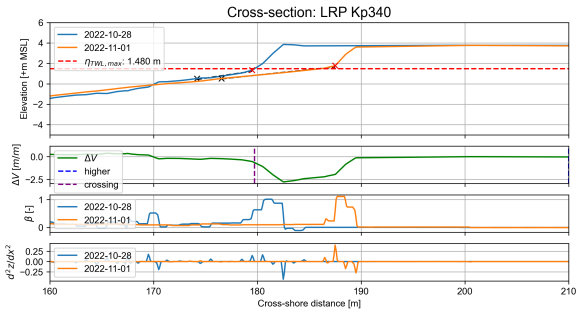

LRP transect Kp340

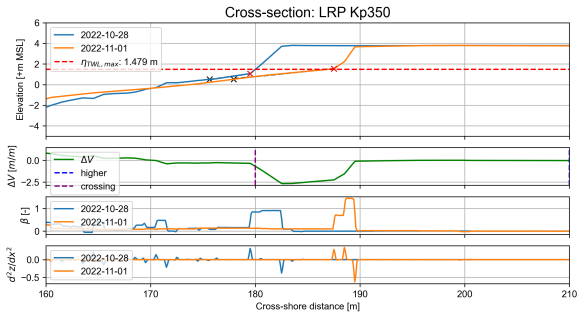

LRP transect Kp350

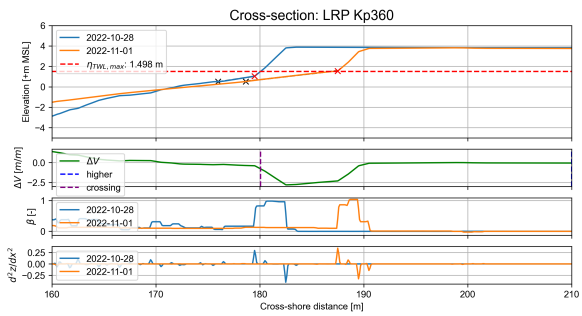

LRP transect Kp360

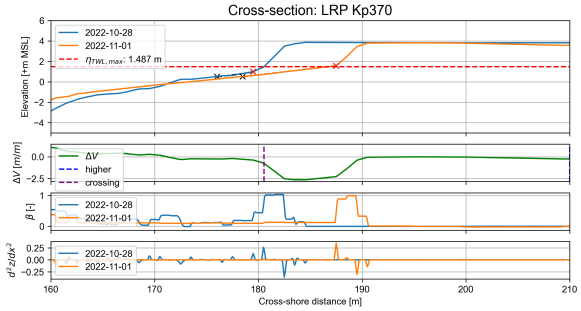

LRP transect Kp370

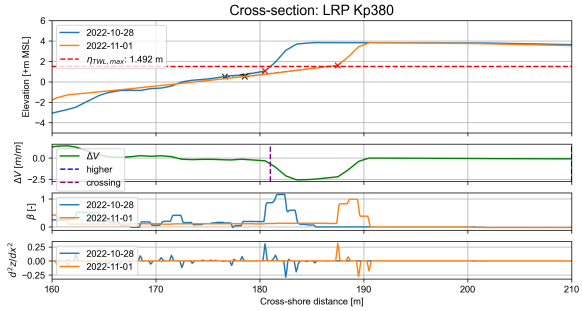

LRP transect Kp380

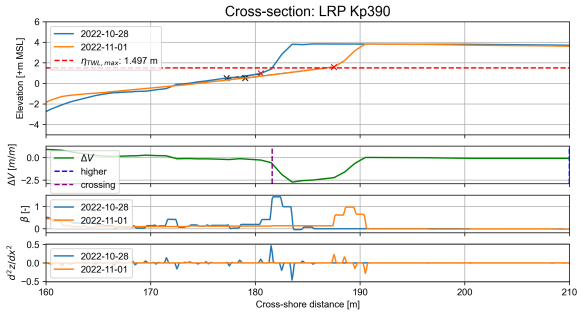

LRP transect Kp390

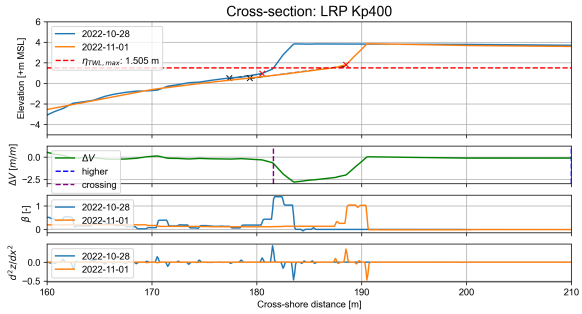

LRP transect Kp400

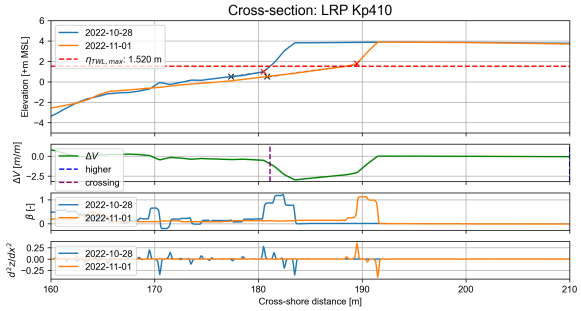

LRP transect Kp410

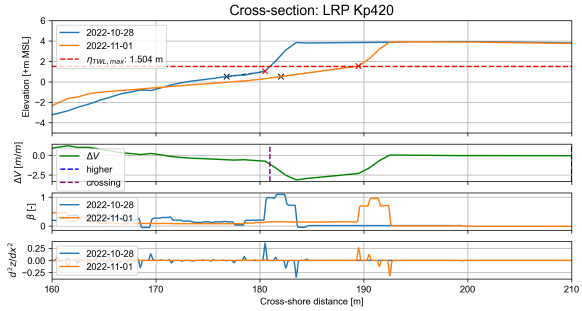

LRP transect Kp420

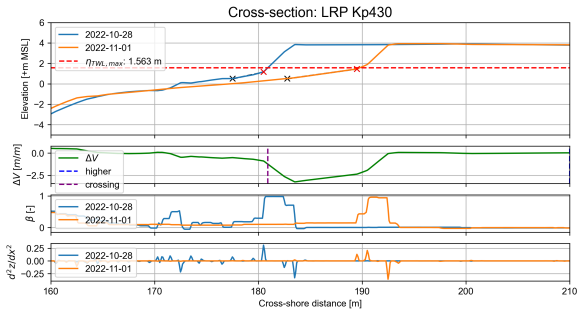

LRP transect Kp430

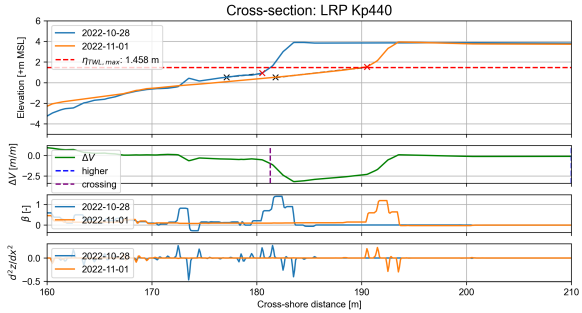

LRP transect Kp440

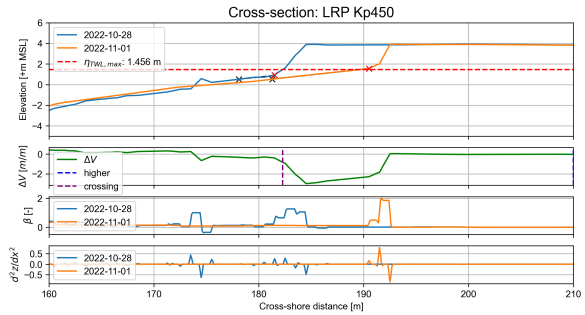

LRP transect Kp450

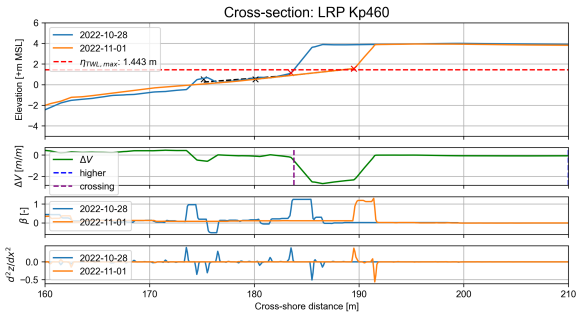

LRP transect Kp460

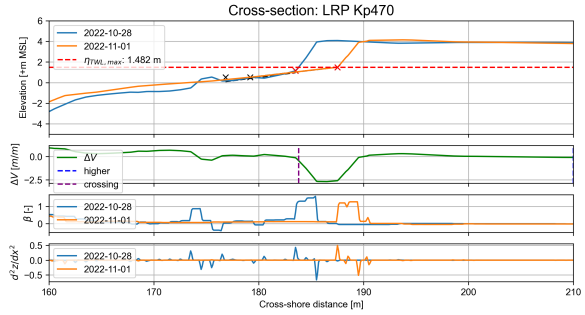

LRP transect Kp470

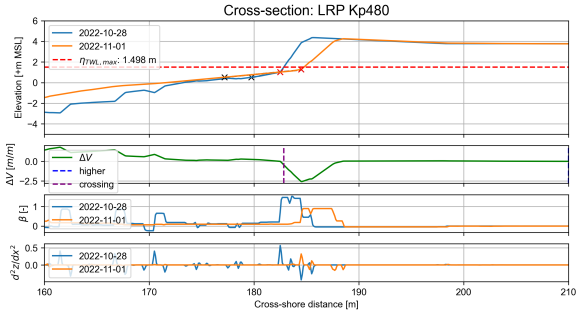

LRP transect Kp480

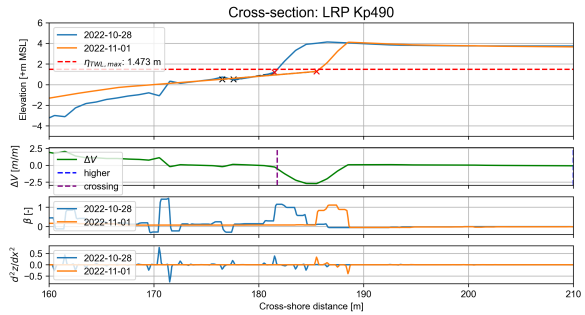

LRP transect Kp490

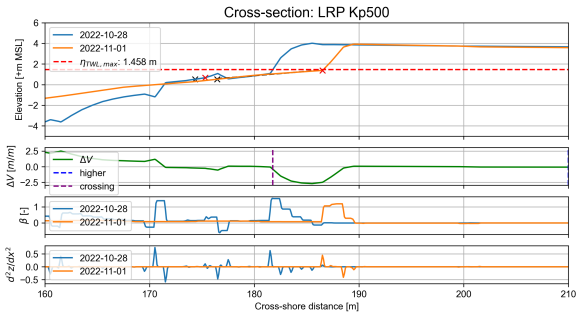

LRP transect Kp500

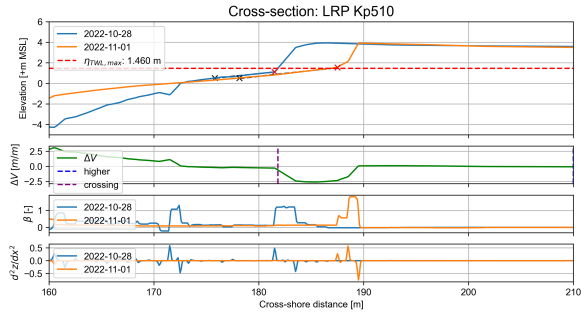

LRP transect Kp510

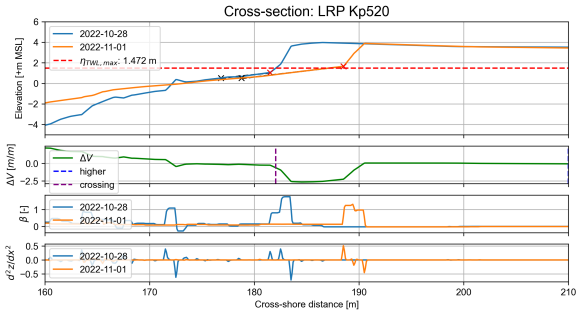

LRP transect Kp520

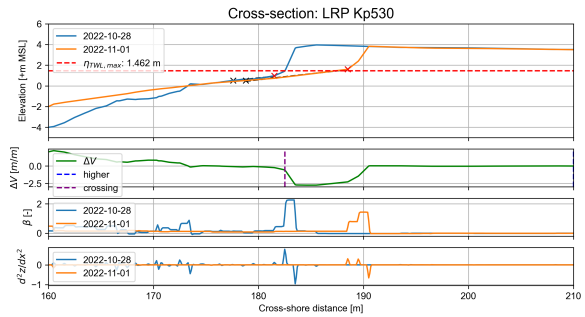

LRP transect Kp530

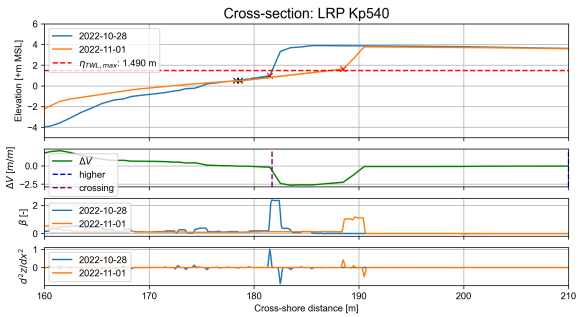

LRP transect Kp540

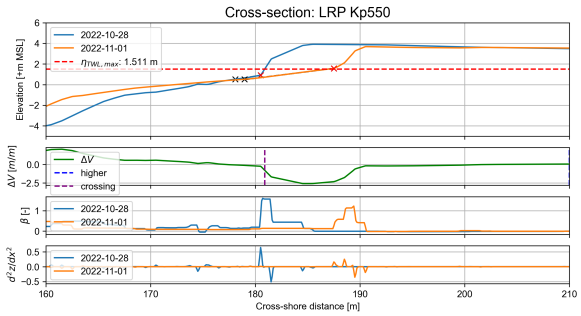

LRP transect Kp550

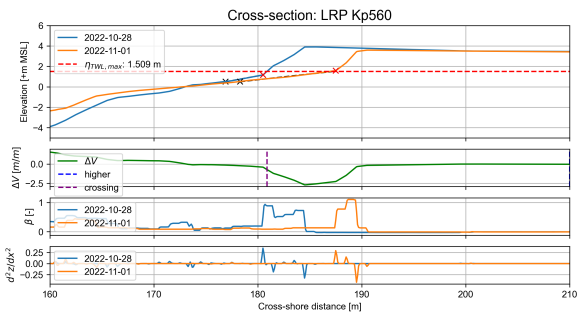

LRP transect Kp560

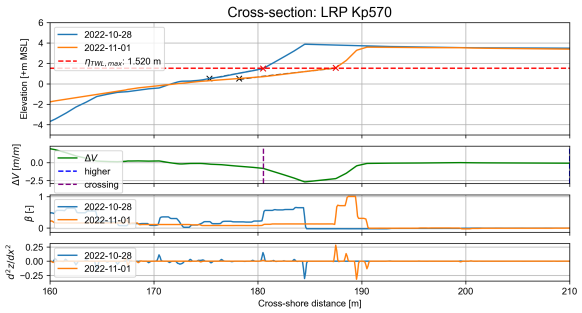

LRP transect Kp570

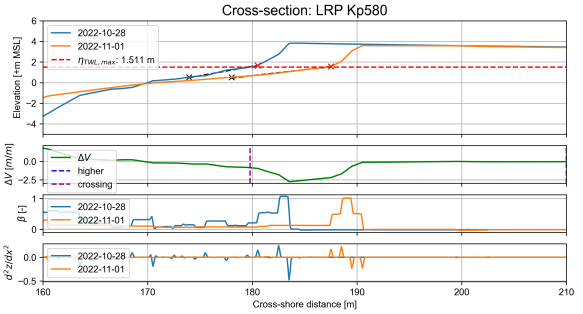

LRP transect Kp580

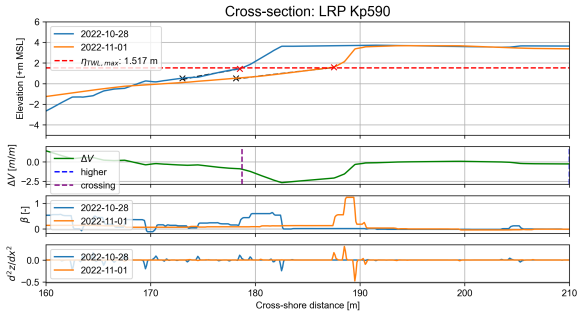

LRP transect Kp590

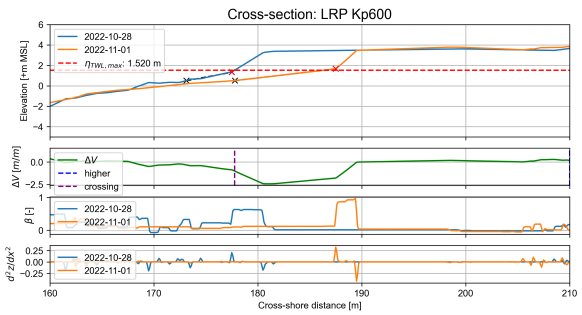

LRP transect Kp600

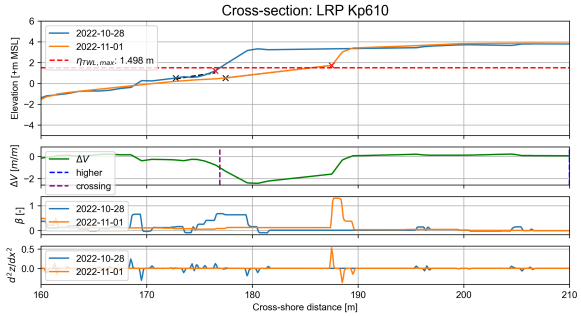

LRP transect Kp610

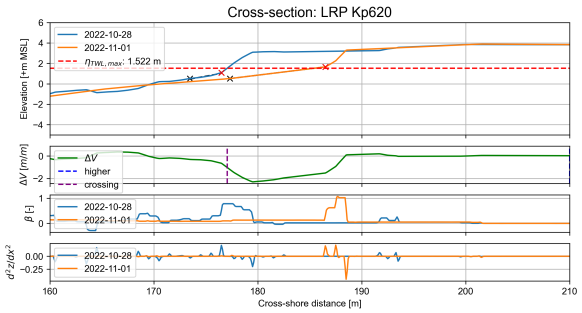

LRP transect Kp620

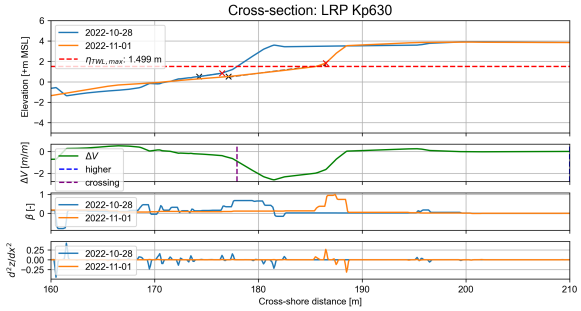

LRP transect Kp630

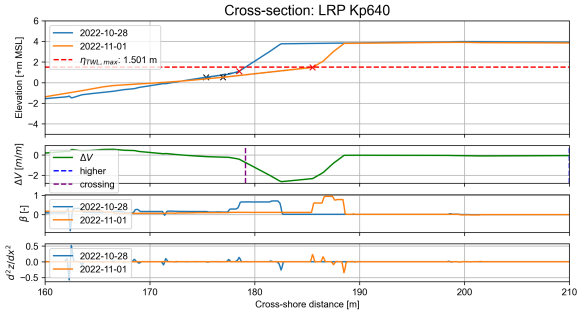

LRP transect Kp640

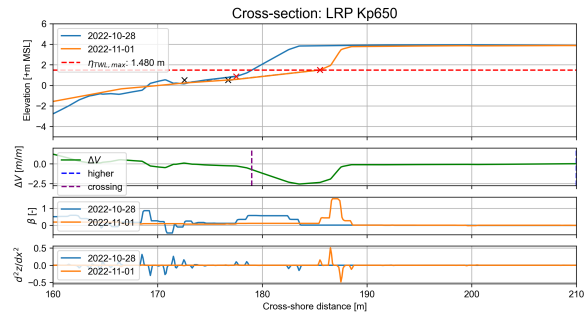

LRP transect Kp650

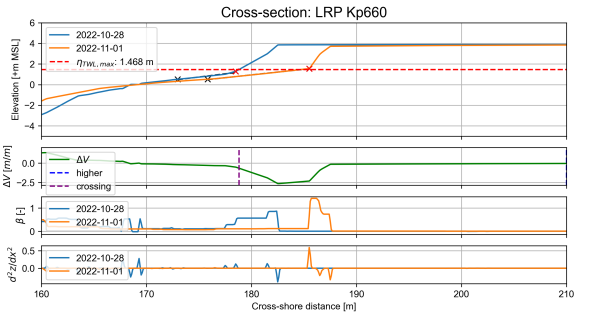

LRP transect Kp660

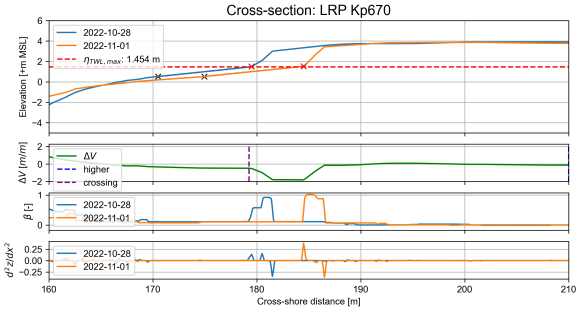

LRP transect Kp670

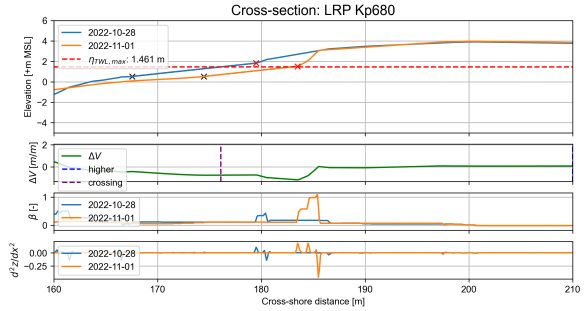

LRP transect Kp680

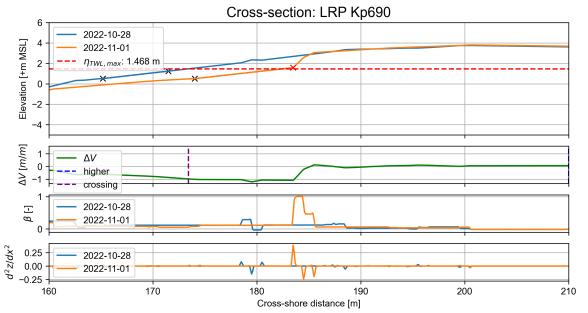

LRP transect Kp690

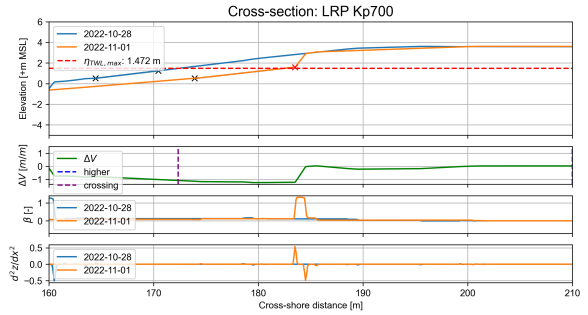

LRP transect Kp700

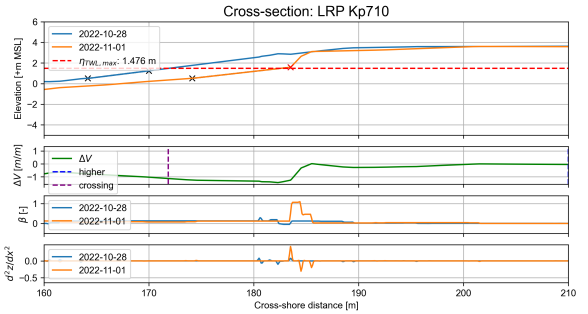

LRP transect Kp710

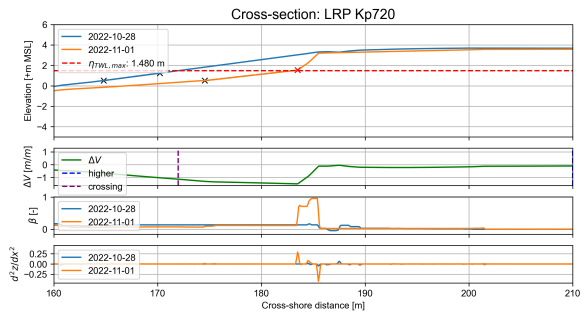

LRP transect Kp720

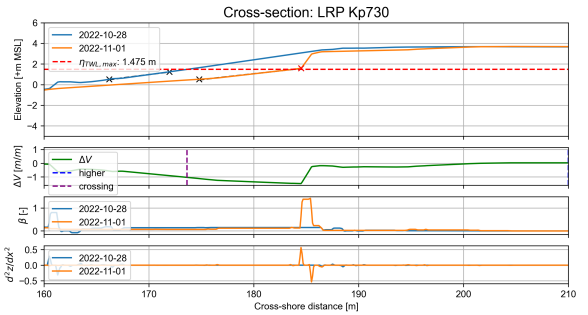

LRP transect Kp730

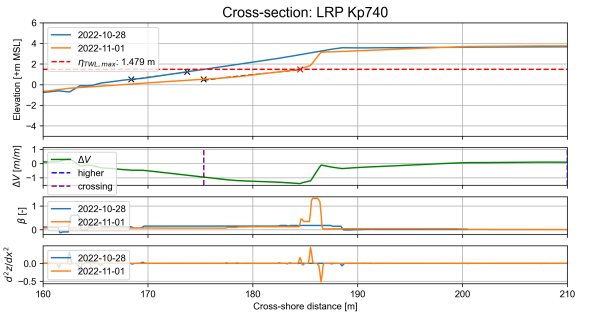

LRP transect Kp740

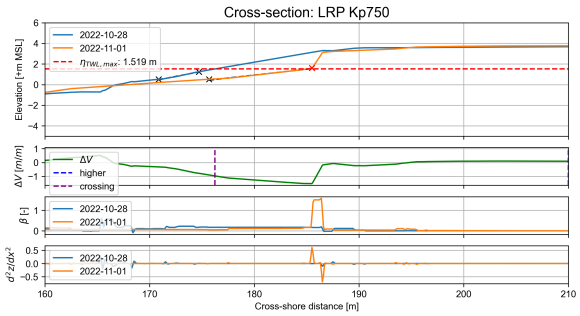

LRP transect Kp750

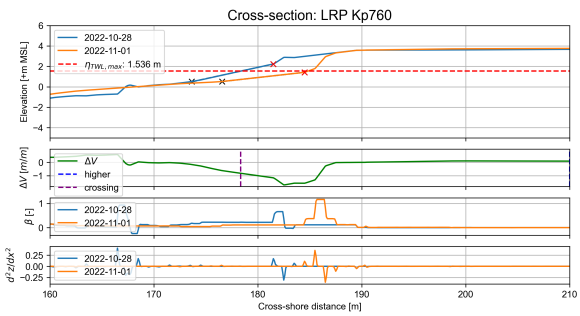

LRP transect Kp760

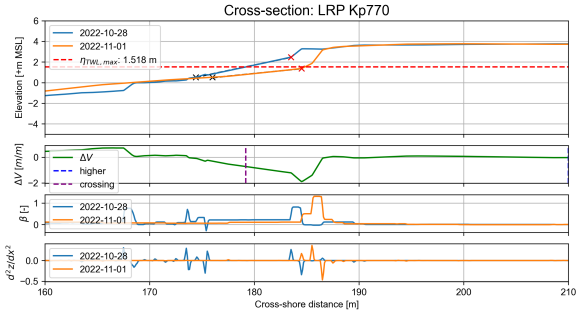

LRP transect Kp770

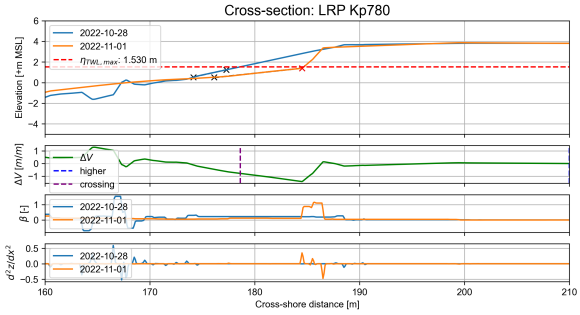

LRP transect Kp780

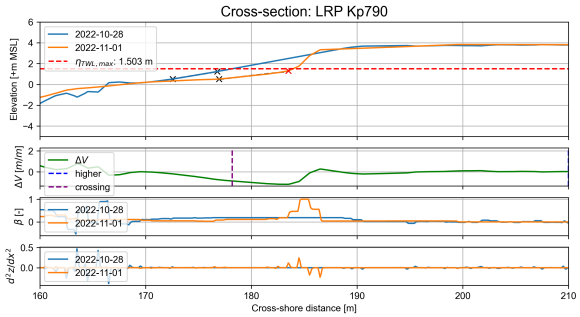

LRP transect Kp790

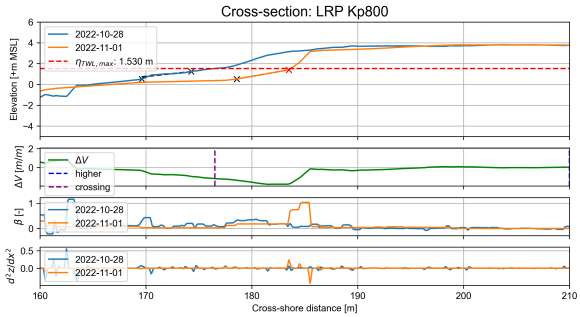

LRP transect Kp800

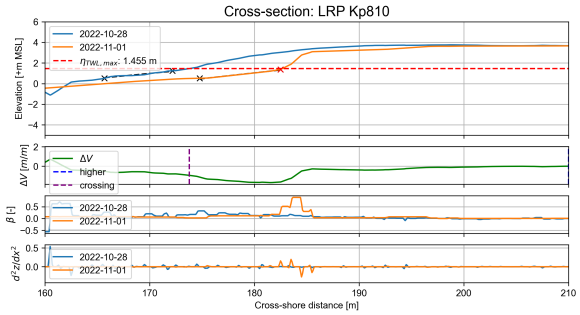

LRP transect Kp810

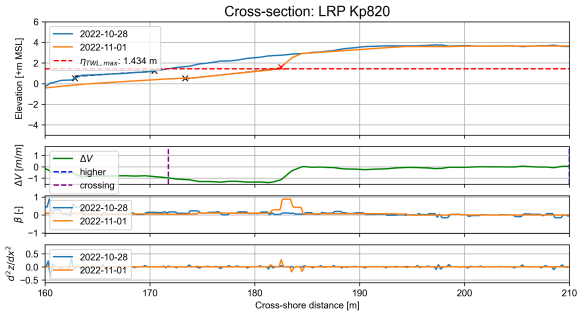

LRP transect Kp820

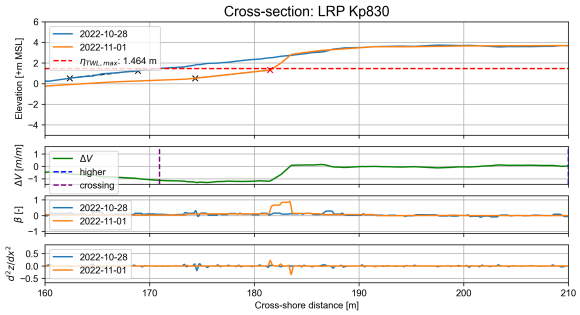

LRP transect Kp830

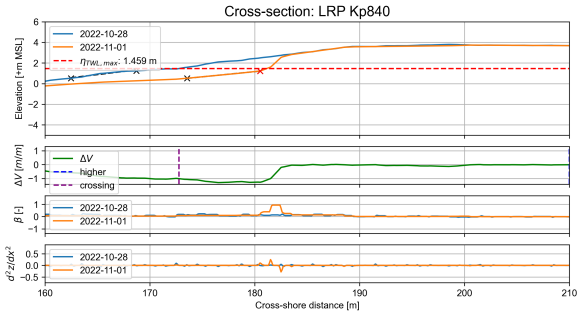

LRP transect Kp840

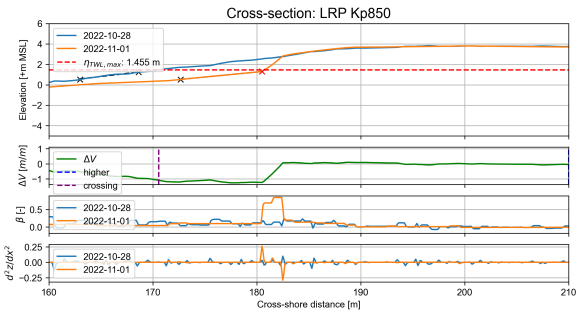

LRP transect Kp850

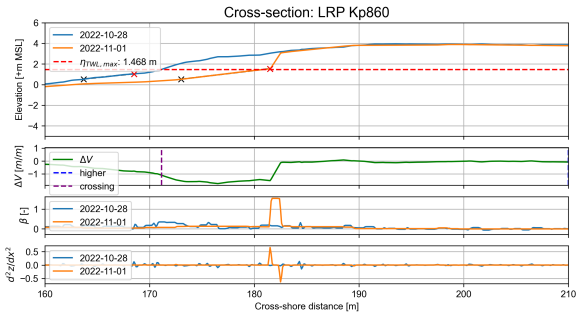

LRP transect Kp860

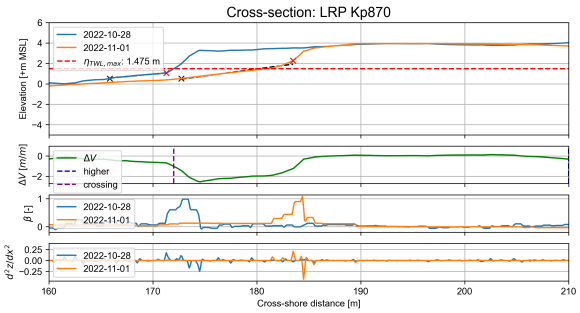

LRP transect Kp870

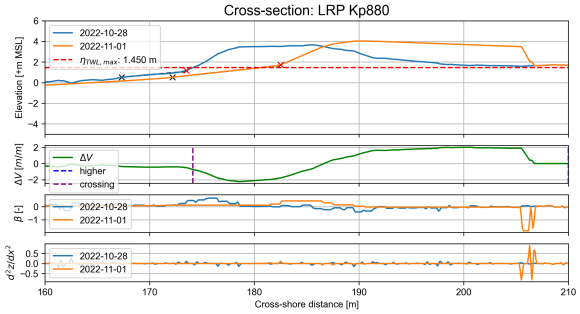

LRP transect Kp880

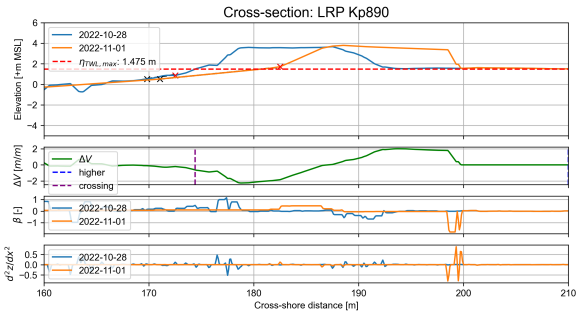

LRP transect Kp890

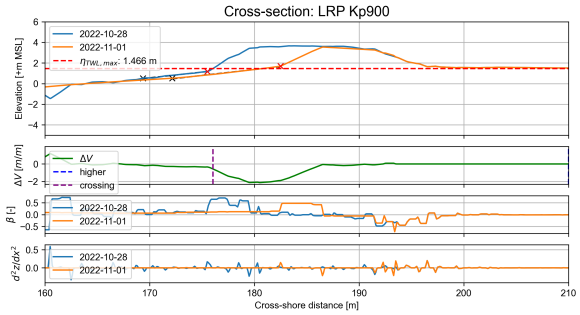

LRP transect Kp900

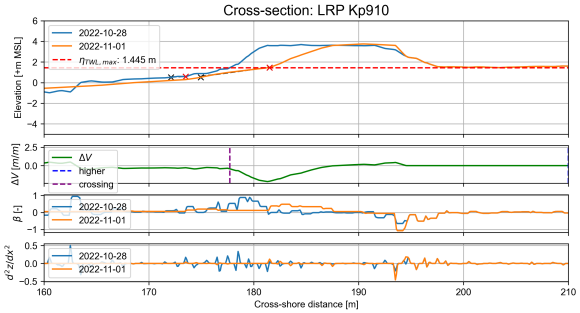

LRP transect Kp910

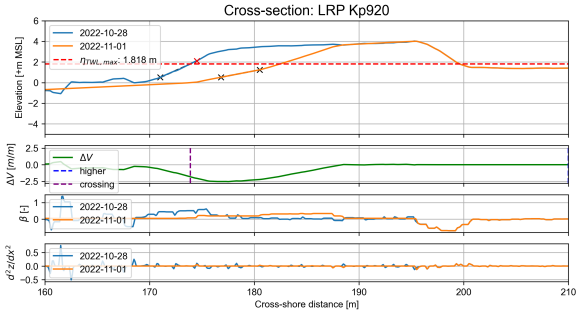

LRP transect Kp920

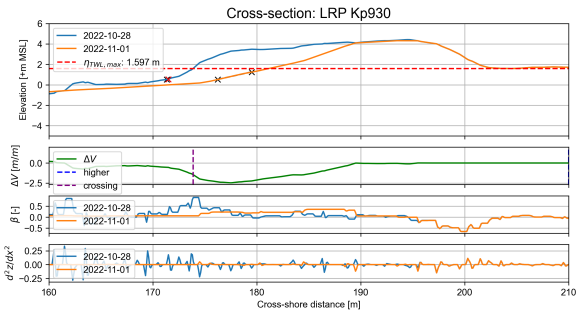

LRP transect Kp930

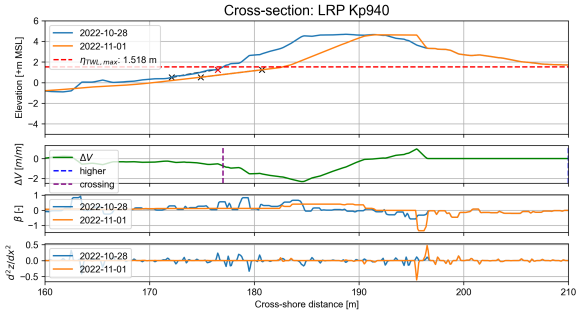

LRP transect Kp940

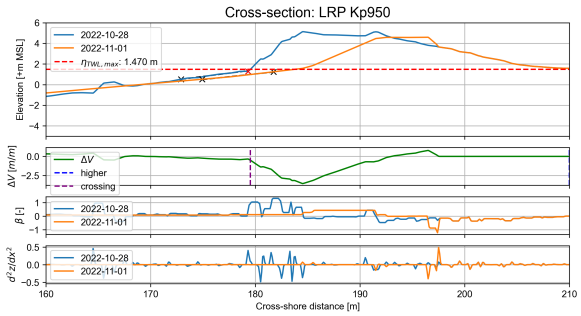

LRP transect Kp950

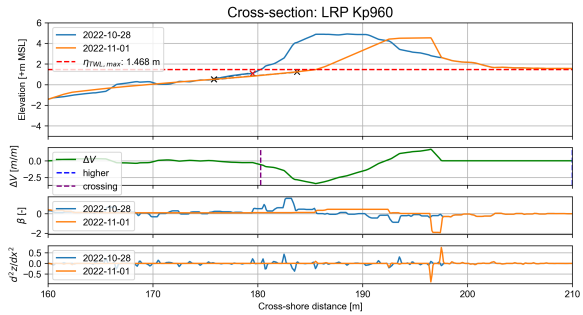

LRP transect Kp960

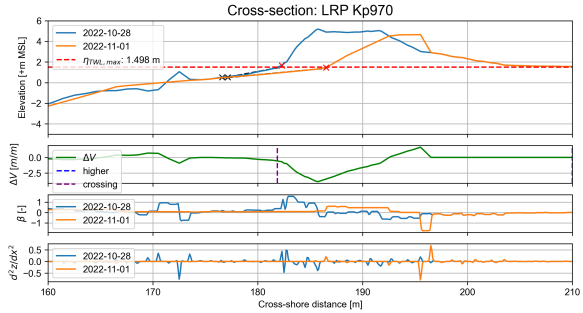

LRP transect Kp970

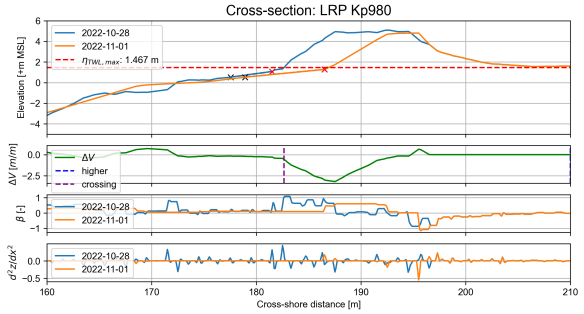

LRP transect Kp980

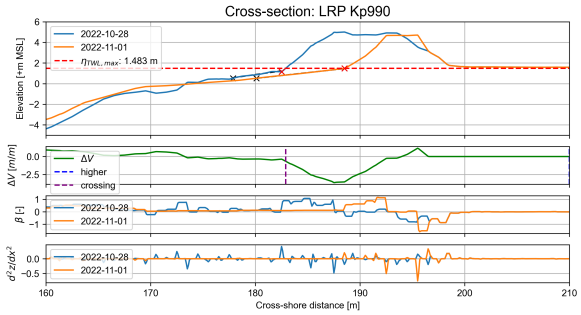

LRP transect Kp990

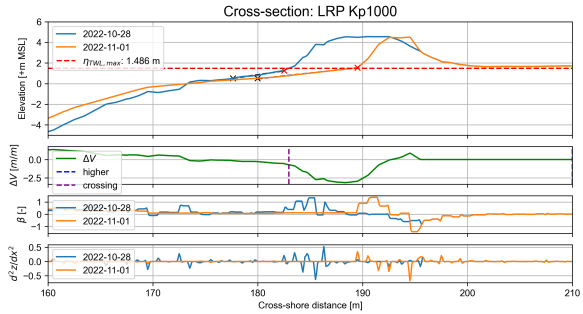

LRP transect Kp1000

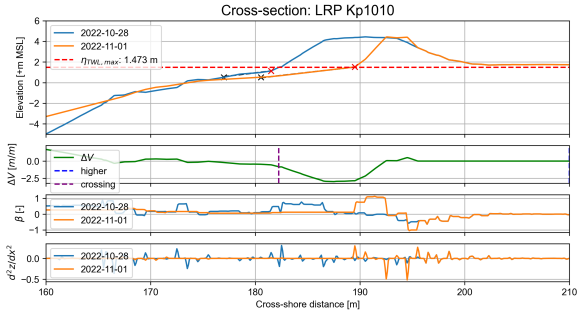

LRP transect Kp1010

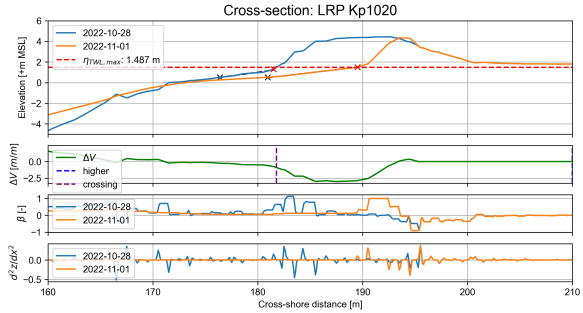

LRP transect Kp1020

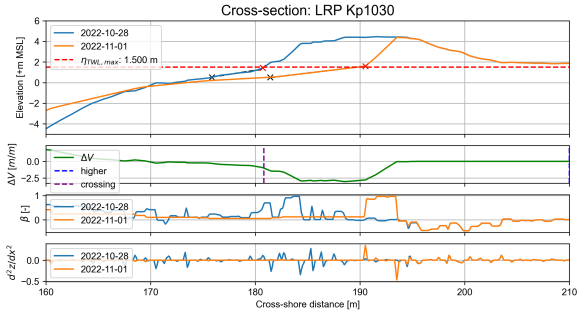

LRP transect Kp1030

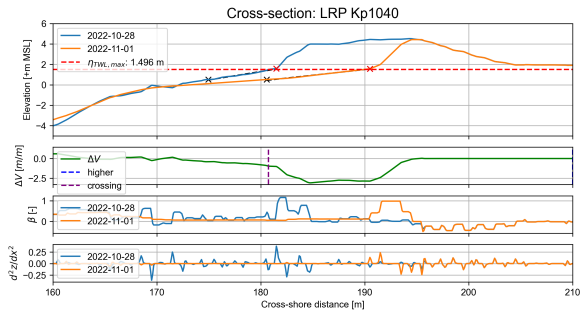

LRP transect Kp1040

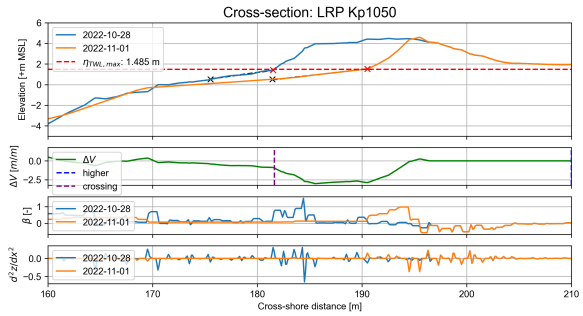

LRP transect Kp1050

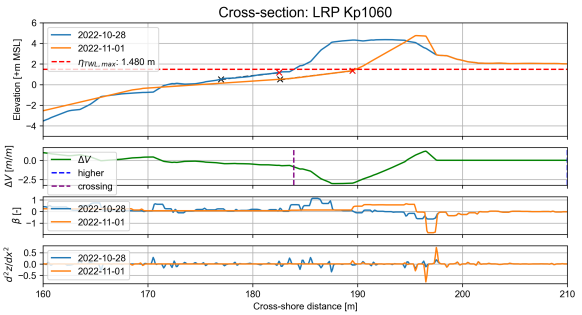

LRP transect Kp1060

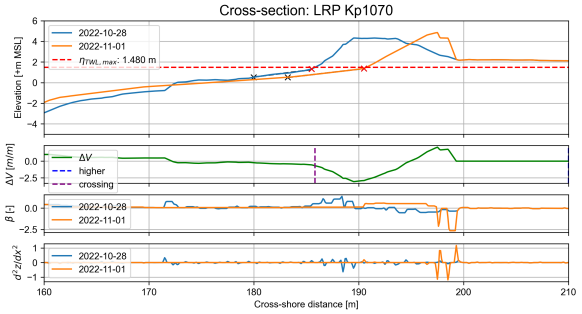

LRP transect Kp1070

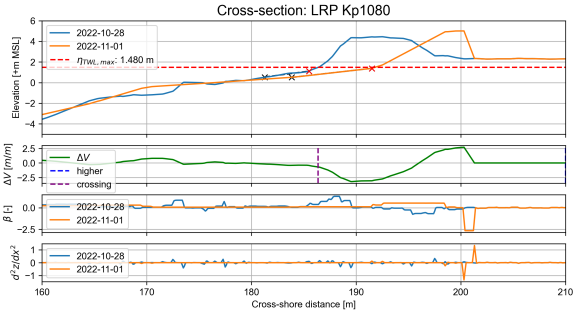

LRP transect Kp1080

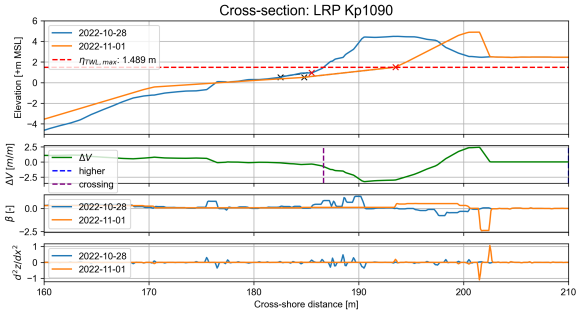

LRP transect Kp1090

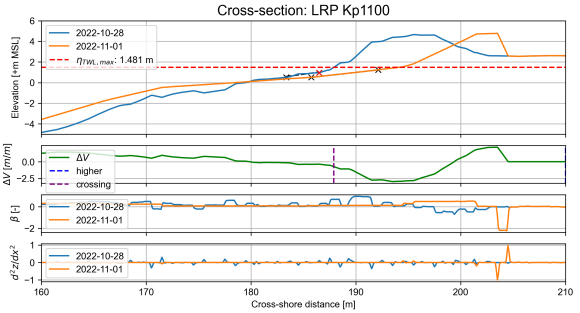

LRP transect Kp1100

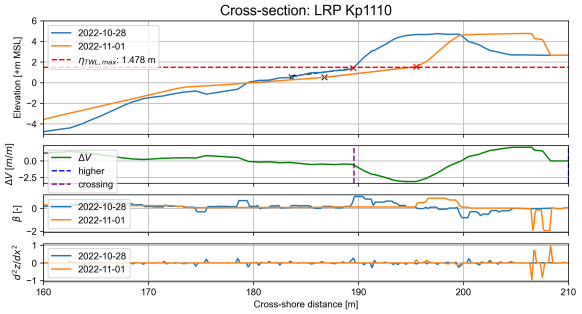

LRP transect Kp1110

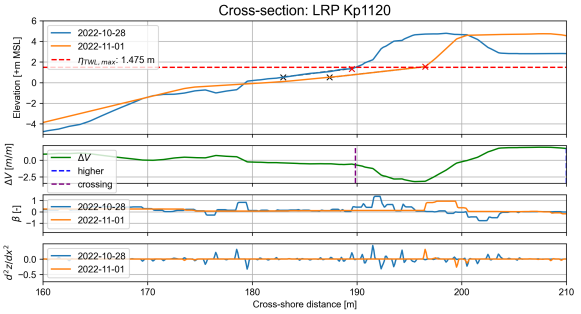

LRP transect Kp1120

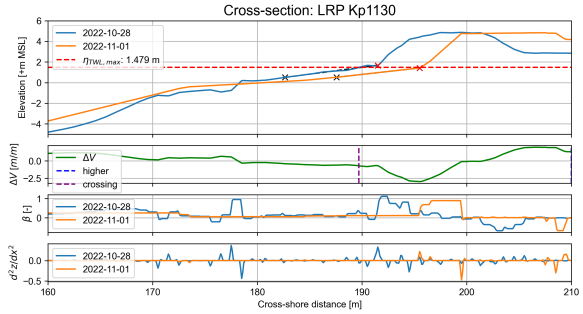

LRP transect Kp1130

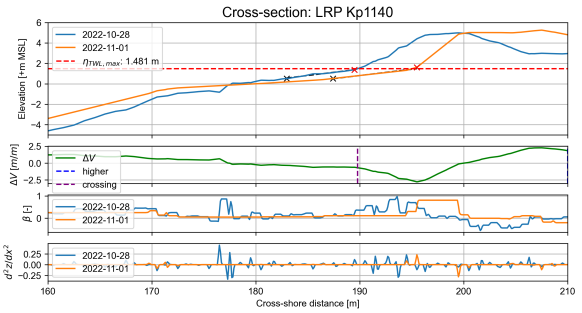

LRP transect Kp1140

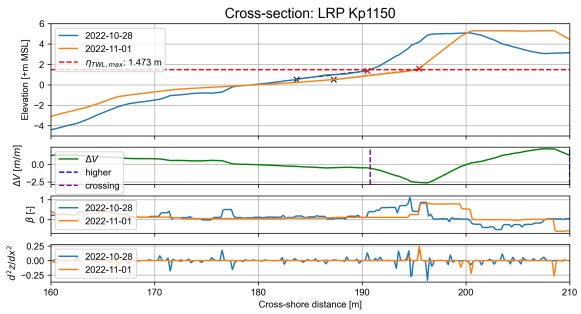

LRP transect Kp1150

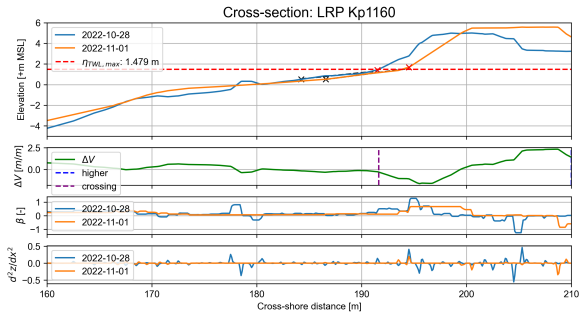

LRP transect Kp1160

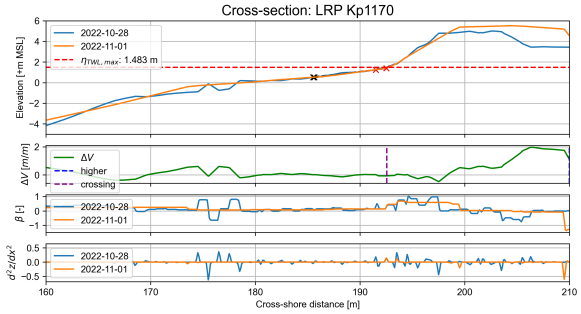

LRP transect Kp1170

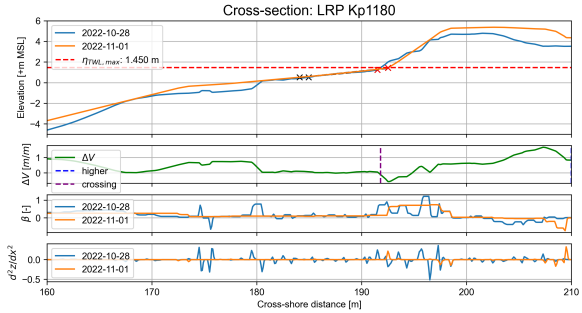

LRP transect Kp1180

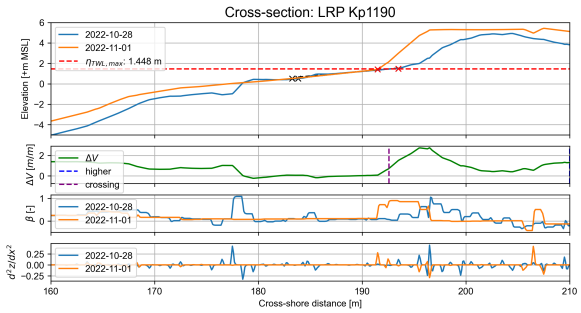

LRP transect Kp1190

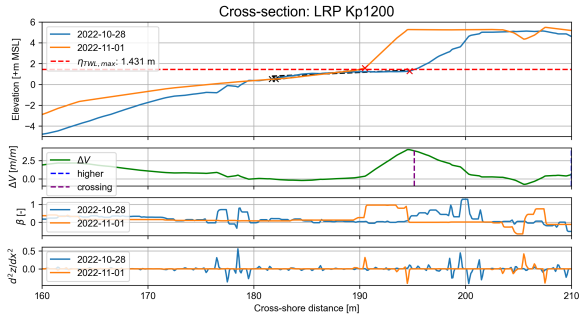

LRP transect Kp1200

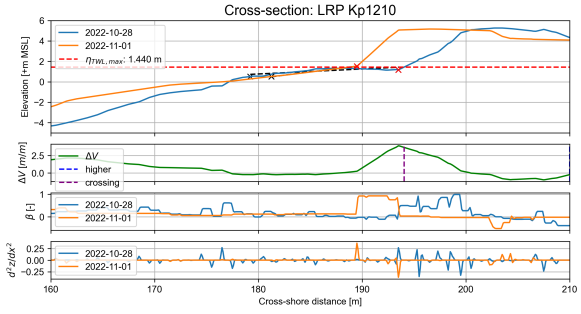

LRP transect Kp1210

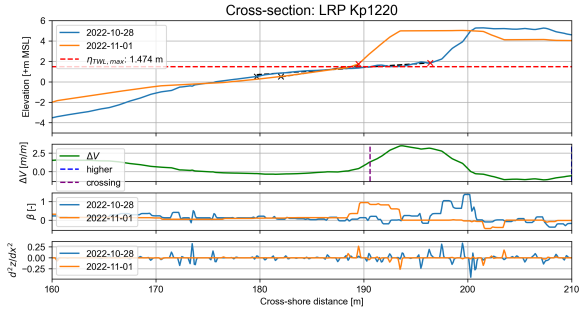

LRP transect Kp1220

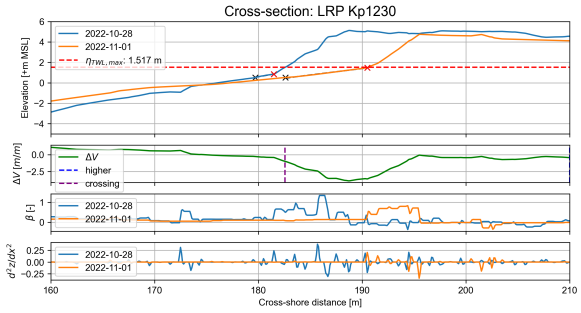

LRP transect Kp1230

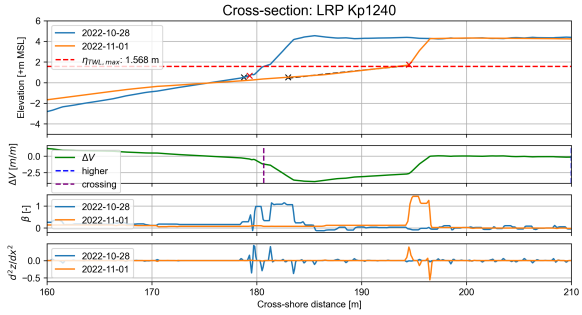

LRP transect Kp1240

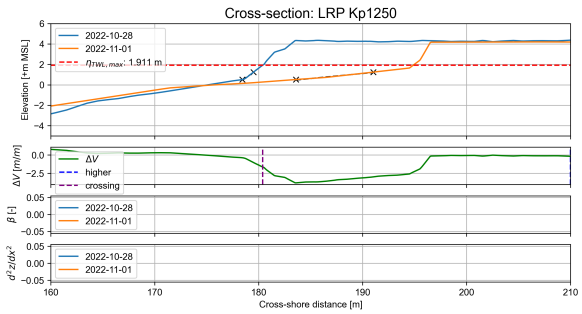

LRP transect Kp1250

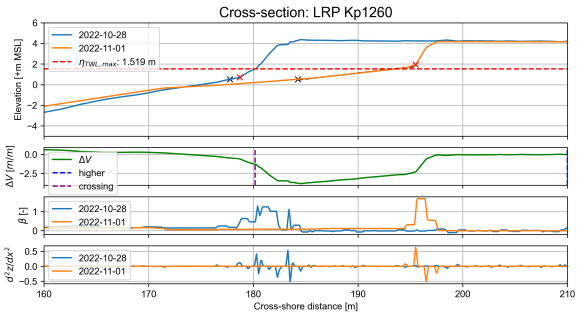

LRP transect Kp1260

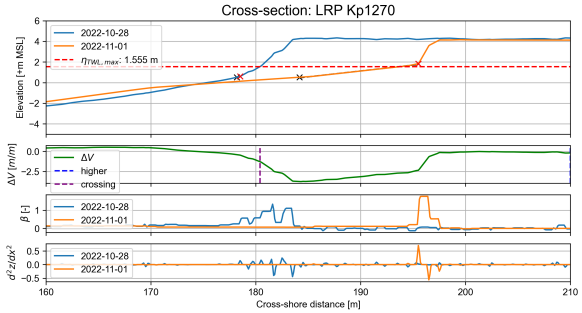

LRP transect Kp1270

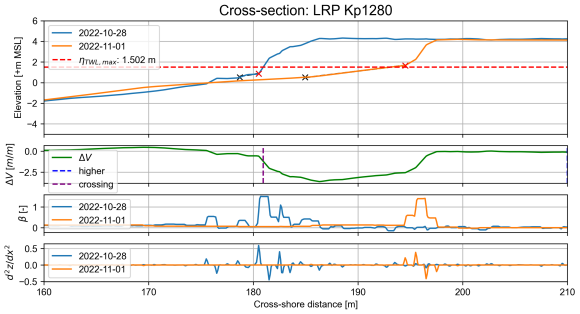

LRP transect Kp1280

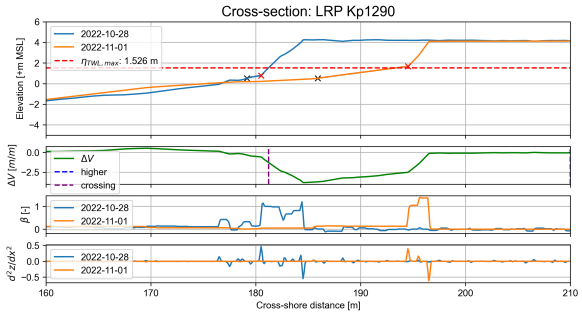

LRP transect Kp1290

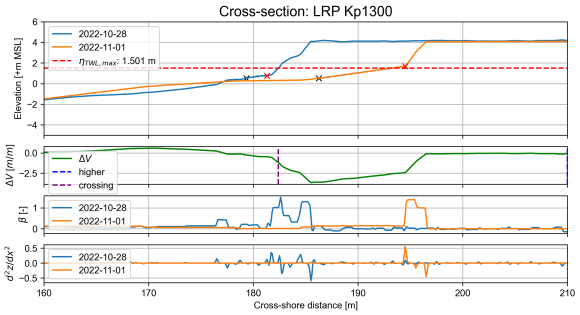

LRP transect Kp1300

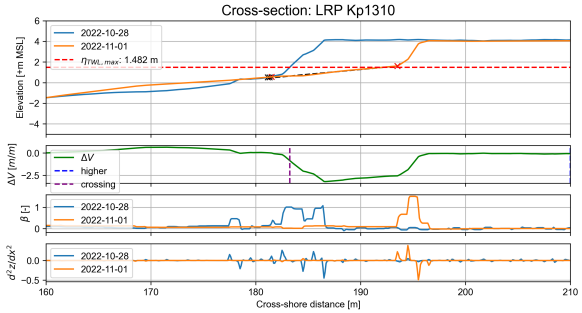

LRP transect Kp1310

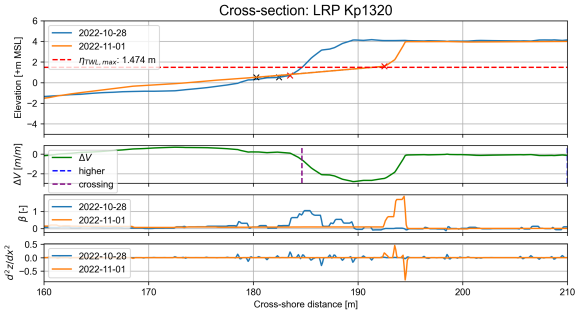

LRP transect Kp1320

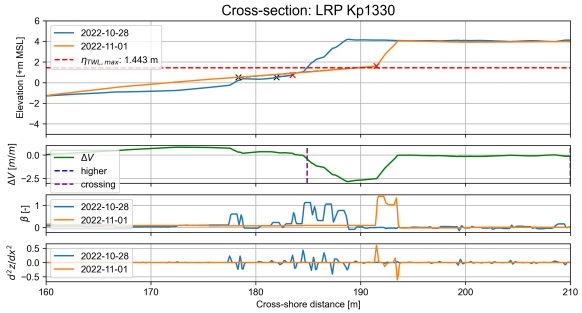

LRP transect Kp1330

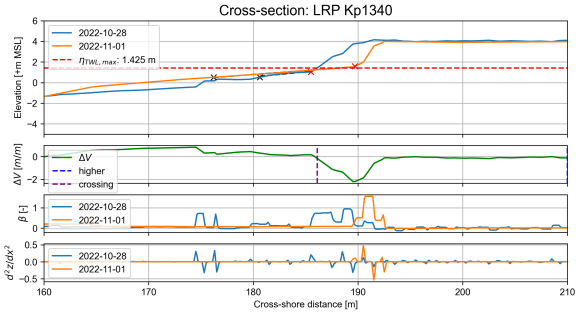

LRP transect Kp1340

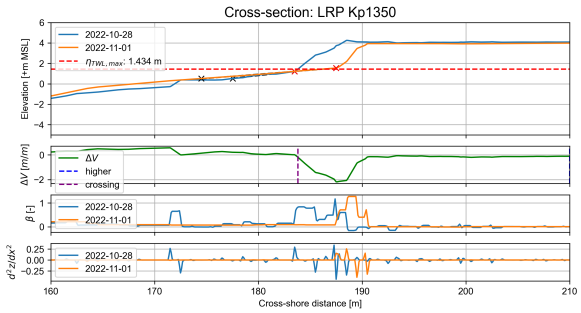

LRP transect Kp1350

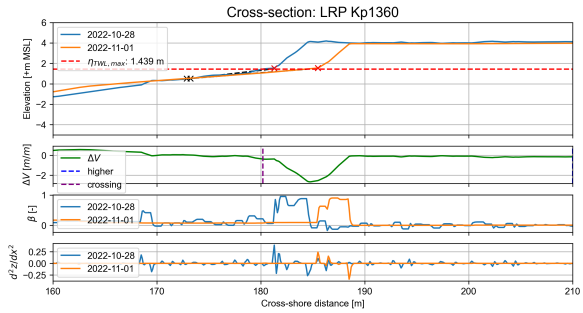

LRP transect Kp1360

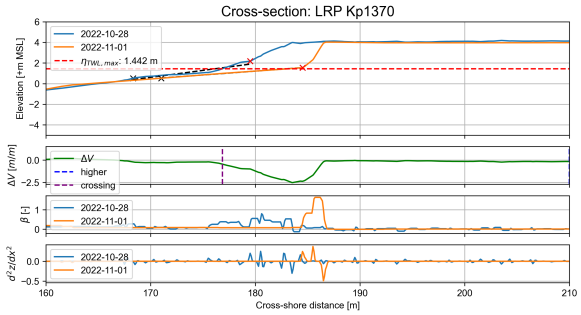

LRP transect Kp1370

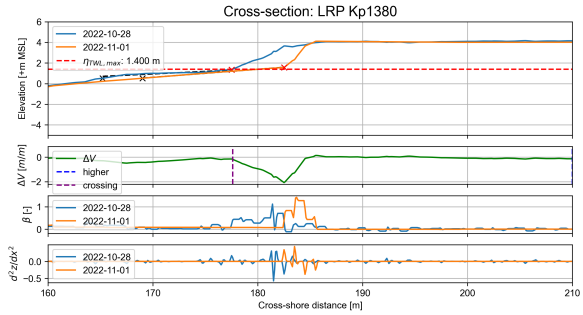

LRP transect Kp1380

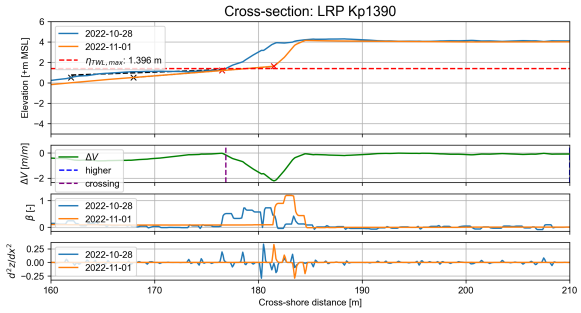

LRP transect Kp1390

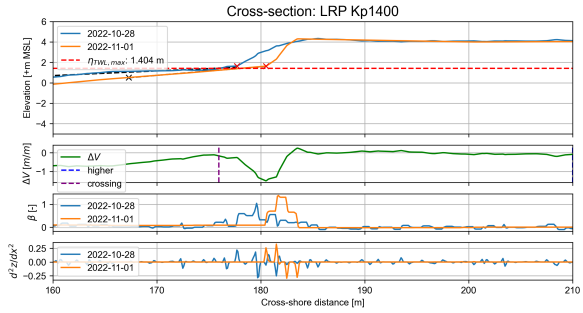

LRP transect Kp1400